TRW

NASA CR- 144848

(NASA-CR-144848) DESIGN STUDY FOR LANDSAT D ATTITUDE CONTROL SYSTEM Interim Technical Report (TRW Defense and Space Systems Group) 175 p HC A08/MF A01 CSCL 22B

N77-15060

Unclas
G3/15 12043

[redacted]

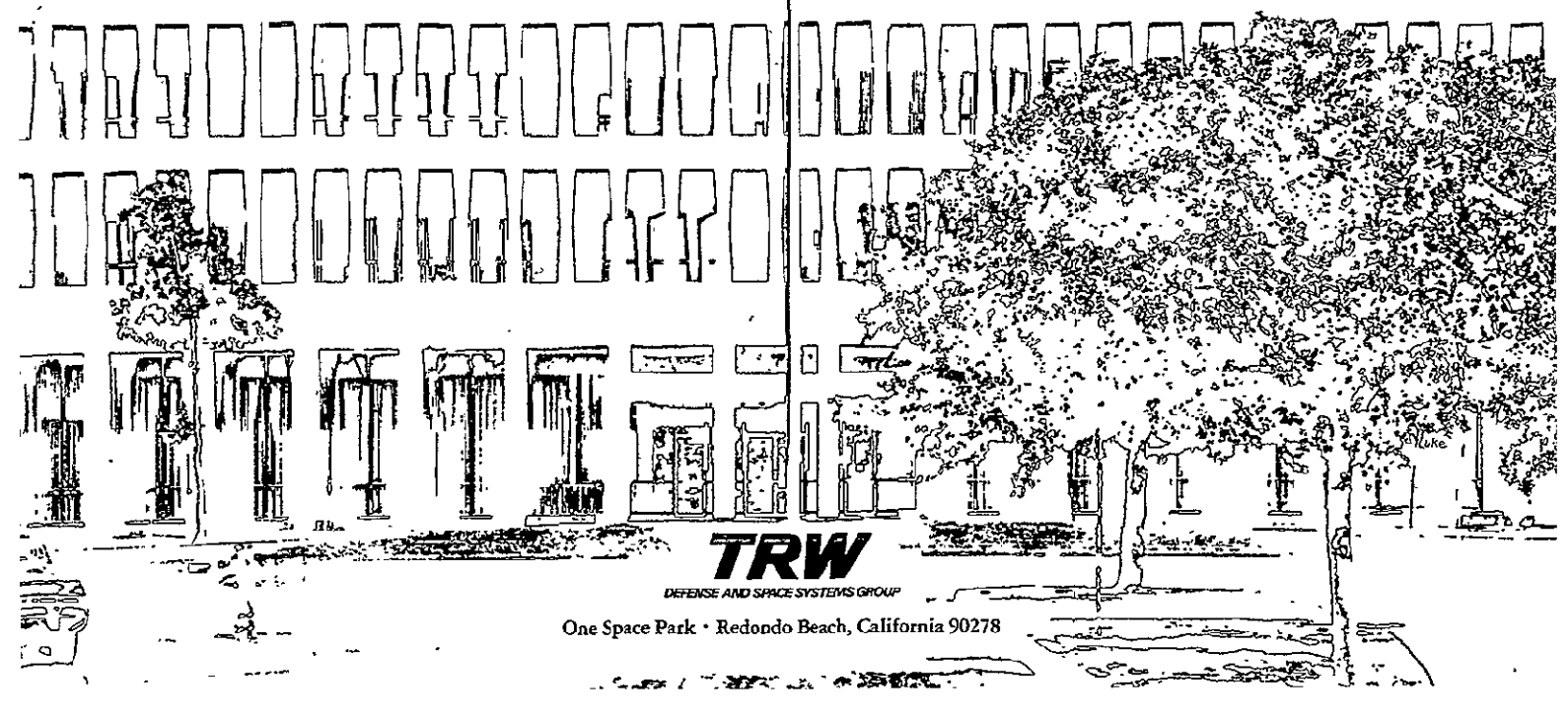

TRW
DEFENSE AND SPACE SYSTEMS GROUP
One Space Park • Redondo Beach, California 90278

INTERIM TECHNICAL REPORT

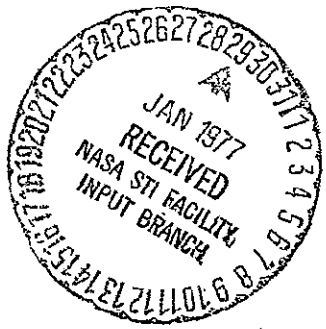

DESIGN STUDY FOR LANDSAT-D ATTITUDE CONTROL SYSTEM

15 December 1976

Prepared by: R. P. Iwens
G. E. Bernier
R. F. Hofstadter

Approved by: _____
A. M. Frew, Manager
Control Systems Engineering Department

Contract NAS5-21188

Prepared for

National Aeronautics and Space Administration
Goddard Space Flight Center
Greenbelt, Maryland 20771

TRW
DEFENSE AND SPACE SYSTEMS GROUP

TABLE OF CONTENTS

TABLE OF CONTENTS
(continued)

1.0 INTRODUCTION AND SUMMARY

TRW Defense and Space Systems has performed a series of Application Studies for NASA Goddard Space Flight Center under contract NAS5-21188. These studies have focused upon three-axis attitude control system designs employing momentum/reaction wheels with magnetic or thruster momentum unloading. The studies encompass conceptual design, system tradeoff, control law development, performance analysis and simulation, and hardware implementation considerations. The current study is directed toward design and performance evaluation of the LANDSAT D attitude control system (ACS). Control and configuration of the gimballed Ku-band antenna system for communication with the Tracking and Data Relay Satellite (TDRS), and control of the solar array drive are considered a part of the ACS and are also addressed here.

This report is an Interim Technical Report and documents only some aspects of the study. A complete final report will be published at the end of the study and the present material will then also be included.

The LANDSAT D mission, a follow-on to LANDSAT's A, B, and C, is currently in the planning stages and it will utilize the NASA Multi-Mission Modular Spacecraft. It will fly at an altitude of 705 km in a sun synchronous, 9:30 a.m. (descending node) orbit. Complete earth coverage is obtained in 16 days; exact revisit time is 233 orbits. Launch is tentatively planned for early in 1981. The payload consists of a Thematic Mapper (TM) and a Multi-Spectral Scanner (MSS). Both sensors collect spectral radiation data of (lighted) land masses. This data will be used to produce land use theme maps to better manage the earth resources. Potential users have a broad spectrum of interests including agriculture, mineralogy, and urban planning, to cite a few. The spatial resolution of the Thematic Mapper is 30 meters corresponding to the 30 meter square footprint on the ground of a square detector in the instrument. The resolution of the MSS is 80 meters. The spacecraft pointing accuracy is specified as 0.01 deg (1σ) with a jitter stability of $\pm$0.5μRad (1σ) over 20 minutes. The ultimately desired temporal registration (essentially

repeatability of ground track after 16 days) of the Thematic Mapper images is to be within 3 meters (1σ).

The primary objective of this study is to assess the adequacy of the Multi-Mission Modular Spacecraft (the MMS attitude control system in particular) to perform the LANDSAT D mission, and to identify and configure mission peculiar equipment that may be required. Examples are the gimballed Ku-band antenna and the single sided solar array and drive. To this end, preliminary design studies and performance assessments were conducted using the MMS as the baseline system concept.

Section 2 describes the LANDSAT D mission in more detail. Important currently available mission data is summarized and a brief description of the MMS and the two payload sensors is provided.

The gimballed Ku-band antenna system for communication with TDRS is discussed in Section 3. By means of an error analysis it is demonstrated that the antenna cannot be open loop pointed to TDRS by an on-board programmer but that an autotrack system is required. After some tradeoffs, a two-axis, azimuth-elevation type gimbal configuration is recommended for the antenna. It is shown that gimbal lock only occurs when LANDSAT D is over water where a temporary loss of the communication link to TDRS is of no consequence. A preliminary gimbal control system design is also presented.

A digital computer program was written that computes antenna gimbal angle profiles, assesses percent antenna beam interference with the solar array (as a function of antenna mast length), and determines whether the spacecraft is over land or water, a lighted earth or a dark earth, and whether the spacecraft is in eclipse. Besides checking for optical blockage of the antenna beam by the solar array paddle, another important application of this program is to determine when the spacecraft is over lighted land, since this is directly proportional to the TM electric power duty cycle. For one typical 15 orbit (24 hrs) case, the spacecraft spent only 16.5% of the time over lighted land.

A solar array control strategy was developed that eliminates interference with the Ku-band antenna beam. The array is driven at orbit rate as long as the spacecraft is within ±45° of the ecliptic plane. When the spacecraft is outside this region the array is kept fixed at the orientation it had at ±45° away from the ecliptic and this orientation is maintained until the earth becomes dark. At that point the array is slewed again to its optimal position normal to the sun line and it continues to track the sun until the spacecraft goes into eclipse. This strategy requires the Ku-band antenna mast to be only 2.11 m (6.9 ft) in length in order to eliminate all interference. The key is the 37.5° cant in the array which permits the antenna to look past the array when it is within ±45° of the ecliptic. Outside this region the array would rapidly obstruct the field-of-view of the antenna if it were not stopped as described above. The total power loss associated with this solar array control strategy is only 4% and it can be easily compensated for by increasing the array area by 4%. The 2.11 meter long antenna mast has been computed for a 4% increased array area.

Section 4 sizes external disturbance torques acting on LANDSAT D. Aerodynamic, gravity gradient, magnetic, and solar pressure disturbance torques are considered. Ku-band antenna mast length and antenna orientation were observed to affect the magnitude of the disturbance torques only insignificantly.

The disturbance torque sizing results were then used to assess whether the four 20 Nms (15 ft-lb-sec) reaction wheels and the three orthogonal 100,000 pole-cm magnetic torque bars provided in the MMS ACS module have sufficient capability for the LANDSAT application. The conclusions were that the spacecraft can operate effectively in its 705 km orbit environment even when using only the 50,000 pole-cm windings on the magnetic bars. Momentum excursions in the wheels were observed within ±2.0 Nms of nominal and since the reaction wheel momentum storage capacity is 20 Nms, it is recommended that all four wheels be run at a biased speed. This avoids wheel speed reversal and associated attitude transients due to nonlinear wheel friction. The four wheels are speed biased such that a net zero momentum system results (not possible with only three

wheels). Should one wheel fail, then the three remaining wheels must be operated about zero speed and the wheel speed reversal attitude transients of about 90 μRad (18.5 arc-sec) must be accepted. This would occur twice per orbit in roll and twice per orbit in yaw.

Initialization of the fine control mode is discussed in Section 5. Two methods to perform fine stellar acquisition, i.e., to initialize the on-board stellar-inertial attitude reference system, are presented. Before entering the stellar acquisition mode the spacecraft is sun pointing (in the fine sun acquisition mode) and only a relatively coarse determination of the spacecraft orientation about the sun line is needed for correct star identification. One method uses magnetic field measurements and is capable of providing attitude knowledge about the sun line within about 2°. The other method correlates observed stars in a swath about the sun line with star catalog entries and determines attitude about the sun line to within approximately 0.2 degree (uncalibrated gyros assumed). The magnetic field measurement method is simpler and the 2° attitude knowledge is sufficient for unambiguously identifying the first few stars when the stellar-inertial attitude reference system is initialized. Using the real star field it is demonstrated that the linearized (extended) Kalman filter algorithm assumed to be used by the on-board attitude reference system, is capable of converging rapidly from large (2°) initial attitude uncertainties. The converged attitude reference filter predicted accuracies in the 5 to 10 arc-sec (1σ) range and the gyro biases were calibrated to within about 0.0013 deg/hr.

The final report will address normal on-orbit ACS design and performance. The effects of flexible and moving appendages such as the Ku-band antenna and the solar array are also considered. Stationkeeping, autonomous Thematic Mapper boresight registration and on-board software sizing will also be addressed.

2.0 LANDSAT-D MISSION

LANDSAT-D is the planned fourth mission in the LANDSAT program whose primary objective is to evaluate and monitor the earth's resources from satellite observations. Formerly, this program was known as the Earth Resources Technology Satellite (ERTS) program. The spacecraft to be flown on the LANDSAT-D mission, as well as the mission itself, have in the past also been referred to as LANDSAT Follow-On (LF/O). The primary mission payload sensor for LANDSAT-D (L-D) is the Thematic Mapper (TM), a large multi-spectral instrument which uses solid state detectors to produce earth imaging data which is digitized and transmitted to the ground in a 120 megabit per second serial data stream. Potential users of TM data have a broad spectrum of interests including agriculture, mineralogy, and urban planning, to cite a few.

Agriculture as it relates to the economy and to the world food supply is one of the driving forces behind the LANDSAT program. Data from the Thematic Mapper can be used to determine how much wheat, corn, barley, etc. have been planted, how well the crops are doing, and combined with watershed data also collected by the Thematic Mapper, predictions of yield can be made. The system can collect this data on a world-wide basis. The public benefit is expected to be enormous. Shortages can be predicted and additional acerage planted - perhaps in a different hemisphere. Surpluses in one crop may be avoided by planting different crops. Effects of disease or insects can be assessed and hopefully minimized by early detection.

Two LANDSAT spacecraft are currently in orbit, LANDSAT's A and B, with an instrument known as the Multi-Spectral Scanner (MSS) being their primary payload sensor; the MSS is basically a smaller and less advanced/less powerful version of a Thematic Mapper type instrument. LANDSAT's A and B are producing image data which is primarily being used for research in remote sensing technology, data interpretation techniques, etc. A third spacecraft, LANDSAT-C, is being prepared for launch with a modestly upgraded Multi-Spectral Scanner instrument which will include a long wave infra red (10.5 to 12 microns) sensing capability in addition to the four

spectral bands carried on LANDSAT's A and B. This upgraded version of the MSS will also be flown as a secondary payload on LANDSAT-D. It will provide continuing service to users who have not yet upgraded their ground stations and data processing capabilities to handle Thematic Mapper data. It will also provide an opportunity to directly compare spectral signature data from the two instruments, maximizing learning transfer and enhancing capability to compare Thematic Mapper data with historic MSS data.

2.1 LANDSAT-D Orbital Data

The LANDSAT-D (L-D) spacecraft will fly in a circular, 9:30 a.m., descending node, sun synchronous orbit. The terminology "sun-synchronous" refers to the property that the line of nodes of the orbit advances at the same rate as the earth's orbital rate about the sun. The orbit altitude is 705 km (380 nautical miles) and the orbit plane inclination is 98.2 degrees. The orbital period can be calculated as 1.648 hours (98.88 minutes), or stating it differently, there are exactly 14 9/16 orbits in a 24 hour period. Figure 2-1 shows the L-D orbit relative to the earth equatorial plane at vernal equinox, illustrating the 9:30 a.m. sun synchronous orbit feature. It simply means that throughout the year the spacecraft will cross the equator on its north-to-south descending pass at 9:30 a.m. local ground time. Since the orbit is almost polar, the ground time is close to 9:30 a.m. over the entire sun lit side of the earth, and close to 9:30 p.m. over the entire dark side of the earth.

Nominally the Thematic Mapper (TM) data is transmitted in real time from the L-D to a geostationary Tracking and Data Relay Satellite (TDRS) which retransmits the data to the ground. By 1981 when L-D is scheduled to be launched, there will at least be two operational TDRS's in geosynchronous equatorial orbit. They will be positioned above the equator at the following longitudes.

- TDRS East: 41° West Longitude
- TDRS West: 171° West Longitude

The TDRS equatorial orbit is also indicated in Figure 2-1.

LANDSAT-D Orbit Summary

- 9:30 a.m., descending node, sun synchronous orbit
- Inclination i = 98.2 deg
- Altitude h = 705 km
- Orbit Period T_o = 1.648 hrs
- Orbit Rate ω_o = 0.06068 deg/sec

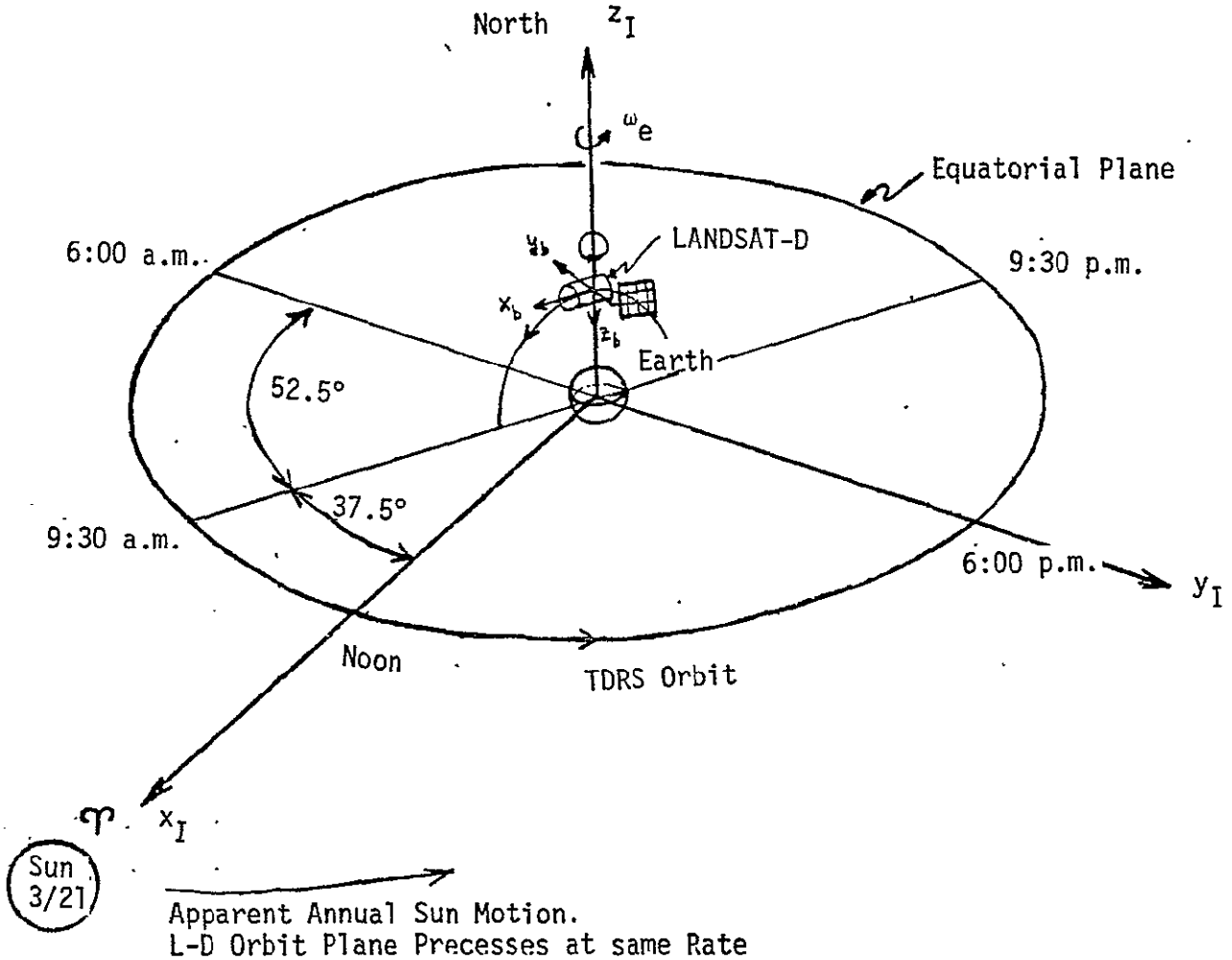

Figure 2-1. LANDSAT-D Orbit

Solar time on earth repeats at integer multiples of 24 hours. Let T_0 be the L-D orbit period in hours. Then the smallest number of orbits n such that $n\,T_0$ is an integer multiple of 24 hours is the L-D revisit time, i.e., the satellite will be exactly above the same point on earth after exactly n orbits (ideal orbits assumed). If the north-south ground path illuminated by the payload sensor field of view is chosen to be of appropriate width, then the revisit time is also the time it takes to obtain total earth coverage, i.e., obtain data from the entire earth surface, with the exception of two small regions about each of the earth's poles which cannot be seen because the orbit inclination is 98.2 degrees, that is, more than 90 degrees. Since the orbit period of L-D is

$$T_0 = \frac{24}{14\ 9/16} = \frac{(24)\ x\ (16)}{233}\ \text{hrs}$$

one must find the smallest integer n such that

$$\frac{(24)\ x\ (16)}{233}\ n = 24\ m$$

where m must be an integer. This leads to m = 16 and n = 233. Thus the revisit time is 16 days during which the spacecraft completes 233 orbits.

L-D is scheduled to be launched in 1981 on a Thor Delta 3910 booster, but the spacecraft and payload designs must also be compatible with future launch, resupply, and retrieval by the Space Shuttle. L-D mission life has been preliminarily specified as 3 years.

After orbit insertion of the spacecraft, initial orbit corrections are performed to assure orbit circularity and correct altitude and orbit inclination. Thereafter, ΔV stationkeeping maneuvers will only be performed to make up for orbit decay due to atmospheric drag. A $\pm$ 6.5 km E-W ground track drift due to spacecraft altitude and attendant orbit period change is the maximum permissible error. Using a conservative drag model, this implies that the orbital velocity must be corrected by applying a ΔV = 0.35 m/second at most every 16 days.

2.2 Spacecraft Configuration

Because the TM is a larger payload sensor than the MSS, the LANDSAT-D mission will require a new spacecraft design to support the TM's greater weight, provide more power, provide more accurate pointing control, and to relay higher data rates to the ground. It has been decided by NASA that the L-D mission will be performed using the Multi-Mission Modular Spacecraft (MMS). The MMS is a concept that has been developed by NASA Goddard Space Flight Center (GSFC) over the past 6 years. It was originally known as the Low Cost Modular Spacecraft and Reference 1 provides an excellent description of its projected characteristics and capabilities. The brief discussion that follows is entirely based on Reference 1, and the illustrations of the MMS in Figures 2-2 through 2-5 are those of Reference 1.

2.2.1 Multi-Mission Modular Spacecraft

The MMS is an independent three-axis stabilized vehicle using three or four reaction wheels in conjunction with a stellar-inertial attitude reference system to provide accurate and stable spacecraft attitude control. As the name implies, the MMS is composed of a set of standard modules: ACS module, Communications and Data Handling (CDH) module and Power module. The propulsion module is generally optional and comes in two standard versions known as SPS-I and SPS-II (L-D will require the SPS-I propulsion module). The baseline MMS configuration contains the above mentioned three subsystem modules supported by a module support structure, as shown in Figure 2-2. A transition adapter and a vehicle adapter complete the structural elements of the system. Mission unique and adapted items include the solar array, the solar array drive, the solar drive deployment mechanisms, a set of deployable TDRS antennas and booms, and a mission adapter and payload (see Figures 2-3 and 2-4). The three spacecraft modules are physically the same size. As shown in Figure 2-3, they measure 18 inches deep, 48 inches high, and 48 inches wide. The ACS module is of particular interest in this study and a preliminary equipment layout of the module is shown in Figure 2-5.

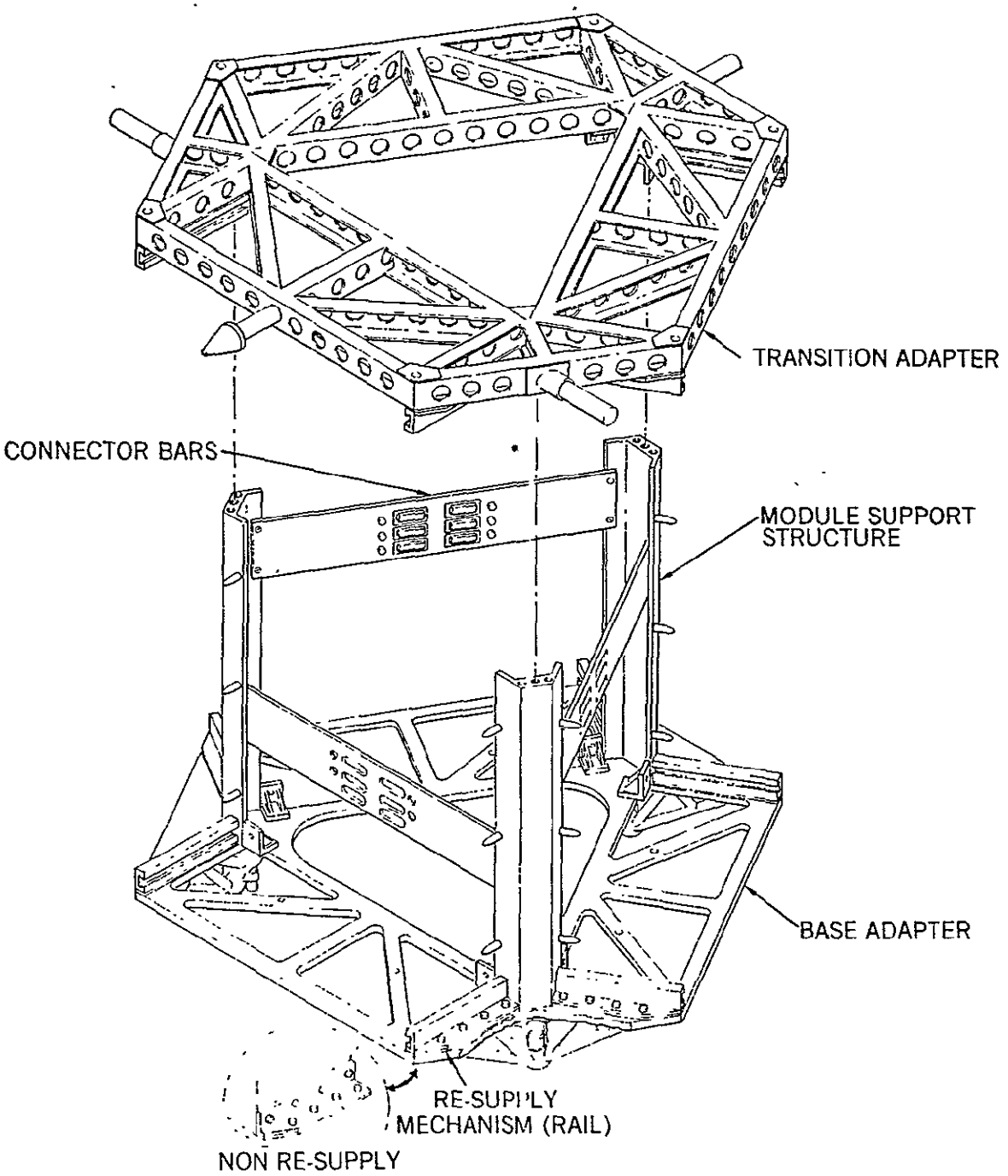

Figure 2-2. Module Support Structure
(Taken from Reference 1)

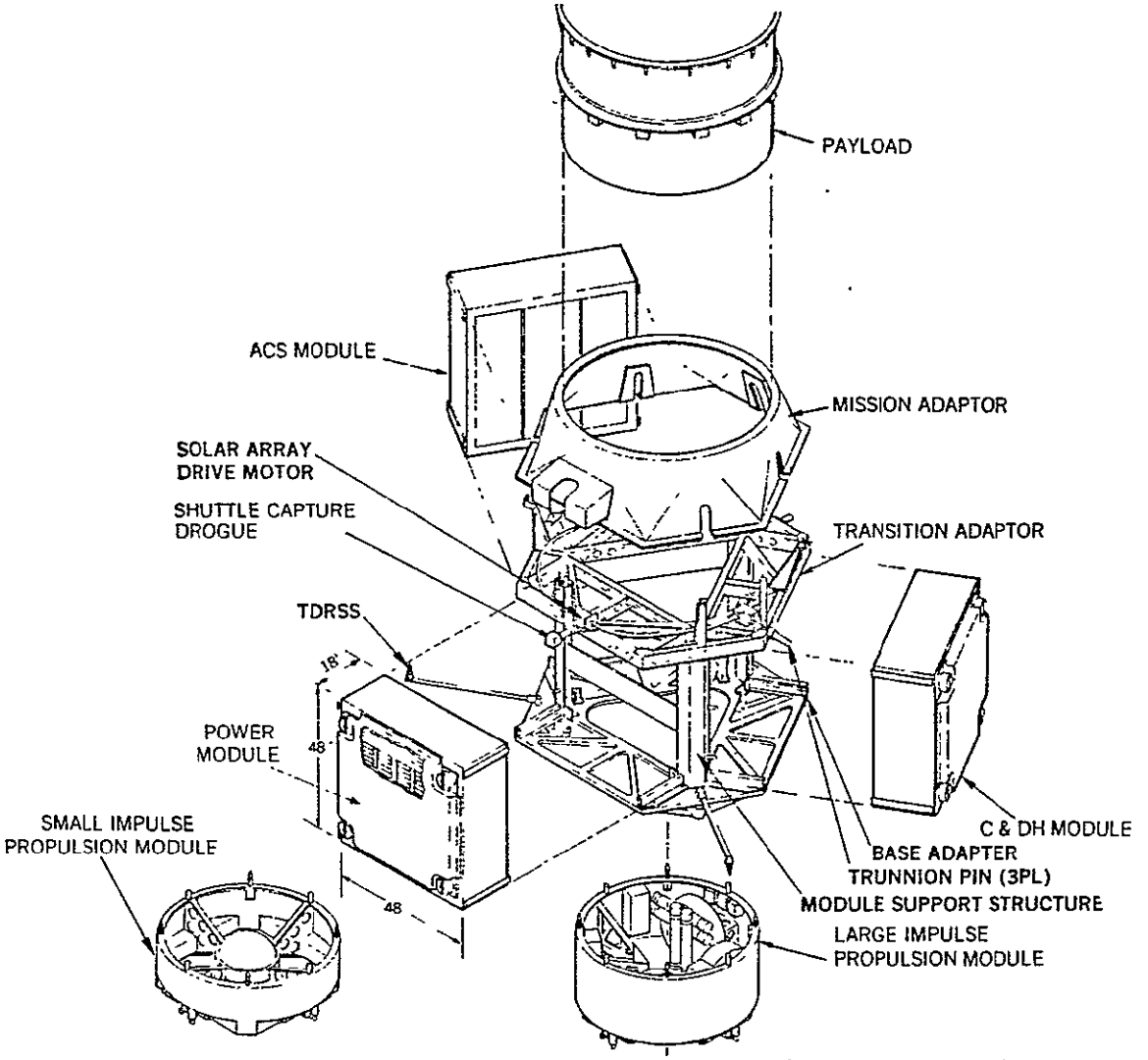

Figure 2-3. Multi-Mission Modular Spacecraft (Exploded View)
(Taken from Reference 1)

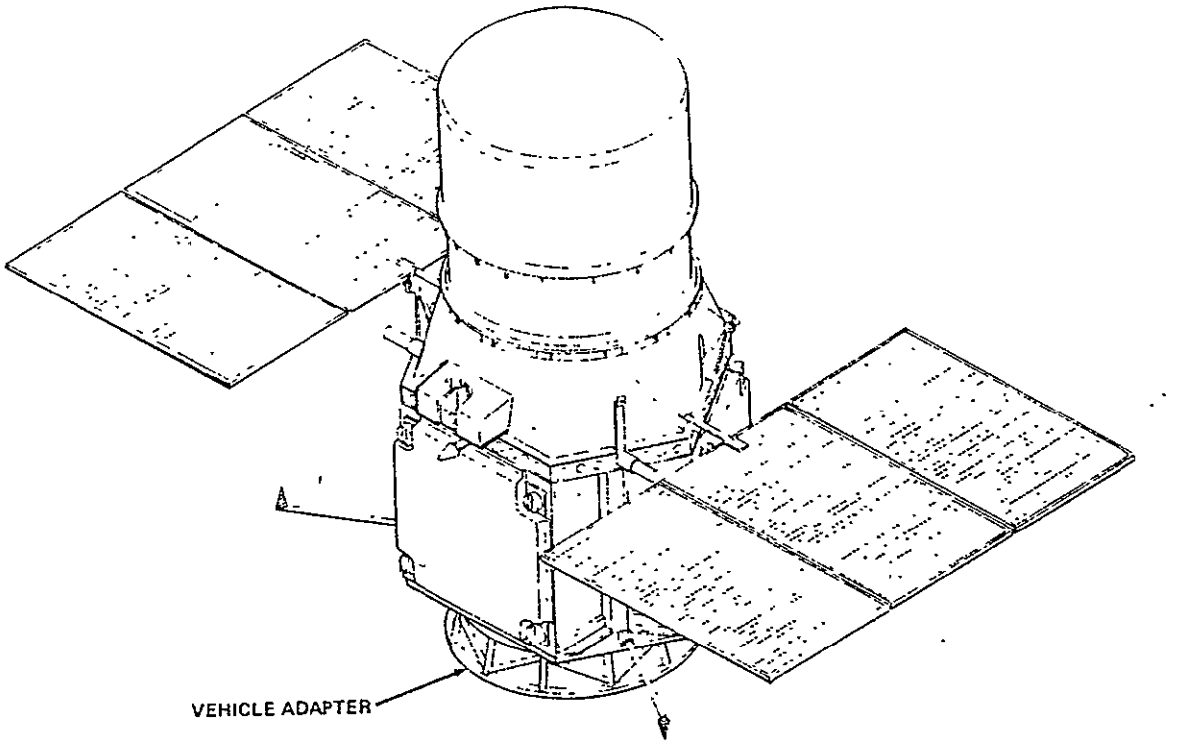

Figure 2-4. Multi-Mission Modular Spacecraft
(Taken from Reference 1)

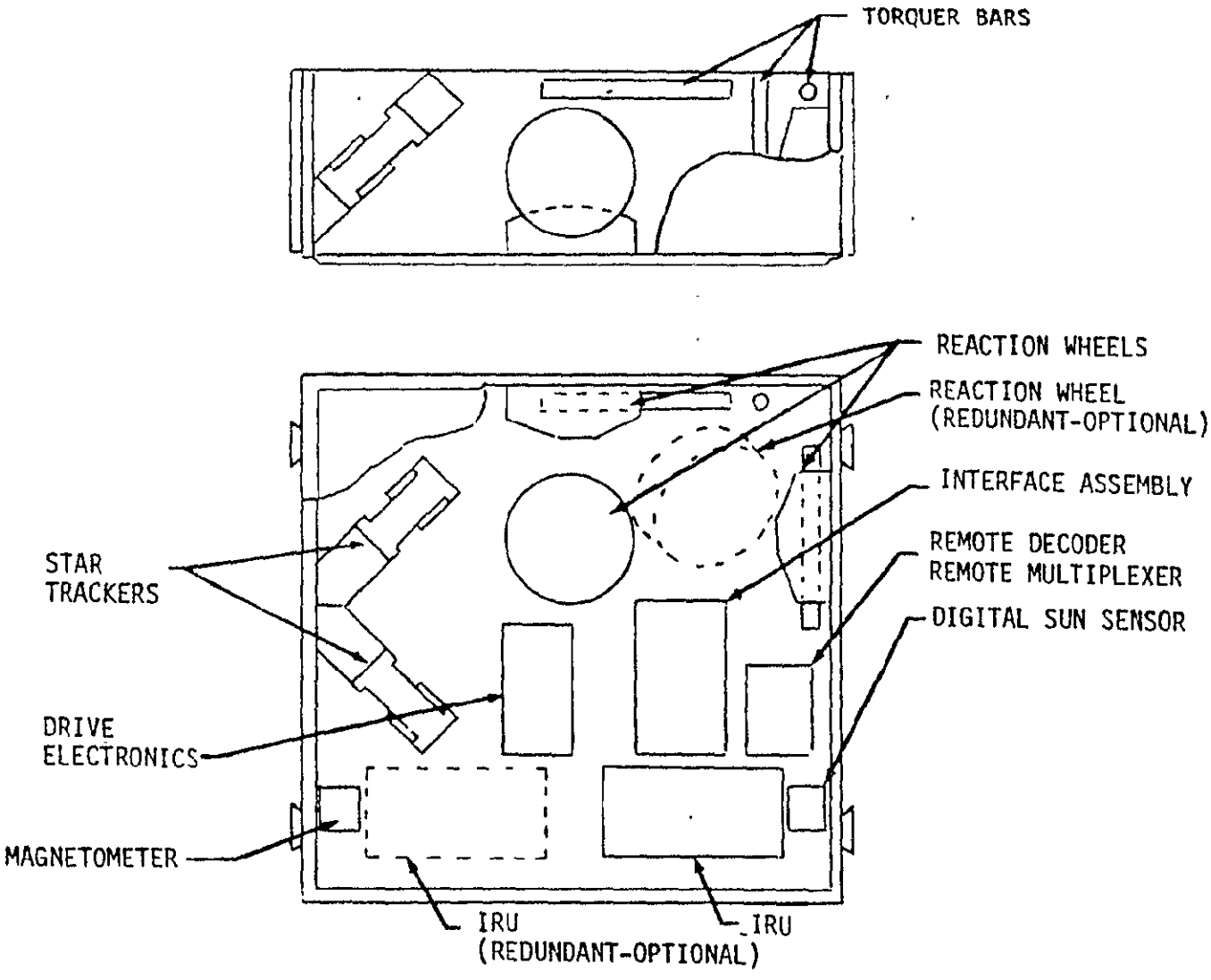

Figure 2-5. ACS Module

Alignment between the attitude control subsystem and the payload reference axis is maintained by the transition adapter during orbit operations. The transition adapter has other unique features which allow a shuttle orbiter capture, docking, retrieval and servicing by a manipulator system. The transition adapter also supports the solar array launch restraint and deployment mechanism and the solar array drive motors. The communication antennas are attached to the spacecraft to suit the mission. Optional attachment points include the area above the separation interface on the base adapter and also the transition adapter. The antennas and boom assembly can be folded into the recess formed by the adjacent edges of the modules. Total spacecraft weight without payload is 1235 pounds for the baseline configuration and 1590 pounds for the fully redundant configuration. This does not include the propulsion module.

2.2.2 LANDSAT-D Configuration and Mass Properties

Figure 2-6 shows a simplified block diagram of the L-D spacecraft system. On the left, the three standardized subsystem modules and their supporting structure is indicated. In the middle of Figure 2-6, the L-D payload is indicated. The payload instruments are supported by a mission unique forward structure and feed their output data to mission unique transmitters and antennas operating at K-band to handle the 120 megabit/second TM data rates. Capability is planned for real time relay via the Tracking and Data Relay Satellite System (TDRSS) to the continental U.S. and for direct downlink to K-band equipped ground stations in view of the spacecraft.

Figure 2-7 shows the overall L-D/MMS spacecraft in its on-orbit configuration with antennas and the solar array deployed. For this mission a one sided solar array is used to maintain clear fields of view for the passive radiation coolers used by both the TM and the MSS. For in flight replacement by the shuttle, the TM can be slid upward away from the nadir direction after disconnecting three attach fittings. The TDRSS compatible K-band antenna dish and transmitter are gimballed and deployed on a boom to allow the antenna more rotational freedom in tracking TDRS and to

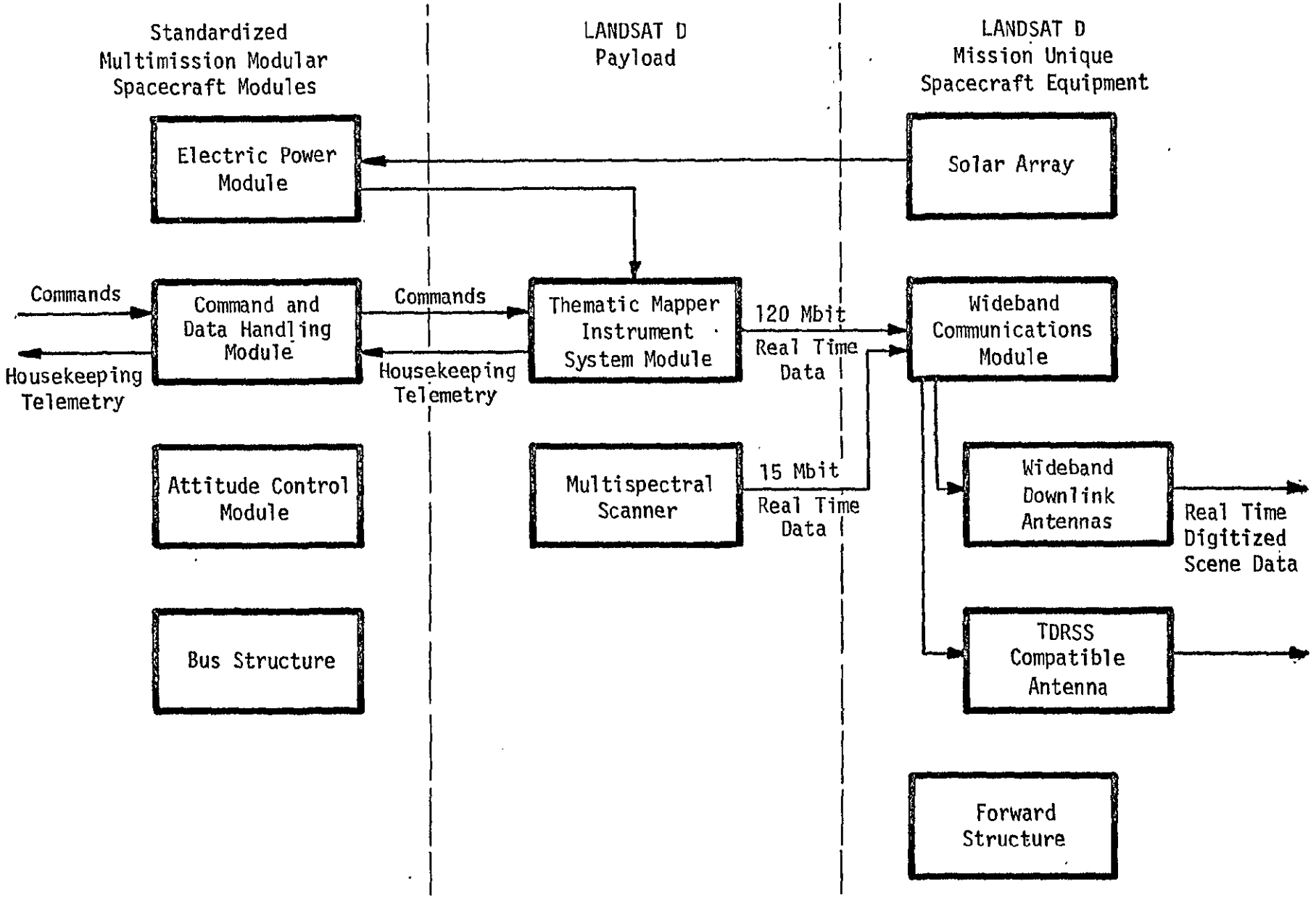

Figure 2-6. Block Diagram of Assumed LANDSAT-D Spacecraft

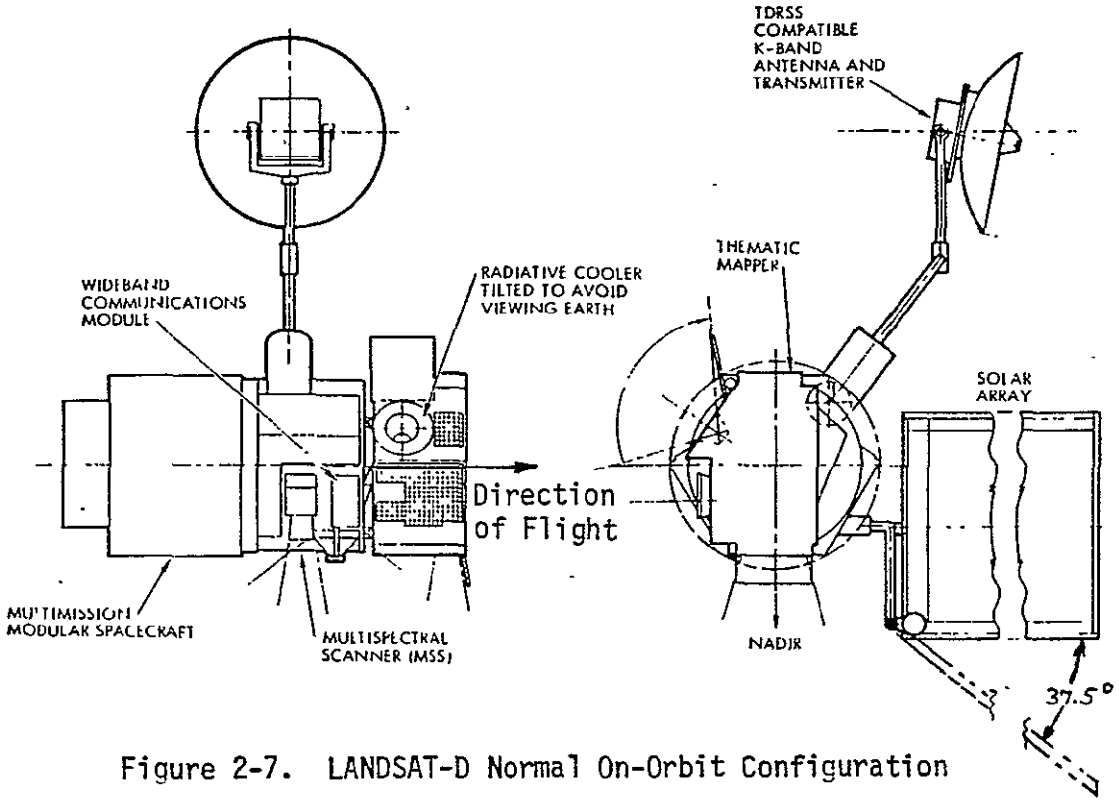

Figure 2-7. LANDSAT-D Normal On-Orbit Configuration

minimize antenna radiation pattern interference with the solar array and other parts of the spacecraft. The direct access antenna for downlink K-band communication is not shown in Figure 2-7.

The driven solar array is of the FRUSA type (Flexible Rolled-Up Solar Array developed by Hughes Aircraft Company) and it is canted 37.5 degrees relative to its axis of rotation (parallel to the spacecraft pitch axis) so that a coincal array envelope results. Because of the 9:30 a.m. orbit of L-D, the cant angle must be 37.5 degrees in order to maintain the plane of the solar array normal to the sun line when the array rotates about the spacecraft pitch axis at orbit rate (see also Figure 2-1). The array dimensions are 6.33 ft x 27 ft (1.93 m x 8.23 m) of which the solar cell area comprises 5 ft x 27 ft (1.525 m x 8.23 m). The array weight is approximately 50 pounds (22.7 kg) and the array efficiency after 3 years on-orbit is about 7.5 watts/square-foot (80.73 watts/m^2), resulting in a little over 1 Kw of generated electric power.

The total spacecraft on-orbit weight is estimated at

$$m = 3500 \text{ lb } (1587 \text{ kg})$$

and preliminary assessments of the principal moments of inertia are (Reference 2)

$$I_x = 1500 \text{ slug-ft}^2 \quad (2034 \text{ kg m}^2)$$
$$I_y = 1970 \text{ slug-ft}^2 \quad (2671 \text{ kg m}^2)$$
$$I_z = 1750 \text{ slug-ft}^2 \quad (2373 \text{ kg m}^2)$$

2.3 Payload Description

2.3.1 Thematic Mapper

The Thematic Mapper is planned as the primary payload instrument for LANDSAT-D, to be launched early in 1981.

The name "Thematic Mapper" derives from the intended use of the instrument to produce land use theme maps which may be tailored to the data requirements of particular researchers, responsible government agencies, or private companies who can make use of remotely sensed data to better manage our earth resources. The Thematic Mapper will provide significant improvements in instrument performance compared to the current generation Multi-Spectral Scanner (MSS). The Thematic Mapper will provide coverage in at least seven spectral bands versus five in the MSS, 30 meter spatial resolution versus 80 for the MSS, better radiometer accuracy, and better geometric accuracy. Figure 2-8 shows a conceptual drawing of LANDSAT-D in operation. The spacecraft is in a circular, nearly polar orbit and provides complete global converage every 16 days.

TRW Defense and Space Systems, teamed with Perkin-Elmer, and Hughes Aircraft Company (HAC) have submitted competing bids to NASA GSFC to develop and build a flight version of the TM. This competition has not yet been decided and for this reason the description of the TM provided here

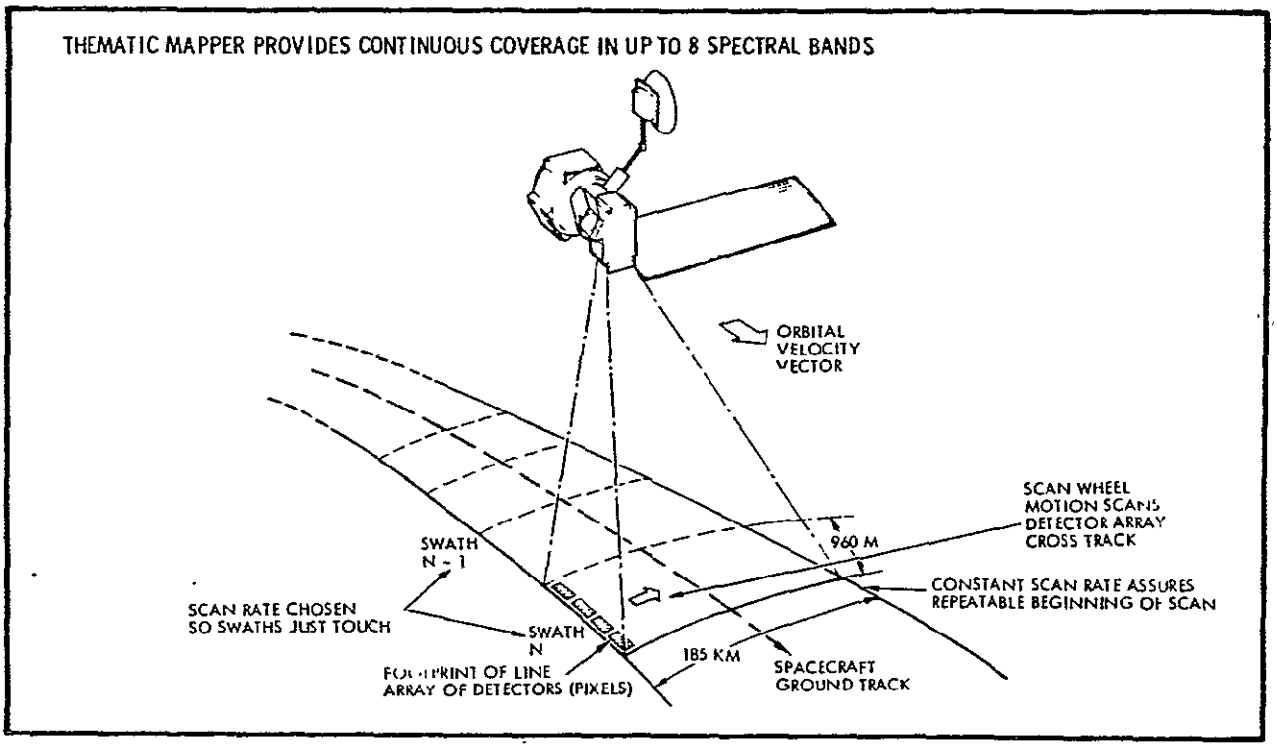

Figure 2-8. Crosstrack Optical Scanning Provides Continuous Coverage of 185 km (100 nmi) Swath

must be more of a general nature, omitting details. The Thematic Mapper optics include a scan mechanism which causes the line of sight of the instrument to scan across track; with the TRW/P-E design each scan is linear and from West to East. The scanned image is relayed to a focal plane assembly where the light is split into at least six spectral bands (options may add a seventh and eighth band). Each 0.004 inch square detector in a line array has a 30 meter square footprint on the ground when projected back through the optics. The six spectral bands are specified as follows where band edge is the wavelength that results in 50% of the maximum response.

Band Number	Lower Band Edge (μm)	Upper Band Edge (μm)	Maximum Edge Slope (μm)
1	0.45 ± 0.01	0.52 ± 0.01	0.02
2	0.52 ± 0.01	0.60 ± 0.01	0.02
3	0.63 ± 0.02	0.69 ± 0.01	0.02
4	0.76 ± 0.02	0.90 ± 0.01	0.03
5	1.55 ± 0.02	1.75 ± 0.02	0.05
6	10.4 ± 0.10	12.5 ± 0.10	0.30

In each spectral band, the moving image scene is swept past a line array of detectors (with the line array parallel to the direction of flight) by the scanning action crosstrack as outlined above. As the ground footprint of each detector moves 30 m across track, the detector output is sampled, converted to an 8 bit digital word, and ultimately multiplexed into a single 120 megabit/second data stream which is relayed to the wideband communications module.

As indicated in Figure 2-8, each scan sweeps out a swath 960 meters (along track) by 185 kilometers (cross track) and the scan rate is chosen so the swaths just touch, providing continuous coverage along the spacecraft ground track.

The major difference between the TRW and HAC TM designs is the scan mechanism. The HAC design uses a reciprocating scan mirror while the TRW design uses a uni-directional scan wheel, referred to as the roof mirror scanning wheel, since it has roof mirrors spaced around its circumference. The roof mirror scanning wheel converts the fixed image from the telescope into an image which moves across the detectors. The concept is illustrated in Figure 2-9.

The scan mechanism of the TM is of some importance for the ACS studies because of potential attitude disturbances resulting from the moving parts. During normal on-orbit operations the TRW scan wheel rotates at a constant

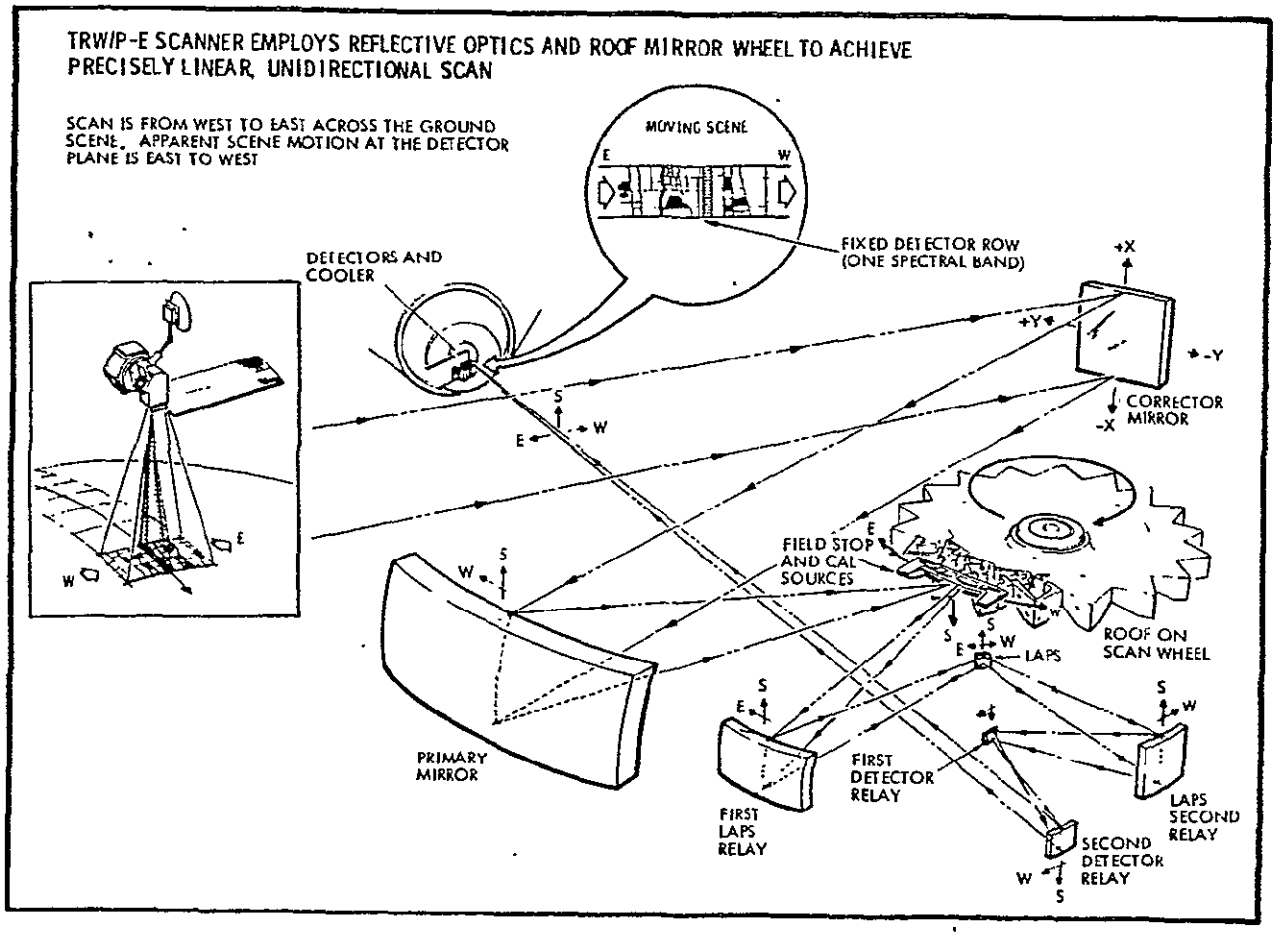

Figure 2-9. Schematic of the Scanning Telescope Optical Path

speed of 23.45 RPM and has a moment of inertia of 224 ounce-inch-seconds^2 (1.58 kg-m^2). No attitude disturbance occurs in steady state operation. The angular position of the HAC reciprocating mirror follows a triangular wave shape with rounded corners at a frequency of 7.14 Hz and $\pm$ 74 mradian (4.24 degrees) amplitude. The moment of inertia of the mirror about its pivot is 0.02614 kg-m^2.

The TM is nominally in a data taking mode only during those portions of the orbit when the L-D is flying over land masses which are in daylight. Data obtained over water (oceans) or a dark earth are of little practical value and consequently this type of data will be acquired only occasionally for experiment's sake. The fact that nominally no TM data need be transmitted to TDRS over water or over a dark earth is an important ground rule

in this study. It is key to the proposed solar array control strategy and the proposed TDRS antenna gimbal configuration and mast length. The proposed configuration does allow, however, for data being taken at night and over water, but not under any arbitrary circumstances. This will be discussed in more detail in Section 3.0.

To give a feel for the size of the TM instrument the following mass property and power data of the TRW design are provided.

Thematic Mapper Physical Parameters (TRW Design)

- Outline Dimensions: 1.12 x 1.94 x 0.96 meters (3.7 x 6.4 x 3.1 ft)
- Overall Weight: 223 kg (490 lb)
- Power Consumption: 228 watts (operating mode) 152 watts (night only)

2.3.2 Multi-Spectral Scanner

The secondary payload for L-D is the Multi-Spectral Scanner (MSS) as it will be flown on LANDSAT-C. The MSS is currently flying on LANDSAT's A and B, but the LANDSAT-C version will contain an additional (fifth) channel.

The MSS is an object plane scanner that was developed by Hughes Aircraft Company to provide radiometric measurements and imagery of the ground scene in the following spectral bands:

(1) 0.5 to 0.6 microns

(2) 0.6 to 0.7 microns

(3) 0.7 to 0.8 microns

(4) 0.8 to 1.1 microns

(5) 10.4 to 12.6 microns (LANDSAT's C and D only)

The uni-directional cross track scanning is provided by a high duty cycle (65%) rocking mirror at a frequency of 18.5 Hz over ± 74 mradians (4.24 degrees). The total weight of the MSS is 125 pounds (56.7 kg) and the power consumption is about 60 watts. The MSS data rate is 15 megabits/second.

2.4 LANDSAT-D Pointing Performance Requirements

Preliminary spacecraft pointing requirements are specified as follows:

- Pointing Accuracy

  Roll and Pitch: 0.01 deg (1σ)
  Yaw: 0.05 deg (1σ)

- Pointing Stability

  Average Rate/Axis: $< 10^{-6}$ deg/sec (1σ)
  Stability over 20 Minutes:
  Roll and Pitch: ± 10.5 μrad (1σ)
  Yaw: ± 80 μrad (1σ)

These requirements are referenced to the spacecraft coordinate reference axes which coincide with the optical cube on the star tracker. This means that the spacecraft to TM misalignments are not included in these performance specifications.

The ultimate temporal registration accuracy desired (essentially repeatability of the ground track after 16 days) for the TM is 3 meters (0.1 of a pixel) which corresponds to an attitude stability of about 4.2 μrad over 16 days if no ephemeris error were incurred. Work on the autonomous on-board Thematic Mapper boresight registration is still being pursued and the study results will be presented in the final report. It is clear, however, that registration within 3 meters is a very stringent performance goal for LANDSAT-D.

3.0 PAYLOAD DATA RELAY SYSTEM

This section addresses various system aspects of the TM data relay system. In particular, system configuration, control, and operational aspects of the mast-deployed, gimballed Ku-band antenna, relaying TM data to TDRS, will be discussed. The antenna will often simply be referred to as the TDRS antenna (of L-D) to distinguish it from the undeployed and ungimballed direct access antenna which must also operate at Ku-band. This section will also discuss the interference of the solar array with the TDRS antenna beam and propose a solution to the problem. A digital computer program that computes on-orbit antenna motion profiles, determines percent solar array interference incurred, and determines whether the spacecraft is over land or sea, over a lighted earth or a dark earth, is also presented.

In order to decide whether the LANDSAT-D TDRS antenna can be pointed open loop by programmed command, or whether closed loop RF tracking, i.e., autotracking, is required, an antenna pointing error analysis was conducted first. This is the subject of the following section.

3.1 TDRS Antenna Pointing Error Analysis

Due to the constraint of limited TWT power, a large size L-D antenna dish (6 feet) is required in order to achieve sufficient EIRP for the return link to the TDRS. This results in a narrow beamwidth of about 0.7 degrees and necessitates very accurate antenna pointing in the order of 0.1 degree (3σ).

This section discusses the antenna pointing accuracies available from two basic antenna tracking techniques: program pointing by ground or onboard stored commands (open loop) and autotrack (closed loop). Detail sources of pointing error are identified for both systems and the associated errors are computed or estimated from accumulated data on current programs and tracking systems hardware.

The results show that the proposed open loop pointing error (Rayleigh circular error probability) is 0.61 (3σ), which corresponds to an antenna gain loss (from peak gain) of 8.2 dB for receive, and 9.9 dB for transmit, and that the proposed closed loop pointing error (Rayleigh CEP) is 0.052 degree (3σ), which corresponds to approximately 0.1 dB antenna gain loss for both receive and transmit.

The major error source for the open loop system comes from thermal distortion of the assumed 20 foot "Astro Mast" type of antenna boom. Since the closed loop system can track out the pointing error caused by antenna boom distortion, as well as many of the other open loop pointing errors identified in the open loop system budget, a considerable reduction in pointing error is realized with the recommended autotrack antenna system.

3.1.1 Program Pointing Performance

Six general sources of error were found to contribute to the inaccuracies involved in open loop pointing the L-D Ku-band antenna at the TDRS. These error sources, their breakdowns, and the error magnitudes are summarized in Table 3-1.

Spacecraft Position

The errors in the target direction arise from uncertainties in the position of the TDRS and the L-D. The maximum error in the TDRS position is 61 m, assuming there is no correction immediately following each TDRS momentum dump (Reference 3). The TDRS orbit radius is 4.224×10^4 km and the L-D orbit radius is 7.083×10^3 km, so the minimum distance between them is about 3.5×10^4 km. At this distance, a 61 m error is equivalent to a 10^{-4} degree line-of-sight error. An L-D position uncertainty of 100 m (Reference 1) contributes 1.64×10^{-4} degrees error. These two effects are negligible compared to the other errors shown in Table 3-1.

Spacecraft Attitude

The spacecraft alignment error is dominated by the 0.01 degree pointing accuracy of the spacecraft and the relative error at the canister mounting surface due to thermal and other distortions of the spacecraft itself.

Table 3-1. Antenna Open Loop Pointing Error Summary

Error Source				3σ Error (degree)	
1. Spacecraft position					1.92×10^{-4}
TDRSS ephemeris, 61 m				1.0×10^{-4}	
LF/O ephemeris, 100 m				1.64×10^{-4}	
2. Spacecraft attitude					0.014
Attitude control of ACS module (gyros, star tracker and RW control errors)				0.010	
Spacecraft structural/thermal alignment (ACS to canister mount)				0.010	
3. Pointing computation and command					0.023
Computer roundoff and quantization (16 bits)				0.005	
Gimbal angle encoder (14 bits)				0.022	
4. Servo and gimballed platform errors					0.023
Servo step size (0.03 degree)				0.015	
Gimbal axes alignment (orthogonality and bearing runout)				0.017	
5. Antenna mast errors (20' Astro-mast)					0.520
Canister mounting and alignment (thermal)				0.017	
Mast deployment/repeatability					
Bending	0.1°	(3σ)	CEP	0.129	
Torsional	0.12°	(3σ)			
Thermal distortion					
Bending	0.05°	(3σ)	CEP	0.503	
Torsional	0.5°	(3σ)			
6. Antenna errors (boresight relative to mounting platform)					0.093
Antenna attachment misalignment				0.057	
Mechanical (thermal) boresight alignment				0.028	
Electrical boresight alignment				0.057	
Precomparator amplitude imbalance				0.036	
Precomparator-postcomparator phase imbalance				0.016	
Total rss error (3σ)					0.529

Pointing Computation and Command

The computation and command error is dominated by the gimbal angle encoder error. The on-board data handling system uses 16 bits in double precision, but the payload drive encoder may well have fewer bits. The computational error, e_N, is found by letting the N bits cover a complete 360 degree range

$$e_N = \frac{360 \text{ deg}}{2^N}$$

The computer roundoff and quantization error is found by letting N = 16 or $e_{16} = 5.49 \times 10^{-3}$ degrees. The gimbal encoder error is $e_{14} = 0.022$ degree. The resultant error is 0.023 degree.

The gimbal, servo, and platform error capabilities were taken from Reference 4 where it was determined that the combined gimbal and steady-state servo error is 1 arc-minute (0.017 degree) and the error due to gimbal step size of 0.03 degree is 0.015 degree. The total error for this category is 0.023 degree.

Antenna Mast Errors

The main source of pointing errors is the Astro-mast. Basically, these errors relate the total error from the canister mounting surface to the gimbal mounts. The baseline mast is assumed to be 20 feet long* and 9 inches in diameter when deployed. The mounting and alignment error in the table (0.017 degree) is the mast mounting error. The other errors are based on information obtained from Mr. Peter Preiswerk of Astro Research.

*It will be shown in subsequent sections that this was a conservative assumption, i.e., the actual mast length is expected to be about 10 feet or less. The conclusions arrived at, namely that autotracking is required, is still believed to be valid, however.

The 3σ numbers provided by Mr. Preiswerk assumed a standard 9-inch diameter, 20-foot long Astro-mast that is canister deployed. These numbers are given in Table 3-1 under item 5. The bending and torsional errors are combined and represented by a Rayleigh circular error. The maximum antenna pointing error due to the Astro-mast is 0.520 degree.

Antenna Errors

The antenna errors category includes all alignment errors from the antenna platform to the beam center. The 0.093 degree error assumes a graphite reflector and the error is compatible with that of a similar 5-foot dish currently being used on another TRW project.

The resultant RSS errors for open loop pointing is 0.529 degrees/axis or a Rayleigh circular error of 0.61 degree (3σ). Since an open loop pointing accuracy of about 0.1 degree (3σ) is required for satisfactory communication with TDRS, it must be concluded that an autotrack system is required.

3.1.2 Autotrack Performance

A description of the recommended antenna autotrack system and acquisition procedure is presented in a companion report on the L-D mission unique communication system, Reference 5. Autotrack performance is given there in terms of the RSS of tracking errors due to thermal noise, precomparator amplitude imbalance, precomparator and post-comparator phase imbalances, and drive step size. The autotrack errors are summarized in Table 3-2.

The single-channel amplitude comparison autotrack system shown functionally in Figure 3-1 has been recommended over other tracking techniques such as interferometer, self (beam)-steering, mechanical scan, conical scan, etc., because of its low risk, low cost, minimum hardware complexity, and its good performance in tracking the Ku-band, spread spectrum RF signal

In summary, the recommended autotrack design provides excellent tracking performance. Practical limits of precomparator amplitude imbalance and precomparator and post-comparator phase imbalances do not cause

Table 3-2. Autotrack Errors (3σ)

Error Source	Error (deg)	Notes
Precomparator amplitude imbalance	0.036	
Precomparator/post-comparator phase imbalances	0.018	
Drive step size	0.015	0.03° step size
Servo loop dynamics	0.015	Estimated
RSS	0.0455	
Thermal noise	0.0004	$(S/N)_{IF}$ = 11 dB
RSS total	0.0455	Per axis
Circular error	0.052	
Antenna pointing loss		
Receive	0.06 dB	3 dB beamwidth = 0.80°
Transmit	0.07 dB	3 dB beamwidth = 0.73°

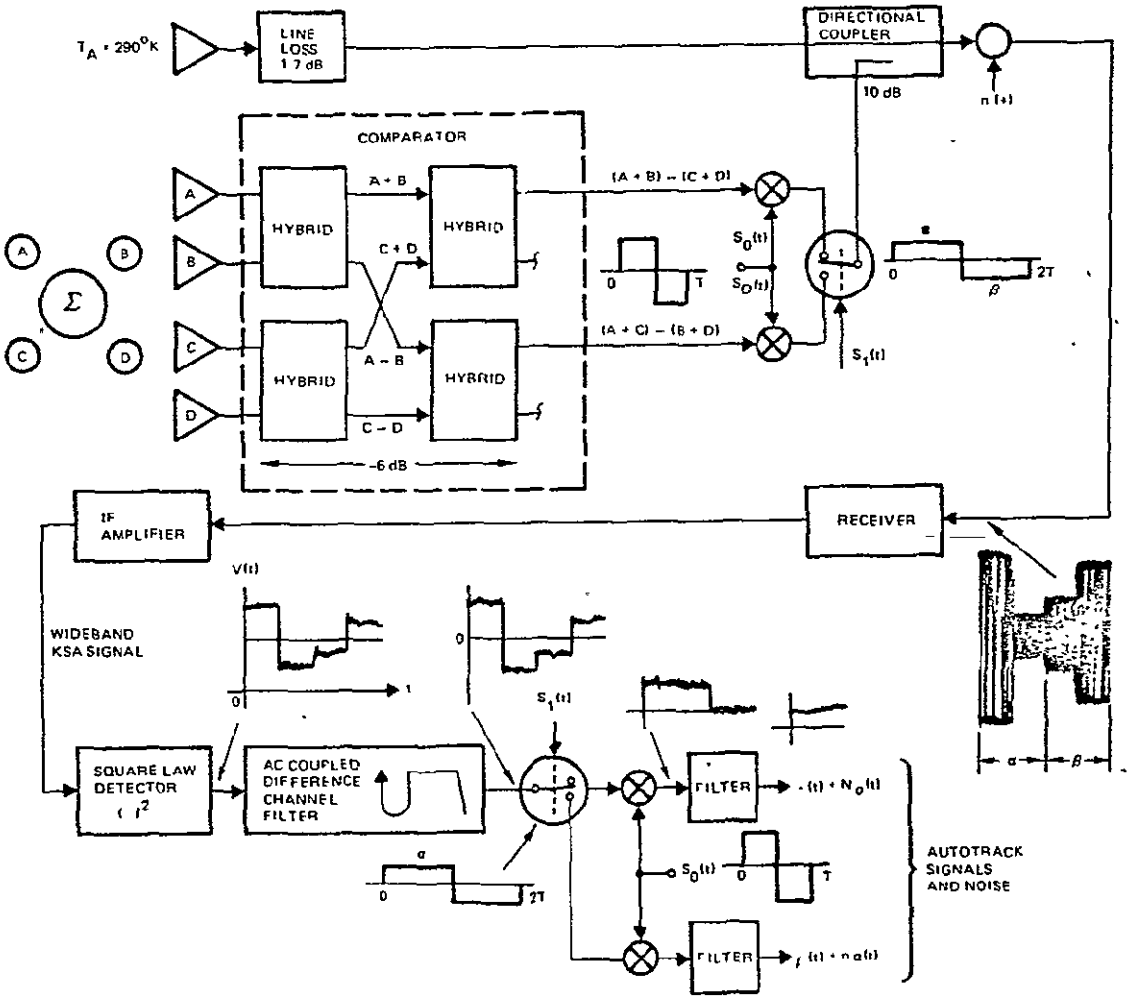

Figure 3-1. Antenna Autotrack Functional Block Diagram

appreciable contributions to the autotrack error. The errors associated with motor step size and servo loop dynamics are also minimal. The tracking error due to thermal noise is negligible at acquisition and autotrack receive signal levels.

3.2 Antenna Gimbal Configuration

Figure 3-2 shows a sketch of L-D in its normal on-orbit orientation. The figure mainly serves to define the body-fixed reference coordinate set, $\{\hat{x}_b, \hat{y}_b, \hat{z}_b\}$, and the earth half cone angle θ_E which equals 64.2 degrees at a spacecraft altitude of 705 km. It follows from the geometry indicated that the gimballed Ku-band antenna must be able to track TDRS in a cone of approximately $\pm$ 120 degrees (exactly: 90° + 25.8° = 115.8 degrees) centered about the $-\hat{z}_b$ axis, and that the maximum antenna dip angle below the spacecraft's local horizontal plane is 25.8 degrees.

The Ku-band antenna target, namely TDRS, follows a cone about the spacecraft's $\hat{y}_b$ axis which is constantly changing in size. This means that a two-gimbal arrangement should have the outer gimbal axis in or near the $\hat{x}_b$-$\hat{z}_b$ plane so that frequent gimbal resetting is not necessary. The problem with a two-axis (2-degree-of-freedom) gimbal lock problem exists and its effects must be carefully considered in the choice of the gimbal configuration and the degress of freedom. Four different gimbal configurations were considered. They are:

(1) x over y* two-axis gimbal.

(2) y over x two-axis gimbal.

(3) Azimuth-elevation two-axis gimbal.

(4) Three-axis gimbal using azimuth-elevation plus a third axis, cross elevation gimbal.

---

*The notation means x rotation <u>after</u> y, i.e., the outer gimbal axis is aligned with the S/C $\hat{y}_b$ axis and the inner gimbal axis (at outer gimbal null) with the S/C $\hat{x}_b$ axis.

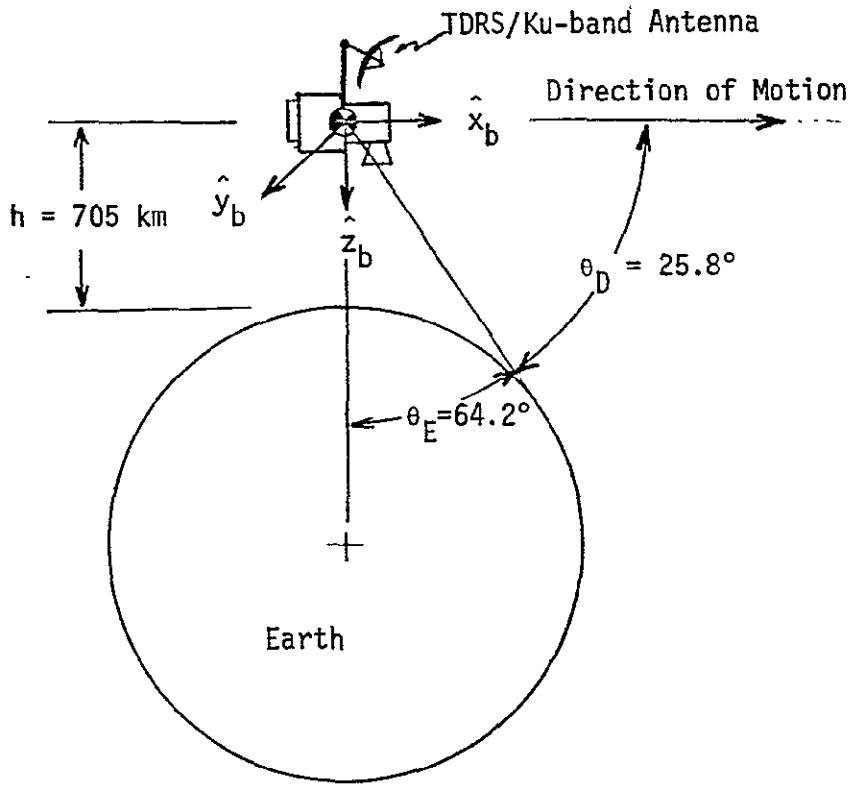

Figure 3-2. LANDSAT-D Normal On-Orbit Attitude and Geometry (not to scale)

The x and y two-axis gimbal would need ± 180 degrees freedom about the y-axis and 0 degrees to 120 degrees in x. Since the line-of-sight to TDRS tends to come around the spacecraft's $\hat{y}_b$ axis, this gimbal configuration would operate often close to gimbal lock and high rates about the y gimbal axis would be required. For the same reason, it would also require frequent resetting of the outer gimbal because of the effective ± 180 degree stops necessitated by the coax cables which are run across the gimbals and do not permit a wind-up motion about $\hat{y}_b$. Since the gimbal lock tends to interfere with the L-D operational scenario, the x over y gimbal arrangement is discarded as a configuration candidate.

The y over x gimbal would need 0 - 120 degree freedom in both gimbal axes. Gimbal lock can occur twice per orbit. Gimbal lock would occur when the TDRS is either straight ahead along the spacecraft velocity vector ($+\hat{x}_b$) or when the TDRS is exactly behind the spacecraft ($-\hat{x}_b$ direction).

These situations would occur when TDRS is crossing the L-D orbit plane at the time L-D descends from the North Pole toward the equator, and again a little later when L-D is half way on its way to the South Pole. The y over x gimbal is a feasible configuration but not particularly attractive since the gimbal lock conditions interfere with normal L-D operations.

The azimuth-elevation gimbal (with azimuth being rotation about the $\hat{z}_b$ axis = mast axis) has one well defined gimbal lock condition per TDRS: whenever TDRS is in the spacecraft zenith, i.e., whenever TDRS is in the L-D orbit plane directly above the spacecraft ($-\hat{z}_b$ direction). Fast antenna rotation near gimbal-lock occurs then mainly about yaw ($\hat{z}_b$ axis) and is expected to cause minimal interaction with the spacecraft which could adversely affect payload pointing. The mechanical design of an azimuth-elevation gimbal is relatively uncomplicated and, moreover, a third gimbal, should it ever be required, can be added quite easily by putting a cross elevation hinge into the antenna mast. The azimuth gimbal about $\hat{z}_b$ should ideally have a freedom of 360 degrees without mechanical stops, but because of a cable transfer across the gimbal hinge, a cable wrap providing $\pm$ 200 degrees of freedom with attendant overlapping $\pm$ 200 degrees mechanical stops, will be required. The elevation gimbal freedom must be at least from -26 degrees to +90 degrees. The azimuth-elevation gimbal configuration looks attractive and will be further considered.

A three-axis gimbal avoids gimbal-lock conditions but the gimbal configuration is mechanically more complex, bulkier, heavier, and costlier. At certain times two gimbal axes may be parallel and control laws and gimbal servo cross-talk problems become more complex. It has been decided to avoid a three-axis gimbal system if satisfactory operation can be achieved with a two-axis gimbal.

3.2.1 Gimbal Lock Problem

The potential gimbal-lock problem for the two-axis gimbal configurations in general, and for the azimuth-elevation configuration in particular, can be solved in one of two ways. Referring to the gimbal-lock point as the keyhole, one can

(1) Show that the target (TDRS) is never in the keyhold.

(2) Place the keyhole so that the data which is lost, by the antenna not tracking TDRS, is not required.

Option 1 can be viewed as: show that whenever one TDRS is in the keyhole, it is acceptable to use the other one as the target. This is best considered in terms of the target location. For an azimuth-elevation arrangement, gimbal-lock occurs when the target is in the L-D orbit plane. At that time the other TDRS is 130 degrees out of the orbit plane where it is hidden by the earth; thus there is no increase in coverage available by switching targets -- in fact, since the other target would have to be tracked for the whole L-D orbit, there would be a larger reduction in coverage by switching targets. This exercise can be repeated for other two-axis gimbal configurations, but the result is the same. Since the outer gimbal axis must be near the $\hat{x}_b$-$\hat{z}_b$ plane, gimbal-lock will occur when a TDRS is near the L-D orbit plane. At that time, the other TDRS is 50 degrees out of the L-D orbit plane and cannot be tracked throughout the L-D orbit.

Option 2 is a feasible solution. Using the azimuth-elevation arrangement, gimbal-lock will occur when the L-D is directly beneath the TDRS, and so loss of the TDRS link will occur at 41 degrees and 171 degrees west longitude, i.e., beneath the station locations of the two TDRS's. These points are over the ocean where coverage is not essential. The loss of the TDRS link at 41 degrees west occurs close to the coast of Brazil, and at 171 degrees west there may be some Pacific islands of interest. Thus it is of some importance to precisely establish the size of the loss of coverage zone on the ground and to investigate if this zone could be shifted if required.

The loss of coverage zone can be shifted by tilting the outer gimbal axis, which for the azimuth-elevation gimbal would mean to tilt the mast. This is demonstrated in Figure 3-3, where tilting the gimbal axis by the angle α, moves the loss of coverage zone by an amount γ. The relationship between these angles is found from:

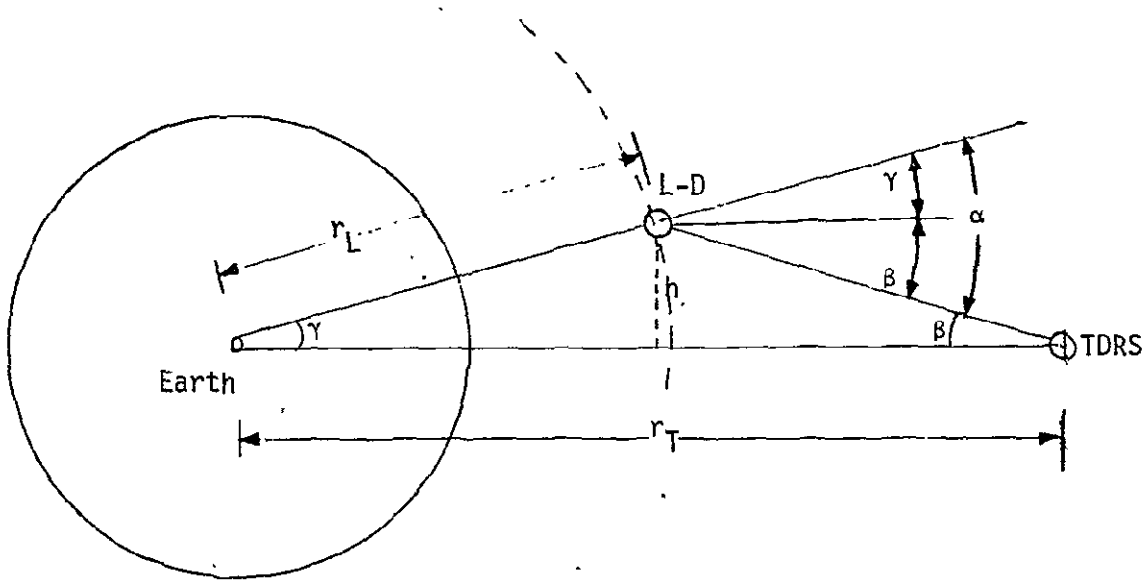

Figure 3-3. Moving the Loss of Coverage Zone by Tilting the Outer Gimbal Axis

$$\alpha = \beta + \gamma \tag{3.2-1}$$

and

$$h = r_L \sin \gamma = (r_T - r_L \cos \gamma) \tan \beta \tag{3.2-2}$$

thus

$$\alpha = \gamma + \tan^{-1} \left\{ \frac{r_L \sin \gamma}{r_T - r_L \cos \gamma} \right\} \approx \frac{r_T}{r_T - r_L} \gamma \tag{3.2-3}$$

where the approximation is for small angles. Using the values r_L = 7074 km and $r_T = 4.224 \times 10^4$ km, a $\approx 1.2\ \gamma$. For example, if the gimbal axis is tilted 6 degrees, the coverage hole moves about 5 degrees.

The size of the loss of coverage zone can be estimated by assuming that normal operation of the antenna gimbal can be maintained until one

gets within ± 2 degrees of gimbal-lock. Using Equation (3.2-3) with $\alpha = \pm 2$ degrees, this becomes $\gamma = \pm 1.664$ degrees of the earth's sphere on the ground which equals ± 185 km. Since a swath of the TM happens to be exactly 185 km wide in the east-west direction, the loss of coverage zone in the worst situation is at most three swaths wide (555 km ≈ 5 degrees on earth sphere), and for the best situation at least two swaths wide (370 km ≈ 3.3 degrees). In the north-south direction, the loss of coverage zone extends always ± 185 km (± 1.664 degrees) if gimbal-lock can be approached to within 2 degrees. This is illustrated in Figure 3-4. Referring to appropriate maps showing the north-east coast of Brazil and the Pacific Ocean, respectively, it can be seen that the loss of coverage zone contains only water (the coast of Brazil is barely missed for the worst situation), with the exception of perhaps some of the Gilbert Islands in the Pacific. Thus, the antenna mast need not necessarily be tilted. If a tilt is considered, because normal tracking operation can only be maintained to within, say, 5 degrees of gimbal-lock, then the mast could be tilted by 6 degrees to 12 degrees toward $+\hat{x}_b$ so that the now larger loss of coverage zone would move 6 degrees to 12 degrees north at the descending node (daylight), where no nearby land masses exist. But this is acceptable only if the loss of coverage due to gimbal-lock is acceptable at night: if the zone is shifted one way at the descending node, it is shifted in the opposite direction at the ascending node. It would be possible to place the zone over the ocean all the time by tilting the gimbal axis 36 degrees from the $\hat{z}_b$ axis in the $\hat{x}_b$-$\hat{z}_b$ plane. This moves the zone 30 degrees north or south depending on the L-D direction at the time.

3.2.2 Baseline Gimbal Configuration

The azimuth-elevation gimbal configuration has been selected as the baseline gimbal for the L-D Ku-band (TDRS) antenna. The occurrence of gimbal-lock is well defined for this gimbal configuration and it was shown that the resultant loss of coverage zone is always situated over water.

The gimbal configuration is shown in its null position in Figure 3-5. Gimbal-lock occurs when the elevation angle $g_2 = 90$ degrees and the antenna views zenith. The coordinates $\{\hat{x}, \hat{y}, \hat{z}\}$ are identical to the body

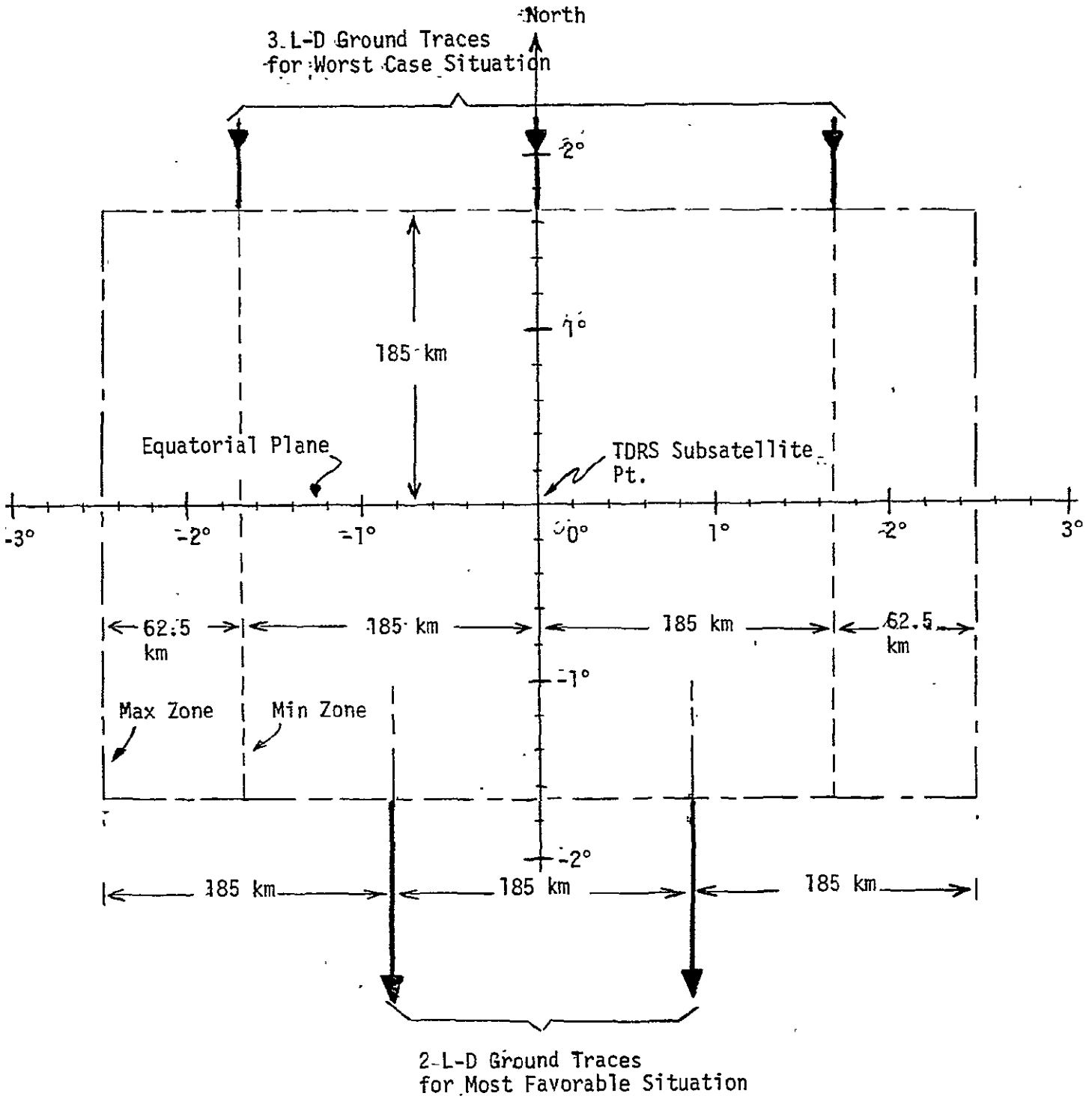

Figure 3-4. Zone of Loss of TDRS Line Due to Gimbal-Lock (Normal Operation Assumed to Within ± 2 degrees of Gimbal-Lock)

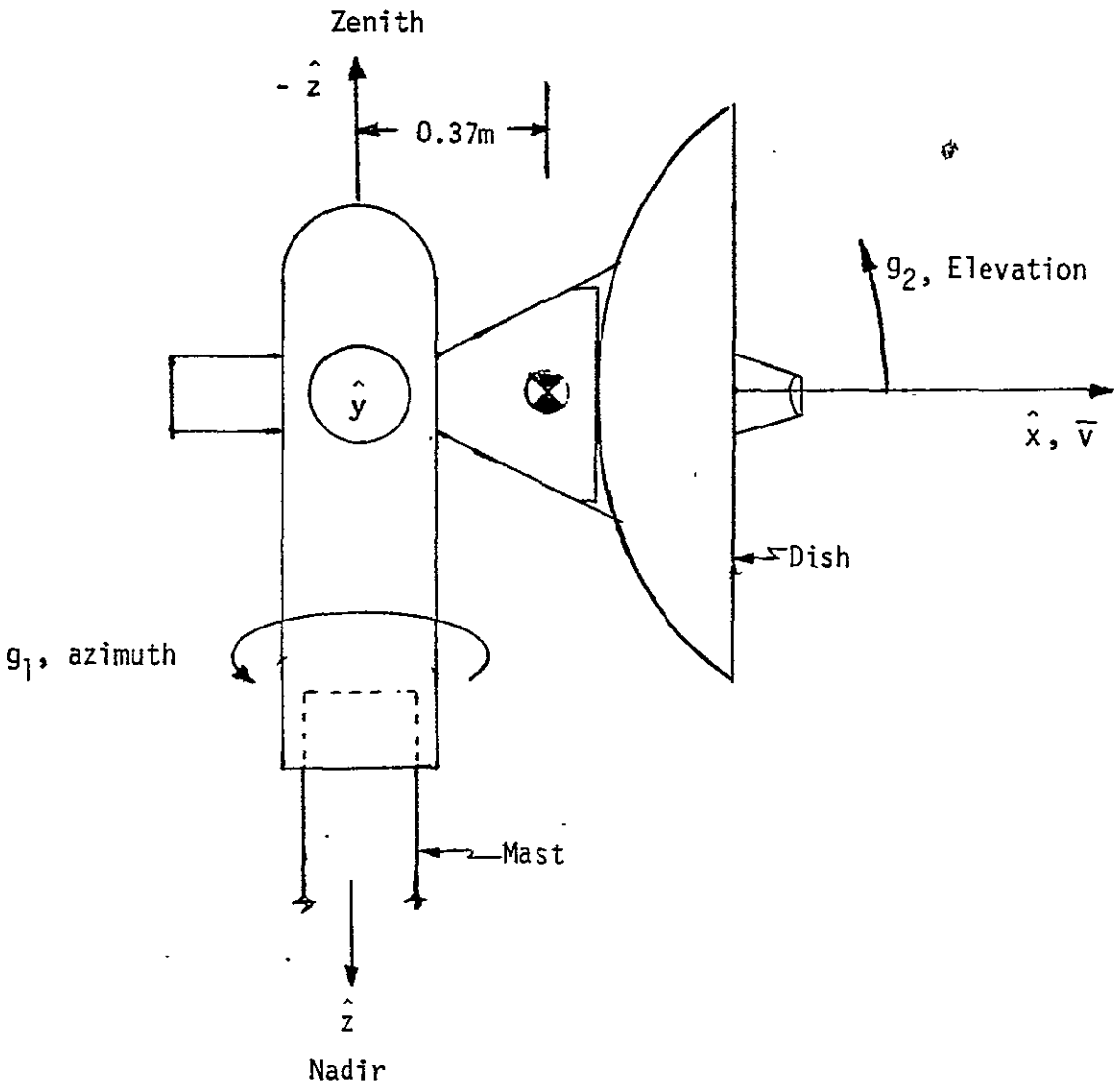

Figure 3-5. Ku-Band Antenna in the Null Position

fixed set defined in Figure 3-2, i.e., in its null position the antenna faces in the direction of travel of the satellite. This is important in view of the cable wrap limits specified as ± 200 degrees from the origin, since near gimbal-lock, the antenna must be able to rotate nearly 180 degrees in azimuth from $+\hat{x}$ to $-\hat{x}$ without crossing a cable wrap limit. A single mechanical stop in azimuth is unacceptable since the antenna must be able to fine-track a TDRS at any arbitrary azimuth angle. Thus, an overlapping cable wrap and attendant overlapping mechanical stops (to

prevent cable damage) are required. The peak gimbal rate occurs in azimuth near gimbal-lock. It can be shown that if gimbal-lock is approached to within ε degrees, then, for small ε, the peak azimuth rate is given by

$$\dot{g}_{1_{max}} = \frac{\omega_o}{\varepsilon} \qquad (3.2\text{-}4)$$

where ω_o is the orbit rate of L-D. For ε = 2 degrees, this yields

$$\dot{g}_{1_{max}} = 1.74 \text{ deg/sec}$$

The peak azimuth rate could be decreased if the elevation angle were allowed to "follow through" beyond 90 degrees, i.e., the elevation gimbal freedom were $-30° \leq g_2 \leq 210$ degrees. The software of the gimbal controller would also become more complicated, however, since gimbal steering is not unique anymore.

Table 3-3 summarizes the baseline gimbal design requirements. A servo loop controlled stepper motor has been assumed for the gimbal drive. Step size and other requirements are compatible with the antenna pointing requirements and the autotracking baseline system established in Section 3.1. The slew rate and acceleration requirements assure that:

- The azimuth can be reoriented by 180 degrees sufficiently fast (1 minute) to resume tracking TDRS when it emerges again from the gimbal-lock zone, assumed at $\pm$ 2 degrees about the keyhole. (That is, the time to reorient the azimuth gimbal is limited by the time it takes L-D to cross the gimbal-lock zone.)

- The antenna can be slewed from one TDRS to the other in less than 2 minutes.

- The system has sufficient acceleration capability for a spiral search pattern to find and lockup on TDRS, in case the open loop pointing command did not bring the target within the acquisition field of view of the autotrack system.

Table 3-3. Baseline Gimbal Configuration Design Requirements

Angular Freedom:	
Azimuth	$\pm$ 200° (overlapping stops)
Elevation	-26° to +90° (minimum) -30° to +210° (desirable)
Maximum Tracking Rate:	2.0 deg/sec
Maximum Slew Rate:	4.0 deg/sec
Maximum Acceleration:	1.5 deg/sec^2
Output Step Size:	< 0.03 deg
Readout Accuracy:	Better than 0.2 deg
Open Loop Pointing:	Better than 0.25 deg

3.3 Antenna Control System Functional Design

This section presents a preliminary design for a control system to point the L-D Ku-Band antenna at a TDRS. There are two major control modes. Mode 1 is an open loop pointing mode in which the on-board computer generates gimbal angle commands based on the computed location of the target. In this mode the gimbal angle readouts provide the feedback. Mode 1 is used to:

(a) Slew from one TDRS to the other.

(b) Reset the azimuth gimbal angle when one of the ± 200 degrees cable wrap stops are close to interferring with nominal operation.

(c) Move the antenna through the zone of TDRS link loss due to gimbal-lock.

(d) Follow TDRS through the zone of exclusion over the Indian Ocean where both TDRS's are hidden by the earth so that autotrack may resume as soon as a TDRS comes again into the field of view.

Operations (a) through (c) will nominally all be accomplished when the spacecraft is near the polar regions so that no data loss (i.e., no effective communication loss) is incurred. The loss of coverage over the Indian Ocean, item (d) above, is not under the control of the L-D mission; it is a characteristic of the TDRSS as currently configured.

If the open loop antenna pointing accuracy is worse than 0.657 degrees, it may not be possible to establish the RF link for locking on to the TDRS. In this case the computer generates a spiral search pattern to bring the TDRS within the field of view of the autotrack system. The search pattern is generated in Mode 1a.

Mode 2 is a closed loop tracking mode which does not use the on-board computer. The pointing error is sensed by the autotrack system, and the controller removes the measured error directly.

3.3.1 Acquisition Procedure

Acquisition procedures between the L-D and the TDRS are outlined in Table 3-4. The data was taken from the TDRSS "User Spacecraft Acquisition Procedures," P-805-1, June 1976, GSFC. For L-D acquisition independent of the S-band TT&C link (except for initial antenna pointing programming and

Table 3-4. TDRSS User Spacecraft Acquisition Procedures

3.1 KSA ACQUSITION SEQUENCE NO. 1

3.1.1 An SSA return link is established with the user spacecraft using the normal SSA acquisition procedure.

3.1.2 The user spacecraft radiates a minimum S-band EIRP of +13 dBw.

3.1.3 TDRSS uses the S-band return link signal to aid antenna pointing. TDRSS radiates, within 5 seconds of user S-band turn-on and in the direction of the user spacecraft, a Ku-band +40 dBw (minimum) signal EIRP compatible with the forward link signal parameters defined in either Table 2-1 or Section 8.2.1.1 of S-805-1. The Ku-band carrier and PN clock shall include doppler compensation as scheduled.

3.1.4 The user spacecraft acquires the TDRSS Ku-band signal, begins autotracking, and begins radiating a +30 dBw (minimum) signal EIRP at Ku-band in the direction of TDRSS.

3.1.5 TDRSS then:

a. Autotracks the user Ku-band signal within 5 seconds of user turn-on (P_{acq} = 0.99 for user EIRP = +30 dBw).

b. Begins radiating normal power mode signal EIRP or high power mode signal EIRP as scheduled.

c. Either establishes return link DG 1 service and/or DG 2 service, or Shuttle Ku-band service within 5 seconds.

3.2 KSA ACQUISITION SEQUENCE NO. 2

3.2.1 An SSA forward link is established with the user spacecraft using the normal SSA acquisition procedure.

3.2.2 The user spacecraft is commanded to point its Ku-band antenna at TDRSS and to transmit in the direction of TDRSS a minimum of +30 dBw EIRP at Ku-band compatible with the return link signal parameters defined in either Table 2-2 or Section 8.2.1.2 of S-805-1.

3.2.3 TDRSS searches for the Ku-band signal and begins autotracking within 10 seconds of user turn-on (P_{acq} = 0.99 for user EIRP = +30 dBw).

3.2.4 TDRSS radiates normal power or high power EIRP at Ku-band in the direction of the user spacecraft compatible with the forward link signal parameters defined in Table 2-1 or Section 9.2.1.1 of S-805-1. The Ku-band carrier and PN clock shall include doppler compensation as scheduled.

3.2.5 The user spacecraft acquires the TDRSS Ku-band signal and begins autotracking.

3.2.6 TDRSS either establishes return link DG 1 service and/or DG 2 service within 5 seconds.

other tracking considerations given below), KSA acquisition sequence 2 is recommended for the L-D mission. The acquisition procedure has also been discussed in Reference 5.

L-D antenna tracking is accomplished as follows. Prior to coming over the horizon, the L-D Ku-band steerable antenna is program-pointed at the TDRS within a factor of 1.8 (open loop pointing error) of the one-sided, half-power beamwidth (0.365 degree). This open loop uncertainty does not reduce the L-D EIRP below the minimum 30 dBW EIRP required for TDRS Ku-band antenna acquisition and autotrack. A margin of greater than 18 dB exists.

Upon acquiring and autotracking the L-D signal beacon, which consists of the normal composite 120 Mbps and 15 Mbps instrument signal, the TDRS begins transmitting a spread spectrum beacon signal to the L-D. The TDRS beacon signal will be within 10 dB of the L-D Ku-band high gain antenna peak. This signal level is above the threshold level which initializes autotrack.

The autotrack design provides for the inclusion of a small acquisition horn (BW $\approx$ 12 degrees) to provide a broadbeam Ku-band beacon for initial TDRS acquisition of the L-D. The acquisition horn is considered as a back-up acquisition aid in the event of temporary pointing anomolies (attitude control, boom distortion, etc.). Furthermore, a preprogram search routine in the communication and data handling module on-board computer provides a search pattern for L-D antenna acquisition and autotrack. This is also considered a backup mode.

3.3.2 System Functional Description

A functional block diagram of the controller is shown in Figure 3-6. The required electronics are shown functionally by the block diagram in Figure 3-6a; a separate compensator may be needed for Modes 1 and 2 due to the different requirements. The autotrack measures the antenna pointing errors - ε_1 and ε_2 - in antenna-fixed axes and they need be resolved

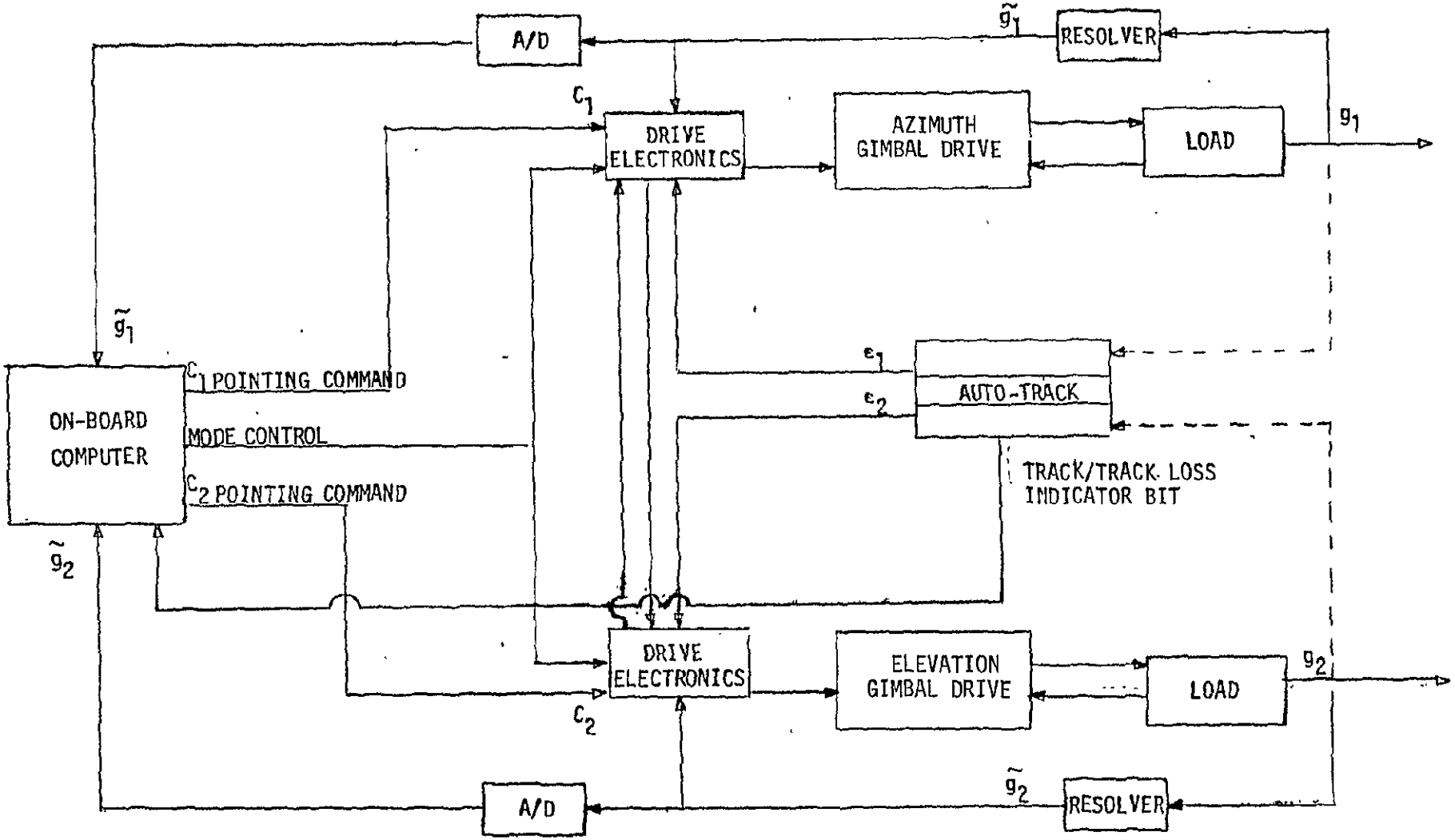

Figure 3-6. Functional Block Diagram of Antenna Control System

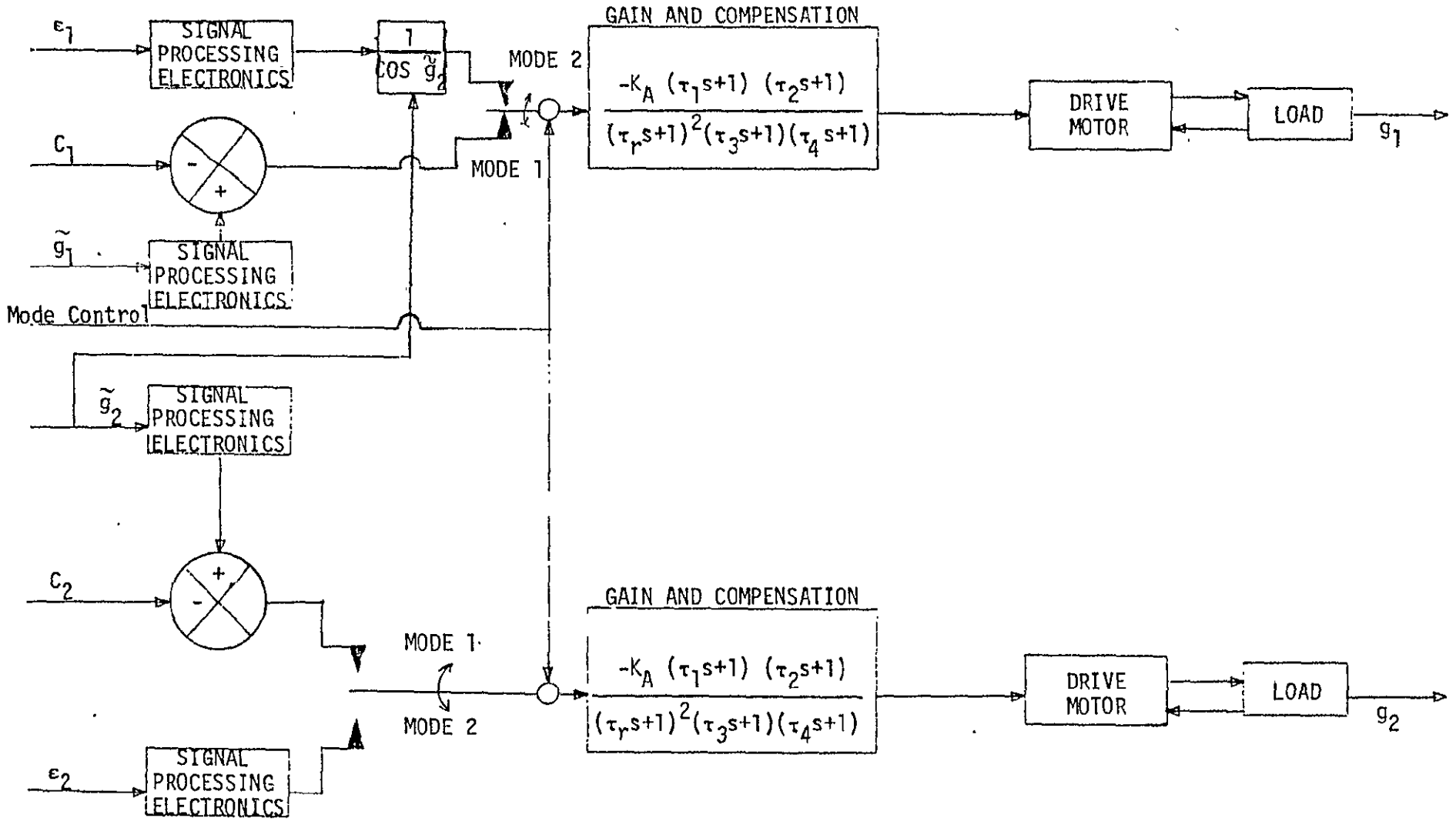

NOTE: K_A AND THE τ_i'S MAY BE DIFFERENT FOR THE TWO MODES

Figure 3-6a. Functional Block Diagram of Drive Electronics

into gimbal coordinates. One of these axes is aligned with the inner gimbal axis, so the measured pointing error is also the gimbal angle error, i.e., for the elevation gimbal,

$$\varepsilon_2 = C_2 - g_2 \tag{3.3-1}$$

where C_2 is the commanded gimbal angle and g_2 the actual (measured) gimbal angle. But, the pointing error about the outer axis (azimuth) differs from the gimbal angle error according to the target location:

$$\varepsilon_1 = \cos g_2 \, (C_1 - g_1) \tag{3.3-2}$$

This factor is removed as shown in Figure 3-6.

In Mode 1, the computer must calculate the required gimbal angles to point the antenna at the target given the TDRS location and the L-D location and attitude. The necessary equations will now be derived.

Assuming that the L-D and TDRS positions are known in the standard earth centered inertial (ECI) coordinate frame {I} ($\hat{z}_I$ axis through North Pole, $\hat{x}_I$ axis toward vernal equinox), denote the L-D and TDRS position vectors by $\{\bar{r}_L\}_I$ and $\{\bar{r}_T\}_I$, respectively. Then the vector pointing from L-D to TDRS is given in ECI coordinates by

$$\{\bar{p}\}_I = \{\bar{r}_T\}_I - \{\bar{r}_L\}_I \tag{3.3-3}$$

and in L-D body coordinates by

$$\{\bar{p}\}_b = A_{bI} \{\bar{p}\}_I \tag{3.3-4}$$

where A_{bI} is the direction cosine matrix of L-D specifying its attitude relative to ECI. Denote the normalized pointing vector to TDRS in L-D body coordinates by

$$\hat{T}_b = \{\bar{p}\}_b / ||\bar{p}|| \qquad (3.3\text{-}5)$$

Denote A_{ab} the direction cosine matrix that transforms from body fixed coordinates to antenna fixed coordinates. Then, performing two ordered rotations g_1 and g_2,

$$A_{ab} = [g_2]_y [g_1]_z$$

$$A_{ab} = \begin{bmatrix} \cos g_2 \cos g_1 & \cos g_2 \sin g_1 & -\sin g_2 \\ -\sin g_1 & \cos g_1 & 0 \\ \sin g_2 \cos g_1 & \sin g_2 \cos g_1 & \cos g_2 \end{bmatrix} \qquad (3.3\text{-}6)$$

Note that when $g_1 = g_2 = 0$, the antenna fixed axes coincide with the body fixed axes and the antenna boresight is aligned with the spacecraft $\hat{x}_b$ axis. The gimbal angles g_1 and g_2 that align the antenna boresight with the normalized pointing vector $\hat{T}_b$, must then satisfy

$$\begin{bmatrix} 1 \\ 0 \\ 0 \end{bmatrix} = A_{ab} \hat{T}_b = A_{ab} \begin{bmatrix} T_{bx} \\ T_{by} \\ T_{bz} \end{bmatrix} . \qquad (3.3\text{-}7)$$

which leads to

$$\text{azimuth:} \quad g_1 = \tan^{-1} (T_{by}/T_{bx}) \qquad (3.3\text{-}8)$$

and

$$\text{elevation:} \quad g_2 = -\sin^{-1} (T_{bz}) \qquad -30° \leq g_2 \leq 90° \qquad (3.3\text{-}9)$$

When the antenna is pointed at the computed target location, Mode 2 is initiated if the autotrack "sees" the TDRS beacon, and Mode 1a

otherwise. In Mode 1a, the computer generates the search pattern and switches to Mode 2 when the autotrack "sees" the beacon. The search pattern assumed here is a spiral:

$$a_1 = g_1 \sin g_2 = K\, t \sin \omega t \tag{3.3-10}$$

$$a_2 = g_2 = K\, t \cos \omega t \tag{3.3-11}$$

At the end of n full periods

$$a_1(n) = \frac{2\pi nK}{\omega} \sin 2\pi n = 0$$

$$a_2(n) = \frac{2\pi nK}{\omega} \cos 2\pi n = \frac{2\pi nK}{\omega}$$

Thus the distance between successive scan centers is $d = \frac{2\pi K}{\omega}$. With the 0.8 degree FOV width, sufficient overlap could be achieved with $d = 0.6$ degree, or $K/\omega = 0.0955$ degree. This scan will cover a circle of radius $r_c = 3$ degrees in $n = 5$ cycles.

The peak gimbal rate within that circle would occur at the end of the fifth cycle, where

$$\dot{a}_1(n) = [K \sin \omega t + K\, \omega t \cos \omega t]_{t = \frac{2\pi n}{\omega}} = 2\pi nK \tag{3.3-12}$$

$$\dot{a}_2(n) = [K \cos \omega t - K\, \omega t \sin \omega t]_{t = \frac{2\pi n}{\omega}} = K \tag{3.3-13}$$

are the rates at the end of the n^{th} cycle. Further, from (3.3-10)

$$\dot{g}_1 \simeq \frac{\dot{a}_1}{\sin g_2} \tag{3.3-14}$$

For acquisition with $g_2 \leq 60$ degrees, this becomes

$$\dot{a}_1 \leq 0.5\ \dot{g}_1 \leq 1 \text{ deg/sec} \qquad (3.3\text{-}15)$$

where $\dot{g}_1$ and $\dot{g}_2$ are each limited to 2 degrees/second by the design requirements. Combining (3.3-12) and (3.3-15)

$$Kn \leq 0.1592 \text{ deg}$$

Since this rate requirement is only necessary thru the fifth cycle, one chooses K = 0.03 degree/second. Since $K/\omega = 0.0955$ degree, this results in $\omega = 0.314$ rad/second, and the period is 20 seconds/cycle. The peak gimbal acceleration can be shown to be 0.6 degree/second^2 where the gimbal design requirement is 1.5 degrees/second^2. In summary, in Mode 1a the computer must compute gimbal angles according to Equations (3.3-10) and (3.3-11) with K = 0.03 degree/second, and $\omega = 0.314$ rad/second. A computer cycle time of 256 msecond would allow the gimbal commands to be updated 80 times per search cycle.

3.4 Digital Program for Antenna Motion Profile and Solar Array Interference

One of the requirements of the LANDSAT-D study was to develop a digital computer program for studying solar array interference with the Ku-band antenna. Program LFO (Landsat Follow-On) satisfies this requirement and is additionally a more general program that can be used to study various other spacecraft/orbital phenomena. In particular, the main outputs of the program are:

- Antenna gimbal angle motion profiles
- Percent transmission to TDRS (interference problem)
- Spacecraft eclipsed or not eclipsed
- Longitude and latitude of the subsatellite point
- Subsatellite point over land or water
- Subsatellite point over lighted earth or dark earth

The objective of this section is to discuss the underlying theory on which the program is based, provide a brief description of the program organization and its use, and to present and discuss some of the results obtained. Program flow diagrams are given in Appendix A and a program listing (FORTRAN IV) is given in Appendix B.

3.4.1 Program Description

This program is primarily used for computations involving a spacecraft in an arbitrary circular orbit -- specifically the LANDSAT-D (L-D) -- and another spacecraft which is in an earth-synchronous orbit -- specifically the TDRS. The geometrical relationships are shown in Figure 3-7; this figure also defines several of the variables and parameters used in the program. The earth centered, sun referenced, coordinate system, s, has the z_s axis pointing north along the polar axis and the sun lying in the $y_s = 0$ plane generally in the $+x_s$ direction; the x_s axis and y_s axis lie in the equatorial plane. The TDRS's are located by the angles γ_1 and γ_2 measured relative to the x_s axis -- nominally TDRS1 is at 41°W longitude and TDRS2 is at 171°W longitude. The L-D orbit is defined by its inclination angle γ_I and the location of its descending node γ_D. In this orbit plane, the spacecraft is located by orbit angle γ_L measured from the point 90 degrees ahead of the equatorial plane. The orbit coordinate system is located at the spacecraft c.m. with the z_o axis pointing at the earth center and the x_o axis in the direction of spacecraft orbital motion. In the program the body coordinate system is assumed to be identical with the orbital frame O -- no pointing errors. The angle between the sun vector and the equatorial plane is γ_s; this varies over the range [-23.5 degrees, 23.5 degrees] depending on the time of year.

The mainline program contains minimal computation. Instead, it primarily ties together the various subroutines; this allows the user to easily supply special purpose subroutines to meet the needs of a particular situation. The flow charts of the total program are given in Appendix A. The subroutines DOT, CROSS, BASIS, CITOO, COTOA, UNIT and ROT are minor computational subroutines used for various vector manipulations and coordinate system transformations; their specific functions are shown in Table 3-5.

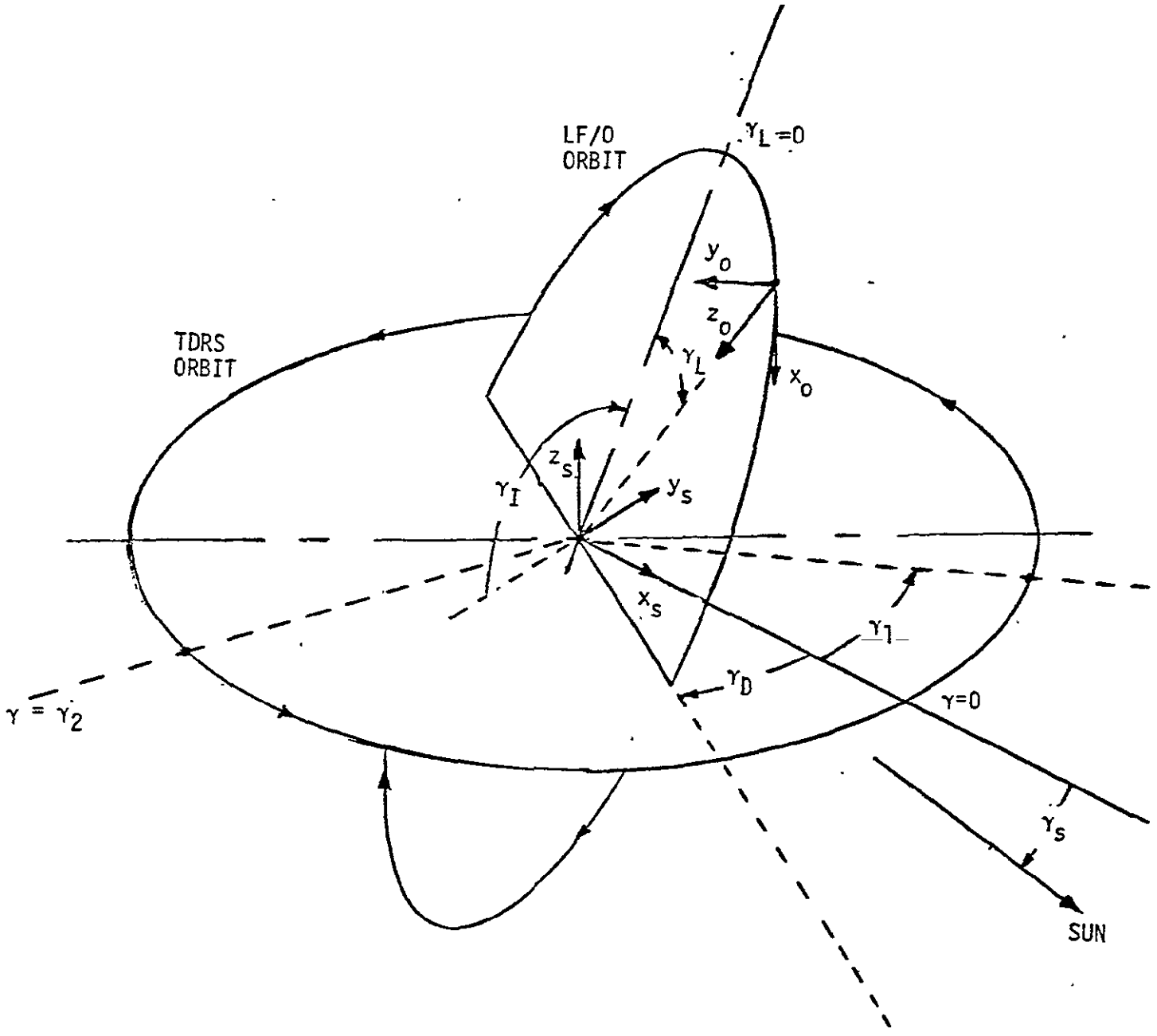

Figure 3-7. Geometrical Relationships

Table 3-5. Minor Subroutines in LFO

Subroutine Name	Inputs	Outputs	Description
DOT	$\overline{X}$, $\overline{Y}$	A	$A = \overline{X} \cdot \overline{Y}$
CROSS	$\overline{A}$, $\overline{B}$	$\overline{C}$	$\overline{C} = \overline{A} \times \overline{B}$
BASIS	$\overline{A}$	$\hat{B}$, $\hat{C}$	The unit vectors $\hat{B}$ and $\hat{C}$ form an orthonormal basis with $\hat{A}$
UNIT	$\overline{X}$	$\hat{Y}$	$\hat{Y} = \overline{X}/\lvert\overline{X}\rvert$
ROT	$\overline{XI}$, A, N	$\overline{XO}$	$\overline{XO} = [A]_N \overline{XI}$, N is nth axis
CITOO	$\overline{X}$, γ_L	$\hat{Y}$	Transforms vector $\overline{X}$ in s coord. system to unit vector $\hat{Y}$ in O coord. system.
COTOA	$\overline{A}$, ρ	$\overline{B}$	Transforms vector $\overline{A}$ in O coord. system to $\overline{B}$ in array centered coord. system (see Section 5).

The subroutines INPUT and OUTPUT do just what their names imply; they are separate subroutines in order to keep the mainline program simple and straightforward. The remaining subroutines are the main computational elements of the program; their functions are described briefly in Table 3-6. More complete descriptions of ARRAY and GIMBAL are given in Section 3.4.3.

Table 3-6. The Main Computational Subroutines in LFO

Subroutine Name	Inputs	Outputs	Description
UPDATE	t, γ_1, γ_2, γ_L	t, γ_1, γ_2, γ_L	Increments variables between computation times
ARRAY	$\hat{T}$, $\hat{S}$	R	With antenna target at $\hat{T}$ and sun at $\hat{S}$, R = Per cent of antenna pattern not blocked by array
ECLIPSE	$\hat{S}$, R_E	ISUN, IDAY	ISUN = { 1, L-D in sun; 0, L-D eclipsed } IDAY = { 1, subsatellite point lighted; 0, subsatellite point dark }
LAT	γ_1, γ_L, γ_I, γ_D, ALAT 1	ALAT, ALONG	Computes geographical latitude and longitude of subsatellite point.
GIMBAL	$\hat{T}$	G_1, G_2	Given antenna target at $\hat{T}$, computes the antenna gimbal angles
LANDSEA	ALAT, ALONG	LAND	LAND = { 0, L-D over water; 1, L-D over land }

The current version of the program assumes uniform step sizes between computation times, a simple rectangular array driven to follow the sun, circular orbits, and the target (TDRS) in a geosynchronous orbit. These assumptions are not necessary, and they could be changed by revising the various subroutines. For example, subroutine UPDATE could be changed to include the effects of an elliptical orbit or to make the intervals between computation times vary -- possibly dependent upon the program outputs.

Subroutine LAT contains an equation for converting true latitude to geographic latitude. The difference is shown in Figure 3-8 where ϕ_T is the true latitude calculated from the L-D position and ϕ_g is the geographic latitude which depends on the "local vertical".

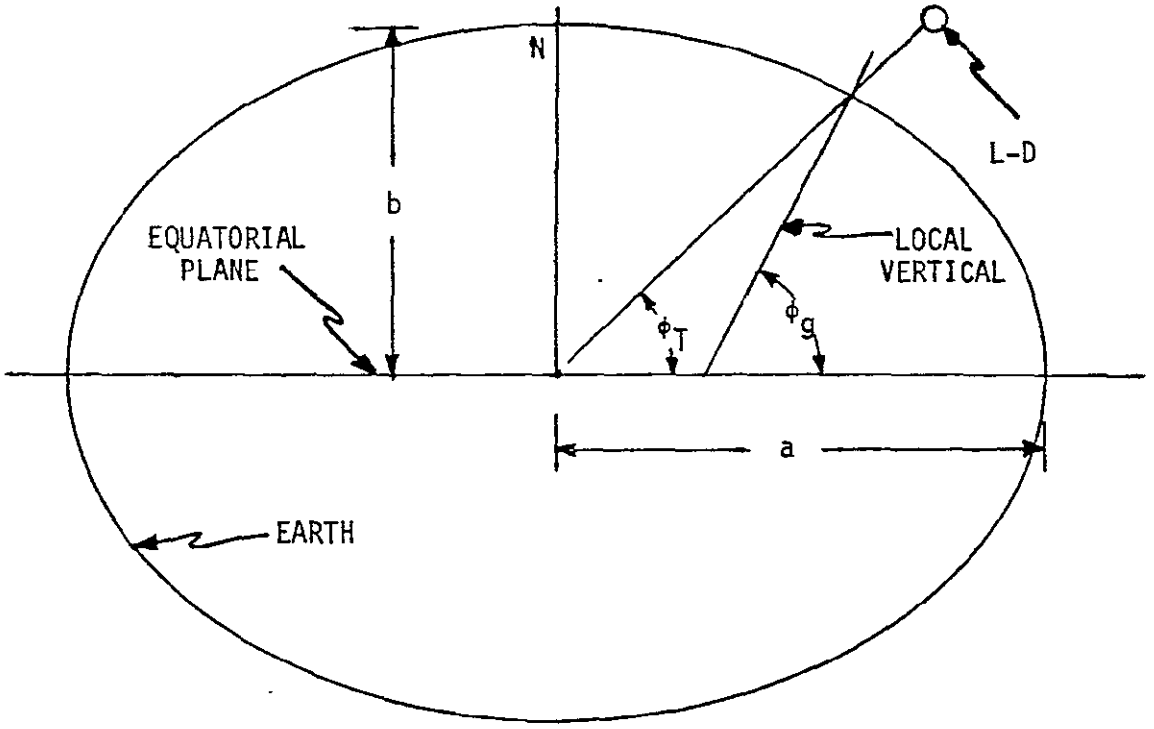

Figure 3-8. Illustration of the Difference Between True and Geographic Latitude

In Reference 6, the two angles are related by the equation

$$\sin \phi_T = \frac{\sin \phi_g}{\left[\sin^2 \phi_g + \left(\frac{a}{b}\right)^4 \cos^2 \phi_g\right]^{1/2}} \qquad (3.4\text{-}1)$$

where

$$\frac{a}{b} = 1.00336417$$

But this easily reduces to the more convenient form

$$\tan \phi_g = \left(\frac{a}{b}\right)^2 \tan \phi_T \qquad (3.4\text{-}2)$$

which is used in the subroutine. This latitude correction changes the latitude by a maximum of 0.2 degree. The longitude computed in LAT is positive for western longitudes and negative for eastern longitudes. The subroutine LANDSEA uses the latitude and longitude to determine whether the point is over land or water. This subroutine was originally written for another program and has been incorporated into this program. The information is stored in 42,261 bits, each representing a 111.2 x 111.2 km piece of the earth's surface -- 1° x 1° at the equator.

3.4.2 Program LFO Abbreviated Users' Guide

The L-D user supplies the program input variables using a namelist file on TAPE3 called "IN". The variables supplied are listed in Table 3-7. The program supplies default values for most of the variables, as shown; the remaining variables must be supplied by the user. Some example runs are given later, but a sample input file is shown in Table 3-8. For the sample input shown, the output file -- from TAPE4 -- is shown in Table 3-9. In practice, the information on the output file would be plotted as in the examples given in Section 3.4.4.

The input variables have the units shown in Table 3-7. The various angles are supplied in degrees for convenience; the program converts the angles to radians for internal use, and then the output angles are reconverted to degrees.

Table 3-7. Program LFO Input Variables

Variable Name	Symbol	Description	Default Value
ALAT1		Longitude of TDRS #1 (Deg)	+41.0
ALPHAS	α_s	Antenna FOV Skirt (Deg)	2.
ARRL	ℓ	Length of Solar Array (Ft)	--
ARRW	ω	Width of Solar Array (Ft)	--
ATMAST	$\bar{a}$	Vector from Edge of Array to Base of MAST (Ft)	$\bar{0}$
CANT	α_c	Solar Array Cant Angle (Deg)	37.5
DELTA1	Δ_1	Rate of Change of γ_1 (Deg/Hr)	15.
DELTAL	Δ_L	Rate of Change of γ_L (Deg/Hr)	220.31
DELTAT	Δ_T	Time Increment (Hr)	--
DIRMAST	$\bar{m}$	Vector Along MAST Toward Antenna	(0,0,-1)
FINALT	T_F	Final Time (Hr)	--
GAMMA1	γ_1	(Initial) Position of TDRS #1 (Deg)	0.
GAMMAD	γ_D	- Angle of Descending Node (Deg)	37.5
GAMMAI	γ_I	L-D Orbit Inclination Angle (Deg)	98.2
GAMMAL	γ_L	(Initial) Position of L-D (Deg)	0.
GAMMAS	γ_s	Angle of Sun Below Equatorial Plane (Deg)	0.
HMAST	h	Antenna Mast Length (Ft)	--
RDISH	R_D	Radius of Ku-Band Antenna Dish (ft)	3.
REARTH	R_E	Earth Half-Angle from L-D (Deg)	64.2
RL	R_L	L-D Orbit Radius (Km)	7074.
RT	R_T	TDRS Orbit Radius (Km)	4.22×10^4

Table 3-8. A Sample LFO Input

```
PSIN
 DELTAT=0.05
 FINALT=1.6
 HMAST=6.34
 ARRW=5.
 ARRL=25.6
 $END
```

Table 3-9. Output with Input Shown in Table 3-8

T	γ_L	γ_1		g_1,Az	g_2,EL	γ_2		g_1,Az	g_2,EL					
TIME	LF/D	TDRS1	TRANS	GIMBAL	ANGLES	TDRS2	TRANS	GIMBAL	ANGLES	DAY	SUN	LAT	LONG	LAND
0.000	0.0	0.0	100.0	-37.2	-4.6	-130.0	100.0	92.5	-17.4	1	1	81.9	-11.5	0
.050	11.0	.7	100.0	-39.1	4.1	-129.2	100.0	90.2	-17.6	1	1	76.4	43.0	1
.100	22.0	1.5	100.0	-42.2	12.6	-128.5	100.0	87.8	-17.2	1	1	66.7	60.6	1
.150	33.0	2.2	100.0	-46.8	20.7	-127.7	100.0	85.7	-16.3	1	1	56.2	68.4	1
.200	44.1	3.0	100.0	-53.1	28.0	-127.0	100.0	83.9	-14.8	1	1	45.5	73.1	1
.250	55.1	3.7	100.0	-61.6	34.1	-126.2	100.0	82.5	-13.0	1	1	34.7	76.6	0
.300	66.1	4.5	100.0	-72.1	38.3	-125.5	100.0	81.7	-10.9	1	1	23.8	79.4	0
.350	77.1	5.2	100.0	-84.1	40.2	-124.7	100.0	81.4	-8.7	1	1	12.8	81.9	0
.400	88.1	6.0	100.0	-96.2	39.3	-124.0	100.0	81.7	-6.4	1	1	1.9	84.2	0
.450	99.1	6.7	100.0	-107.1	35.9	-123.2	100.0	82.6	-4.1	1	1	-9.1	86.6	0
.500	110.2	7.5	100.0	-115.8	30.7	-122.5	100.0	84.0	-2.1	1	1	-20.1	89.0	0
.550	121.2	8.2	100.0	-122.3	24.2	-121.7	100.0	86.0	-.5	1	1	-31.0	91.7	0
.600	132.2	9.0	100.0	-126.9	16.9	-121.0	100.0	88.3	.7	1	1	-41.8	94.9	0
.650	143.2	9.7	100.0	-129.8	9.3	-120.2	100.0	91.0	1.2	1	1	-52.6	99.0	0
.700	154.2	10.5	100.0	-131.4	1.6	-119.5	100.0	93.7	1.2	1	1	-63.2	105.5	0
.750	165.2	11.2	100.0	-131.8	-5.9	-118.7	100.0	96.5	.4	1	1	-73.3	118.2	0
.800	176.2	12.0	100.0	-131.0	-13.2	-118.0	100.0	99.0	-.9	0	1	-81.0	155.8	0
.850	187.3	12.7	91.4	-129.2	-20.0	-117.2	100.0	101.3	-2.9	0	1	-79.1	-137.0	1
.900	198.3	13.5	-20.0	-126.2	-25.8	-116.5	100.0	103.0	-5.4	0	1	-70.1	-111.4	1
.950	209.3	14.2	-20.0	-122.0	-25.8	-115.7	100.0	104.2	-8.3	0	0	-59.8	-101.5	0
1.000	220.3	15.0	-20.0	-116.5	-25.8	-115.0	100.0	104.8	-11.4	0	0	-49.2	-96.0	0
1.050	231.3	15.7	-20.0	-109.7	-25.8	-114.2	100.0	104.6	-14.6	0	0	-38.4	-92.3	0
1.100	242.3	16.5	-20.0	-102.0	-25.8	-113.5	100.0	103.7	-17.8	0	0	-27.5	-89.3	0
1.150	253.4	17.2	-20.0	-93.8	-25.8	-112.7	100.0	102.1	-20.8	0	0	-16.6	-86.7	0
1.200	264.4	18.0	-20.0	-85.7	-25.8	-112.0	100.0	99.7	-23.5	0	0	-5.6	-84.3	0
1.250	275.4	18.7	-20.0	-78.3	-25.8	-111.2	100.0	96.6	-25.6	0	0	5.4	-82.0	0
1.300	286.4	19.5	-20.0	-72.1	-25.8	-110.5	-20.0	92.9	-25.8	0	0	16.3	-79.6	1
1.350	297.4	20.2	-20.0	-67.1	-25.8	-109.7	-20.0	88.8	-25.8	0	0	27.3	-77.0	1
1.400	308.4	21.0	-20.0	-63.5	-25.8	-109.0	-20.0	84.4	-25.8	0	0	38.2	-74.0	1
1.450	319.4	21.7	48.3	-61.2	-22.7	-108.2	-20.0	80.1	-25.8	0	0	49.0	-70.3	1
1.500	330.5	22.5	56.9	-59.9	-17.2	-107.5	100.0	76.0	-25.3	0	1	59.6	-64.9	1
1.550	341.5	23.2	66.9	-59.8	-11.6	-106.7	100.0	72.4	-22.7	0	1	69.9	-55.2	0
1.600	352.5	24.0	100.0	-60.6	-6.0	-106.0	100.0	69.4	-19.4	0	1	79.0	-30.2	0
1.650	363.5	24.7	100.0	-62.4	-.8	-105.2	100.0	67.2	-15.5	1	1	81.1	36.5	1

3.4.3 Two Key Subroutines

The purpose of the subroutine ARRAY is to compute the fraction of the Ku-band antenna field-of-view pattern that is blocked by the solar array. The solar array is assumed to be a rectangular array of length ℓ and width w. It is also assumed that the array is mounted in such a way that it is canted to the spacecraft $-\hat{y}_o$ axis and is driven to rotate about the $\hat{y}_o$ axis to track the sun. This is illustrated in Figure 3-9, where $\hat{s}$ is the sun vector, $\hat{T}$ is the target vector and θ_c is the array cant angle. The distance indicated as L in Figure 3-9 is the distance from the x-y plane to the top of the mast; this has been referred to as the "mast length" in previous work. In the program, the variable HMAST is used instead to represent the true mast length as measured from the spacecraft mounting point to the hinge.

The field-of-view of the antenna is a cylindrical beam of radius R_D extending out from the antenna dish plus a 1 to 2 degree skirt all around the cylinder. The solar array interference is found by:

(1) The solar array orientation is determined from the sun vector $\hat{s}$.

(2) A ray of the antenna beam at the center of the dish is found and used to determine the average distance from the dish to the plane of the array.

(3) That distance is used to determine the FOV diameter at the plane of the array -- this includes the skirt.

(4) A pair of unit vectors that form an orthonormal basis with $\hat{T}$ are used to construct a uniform distribution of points in the FOV.

(5) A ray of the antenna beam through each of those points is extended to the plane of the array.

(6) The portion of those rays that intersect the array is the interference.

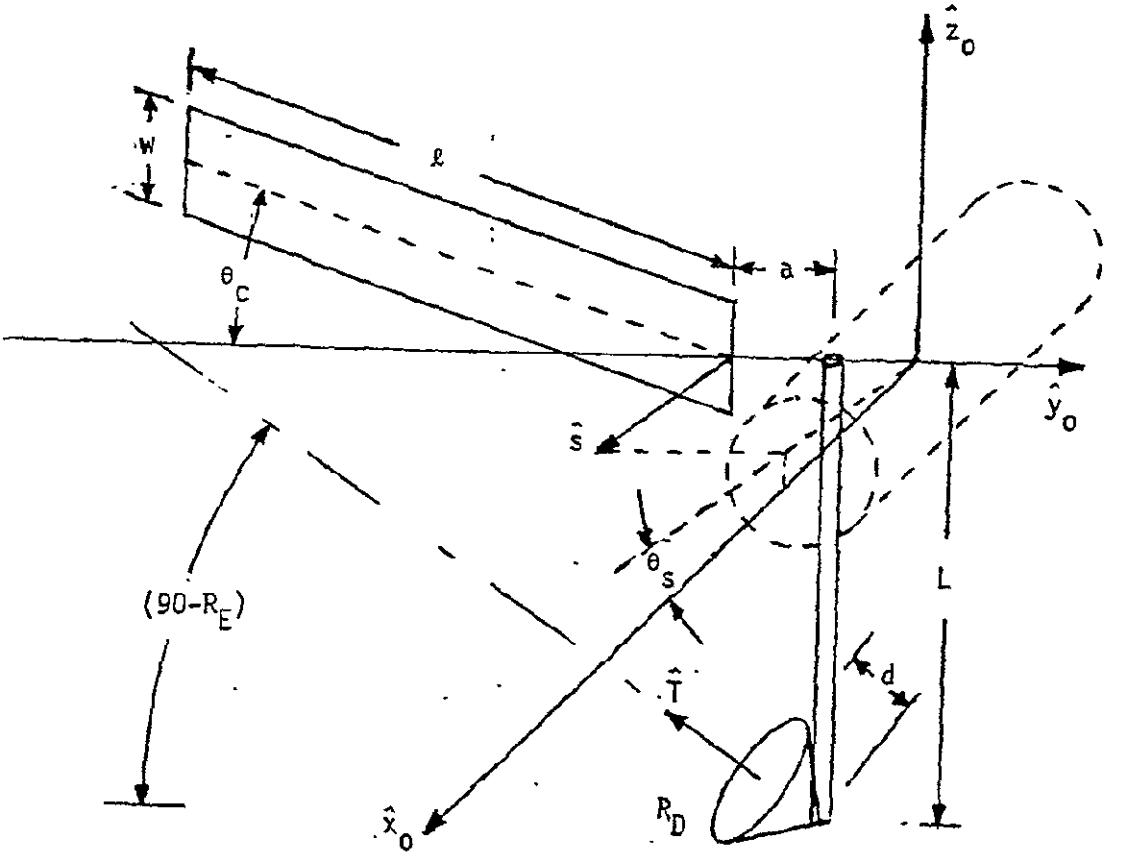

Figure 3-9. The Antenna and Solar Array in Orbit Coordinates

Given the sun unit vector, $\hat{s} = [s_x, s_y, s_z]^T$, the array rotation angle θ_s in Figure 3-9 is given by

$$\theta_s = \tan^{-1}\left(\frac{s_x}{s_z}\right) \qquad (3.4\text{-}3)$$

where θ_s is the angle between the x axis and the projection of the sun vector onto the $\hat{x}$-$\hat{z}$ plane. This means θ_s is zero when the spacecraft is over the North Pole -- 8.2 degrees away, actually -- at a solstice. If the array cant angle is θ_c, then a vector in body coordinates O can be written in array coordinates A as

$$\bar{r}_A = [\theta_c]_x [-\theta_s]_y \bar{r}_o = T_{AO} \bar{r}_o \qquad (3.4\text{-}4)$$

This assumes that the two coordinate systems have the same origin, which is an acceptable assumption in the case of the sun and TDRS vectors. The coordinate system A is the one in which the solar array lies in the x_A-y_A plane with its inner edgelying on the x_A axis.

In the program, the mast length h is called HMAST, the mast direction $\hat{m}$ is given by the vector DIRMAST and the antenna mast base is located by the vector ATMAST ($\bar{a}$) relative to the origin of the coordinate system A -- the above vectors are given in the O coordinate system. Thus, in array coordinates, the antenna hinge is at the point

$$\bar{v} = T_{AO} \{\bar{a} + h \hat{m}\} \qquad (3.4\text{-}5)$$

Since the antenna is pointed at the target, the center ray of the beam -- which is aligned with the hinge -- intersects the points

$$\bar{r}_o = \bar{v} + \alpha \hat{T} \qquad (3.4\text{-}6)$$

where α is a parameter. Thus the distance from the hinge to the plane of the array is given by

$$\alpha_o = - \frac{(\bar{v})_z}{(\hat{T})_z} \qquad (3.4\text{-}7)$$

because that is the value which makes $(\bar{r}_o)_z \equiv 0$. This can be used to compute the FOV radius at the plane of the array:

$$R_c = R_D + (\alpha_o - d) \tan (\alpha_s) \qquad (3.4\text{-}8)$$

where R_D is the radius of the dish, α_s is the angle of the skirt and

$$d = \frac{R_D}{\tan(R_E)} \tag{3.4-9}$$

where R_E is the earth half-angle.

Given $\hat{T}_A$ -- the target unit vector in array coordinates -- and a suitable unit vector $\hat{e}_o$, a pair of orthogonal unit vectors in the plane P perpendicular to $\hat{T}_A$ are formed as

$$\hat{e}_1 = (\hat{T}_A \times \hat{e}_o)/(|\hat{T}_A \times \hat{e}_o|) \tag{3.4-10}$$

and

$$\hat{e}_2 = \hat{T}_A \times \hat{e}_1 \tag{3.4-11}$$

These basis vectors are then used to form a set of 625 points uniformly distributed over the square in P that circumscribes the FOV circle of radius R_c. A particular point is given by

$$\overline{c} = a_1 \hat{e}_1 + a_2 \hat{e}_2 \tag{3.4-12}$$

where

$$a_1 = \frac{2i - n - 1}{n} R_c \quad , \quad i=1,\ldots,n \tag{3.4-13}$$

and

$$a_2 = \frac{2j - n - 1}{n} R_c \quad , \quad j=1,\ldots,n \tag{3.4-14}$$

where n = 25.

The ray parallel to $\hat{T}_A$ through one of the points is given by

$$\bar{r} = \bar{r}_o + \bar{c} = \bar{v} + \bar{c} + \alpha \hat{T}_A \tag{3.4-15}$$

If α is chosen so that $(\bar{r})_z = 0$, then $\bar{r}$ is the intersection of the ray with the plane of the solar array. This point of intersection is compared with the array boundaries to determine whether or not it intersects the array. The subroutine output is the percent transmission of the antenna which is

$$R = 100 \left[1 - \left(\frac{M_2}{M_1}\right)\right] \tag{3.4-16}$$

where M_1 is the number of points lying in the circle and M_2 is the number of those points that emanate rays which intersect the solar array.

Subroutine Gimbal

The purpose of this subroutine is to compute the gimbal angles required to point the Ku-band antenna at the target. In the subroutine, it is assumed that there are two gimbals with the inner gimbal angle being the elevation angle and the outer gimbal angle being the azimuth angle. In the normal or null position, the antenna is pointed along the roll axis and the elevation axis is the spacecraft pitch axis -- see Figure 3-10. Thus for a normalized target vector $\hat{T}$, the required gimbal angles g_1 and g_2 are found from

$$\begin{bmatrix} 1 \\ 0 \\ 0 \end{bmatrix} = [g_2]_y [g_1]_z \hat{T} \tag{3.4-17}$$

which is rearranged to obtain

$$T = \begin{bmatrix} T_x \\ T_y \\ T_z \end{bmatrix} = \begin{bmatrix} \cos g_1 \cos g_2 \\ \sin g_1 \cos g_2 \\ -\sin g_2 \end{bmatrix} \tag{3.4-18}$$

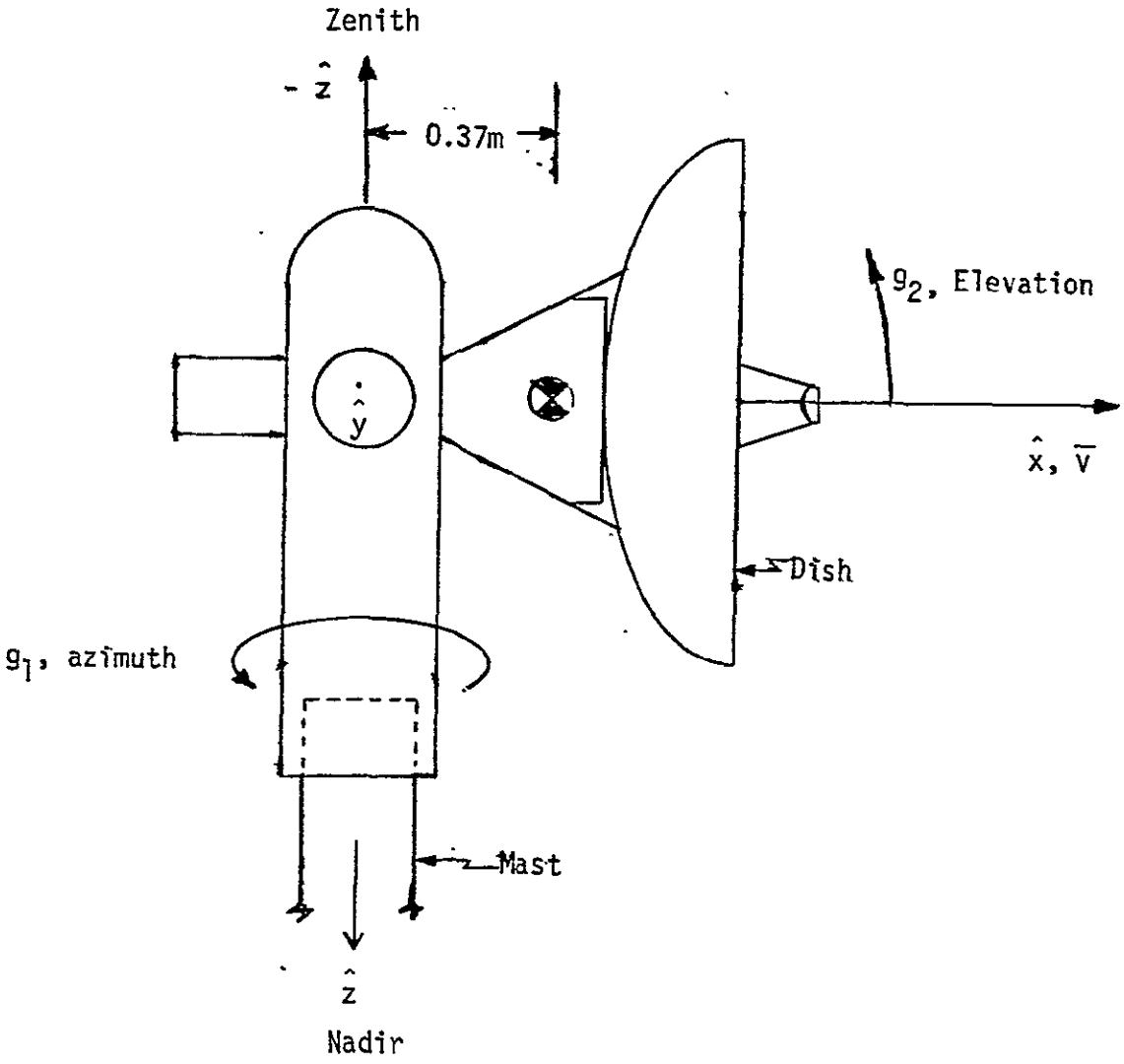

Figure 3-10. Ku-Band Antenna in the Null Position

Solving this for the gimbal angles:

$$g_1 = \tan^{-1}\left[\frac{T_y}{T_x}\right] \tag{3.4-19}$$

$$g_2 = \sin^{-1}\left[-T_z\right] \tag{3.4-20}$$

The gimbal equations for several two-gimbal configurations are given in Table 3-10. As discussed earlier, a third gimbal would be used only to overcome a severe gimbal-lock problem. Because there are several ways to utilize the third gimbal, it is not convenient to include the three-gimbal configuration in Table 3-10.

Table 3-10. Antenna Gimbal Equations

Outer Gimbal Axis	Inner Gimbal Axis	Nominal Antenna Direction	Outer Gimbal Angle, g_1	Inner Gimbal Angle, g_2
$\hat{z}$	$\hat{y}$	$[1 \quad 0 \quad 0]^T$	$\tan^{-1}[T_y/T_x]$	$\sin^{-1}[-T_z]$
$\hat{z}$	$\hat{y}$	$[0 \quad 0 \quad -1]^T$	$\tan^{-1}[T_y/T_x]$	$\cos^{-1}[-T_z]$
$\hat{z}$	$\hat{x}$	$[0 \quad 0 \quad -1]^T$	$\tan^{-1}[(-T_x)/T_y]$	$\cos^{-1}[-T_z]$
$\hat{y}$	$\hat{x}$	$[0 \quad 0 \quad -1]^T$	$\tan^{-1}[(-T_x)/(-T_z)]$	$\sin^{-1}[T_y]$
$\hat{x}$	$\hat{y}$	$[0 \quad 0 \quad -1]^T$	$\tan^{-1}[T_y/(-T_z)]$	$\sin^{-1}[-T_x]$

3.4.4 Examples

Although the cases in this section are examples of the use of Program LFO, they are also meaningful cases to the L-D study. In all cases the antenna mast length above the attachment point has been chosen as 6.34 feet. In the first example, the L-D passes through the "zone of exclusion" -- an area over the Indian Ocean where the earth blocks transmission to both TDRS's simultaneously. The input file is shown in Table 3-11, and the results of the run are shown in Figures 3-11 through 3-15. Figure 3-11 shows the percent transmission for the two potential targets. Note that toward the end of the first orbit shown, the earth blocks both targets -- this is the "zone of exclusion" (ZOE). Figure 3-12 indicates when the L-D is over a lighted earth, when it is eclipsed, and when it is over land. Note that the earth blockage of both TDRS's occurs over a dark earth in this case, but it could just as easily occur over a lighted earth. The solar array interference is much worse over this dark earth than over a lighted earth because the array follows the hidden sun. For the few orbits shown, TDRS2 would be chosen as the target because of the 100 percent transmission over the lighted earth.

Table 3-11. Input for First Example Showing the Zone of Exclusion

```
$SIN
 DELTAT=0.02
 FINALT=7.
 HMAST=6.34
 ARRW=5.
 ARRL=25.6
 GAMMA1=8.9
 $END
```

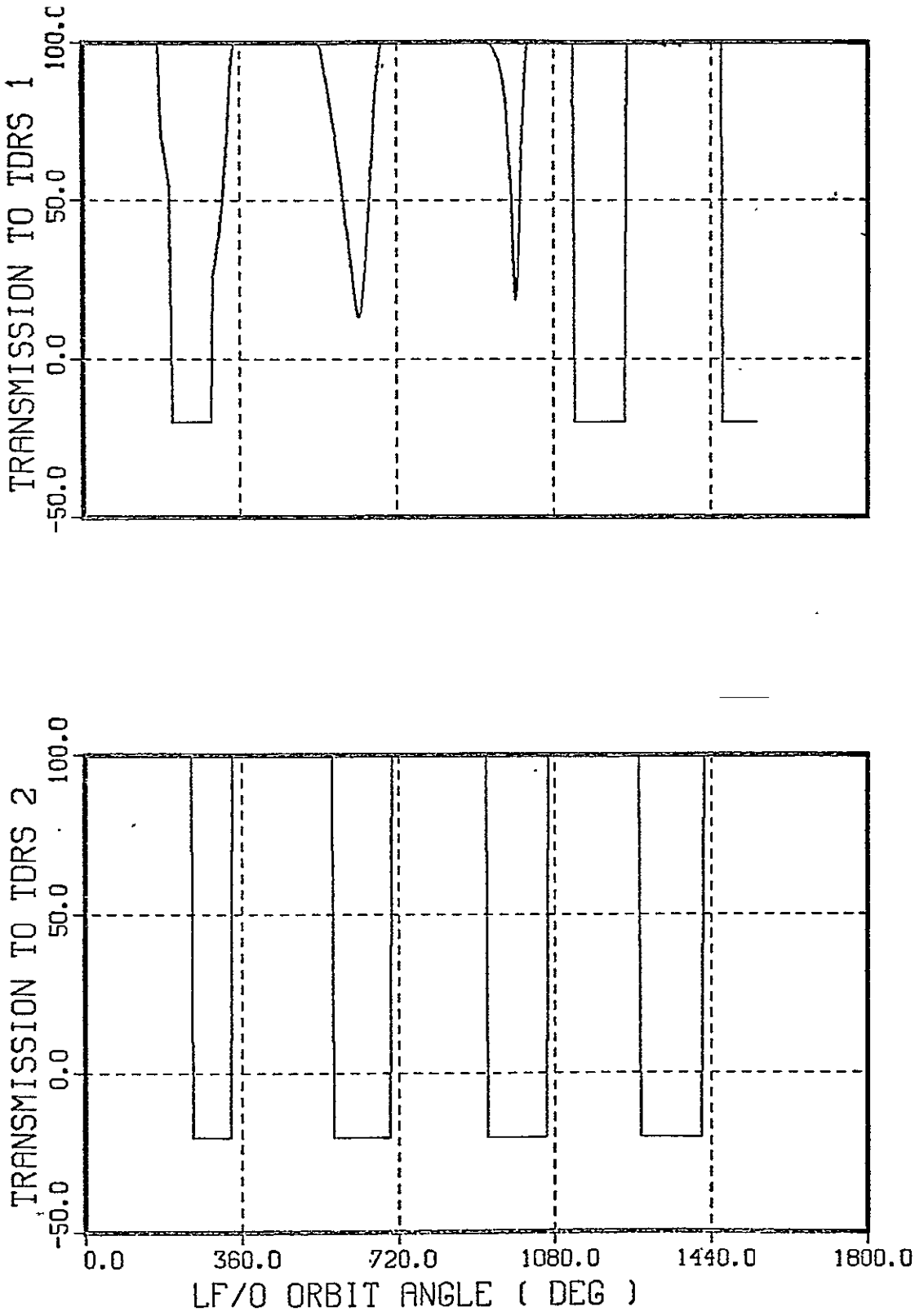

Figure 3-11. Zone of Exclusion at Night

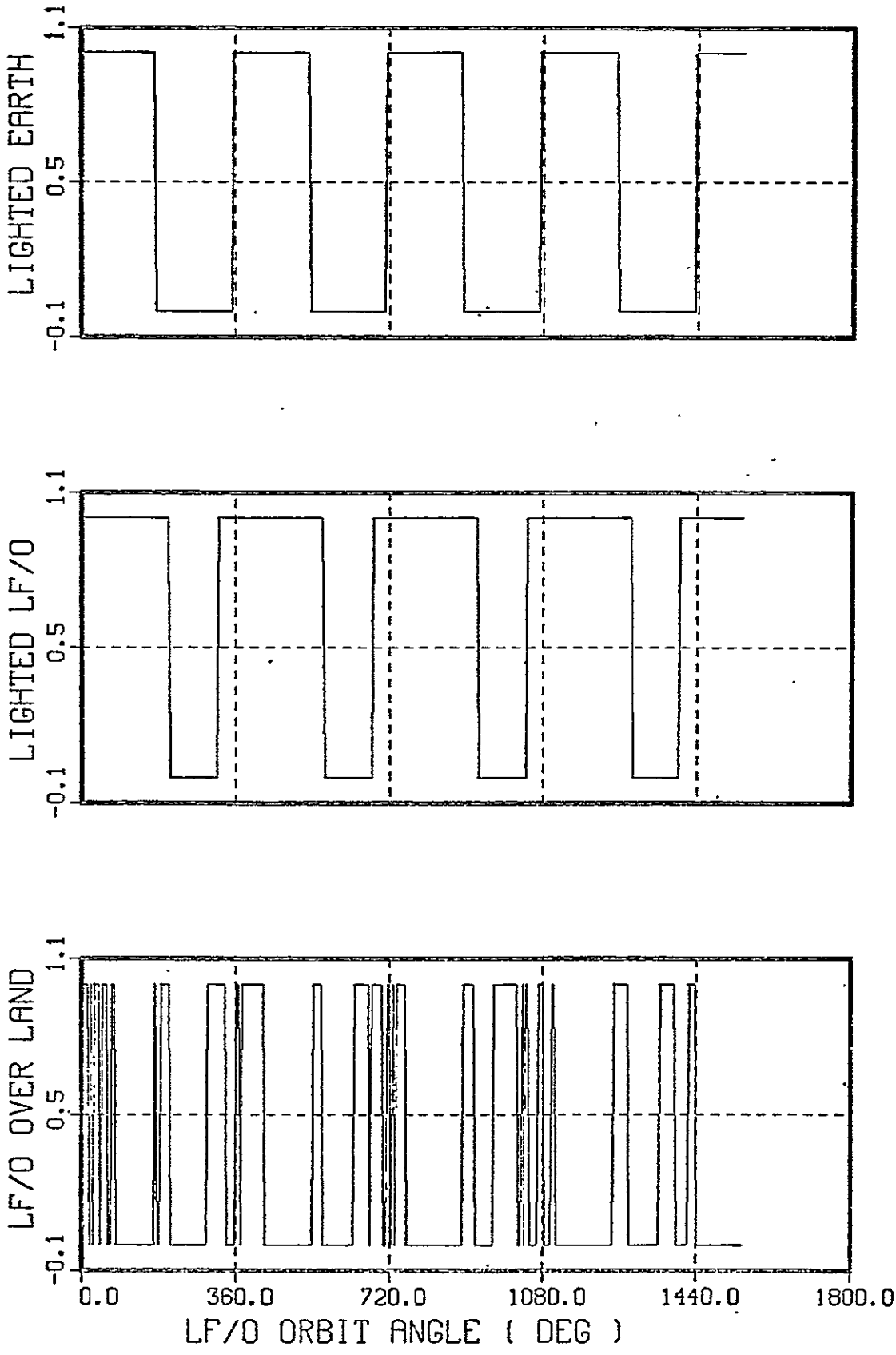

Figure 3-12. Zone of Exclusion at Night

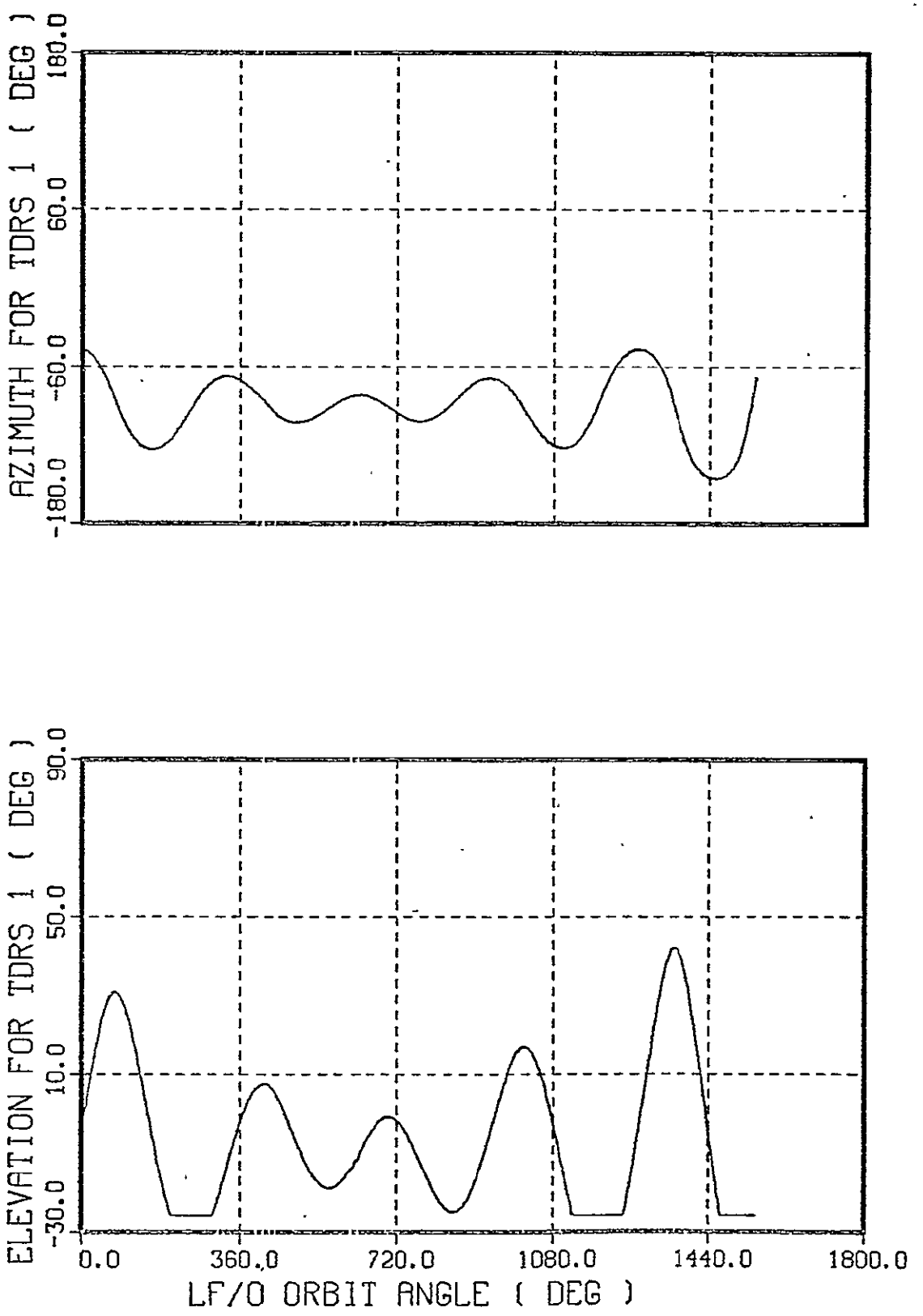

Figure 3-13. Zone of Exclusion at Night

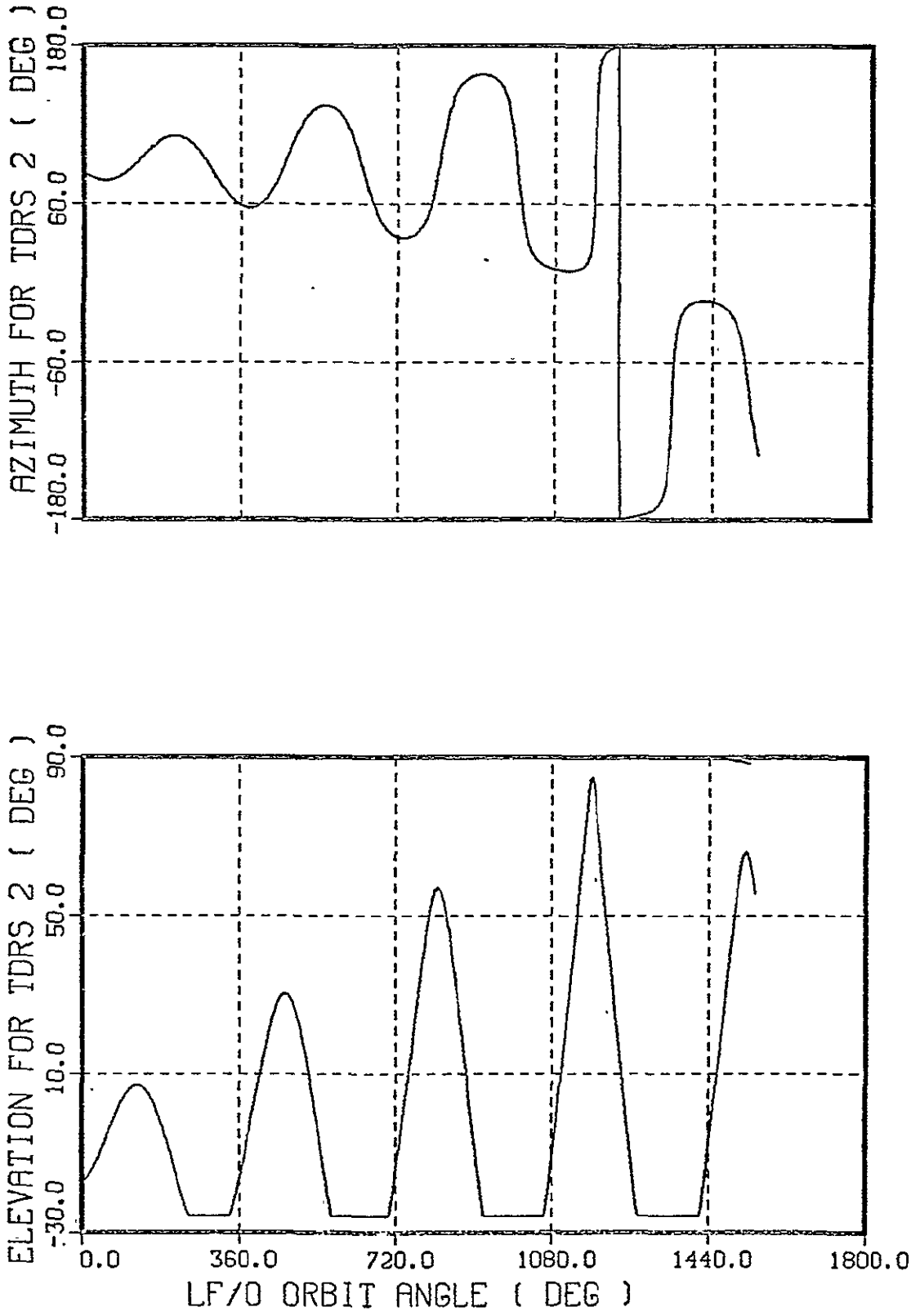

Figure 3-14. Zone of Exclusion at Night

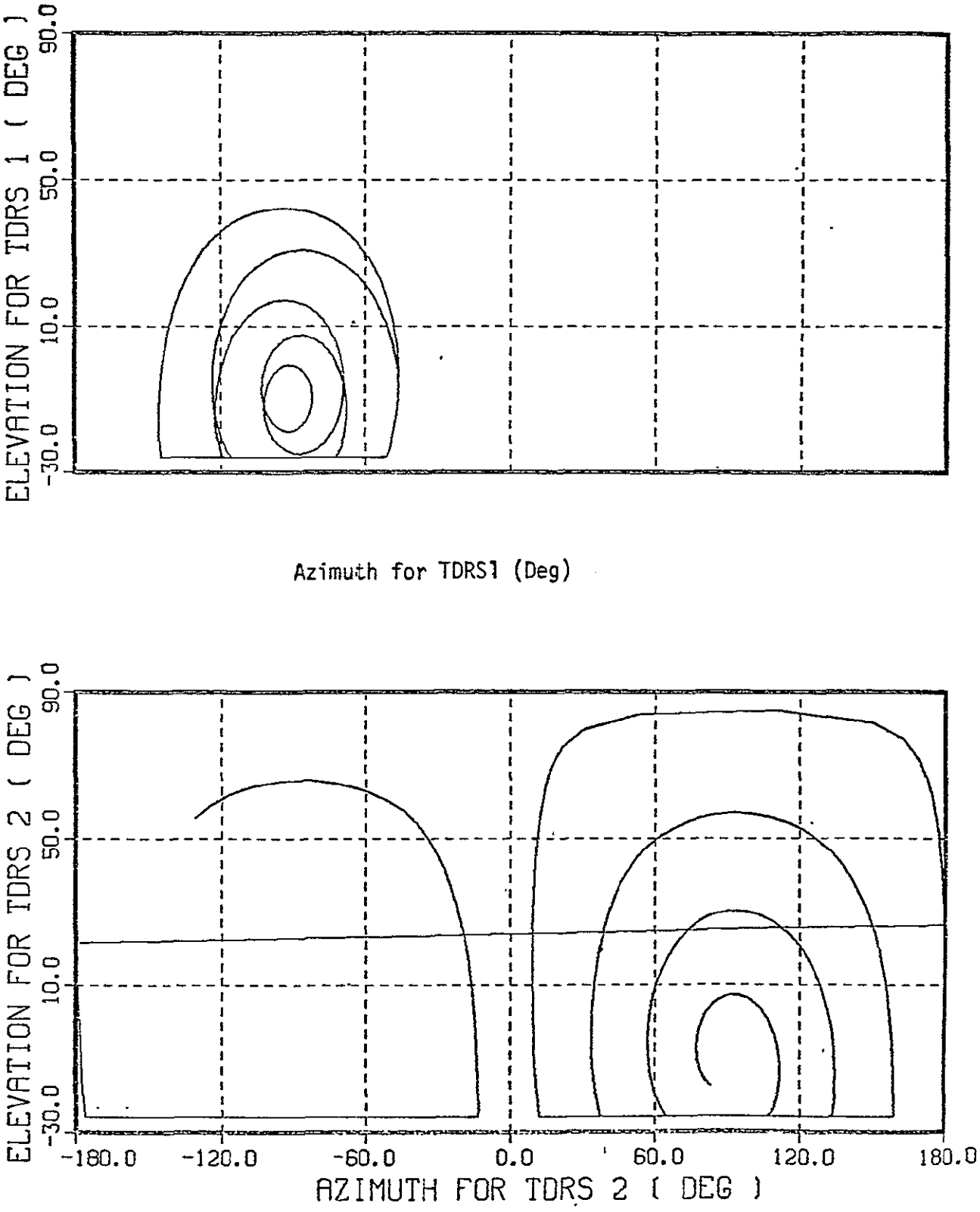

Figure 3-15. Zone of Exclusion at Night

Figures 3-13 and 3-14 show the required antenna gimbal angles. The elevation angle stops at -25.8 degrees because that is the edge of the earth: when the TDRS position is at an elevation beyond -25.8 degrees, it is hidden behind the earth. Note in Figure 3-14 that TDRS2 passes through the L-D orbit plane, requiring that the azimuth gimbal be reset. Also, the elevation angle is very nearly 90 degrees -- gimbal-lock occurs when the elevation angle is 90 degrees. Finally, Figure 3-15 shows the elevation angle plotted versus the azimuth angle.

The results of the second example are shown in Figures 3-16 through 3-20; the input file is in Table 3-12. This run shows the gimbal-lock case as indicated in Figure 3-20. According to Figure 3-16, the target should be TDRS2 during these four orbits. When the gimbal-lock occurs -- for a L-D orbit angle of about 800 degrees as seen in Figure 3-19 -- the earth blocks TDRS1, so TDRS2 is still the proper target.

The third example shows the L-D passing through the ZOE over a lighted earth. The input file is in Table 3-13, and the results are shown in Figures 3-21 through 3-25. Note that the solar array interference is much less than it was in the first example, this is because the solar array is rotated away from the antenna when the sun is overhead.

A fourth example consists of a 24 hour run (15 orbits) at vernal equinox conditions. Of main interest here is a summary of the percent of lighted land encountered. The program was initialized so that the first orbit contained the longest continuous land swath extending from the northern rim of Russia, across the middle east, to the southern tip of Africa. The lighted land data is important for the spacecraft power budget since nominally the TM needs be in the active data taking mode only when the spacecraft is over lighted land. The results are summarized in Figure 3-26 which gives percent lighted land per half and full orbit and percent land per orbit. For this particular 24 hour run (repetition occurs only after 16 days!) the L-D was over lighted land only 16.56% of the 24 hour period. The spacecraft was over land, lighted or dark, 34.23% of the 24 hour period.

Table 3-12. Input for Second Example Showing Gimbal Lock

```
P$IN
 DELTAT=0.02
 FINALT=7.
 HMAST=6.34
 ARRW=5.
 ARRL=25.6
 GAMMA1=38.
 $END
```

Table 3-13. Input for Third Example Showing the ZOE Over a Lighted Earth

```
P$IN
 DELTAT=0.02
 FINALT=7.
 HMAST=6.34
 ARRW=5.
 ARRL=25.6
 GAMMA1=-159.
 $END
```

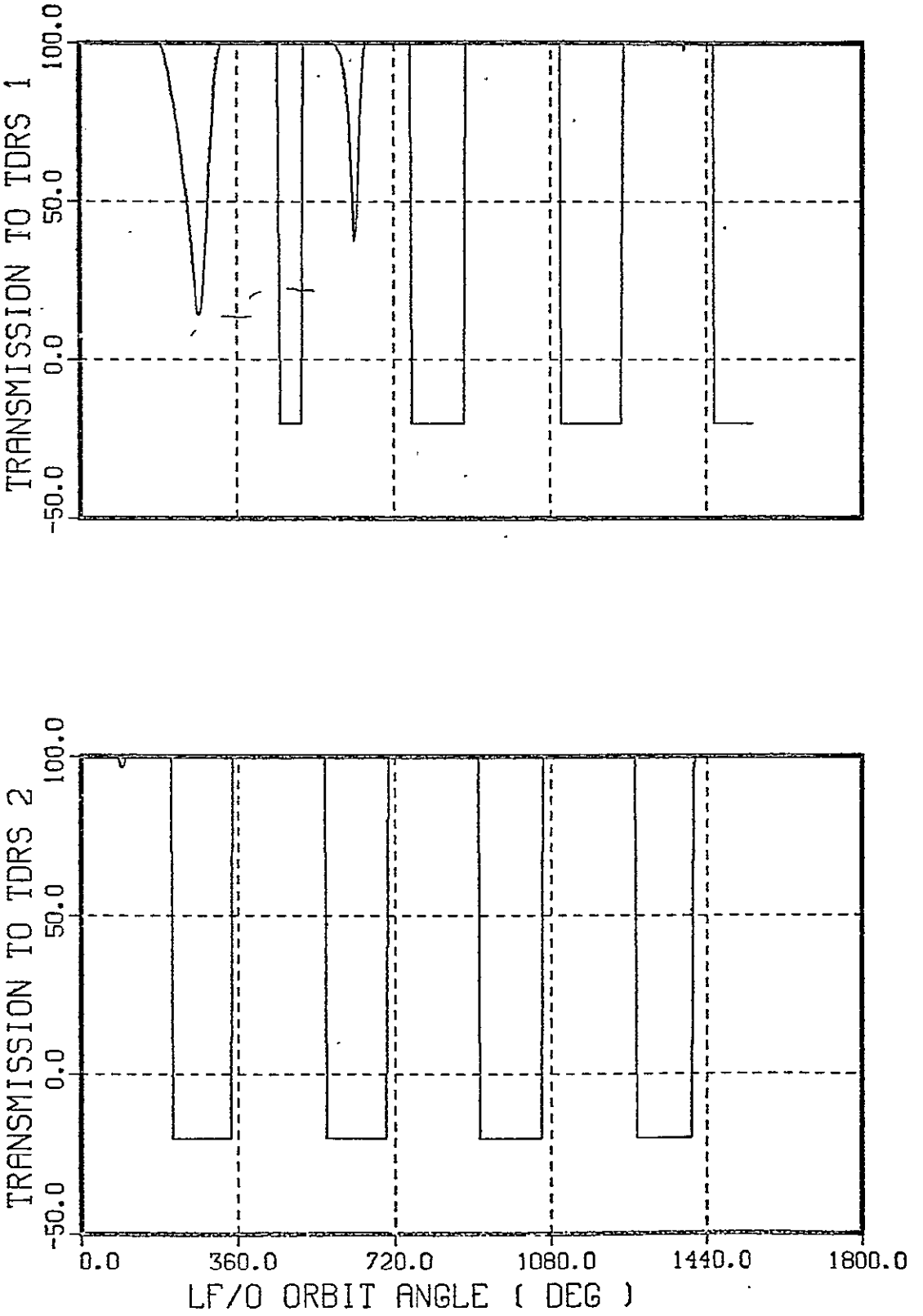

Figure 3-16. Gimbal Lock

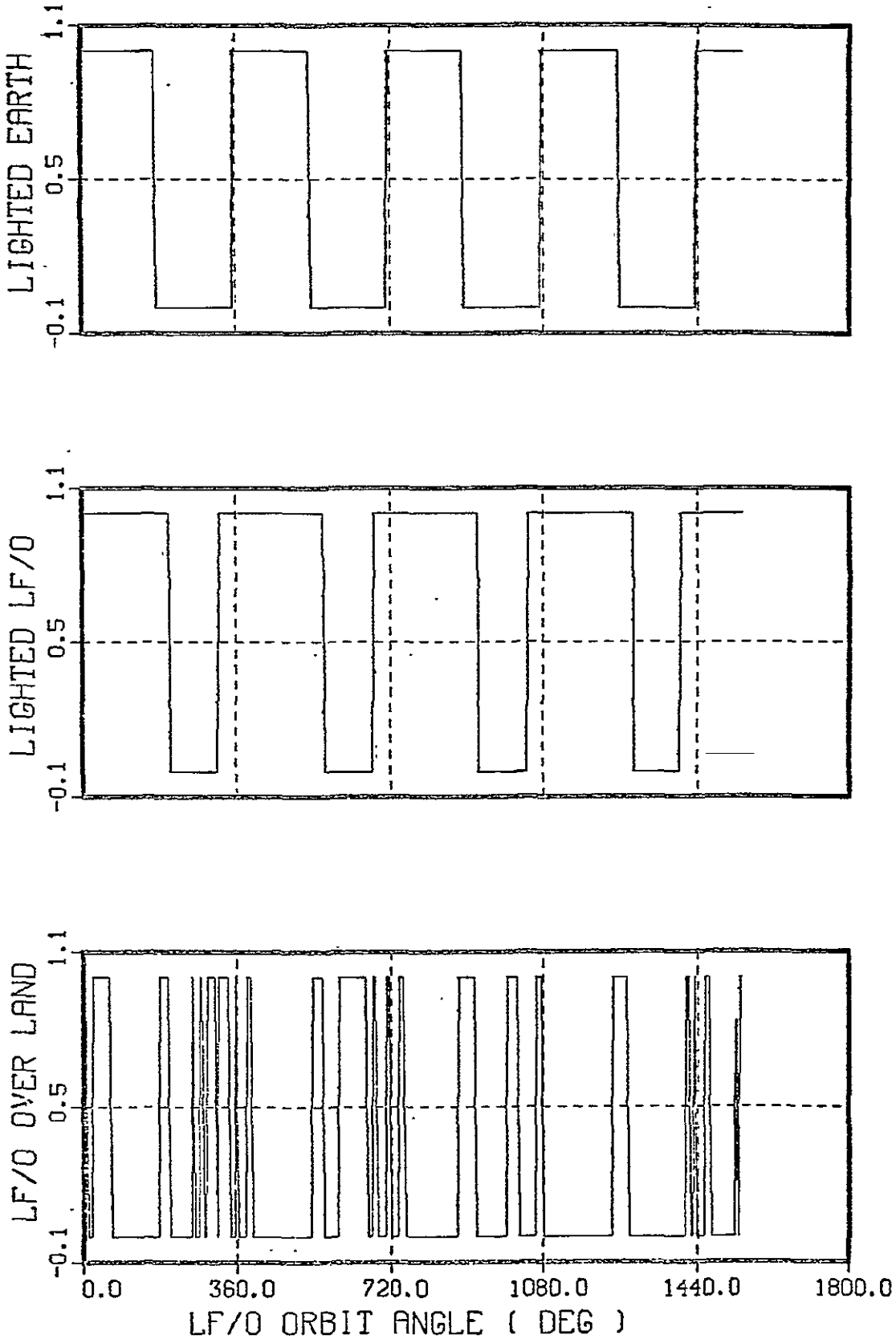

Figure 3-17. Gimbal Lock

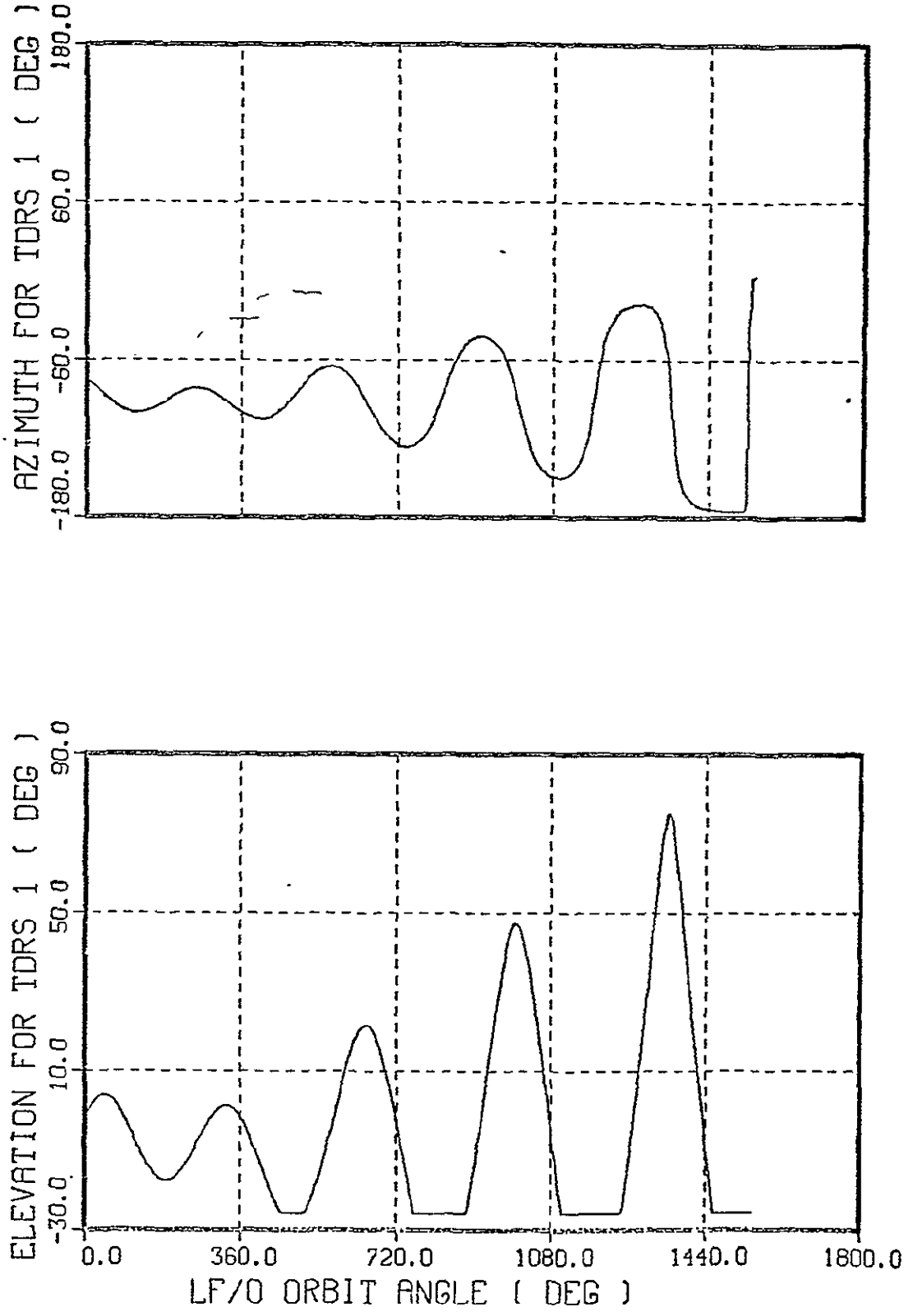

Figure 3-18. Gimbal Lock

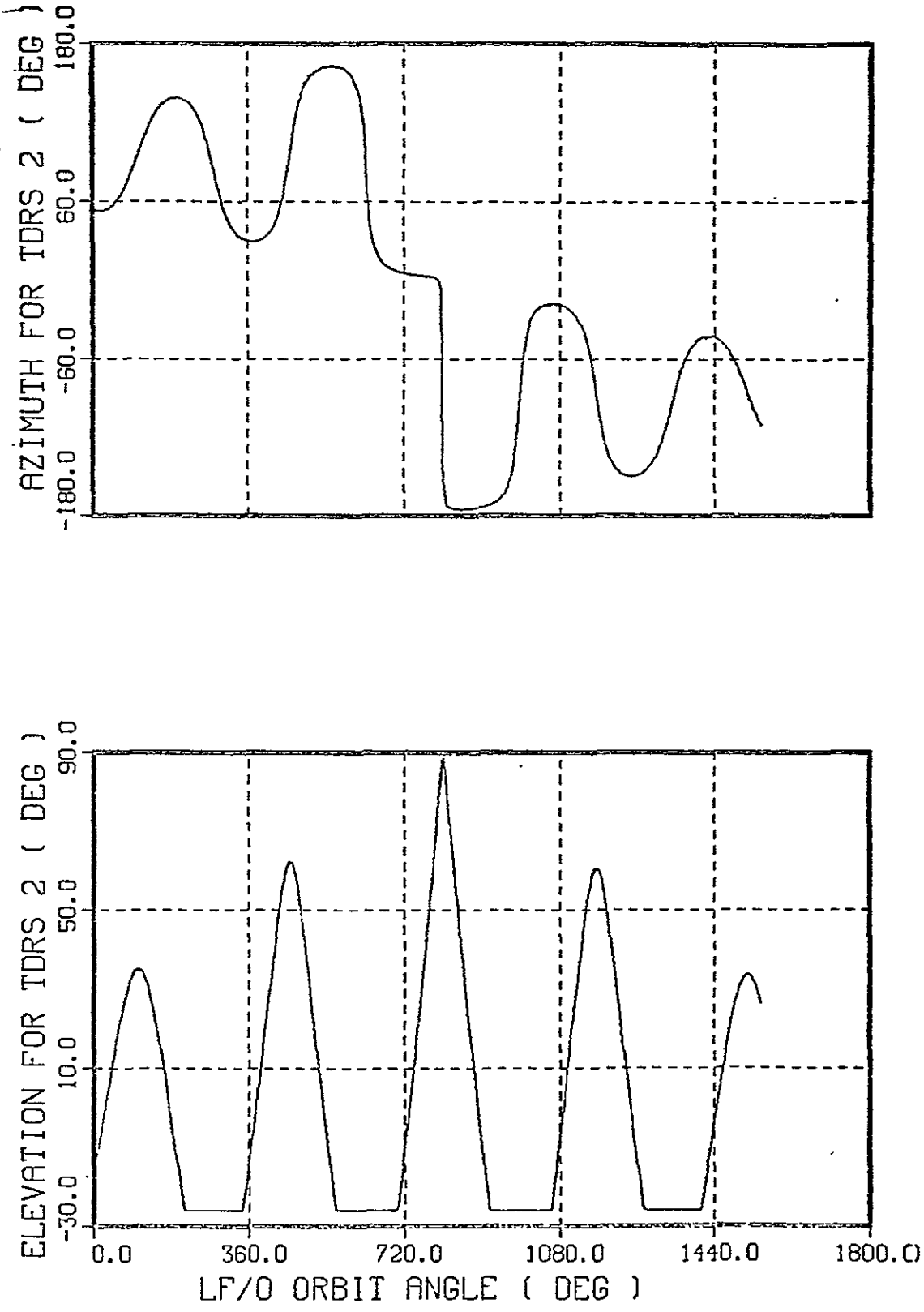

Figure 3-19. Gimbal Lock

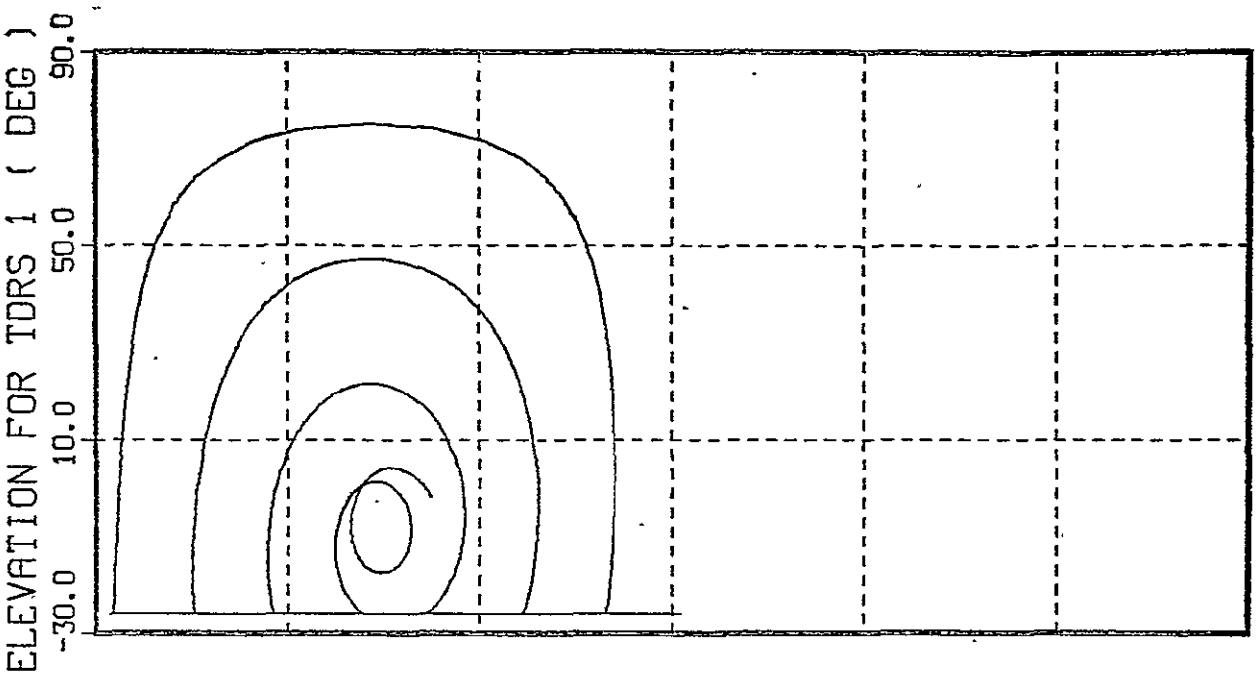

Azimuth for TDRS1 (Deg)

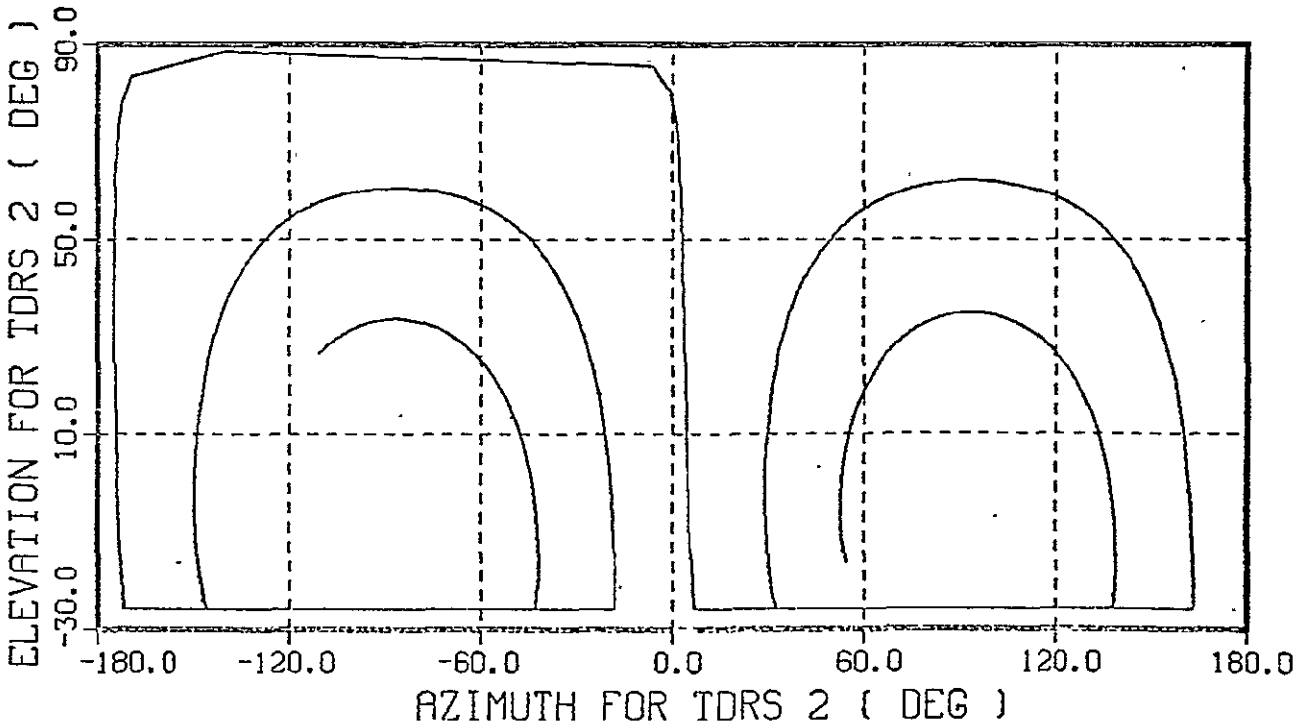

Figure 3-20. Gimbal Lock

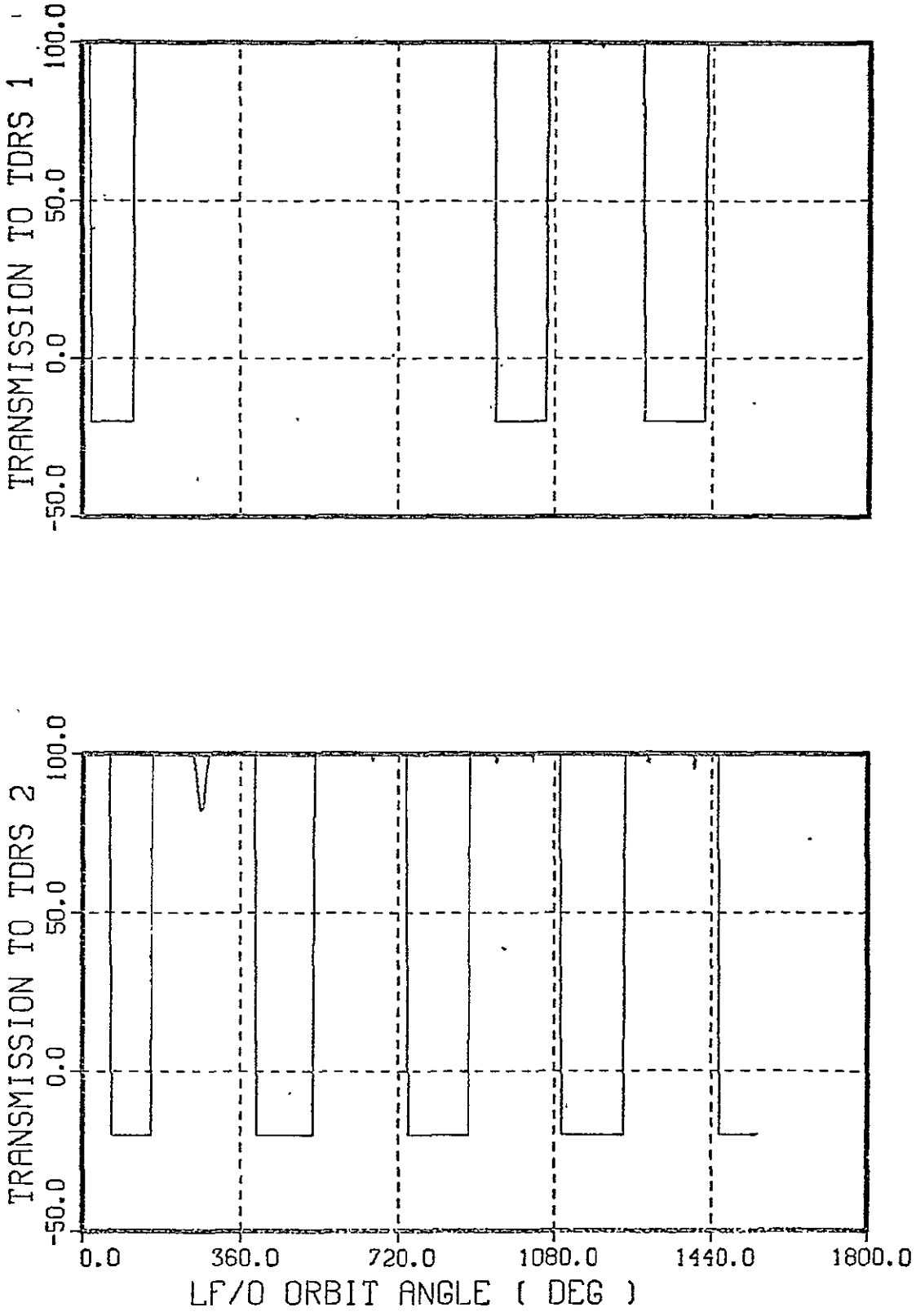

Figure 3-21. Zone of Exclusion Over Daylight

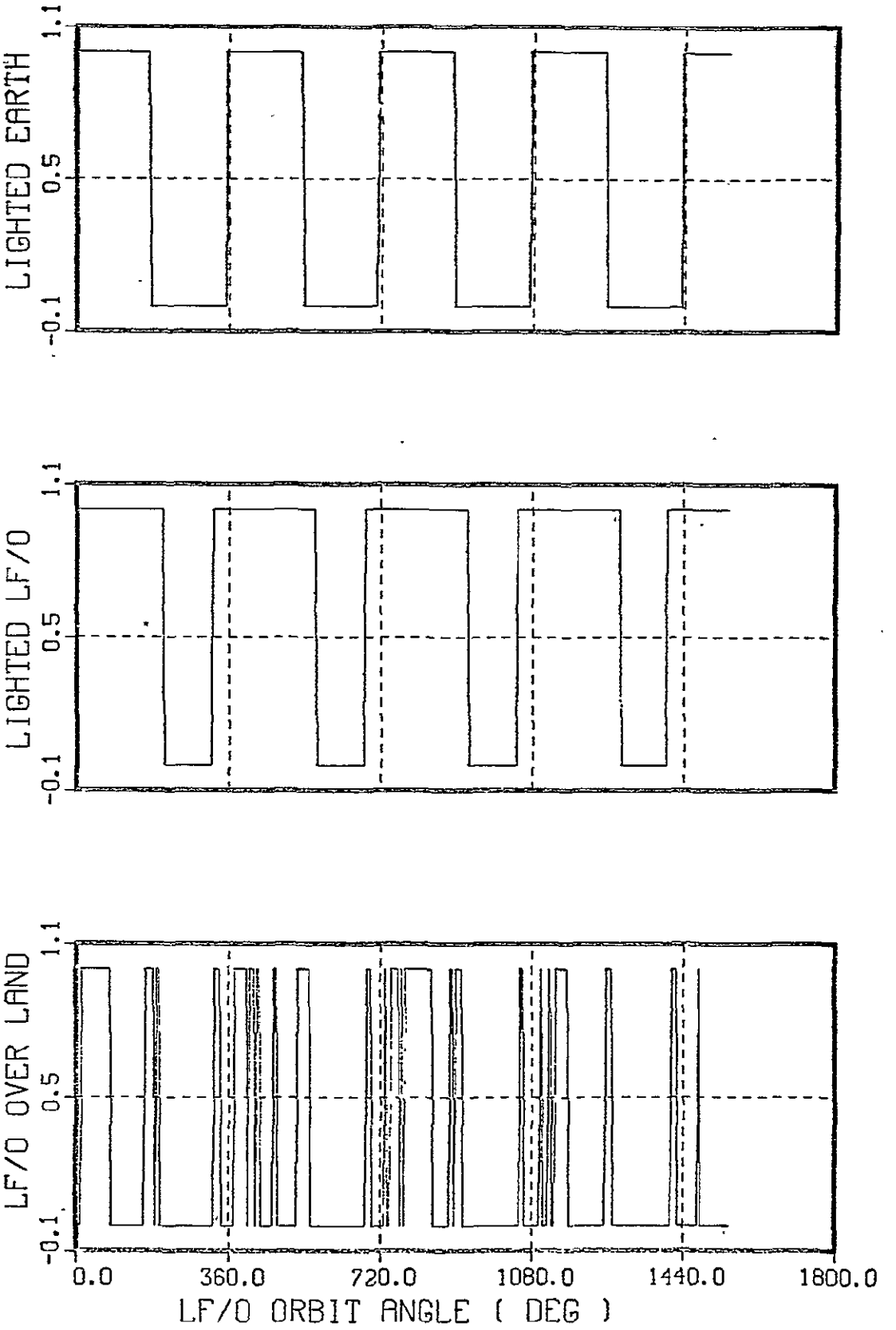

Figure 3-22. Zone of Exclusion Over Daylight

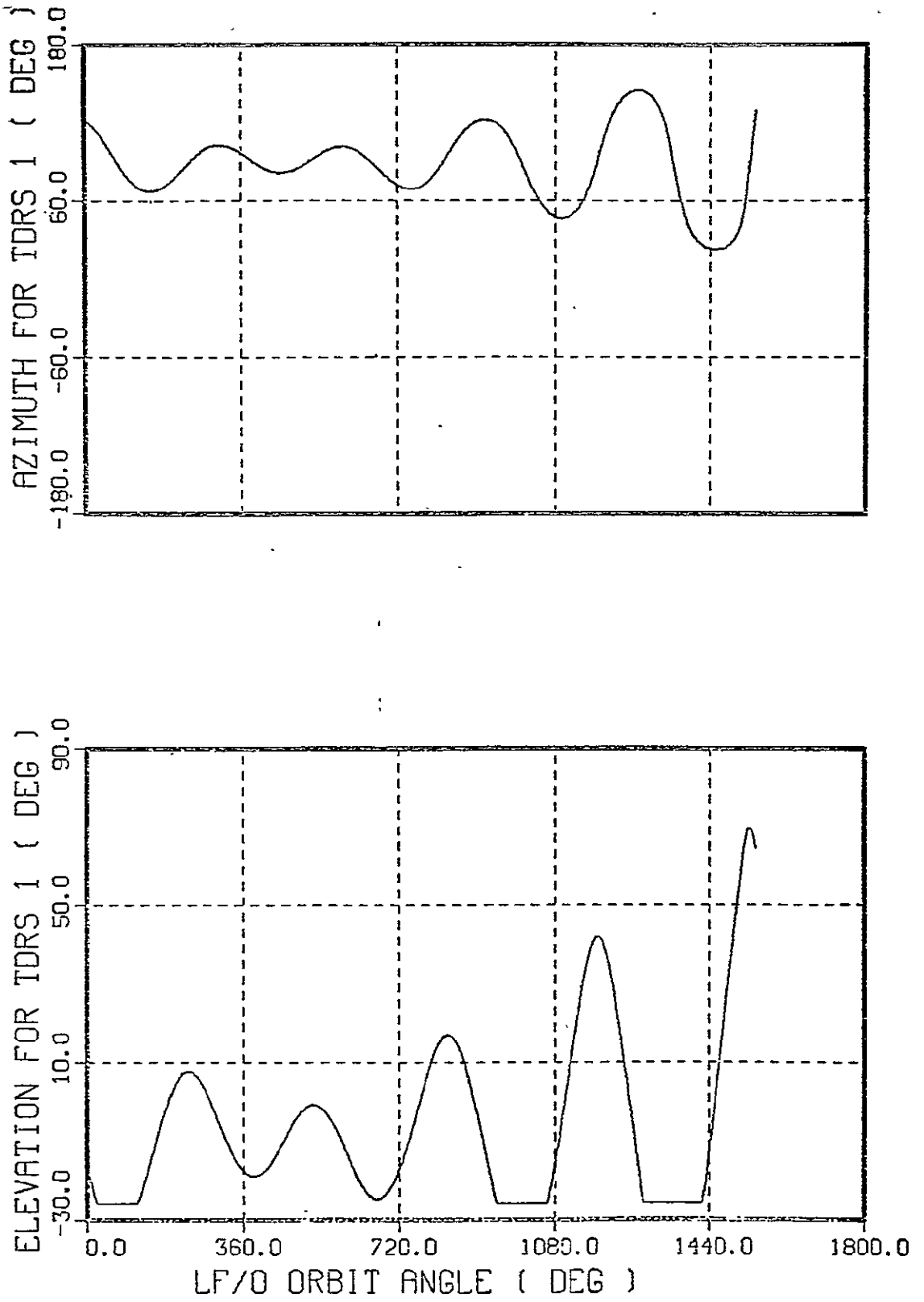

Figure 3-23. Zone of Exclusion Over Daylight

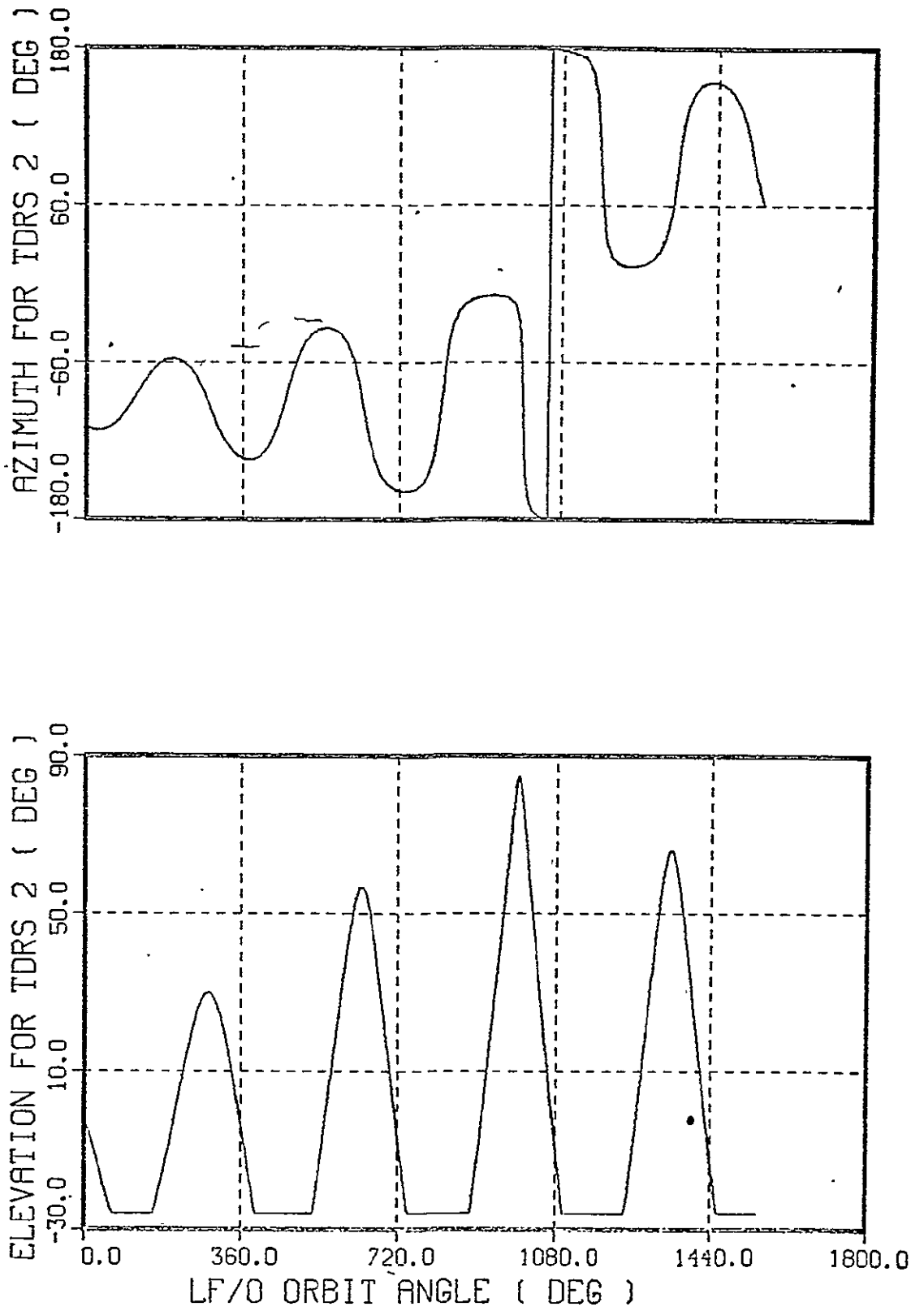

Figure 3-24. Zone of Exclusion Over Daylight.

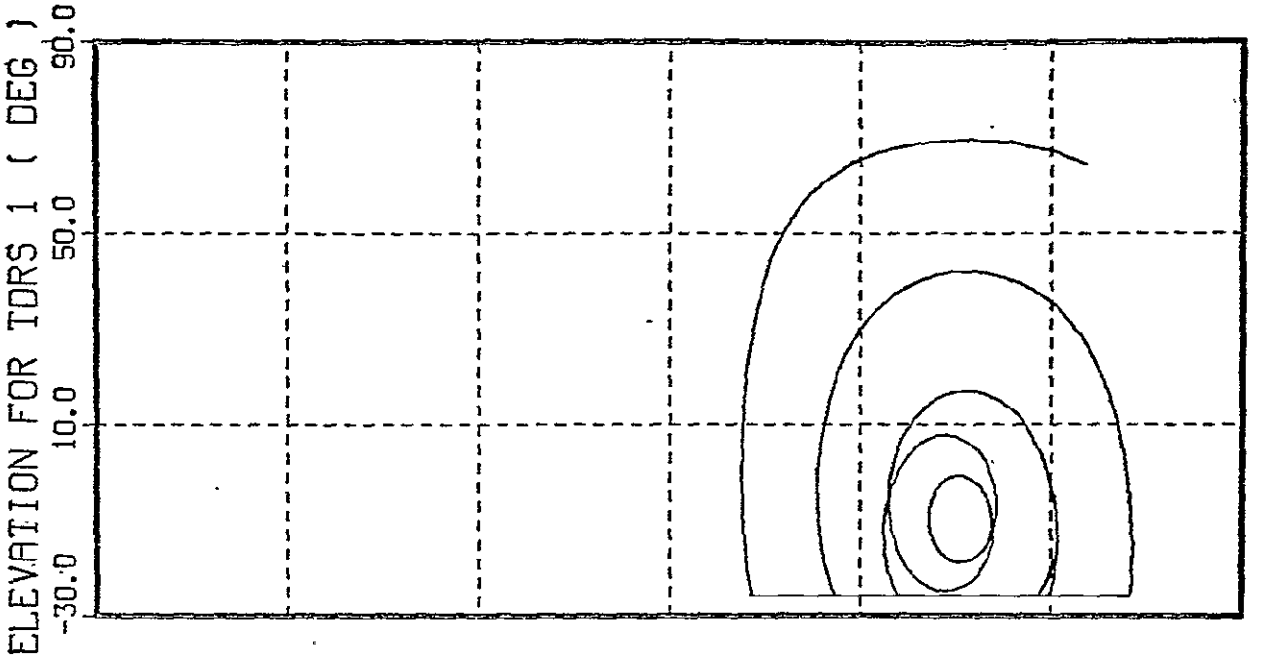

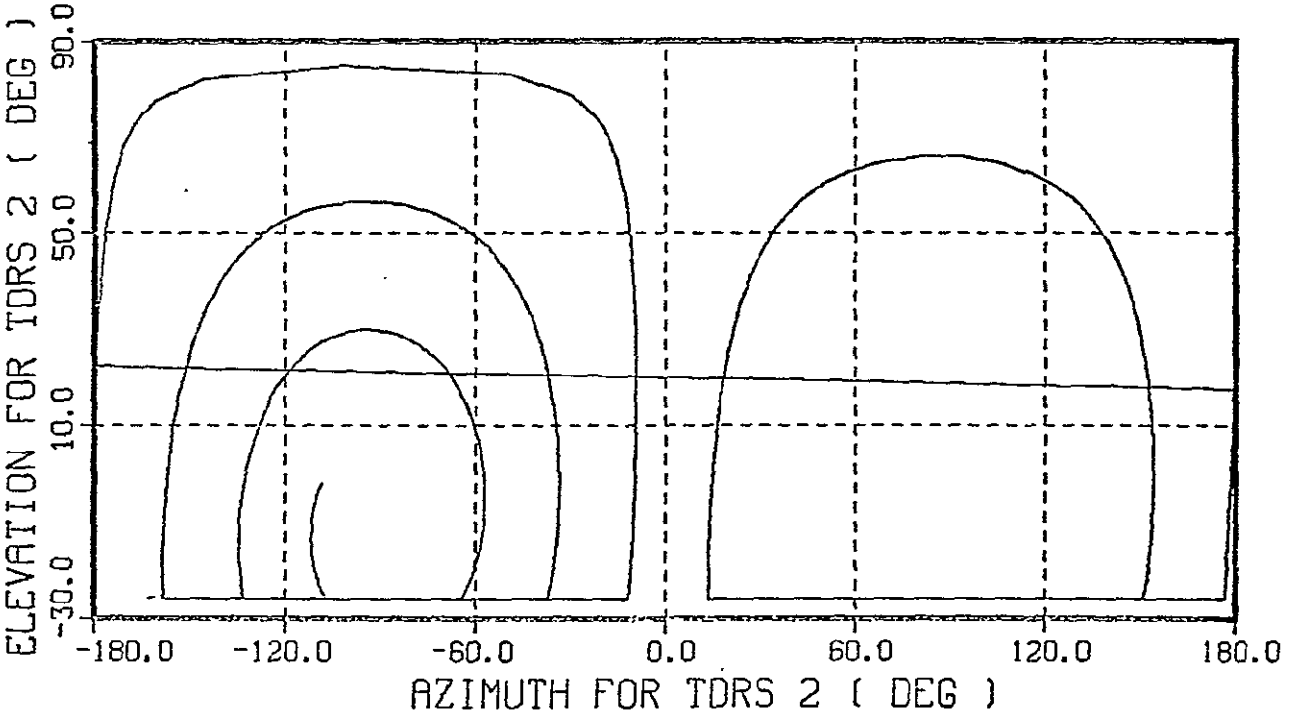

Figure 3-25. Zone of Exclusion Over Daylight

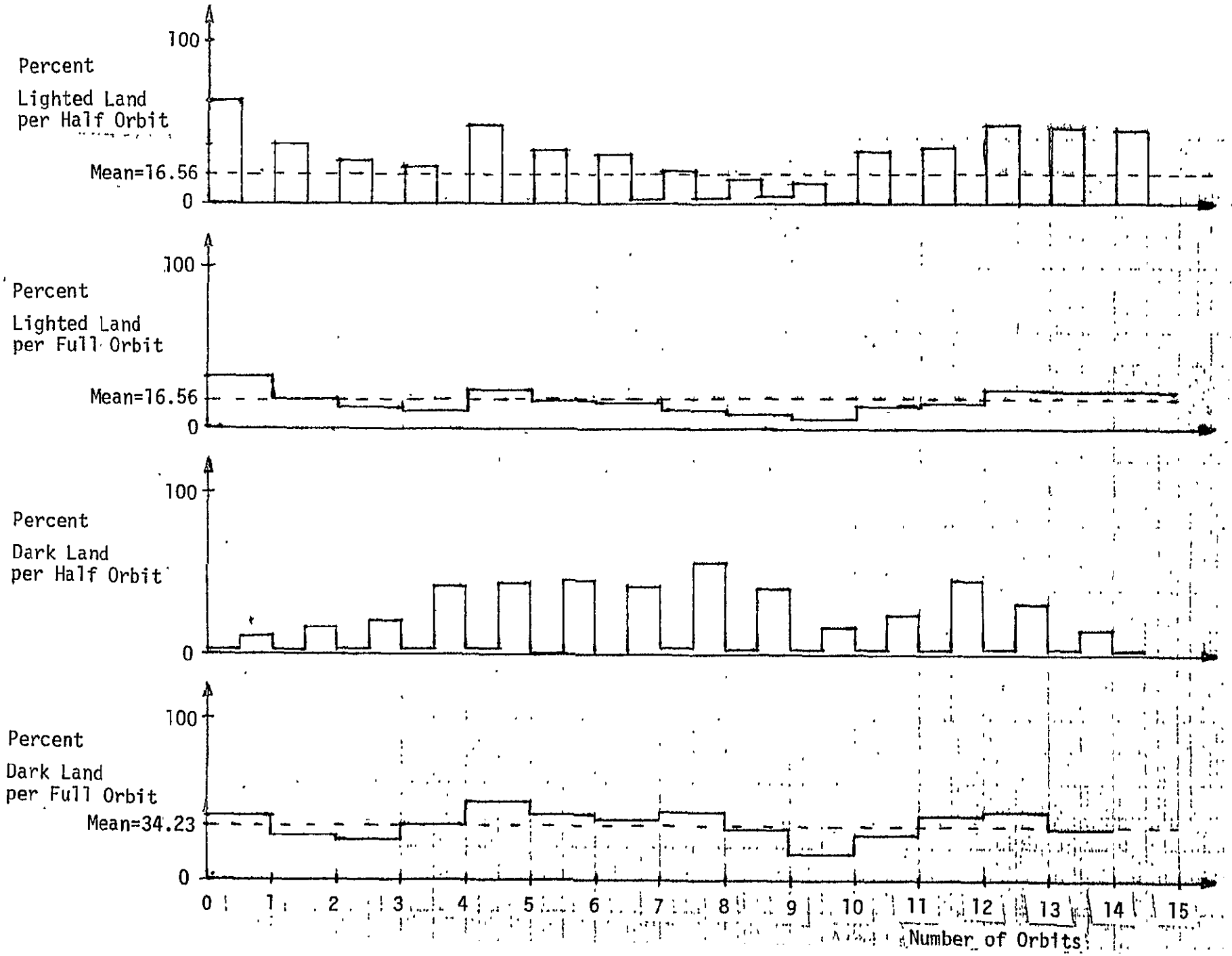

Figure 3-26. 24-Hour Run: Percent Lighted Land

Note that in the percent per half orbit plots in Figure 3-26, the lighted or dark land does not always split exactly along the half orbit time line. The reason for this is the 98.2 degree orbit inclination and the half orbit definition as $\pm$ 90 orbital degrees from crossing the equator. On the light side of the orbit (descending path), for example, the spacecraft will reach dark land (the Antarctic) near its "southern" most point (90 orbital degrees after crossing the equator). This can be seen best on the "Percent Dark Land per Half Orbit" graph in Figure 3-26.

3.5 Solar Array Control to Minimize Interference with Antennta Beam

The purpose of this section is to support the recommendation of a solar array configuration and array control strategy such that optical interference with the Ku-band antenna beam is eliminated. This is to be accomplished under the constraint of keeping the antenna mast as short as possible (mainly for spacecraft for structural reasons), since a sufficiently long mast permitting the antenna a field of view above all obstacles presents itself as an obvious solution to the problem.

The L-D solar array can be stationary relative to the spacecraft, or it can be driven to rotate about the $\hat{y}_b$ axis and follow the sun. The former design has the advantage of not requiring a drive mechanism, but it also has the potential disadvantage of necessitating a longer Ku-band antenna mast. There are many options available in designing the solar array. Two assumptions were made to eliminate some of the unnecessary options:

(1) It is assumed that interference with TDRS transmission over earth night is acceptable.

(2) It is assumed that the array shape will be rectangular.

The spacecraft with the Ku-band antenna is shown in Figure 3-27. The antenna is a circular dish with a 0.91 meter (3 foot) radius mounted on and rotating about the end of the mast. The mast is mounted parallel to the $\hat{z}_b$ axis, as shown, but generally lies near the edge of the spacecraft

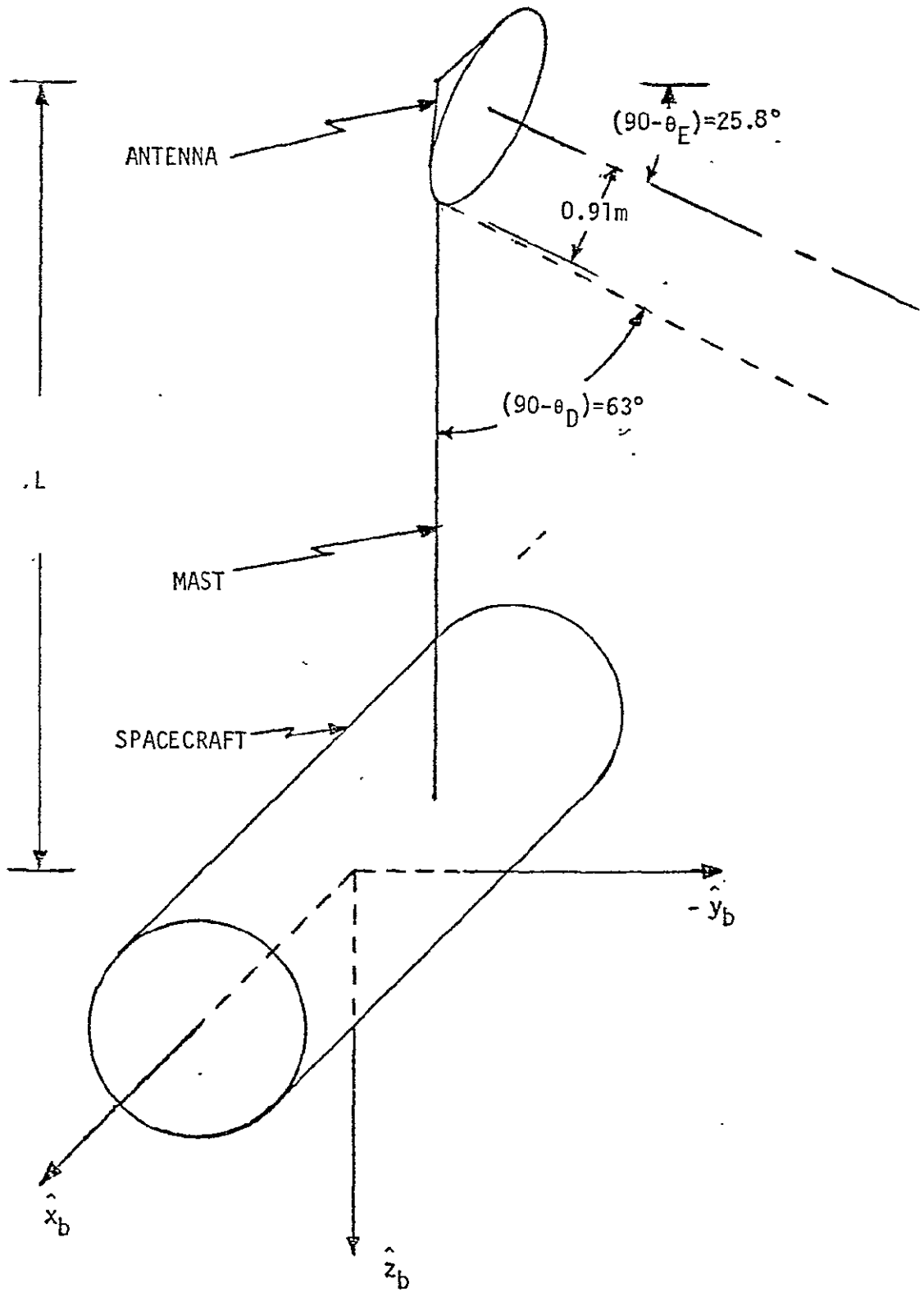

Figure 3-27. Ku-Band Antenna Mounted on Spacecraft

body rather than at the c.m. The mast length, L, is measured from the $\hat{x}_b$-$\hat{y}_b$ plane to the hinge point of the antenna; but note that the actual mast could be made shorter than this by mounting it on the top of the spacecraft instead of in the $\hat{x}_b$-$\hat{y}_b$ plane. The antenna field-of-view pattern is the 6 foot diameter cylinder extending out from the dish plus a 1 to 2 degree skirt -- the skirt is assumed to be 1.2 degrees in Figure 3-27. The antenna is only allowed to dip 25.8 degrees below the spacecraft horizontal, because that is where its line-of-sight grazes the earth -- 64.2 degree half angle.

The region which does not interfere with the antenna FOV is the 63 degree half angle cone centered on the mast with its apex at the point where the edge of the dish touches the mast. This apex of the cone is then given by A = (0.91 m)/(sin 64.2°) = 1.01 meter (3.33 feet) below the hinge point. Define a new coordinate system by shifting the body coordinate system so that the origin coincides with the base of the mast. Now, if the 3-tuple (x, y, z) is used to specify a point in this coordinate system, the set of points lying within the cone satisfies the inequality

$$x^2 + y^2 \leq L - \left(\frac{0.91}{\sin \theta_E}\right) + z^2 \cot^2 \theta_D \qquad (3.5\text{-}1)$$

where θ_E is the earth half angle and θ_D is the maximum angle by which the antenna beam dips below the horizontal.

3.5.1 The Driven Array

The driven array will be a rectangular array canted 37.5 degrees to the $-\hat{y}_b$ axis and rotating about the $\hat{y}_b$ axis so that its face remains normal to the sun line. When the spacecraft is in the ecliptic plane over earth day, this array is in the position shown in Figure 3-28, which is the position of least interference with the Ku-band antenna. As the L-D rotates out of the ecliptic, the array rotates about the $\hat{y}_b$ axis and moves toward the cone where it may interfere with the antenna. That interference is avoided by mounting the antenna at the end of a mast, but that mast should be as short as possible.

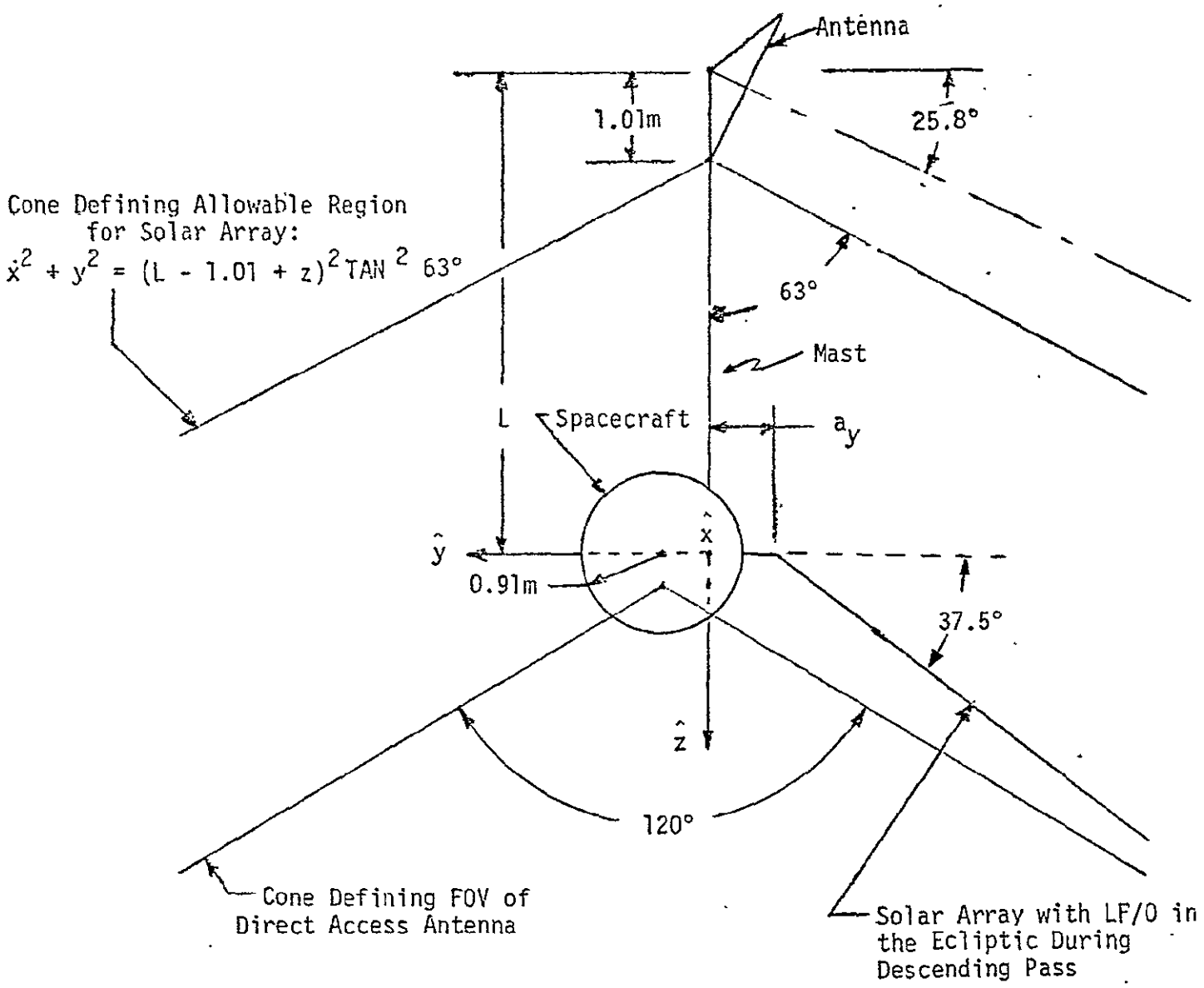

Figure 3-28. The Spacecraft with the Driven Array

The mast length can be minimized by proper choice of the shape of the rectangular array. The mast can also be kept short by keeping the array close to the position shown in Figure 3-28 while the antenna is transmitting. This can be accomplished by letting the array follow the sun whenever the spacecraft is over earth night but not eclipsed -- interference is acceptable -- and whenever the spacecraft is within some predetermined angle, θ_L, of the ecliptic. When the spacecraft is in the

remaining region, the array will be stationary at the position which would have it aligned with the sun at θ_L from the ecliptic (see Figure 3-29).

This approach reduces the average solar array power over an orbit. That average power is computed using

$$P_{avg} = \frac{1}{360} \int_0^{360} P(\theta)\, d\theta \qquad (3.5\text{-}2)$$

where θ is the orbit position of the L-D and $P(\theta)$ is the normalized instantaneous power measured as the projected array area normal to the sun line divided by the nominal area 11.89 m^2 (128 $foot^2$). The L-D is eclipsed by the earth when within $\pm$ 56.73 degrees of the ecliptic over the earth night, so if the array follows the sun throughout the orbit,

$$P(\theta) = \begin{cases} 0, & \text{in eclipse region} \\ 1, & \text{outside eclipse region} \end{cases} \qquad (3.5\text{-}3)$$

Thus,

$$P_0 = \frac{1}{360} \left\{ \int_{-33.27}^{213.27} \right\} d\theta = 0.6848 \qquad (3.5\text{-}4)$$

for this ideal case, where the zero angle is taken to be the point of the orbit where the L-D is 90 degrees of revolution ahead of the daylight crossing of the ecliptic. This number, P_0, represents the required average normalized power per orbit.

Now, if the array is stopped when the L-D is more than θ_L from the ecliptic, the average power per orbit with a 11.89 m^2 (128 $foot^2$) array would be given by:

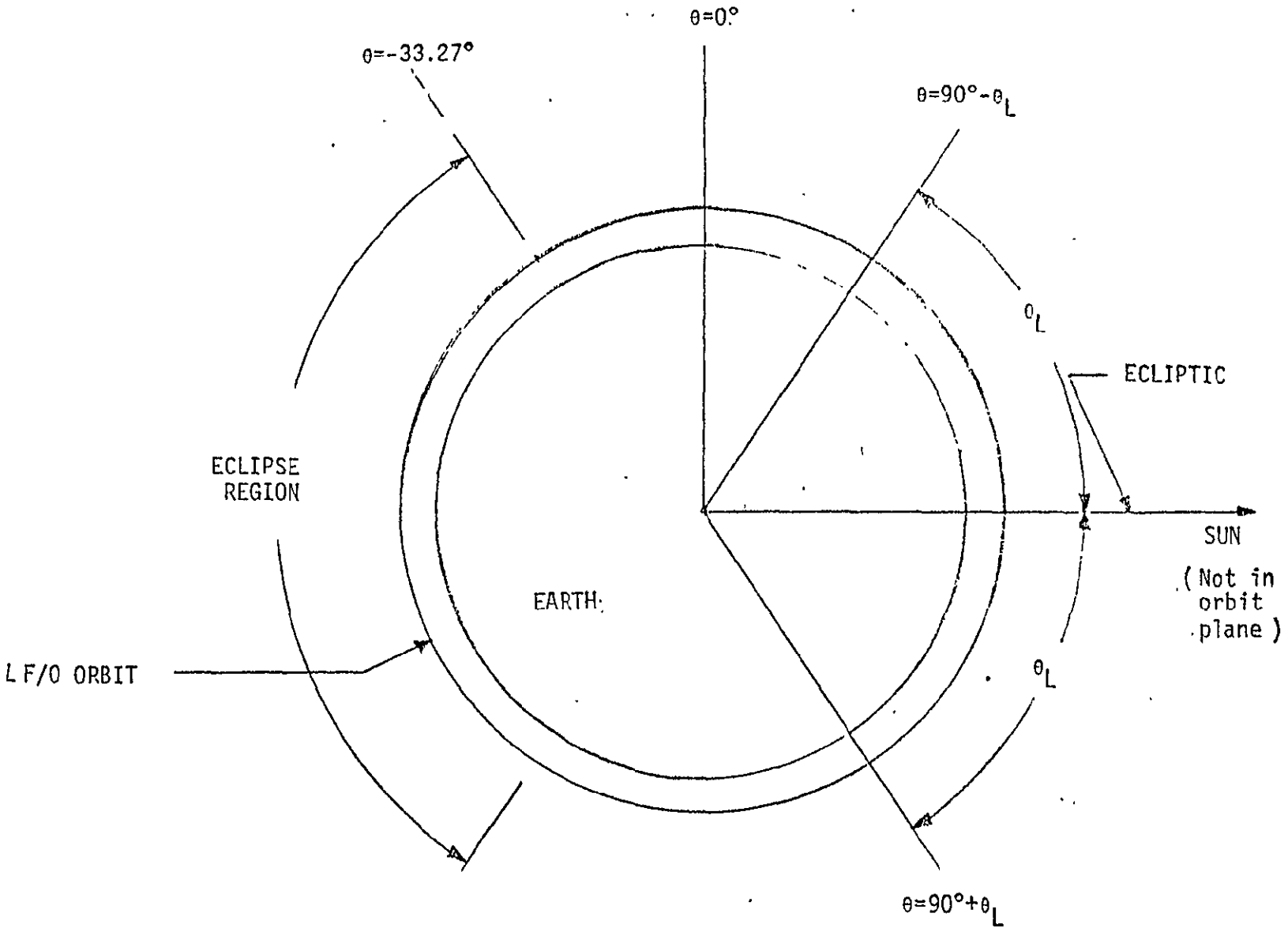

Figure 3-29. The LF/O Orbit

$$P_{avg} = \frac{2}{360} \left\{ \int_{-33.27}^{0} d\theta + \frac{180}{\pi} \int_{0}^{90-\theta_L} \cos(90 - \theta_L - \theta)\, d\theta + \int_{90-\theta_L}^{90} d\theta \right\} = \left[\frac{\theta_L + 33.27}{180} + \frac{\sin(90 - \theta_L)}{\pi} \right] \qquad (3.5\text{-}5)$$

The efficiency is given by

$$\eta = \frac{P_{avg}}{P_0} \times 100\% = \frac{100\%}{P_0} \left\{ \frac{\theta_L + 33.27}{180} + \frac{\sin(90 - \theta_L)}{\pi} \right\} \qquad (3.5\text{-}6)$$

The efficiency is plotted versus θ_L in Figure 3-30.

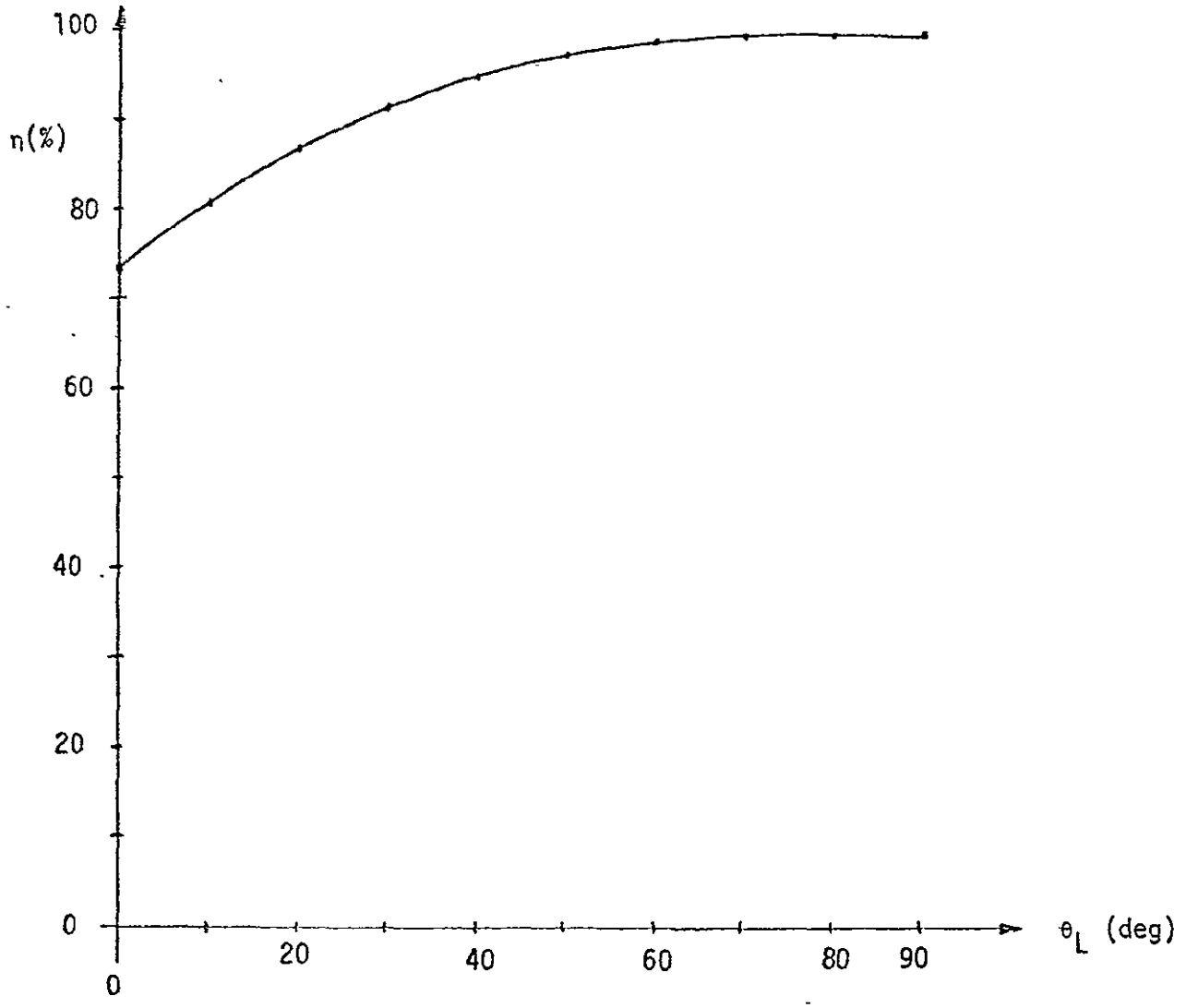

Figure 3-30. Solar Array Efficiency versus Stop Angle θ_L from the Ecliptic

In summary, the approach, wherein the array does not follow the sun throughout the orbit, reduces the average solar array power over an orbit. The overall reduction is on the order of 4% and relatively insignificant. It can also easily be compensated by a correspondingly small increase in array area.

The minimum mast length can be determined by comparing the location of the worst-case point of the array with the cone represented by Equation (3.5-1). The worst case point on the array is some point on the "top" edge when the array is rotated the maximum amount toward the antenna -- θ_L degrees from the lowest point as shown in Figure 3-28. It is obvious that because the cone is convex the worst case point is at one end or the other of the top edge. Let the vector representing one of these points be $\bar{c}$. Then, from Equation (3.5-1), the minimum mast length so that the point $\bar{c}$ does not lie in the FOV of the antenna is given by

$$L_{MIN} = \sqrt{c_x^2 + c_y^2} \tan \theta_D + \frac{3}{\sin \theta_E} - c_z \qquad (3.5\text{-}7)$$

Let the array have length ℓ, measured along the shaft, and width ω. Now, the unit vector along the array shaft is

$$\hat{\ell} = [\theta_L - 90]_y [\theta_c]_z \begin{bmatrix} 0 \\ -1 \\ 0 \end{bmatrix} = \begin{bmatrix} -\sin \theta_c \sin \theta_L \\ -\cos \theta_c \\ \sin \theta_c \cos \theta_L \end{bmatrix} \qquad (3.5\text{-}8)$$

where θ_c is the array cant angle -- nominally 37.5 degrees -- and the rotation $[a]_v$ means a rotation of the coordinate system through the angle α about the v axis. The unit vector along the end of the array is

$$\hat{\omega} = \begin{bmatrix} -\cos \theta_L \\ 0 \\ -\sin \theta_L \end{bmatrix} \qquad (3.5\text{-}9)$$

Using these unit vectors, the vector representing an arbitrary point of the top edge of the array is

$$\bar{c}_\alpha = \alpha \ell \hat{\ell} + \frac{\omega}{2} \hat{\omega} + \bar{a} \qquad (3.5\text{-}10)$$

where $\bar{a}$ is the vector representing the close end of the array shaft and $\alpha \in [0,1]$ determines the particular point of the top edge -- the two points of interest are $\bar{c}_0$ and $\bar{c}_1$. The vector elements a_x and a_z are assumed to be 0, and a_y is nominally 0 but may be as much as -0.91 (3 feet). Equations (3.5-6), (3.5-7) and (3.5-10) were used to create Table 3-14 showing the baseline design and several variations.

It is evident by comparing the first and last entries of Table 3-14 that the baseline design is much better than having the array follow the sun throughout the orbit. Note also that for a shallow array rotation angle such as θ_L = 45 degrees the FRUSA* array is nearly as good as the best rectangular array. Further, the table shows that only a slight increase in array area is needed to bring the efficiency up to 100%. Recalling that the actual mast length could be smaller than that shown by mounting it higher up on the spacecraft, it is concluded that a normal boom rather than an Astro-mast type boom is sufficient for mounting the antenna.

This baseline design is recommended as the rotating array design. The array rotation scenario for an orbit is as follows: as the L-D comes out of eclipse, the array tracks the sun until the northern terminator is reached -- this is within 23.5 degrees of the North Pole depending on the season; during this period the array could be in the antenna FOV, but there is no Thematic Mapper data to transmit. At the northern terminator, the array "jumps" ahead approximately** 45 degrees and stops until the L-D travels a compensating 45 degrees. At this time, the array is again driven to follow the sun through 90 degrees of L-D travel where it again stops

*6.33 foot wide Flexible, Roll Up Solar Array with 5 foot wide cell region.
**Inclination i = 98.2° $\pm$ 90°.

Table 3-14. Various Driven Array Configurations

Mast-Array Separation a_y (m) (Fig. 2-2)	Array Cant Angle, θ_c (deg)	Angle from Ecliptic within which the Array tracks the Sun θ_L (deg)	Maximum Antenna Dip Angle, θ_D (deg)	Solar Array Actual Surface Area, (m^2)	Efficiency (%)	Minimum Mast Length for FRUSA (m) (1.52 m = 5 ft wide cell reg.)	Optimal Array Width (m)	Minimum Mast Length (m)
0	37.5	45	27	12.32	100	2.11	0.90	1.82
0	37.5	45	27	11.89	96.37	2.11	0.89	1.80
0	37.5	40	27	12.49	100	2.01	----	----
0	37.5	50	27	12.20	100	2.55	1.41	2.35
0	30	45	27	12.32	99.14	2.84	1.85	2.63
0	30	45	27	12.43	100	2.85	1.85	2.64
0	37.5	45	28	12.32	100	2.28	1.16	2.06
-0.61	37.5	45	27	12.32	100	2.38	0.91	2.09
0	37.5	60	27	11.89	98.91	3.41	2.04	3.11
0	37.5	70	27	11.89	99.68	4.29	2.56	3.70
0	37.5	90	27	11.89	100	5.96	2.75	4.50

until the L-D reaches the southern terminator at which point the array catches up. Finally, the array tracks the sun into eclipse and the process is repeated for the next orbit. This design insures that the array will not interfere with the antenna during transmission periods, but on many orbits the array can follow the sun throughout without interference due to the favorable TDRS locations. This subject can be studied more thoroughly using the computer program presented in Section 3.4. Note also that while the L-D is eclipsed by the earth, the array position is immaterial; thus it could be moved out of the way of the antenna to allow data transmission at night.

3.5.2 The Fixed Array

If the solar array is to be fixed relative to the spacecraft so that it can not follow the sun, it should always have the same area normal to the sun line. Since the sun cones about the vehicle pitch axis, the array should be mounted normal to this axis as shown in Figure 3-31. In this configuration, the solar array position can be moved along the $\hat{z}_b$ axis. Thus, the only fixed distance to be considered is the distance from the lower edge of the array to the antenna pivot point; this is the dimension h in Figure 3-31. The antenna position is assumed to be directly over the array in the baseline design.

The largest rectangular array that can be enclosed by the triangle as shown has height a and base b where

$$a = \frac{1}{2}\left(h - \frac{0.91}{\sin \theta_E}\right) \tag{3.5-11}$$

and

$$b = \frac{1}{\tan \theta_D}\left(h - \frac{0.91}{\sin \theta_E}\right) \tag{3.5-12}$$

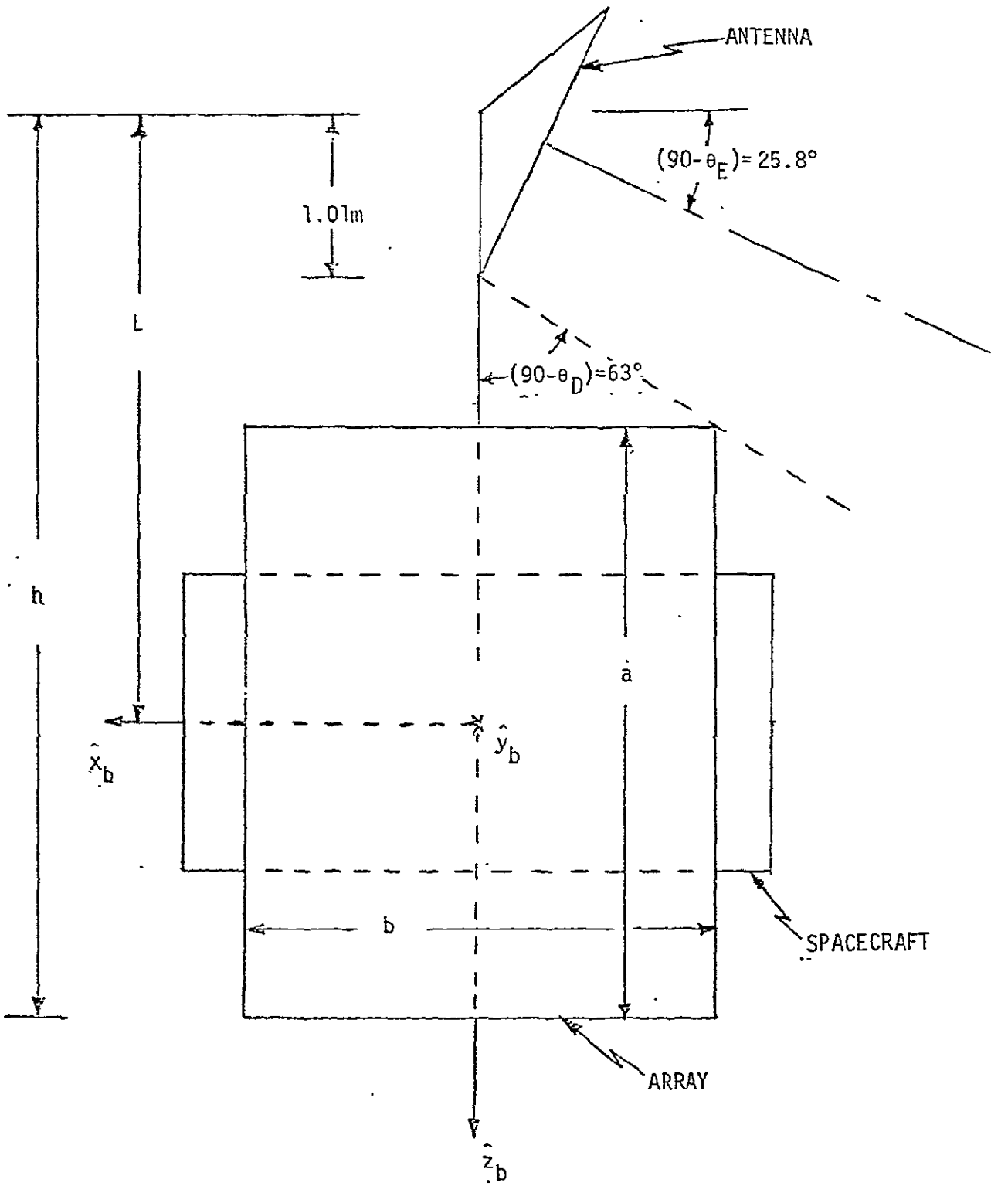

Figure 3-31. Location of Fixed Array on Spacecraft

Then the area is given by

$$A = ab = \frac{1}{2 \tan \theta_D} \left(h - \frac{0.91}{\sin \theta_E} \right)^2 \qquad (3.5\text{-}13)$$

For this design, the sun strikes the array at an angle of 52.5 degrees, so the area must be

$$A = (11.89\ m^2)/(\cos 52.5°) = 19.53\ m^2\ (210.26\ ft^2) \qquad (3.5\text{-}14)$$

and Equation (3.5-13) results in h_{min} = 5.47 m (17.95 feet).. The lower edge of the array can not be much more than 0.61 m (2 feet) below the $\hat{x}_b$-$\hat{y}_b$ plane without interfering with the direct access antenna. Thus the mast length, L, as defined earlier would have to have a length at least L = 4.88 m (16 feet).

This required mast length would be increased still further if the antenna were laterally offset from the array. Also, any change in the sun incidence angle would cause a change in the array size and thus the mast length. For example, if the descending node occurred at 10:00 a.m. instead of 9:30 a.m., the array area would become A = 23.78 m^2 (256 $foot^2$) and the required mast length would be increased to 5.33 m (17.5 feet).

3.5.3 Recommended Solar Array Configuration

Each of the two solar array configurations -- the fixed array and the driven array -- described above are satisfactory. The fixed array has the advantage of not requiring a drive mechanism, but it has the disadvantages of increased size, weight and cost. Also, the fixed array requires a much longer antenna mast; this extra mast length is undesirable because it affects the spacecraft and antenna flexible dynamics. The driven array would exhibit dynamic interaction with the spacecraft, but this would probably be a smaller effect than that due to the structural flexibility of the large fixed array. Based on the above tradeoffs, the driven FRUSA array as shown in line 1 of Table 3-14 is recommended.

4.0 DISTURBANCE TORQUES AND MOMENTUM MANAGEMENT FOR LANDSAT-D

This section summarizes the results of a disturbance torque-momentum management investigation for the present concept of the LANDSAT spacecraft configuration. The purpose is to determine magnetic unloading torque levels and associated peak stored momentum values which will indicate if standard reaction wheels and torquer magnets are sufficient for the design of the system. Detailed disturbance torque models and an ideal spacecraft with zero attitude errors are used to establish torque and momentum patterns and magnitudes. Based on the disturbance torque signals for one orbit, a Fourier coefficient set is compiled which approximates the spectral content of the disturbances. These may be used in later simulations as simplified disturbance models. Eclipse conditions occurring for the 9:30 a.m. sun-synchronous orbit are included in the disturbance model.

Based on the results of this study, it appears that the single 50,000 pole-cm magnet windings are sufficient for momentum unloading. Thus the two windings per magnet may be used in a redundant mode. Only a short interval of magnet command limiting at 50,000 pole-cm is observed per orbit.

Momentum excursions of less than 2.0 N-m-s occur at all axes. This is considerably less than the allowable excursion of 7.32 N-m-s for speed-biased operation of the wheels with equal allowed excursions for all wheels. Thus it is concluded that the 20 N-m-s NASA Standard Reaction Wheels are sufficient for the design.

Sensitivity to antenna mast heights is not dramatic for the heights presently under consideration. These effects, and the effects of antenna orientation, are thus not a major concern with regard to momentum storage and disturbance torques.

4.1 Spacecraft Model

The diagrams in Figure 4-1 display the pertinent measurements for the LANDSAT. Since antenna height has not been definitely decided upon, it is treated as a parameter to obtain an estimate of its effects on the

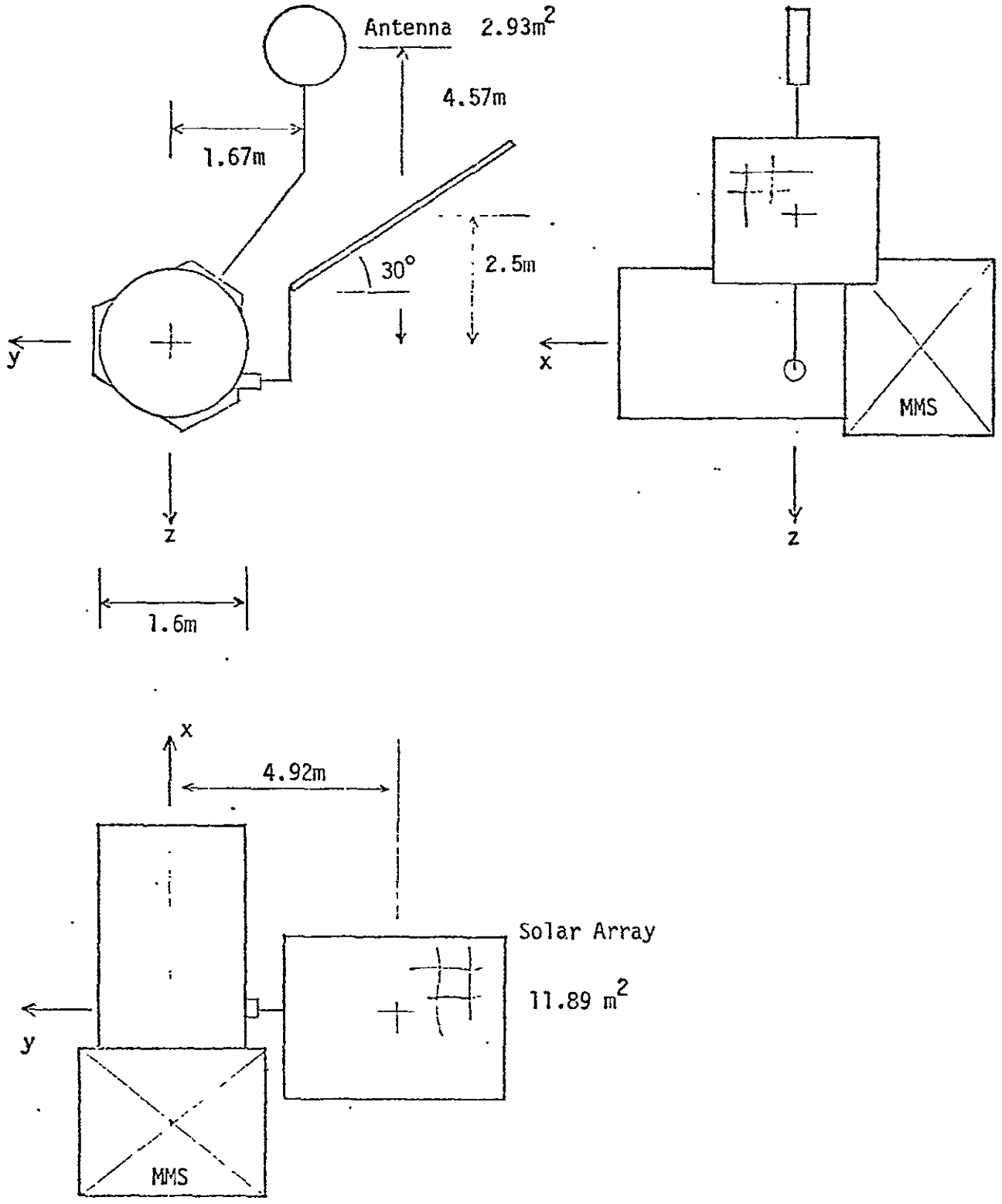

Figure 4-1. Simplified LANDSAT Configuration Schematic for Solar and Aero Disturbances

disturbance torques. Various antenna orientations, primarily looking forward or zenith, are considered to also determine their effect on disturbance levels. These orientations are chosen because the antenna coverage pattern is approximately a hemisphere over the minus $\hat{Z}$ body axis. The spacecraft model consists of a standard configuration for the MMS ACS, CDH, power modules, and adapter plate. For simplicity, the payload is modelled as a cylinder with an end plate since more refined surface models are not available. The sun pointing array is modelled as a flat plate that rotates at a cone angle of *30 degrees in body coordinates, and the antenna is modelled as a thin wide cylinder at mast heights of 3.05 m (10 feet), 4.57 m (15 feet) and 6.10 m (20 feet).

Since the array rotates in body coordinates, its center of pressure varies for aerodynamic torque calculations. This time varying function is modelled in the simulation. The time varying surface normal to the solar panel from the sun is also computed.

Moments of inertia for the present configurations are I_{xx} = 2033.7 kg-m^2, I_{yy} = 2670 kg-m^2, and I_{zz} = 2372.7 kg-m^2. Weights are 1496.6 kg for the spacecraft and 22.7 kg for the solar array and for the antenna. The relatively small effects of a time varying inertia matrix are not modelled. Cross products of inertia are also time-varying, depending primarily on array position. These affect primarily the gravity gradient torques, and are modelled as an average of 271.2 kg-m^2 in all axes.

For a specified antenna mast size, the center of mass (c.m.) of the spacecraft moves slightly as the antenna is rotated. The maximum distance is on the order of 1 inch (2.54 cm), and thus a fixed average c.m. is chosen for the model. Changes are included for various antenna heights.

Table 4-1 summarizes the solar-aero surface model data for the present study. An antenna height of 4.57 m (180 inches) is shown in the table.

---

*Based on Grumman layout drawing; a 9:30 a.m. orbit would correspond to an array cant angle of 37.5 degrees. The difference in the resultant disturbance torque is insignificant.

Table 4-1. LANDSAT Solar-Aero Model

Surface Description	Surface Number	Area (in^2)	Center of Pressure (in)			Inward Normal Vector			Reflect. ν	Acc. Coef. f_n, f_T
			r_x	r_y	r_z	n_x	n_y	n_z		
Solar Array Front	1	18432.	Time Varying, Inernal			Time Varying, Internal			0.2	0.85
Solar Array Back	2	18432.							0.56	0.85
Interface Back	3	828.	48	0	0	1	0	0	0.56	0.85
(Spare)	4	0	0	0	0	0	0	1	0.56	0.85
ACS Module	5	2304	24	31.9	0	0	-1	0	0.56	0.85
	6	864	24	22.9	-24	0	0	1	0.56	0.85
	7	864	24	22.9	24	0	0	-1	0.56	0.85
CDH Module	8	2304	24	-15.95	-27.6	0	0.5	0.866	0.56	0.85
	9	864	24	19.5	-31.8	0	-0.866	0.5	0.56	0.85
	10	864	24	-32.2	-7.79	0	0.866	-0.5	0.56	0.85
Power Module	11	2304	24	-15.9	27.6	0	0.5	-0.866	0.56	0.85
	12	864	24	19.5	31.8	0	-0.866	-0.5	0.56	0.85
	13	864	24	-32.2	7.79	0	0.866	0.5	0.56	0.85
Spacecraft Bottom	14	4010	0	0	0	1	0	0	0.56	0.85
Interface Front	15	1979	48	0	0	-1	0	0	0.56	0.85
Payload Front	16	3040	145	0	0	1	0	0	0.56	0.85
Antenna Front	17	4536	72.58	-66	-180	0	0	1	0.56	0.85
Antenna Back	18	4536	72.58	-66	-180	0	0	-1	0.56	0.85
Payload Body Cyl.	19	*	100	0	0	1	0	0	0.56	0.85
Antenna Edge	20	**	72.58	-66	-180	0	0	1	0.56	0.85

*Dia = 62.2, Length = 89.9
**Dia = 76.0, Length = 10.0

4.2 Disturbance Models

A standard detailed earth magnetic dipole field model is used as the source of the magnetic disturbance torques and for the generation of the unloading torques. It is described, for example, in [1] and is not repeated here. A spacecraft residual magnetic moment of 10,000 pole-cm at a fixed random orientation is used. Based on a commonly used estimate of 1 pole-cm per pound of weight, the 10,000 pole-cm value is conservative. Provision is made for rotation of the dipole field as a result of earth rotation, but over the short time of one or three orbits considered here, this effect is very small and is set to zero.

Solar torques are computed as a function of position in orbit and relative sun location using the detailed surface model. An eclipse condition is included to zero the solar torques within an angle of $\pm$ 56.7 degrees of the ascending node*. Shading effects which may be present during portions of the orbit are not included.

Aerodynamic torques are computed with the detailed surface model used for the solar torques. Gravity gradient torques are computed using the complete theoretical expressions, but the use of an idealized spacecraft with zero attitude errors results in constant gravity gradient torques resulting from the assumed cross products of inertia. Otherwise the periodic orbital variations in other disturbance torques would result in small attitude errors and resulting periodic content in the gravity gradient torques.

The theoretical expression for the gravity gradient torque is given by

$$\overline{T}_g = 3 w_o^2 \overline{R} \times (\overline{\overline{I}} \cdot \overline{R})$$

*Assuming an equinox.

where

w_o - is the orbit rate

$\bar{R}$ - is the distance to the center of the earth

$\bar{\bar{I}}$ - is the inertia dyadic

From the preceding equation, the gravity gradient torque expressions are

$$T_{gx} = 3 w_o^2 [(I_{zz}-I_{yy}) \phi - I_{xy} \theta + I_{yz}]$$

$$T_{gy} = 3 w_o^2 [-(I_{xx}-I_{zz}) \theta - I_{xy} \phi - I_{xz}]$$

$$T_{gz} = 3 w_o^2 [I_{xz} \phi + I_{yz} \theta]$$

and by setting the pitch angle error θ to zero, the following expressions are obtained for small ϕ angles.

$$\frac{T_{gx}}{\phi} = 3 w_o^2 (I_{zz}-I_{yy}) \quad \frac{N\text{-}m}{rad}$$

$$\frac{T_{gy}}{\phi} = -3 w_o^2 I_{xy} \quad \frac{N\text{-}m}{rad}$$

$$\frac{T_{gz}}{\phi} = 3 w_o^2 I_{xz} \quad \frac{N\text{-}m}{rad}$$

These may be used to estimate gravity gradient torques for small ϕ angles. Similarly, the relations

$$\frac{T_{gx}}{\theta} = -3\,\omega_o^2\,I_{xy} \quad \frac{N\text{-}m}{rad}$$

$$\frac{T_{gy}}{\theta} = -3\,\omega_o^2\,(I_{xx}-I_{zz}) \quad \frac{N\text{-}m}{rad}$$

$$\frac{T_{gz}}{\theta} = 3\,\omega_o^2\,I_{yz} \quad \frac{N\text{-}m}{rad}$$

yield torques for small θ attitude errors.

4.3 Momentum Unloading System

Magnetometers are used to sense the earth's $\overline{B}$ field, and a magnetic moment $\overline{M}$ is generated by the three-axis arrangement of the bars. The command $\overline{M}$ is generated according to the linear law

$$\overline{M} = -K\,\overline{B} \times \overline{H}_e$$

where K is a suitable constant and $\overline{H}_e$ is the momentum error vector. The preceding unloading law may be arrived at either by minimization of an error $\overline{e}$ between $\overline{M} \times \overline{B}$ and $-K\,\overline{H}_e$ or by geometric considerations. This control law is simulated to obtain continuous momentum unloading of the reaction wheels.

The dipole magnets for the generation of $\overline{M}$ are available in standard sizes of two 50,000 pole-cm windings on a single core. Those windings may be used singly in which case one winding is redundant for backup purposes, or they may be used together to obtain 1×10^5 pole-cm with no redundancy. The choice is determined by the on-orbit torque levels that are required.

4.4 Stored Momentum Determination

It is desired to use the NASA Standard Reaction Wheel (SRW) for reaction torque and angular momentum storage. This is a 20 N-m-s wheel and in the present application four of them will be used in a speed-biased

arrangement. It is thus necessary to determine if the orbital momentum variations remain below the maximum allowable as measured from the nominal speed-biased momentum value. In fact, it is desired to operate the wheels as closely as possible to the speed bias.

To do that, disturbance and magnetic unloading torques are computed for an idealized spacecraft in a simulation. The net external torque on the spacecraft is transformed to inertial space, integrated to provide inertial momentum, and transformed back to body coordinates. Since perfect attitude control is assumed, the momentum in body coordinates represents stored wheel momentum as a function of orbital position. The roll, pitch and yaw momenta may be resolved into wheel axes to obtain the excursions from nominal speed-biased momenta.

4.5 Results

Initial results indicated that magnet signals slightly in excess of 50,000 pole-cm would be required for momentum unloading. Thus magnet command limits of 50,000 pole-cm were applied to determine if unloading could be accomplished using just one winding. The results are summarized in Table 4-2 for 4.57 and 6.10 meter antenna heights.

Table 4-2. Maximum Magnet Commands and Reaction Wheel Momenta

Antenna, Position	$\lvert\bar{M}\rvert_{max}$ pole-cm	$\lvert\bar{h}\rvert_{max}$ N-m-s
4.57 m, looking $-\hat{Z}$	61,864	1.78
4.57 m, looking $+\hat{X}$	60,073	1.86
6.10 m, looking $+\hat{X}$	58,947	1.85

The magnet commands and limiting are more apparent in the plots of Figure 4-2a. There it is seen that only the pitch magnet is saturated at 50,000 pole-cm, and only for a brief portion of the orbit near the descending node. Although the desired unloading level is not achieved during this time, the system carries the momentum error until it can be unloaded thus keeping the resultant momentum less than 2.0 N-m-s. Later paragraphs examine allowable momenta levels, but accepting the 1.86 N-m-s as permissible it can be concluded that the single winding 50,000 pole-cm is sufficient. Thus the magnets may be used in redundant mode.

The total external disturbance torques are shown in Figure 4-2b. Since eclipse occurs at $\pm$ 56.7 degrees from the ascending node, a check is easily made on the magnitude of the jump in the solar torques. Without allowing for antenna effects, the values should be

$4.07 \times 10^{-4} \cos 56.7° = 2.23 \times 10^{-4}$ N-m roll

$4.07 \times 10^{-4} \sin 56.7° = 3.40 \times 10^{-4}$ N-m yaw

These agree closely with the plot values.

From Table 4-2 and from the series of plots in Figure 4-2, it is also seen that the sensitivity to antenna mast height and antenna orientation is fairly small. This is of interest in estimating effects of possible configuration changes. Studies made with a 3 m antenna height show disturbance torques and stored momenta slightly less than for the 4.57 m antenna mast. Since the latter are acceptable, the 3 m results are also acceptable and are not tabulated here.

For four reaction wheels in speed-biased operation, with one wheel on each of three major body axes and the fourth wheel equiangularly placed from the other three, a vector diagram shows that the fourth wheel should have $-\sqrt{3}$ time the (equal) momentum in the other three wheels for a net zero momentum. And to give all wheels equal momentum ranges, a simple calculation shows that the bias momentum should be 7.32 N-m-s for wheels

Figure 4-2a. 4.57 m Antenna, Zenith Pointing: Magnetic Moments

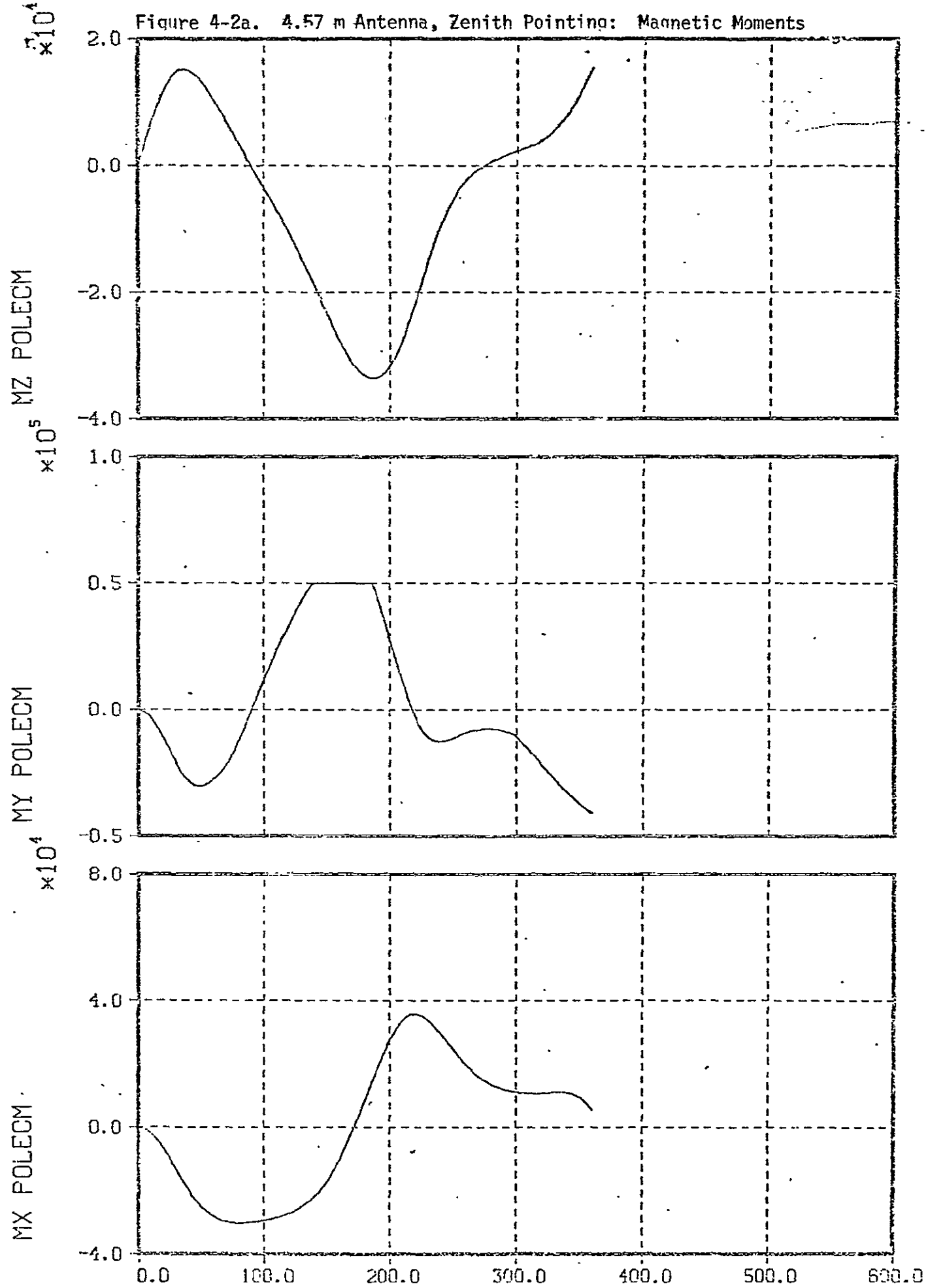

Figure 4-2b. 4.57 m Antenna, Zenith Pointing: Disturbance Torques

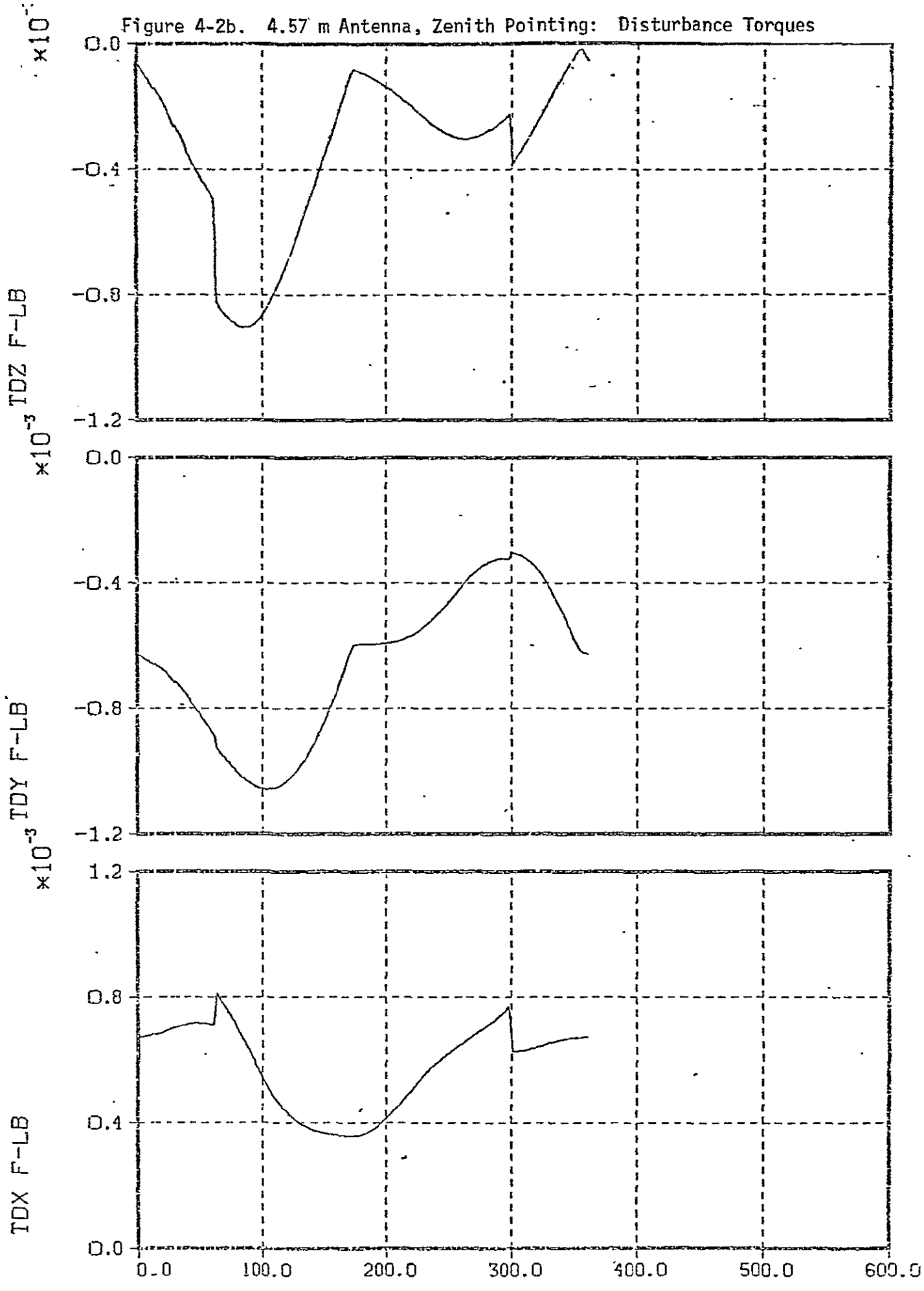

Figure 4-2c. 4.57 m Antenna, Zenith Pointing: Wheel Momenta

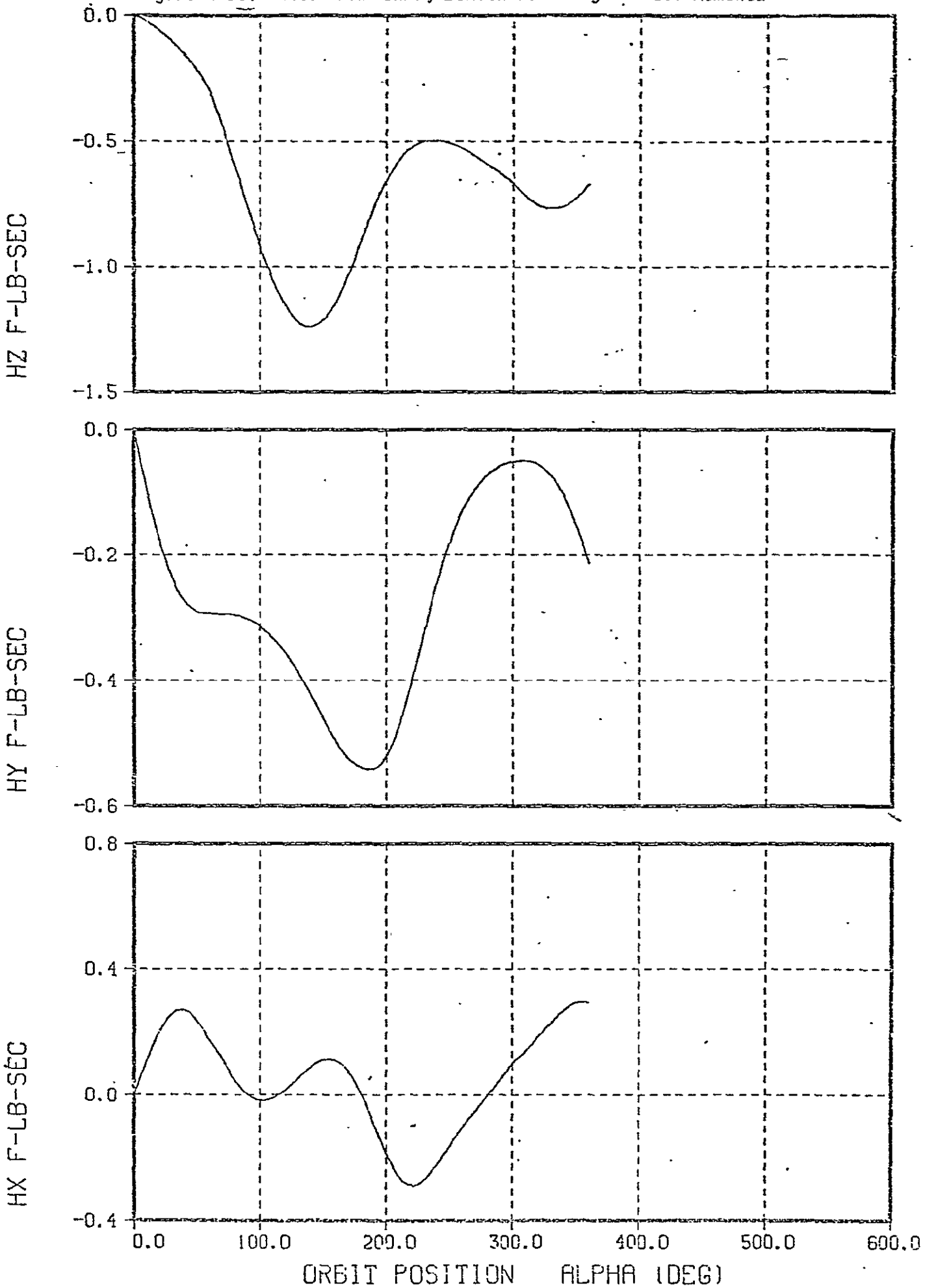

Figure 4-2d. 4.57 m Antenna, Pointing Ahead: Magnetic Moments

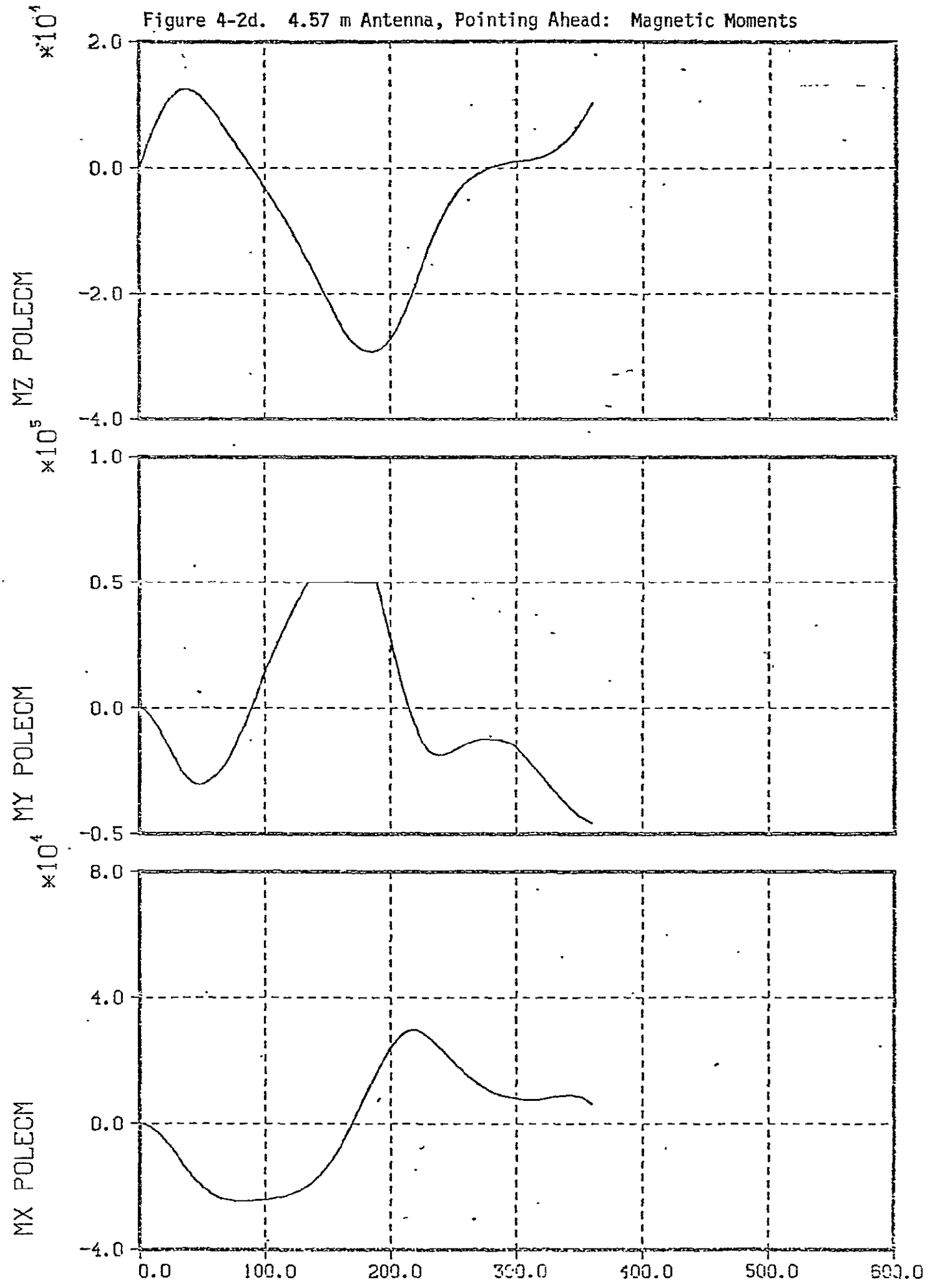

Figure 4-2e. 4.57 m Antenna, Pointing Ahead: Disturbance Torques

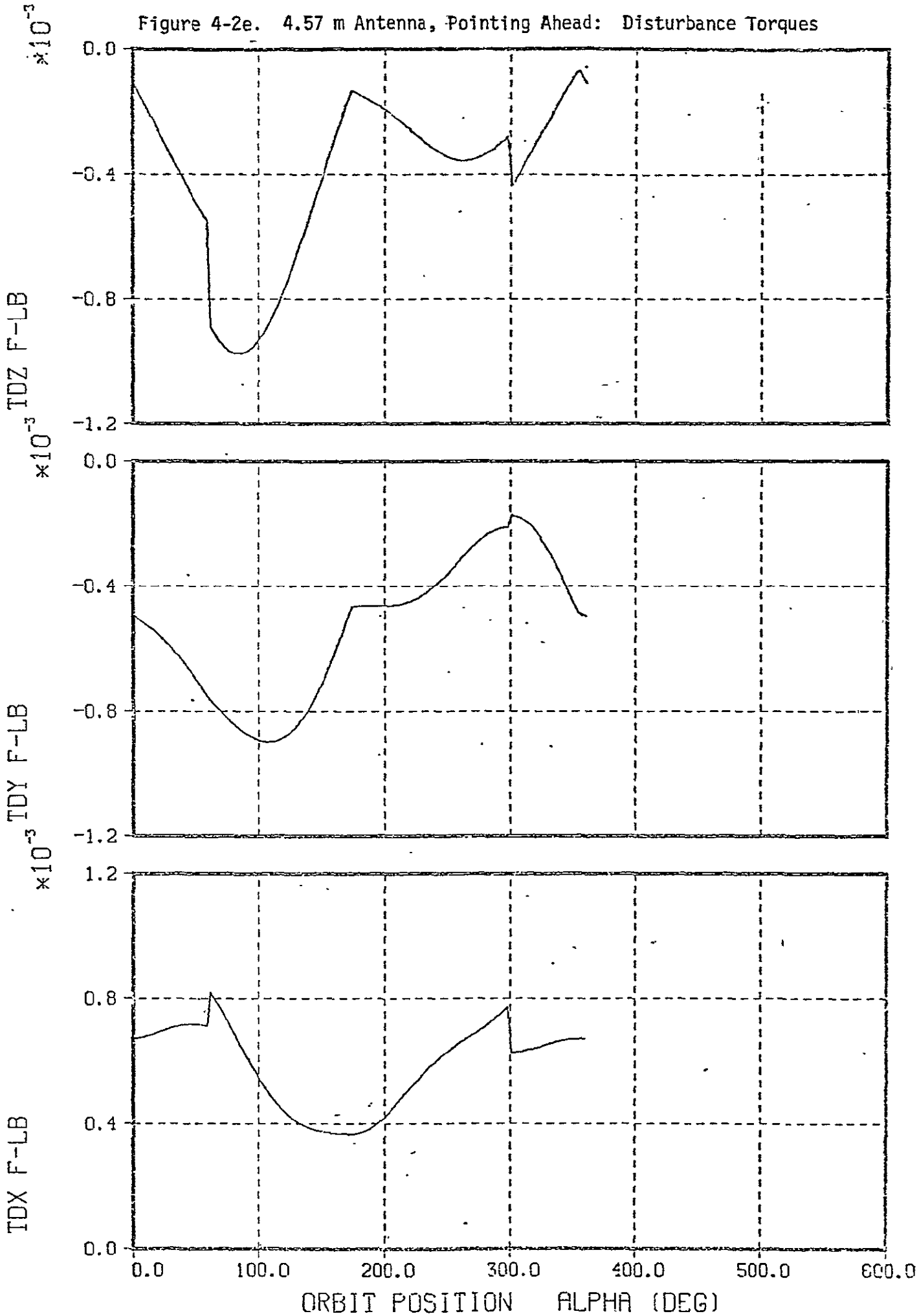

Figure 4-2f. 4.57 m Antenna, Pointing Ahead: Wheel Momenta

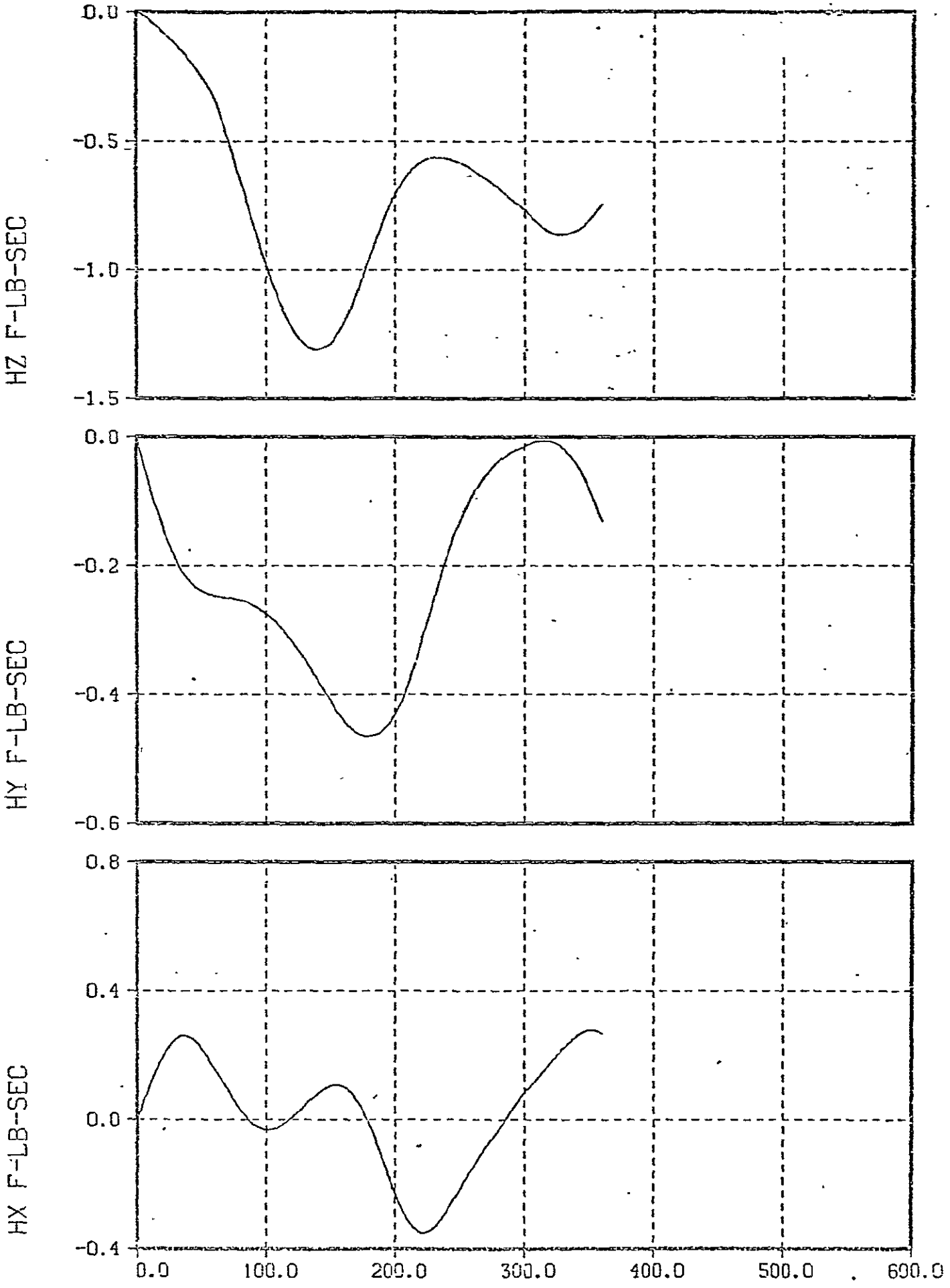

Figure 4-2g. 6.1 m Antenna, Pointing Ahead: Magnetic Moments

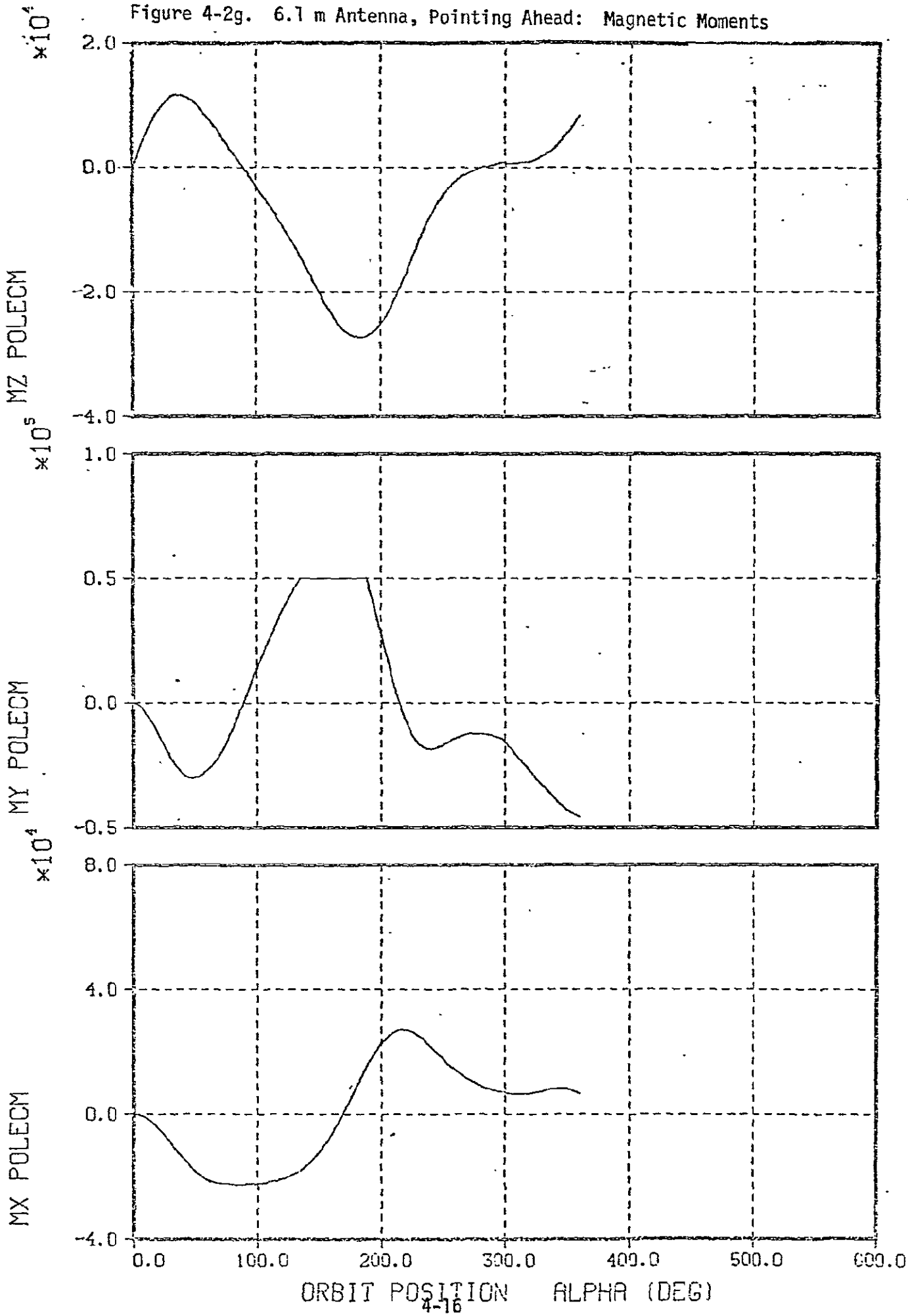

Figure 4-2h. 6.1 m Antenna, Pointing Ahead: Disturbance Torques

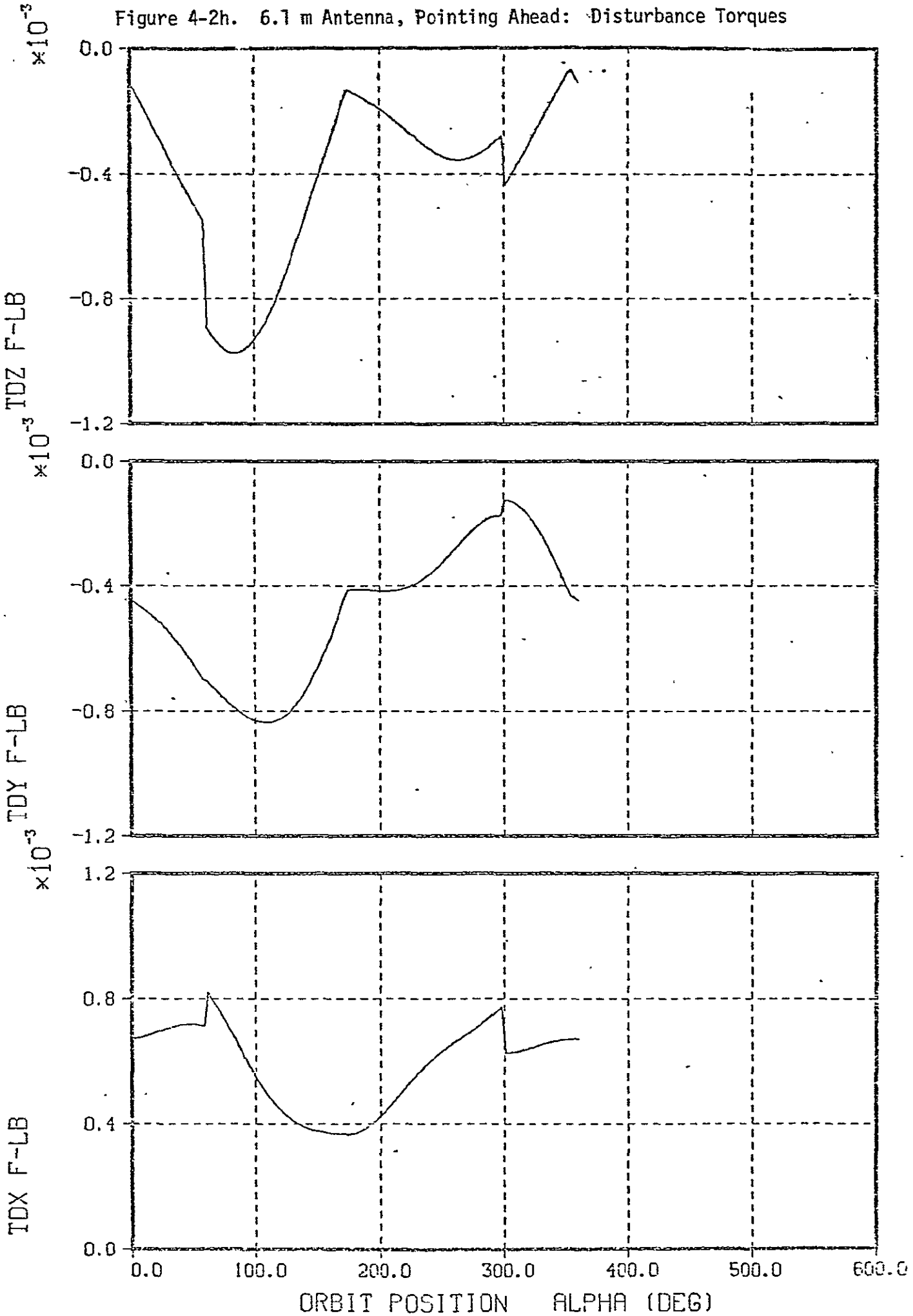

Figure 4-2i. 6.1 m Antenna, Pointing Ahead: Wheel Momenta

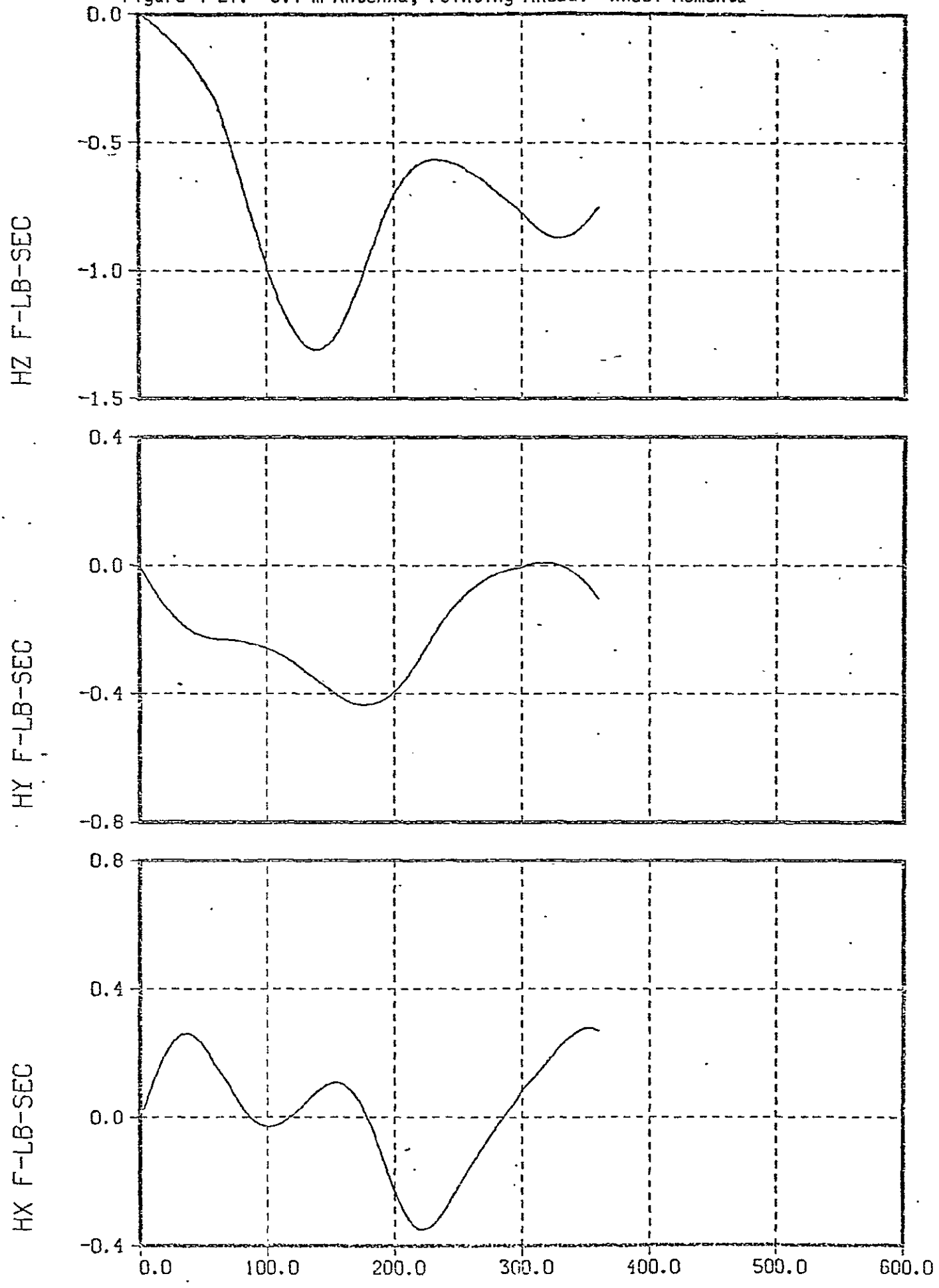

on the axes and -12.68 N-m-s for the fourth wheel. This will allow the fourth wheel to accumulate -7.32 N-m-s before momentum saturation, and will allow each of the other three wheels to lose 7.32 N-m-s before dropping to zero speed.

The preceding bias set point may be tailored slightly to specific orbits if it is known that the stored momentum will show a bias. However, the range of $\pm$ 7.32 N-m-s is used here. Based on it, the 1.86 N-m-s maximum excursion shown in Table 4-2 can be easily handled by the proposed 20 N-m-s SRW's.

Figure 4-2c contains plots of the roll, pitch, and yaw wheel momenta which show that the roll momentum is approximately zero biased. Although the initial momentum was zero at the ascending node, a complete orbit shows that there is a net accumulated momentum. To insure that the momentum does not continue to accumulate on succeeding orbits, three-orbit simulation plots are shown in Figure 4-3. These show more clearly that the roll momentum is zero biased and periodic. However, although the pitch and yaw momenta are periodic after an initial transient, there is a net bias momentum.

This bias is caused by the magnetic unloading law which requires that a certain momentum error $\bar{H}_e$ exists before any unloading torques are generated. The observed bias values thus reflect the equilibrium condition of the magnetic unloading law. These biases may be reduced by increasing the unloading gain K or by changing the magnetic control law to include a lead term representing an estimate of the disturbance torque in body coordinates. In inertial coordinates, the momentum biases are about equal in all axes, but in body coordinates they mainly appear in pitch and yaw. The results of the present investigation into the adequacy of the wheels and the magnetic torque bars are not affected by the biases since they are relatively small compared to the reaction wheel momentum capacity. Thus reduction of the biases will not be further pursued at this time.

Figure 4-3a. 4.57 m Antenna, Pointing Ahead: Magnetic Moments

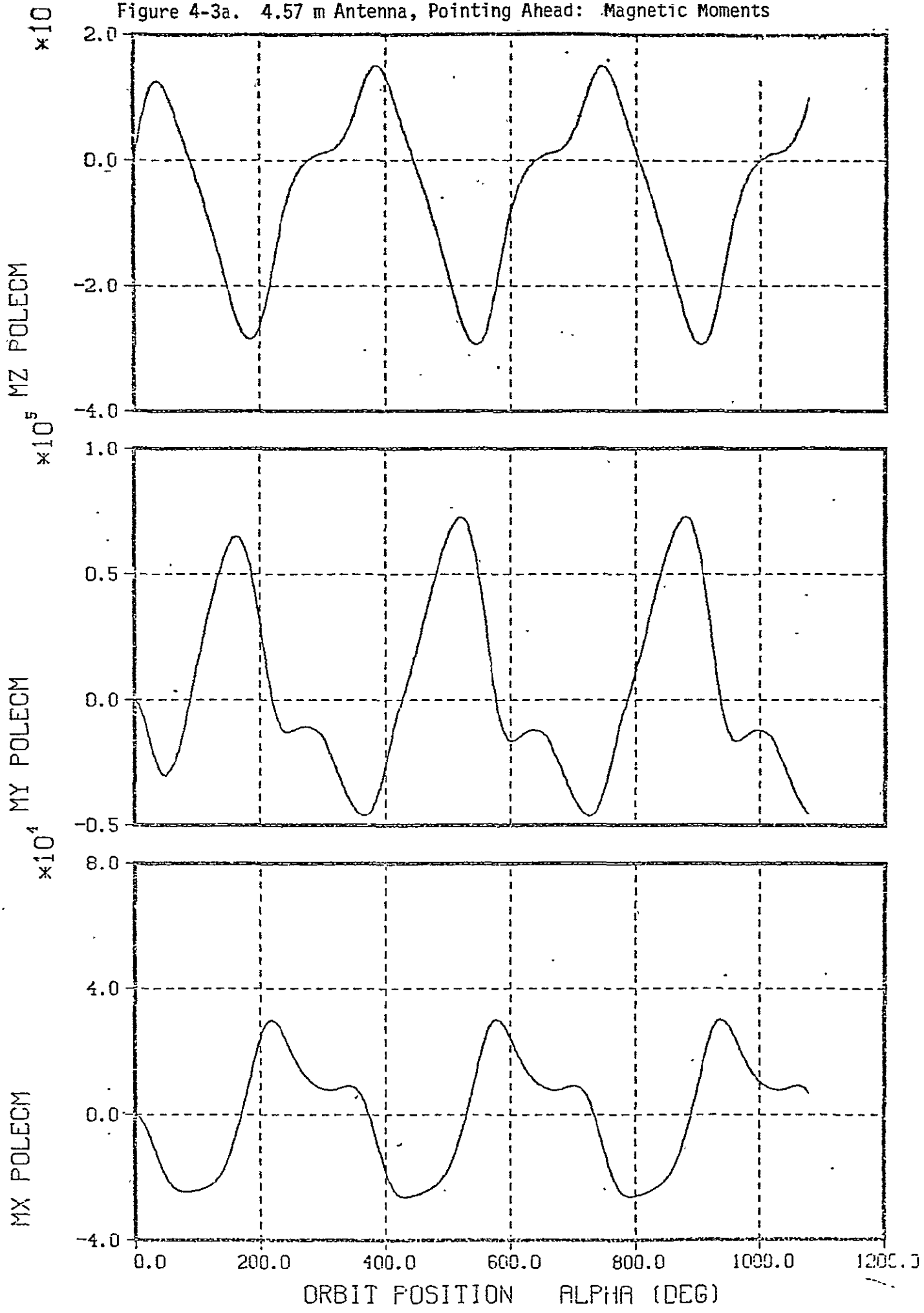

Figure 4-3b. 4.57 m Antenna, Pointing Ahead: Disturbance Torques

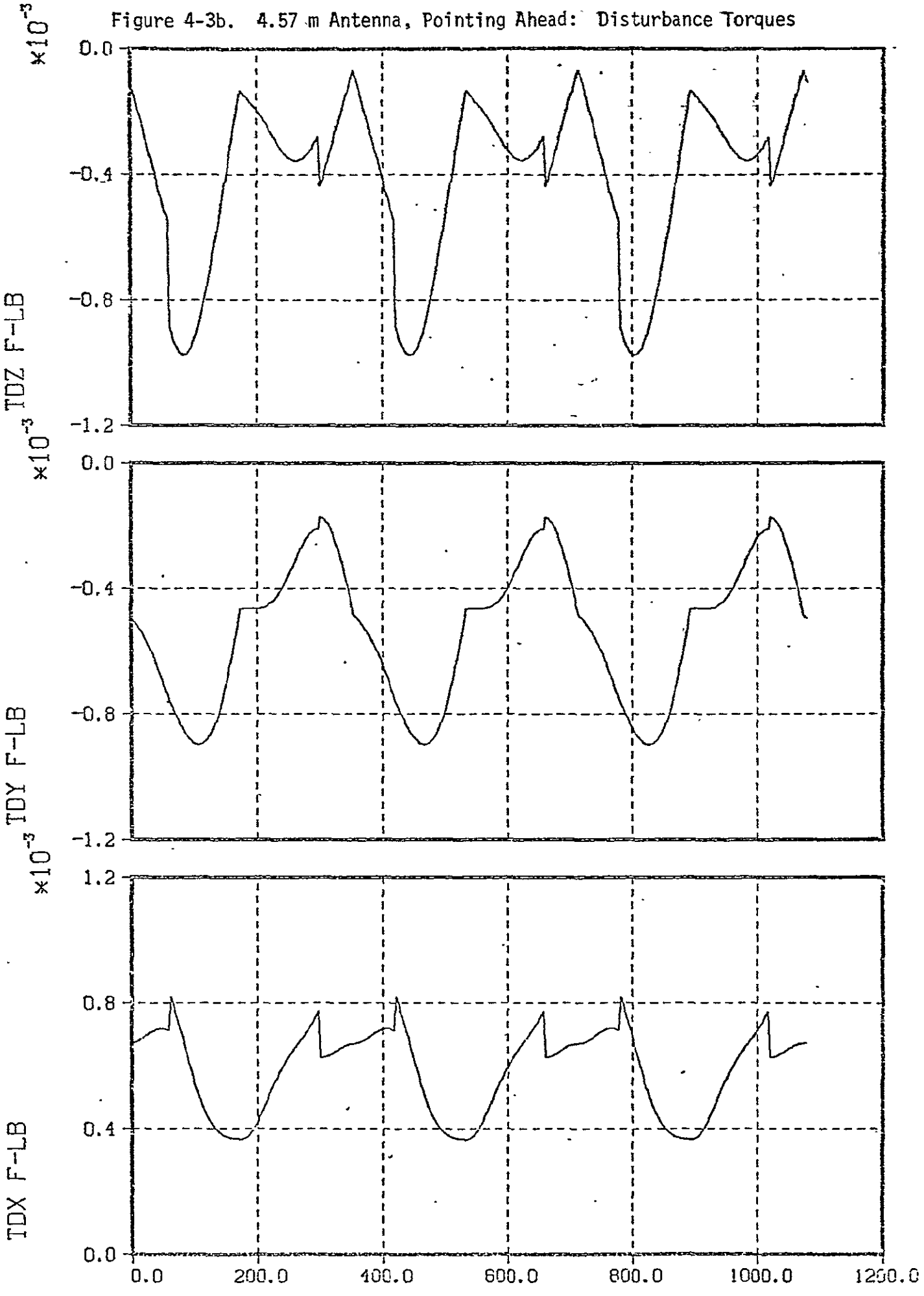

Figure 4-3c. 4.57 m Antenna, Pointing Ahead: Wheel Momenta

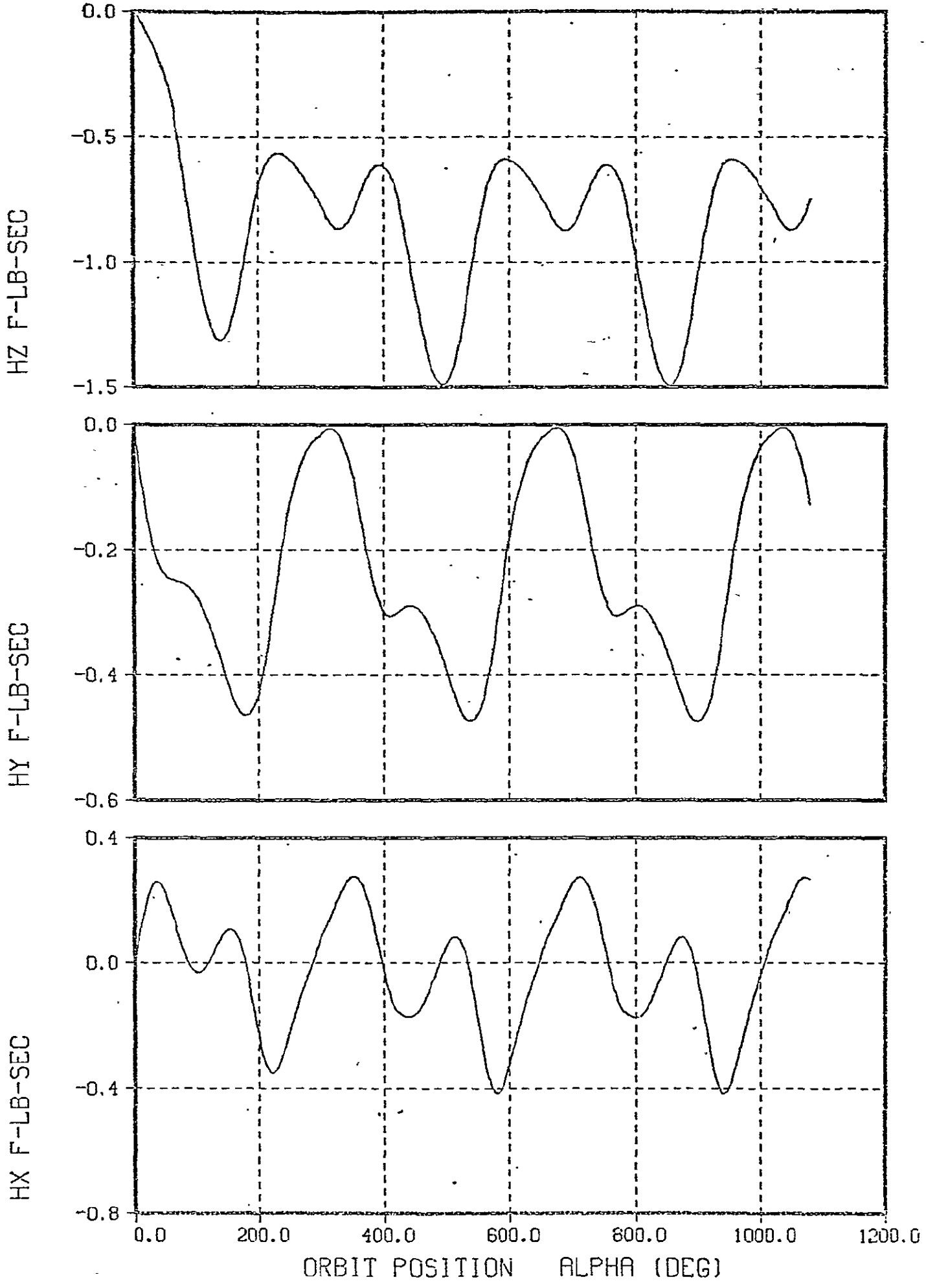

For the plots shown in Figures 4-2 and 4-3, the spacecraft was started in orbit at the ascending node with zero wheel momenta. Other plots not included here show that the wheel momenta appearance varies when the spacecraft is started at orbit positions of 90 and 180 degrees with zero initial momenta. The reason is that an unloading error exists depending on the relative orientations of the $\overline{H}_e$ and $\overline{B}$ vectors, which in fact depends on the initial conditions. Additional studies should examine the possibility of reducing the bias momentum on succeeding orbits. This may require a more detailed study of unloading gains.

Figure 4-4 shows the momentum for the three axes as it accumulates when no unloading torques are commanded. The RSS value for one orbit is approximately 4.6 N-m-s. In the pitch axis, the aerodynamic torque on the antenna (looking ahead) is primarily causing the constant buildup, while the small superimposed oscillation is from solar effects.

To show the sensitivity of the disturbance torques to the mast height and antenna orientation, the Fourier coefficients for the fundamental and first harmonic are tabulated in Table 4-3. These may also be used later for simulation models. In the Table, T_{sx}, T_{sy}, T_{sz} denote the solar roll, pitch, and yaw torques, T_{ax}, T_{ay}, T_{az}, the aerodynamic roll, pitch, and yaw torques, T_{gx}, T_{gy}, T_{gz}, the gravity gradient roll, pitch, and yaw torques, T_{mx}, T_{my}, T_{mz}, the residual magnetic torques, and T_{dx}, T_{dy}, T_{dz} denote the total disturbance torques. The Fourier model is

$$T_{ij} = a_o + \sum_{n=1}^{2} a_n \cos n w_o t + b_n \sin n w_o t$$

where

$i = s, a, g, m, d$

$j = x, y, z$

Figure 4-4. No Unloading, 4.57 m Antenna Looking Ahead: Wheel Momenta

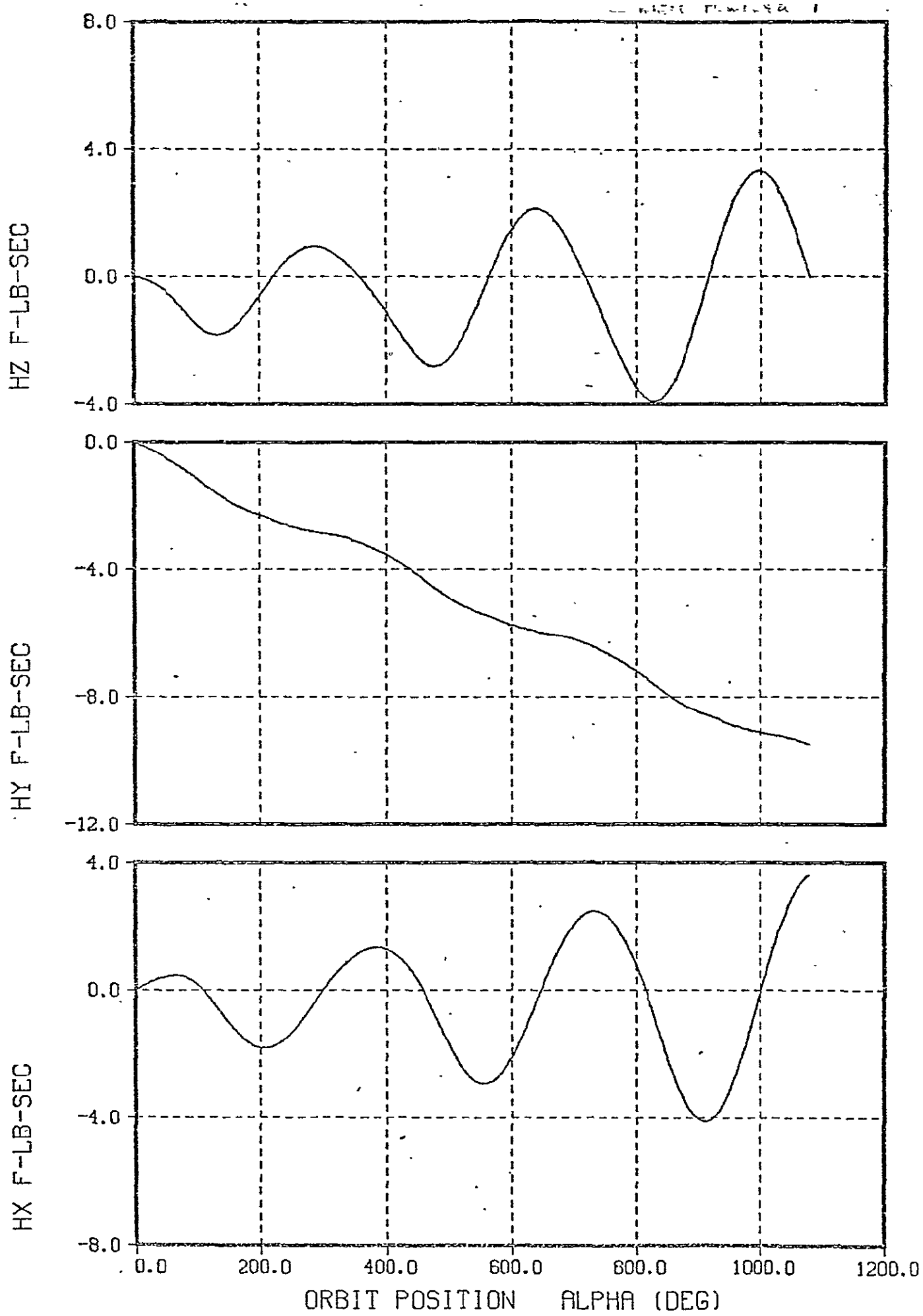

Table 4-3. Fourier Coefficients for Disturbance Torques

4.57 m Antenna, Pointing Zenith

Torques N-m	Fourier Coefficients				
	a_0	a_1	b_1	a_2	b_2
T_{sx}	-12.5×10^{-5}	2.19×10^{-4}	-2.17×10^{-5}	-1.03×10^{-4}	1.20×10^{-5}
T_{sy}	4.07×10^{-5}	-6.49×10^{-5}	-1.05×10^{-5}	2.39×10^{-5}	3.09×10^{-6}
T_{sz}	-4.66×10^{-5}	2.63×10^{-5}	-2.97×10^{-4}	3.32×10^{-5}	1.09×10^{-4}
T_{ax}	2.77×10^{-6}	-1.26×10^{-6}	-1.15×10^{-5}	1.00×10^{-5}	6.07×10^{-5}
T_{ay}	-2.96×10^{-5}	1.53×10^{-4}	2.36×10^{-5}	3.88×10^{-5}	-2.49×10^{-5}
T_{az}	-4.68×10^{-4}	-3.29×10^{-6}	-3.00×10^{-5}	3.15×10^{-4}	-6.72×10^{-5}
T_{gx}	9.10×10^{-4}	0.	0.	0.	0.
T_{gy}	-9.10×10^{-4}	0.	0.	0.	0.
T_{gz}	-1.53×10^{-13}	0.	0.	0.	0.
T_{mx}	0.	0.	0.	0.	0.
T_{my}	-2.10×10^{-10}	2.64×10^{-8}	-4.47×10^{-10}	-4.19×10^{-10}	-1.14×10^{-8}
T_{mz}	1.87×10^{-4}	0.	0.	0.	0.
T_{dx}	7.95×10^{-4}	2.18×10^{-4}	-3.32×10^{-5}	-9.34×10^{-5}	7.27×10^{-5}
T_{dy}	-8.98×10^{-4}	8.79×10^{-5}	-4.34×10^{-4}	6.26×10^{-5}	-2.18×10^{-5}
T_{dz}	-4.81×10^{-4}	2.30×10^{-5}	-3.27×10^{-4}	3.47×10^{-4}	4.15×10^{-5}

Table 4-3. Fourier Coefficients for Disturbance Torques (continued)

4.57 m Antenna, Pointing Ahead

Torques N-m	Fourier Coefficients				
	a_0	a_1	b_1	a_2	b_2
T_{sx}	-1.19×10^{-4}	2.10×10^{-4}	-2.17×10^{-5}	-1.04×10^{-4}	1.28×10^{-5}
T_{sy}	3.97×10^{-5}	-6.22×10^{-5}	2.09×10^{-5}	2.35×10^{-5}	-3.24×10^{-6}
T_{sz}	-5.07×10^{-5}	2.75×10^{-5}	-3.02×10^{-4}	3.84×10^{-5}	1.08×10^{-4}
T_{ax}	2.77×10^{-6}	-1.26×10^{-4}	-1.15×10^{-5}	1.00×10^{-5}	6.07×10^{-5}
T_{ay}	1.49×10^{-4}	1.53×10^{-4}	2.36×10^{-5}	3.88×10^{-5}	-2.49×10^{-5}
T_{az}	-5.42×10^{-4}	-3.29×10^{-6}	-3.00×10^{-5}	3.15×10^{-4}	-6.72×10^{-5}
T_{gx}	9.10×10^{-4}	0.	0.	0.	0.
T_{gy}	-9.10×10^{-4}	0.	0.	0.	0.
T_{gz}	-1.53×10^{-13}	0.	0.	0.	0.
T_{mx}	0.	0.	0.	0.	0.
T_{my}	2.10×10^{-10}	2.64×10^{-8}	-4.47×10^{-10}	-4.19×10^{-10}	-1.14×10^{-8}
T_{mz}	3.23×10^{-5}	0.	0.	0.	0.
T_{dx}	7.93×10^{-4}	2.13×10^{-4}	-3.32×10^{-5}	-9.40×10^{-5}	7.35×10^{-5}
T_{dy}	-7.20×10^{-4}	9.06×10^{-5}	-4.03×10^{-4}	6.22×10^{-5}	-2.82×10^{-5}
T_{dz}	-5.60×10^{-4}	2.43×10^{-5}	-3.32×10^{-4}	3.53×10^{-4}	4.11×10^{-5}

Table 4-3. Fourier Coefficients for Disturbance Torques (continued)

6.10 m Antenna, Pointing Ahead

Torques N-m	Fourier Coefficients				
	a_o	a_1	b_1	a_2	b_2
T_{sx}	-1.17×10^{-4}	2.12×10^{-5}	-2.17×10^{-5}	-1.06×10^{-4}	1.30×10^{-5}
T_{sy}	3.95×10^{-5}	-6.13×10^{-5}	3.40×10^{-5}	2.30×10^{-5}	-6.87×10^{-6}
T_{sz}	-5.14×10^{-5}	2.75×10^{-5}	-3.02×10^{-4}	3.84×10^{-5}	1.08×10^{-4}
T_{ax}	2.77×10^{-6}	-1.30×10^{-6}	-1.18×10^{-5}	1.00×10^{-5}	6.07×10^{-5}
T_{ay}	2.17×10^{-4}	1.53×10^{-4}	2.36×10^{-5}	4.01×10^{-5}	-2.52×10^{-5}
T_{az}	-5.42×10^{-4}	-3.29×10^{-6}	-3.00×10^{-5}	3.15×10^{-4}	-6.72×10^{-5}
T_{gx}	9.10×10^{-4}	0.	0.	0.	0.
T_{gy}	-9.10×10^{-4}	0.	0.	0.	0.
T_{gz}	-1.53×10^{-13}	0.	0.	0.	0.
T_{mx}	0.	0.	0.	0.	0.
T_{my}	-2.10×10^{-16}	2.64×10^{-8}	-4.47×10^{-4}	-4.19×10^{-10}	-1.14×10^{-9}
T_{mz}	3.23×10^{-5}	0.	0.	0.	0.
T_{dx}	7.96×10^{-4}	2.12×10^{-4}	-3.36×10^{-5}	-9.59×10^{-5}	7.38×10^{-5}
T_{dy}	-6.54×10^{-4}	9.17×10^{-5}	-3.90×10^{-4}	6.32×10^{-5}	-3.20×10^{-5}
T_{dz}	-5.60×10^{-4}	2.43×10^{-5}	-3.32×10^{-4}	3.53×10^{-4}	4.11×10^{-5}

Note that the cross products of inertia contribute small constant gravity gradient torques. These may be computed to be 9.1×10^{-4} and -9.1×10^{-4} N-m in roll and pitch, respectively. These compare very well with the table values for roll and pitch.

5.0 INITIALIZATION OF FINE CONTROL

After completion of the initial orbit acquisition, and later on if necessary after stationkeeping or any other maneuvers, the fine control mode must be initiated. The TDRS antenna must be deployed and the solar array drive placed into normal operation.

Normal on-orbit attitude control of the L-D is accomplished using reaction wheels (RW's) and only two areas important to fine control mode initialization must be examined.

(1) When entering the RW attitude control mode, the spacecraft body rates must be compatible with the RW capabilities and the minimum impulse bit of the reaction control system (RCS) used for momentum unloading.

(2) An accurate and stable attitude reference for earth pointing must be available.

Since the L-D mission will be flown on an MMS bus, point 1 above hardly needs any further examination. The mass expulsion RCS and the torque and momentum capabilities of the RW's specified for the MMS [1,2], are compatible. When under mass expulsion attitude control, the MMS is capable of reducing spacecraft rates to less than 0.1 deg/sec per axis. The RW attitude control system (ACS) is capable of stabilizing the spacecraft within 30 minutes from initial rates of up to 0.25 deg/sec about any axis [2]. The minimum torque impulse bit available from the 0.2 lbf thruster is conservatively estimated for L-D as 0.06 ft-lb-sec which is more than two orders of magnitude smaller than the wheel capacity of 15 ft-lb-sec (20 Nms) and the ability to unload the wheel is assured. In conclusion, there exists no problem in transferring from RCS to RW attitude control.

Establishing an accurate and stable attitude reference for earth pointing is thus the main problem encountered when initializing the fine control mode and this section is therefore mainly concerned with the

nitialization of the MMS stellar-inertial attitude reference system. The atter task separates into two sub-tasks. Following the normal MMS acquisition procedure (described below) it must first be shown that stars sighted by the on-board star trackers can be identified, and secondly, chat the on-board attitude reference algorithm (filter) will converge from the attendant, relatively large, initial attitude uncertainty. Sections 5.2 and 5.3, respectively, will address two different methods of star identification for initializing the on-board stellar-inertial attitude reference system (ARS). The method presented in Section 5.2 utilizes earth magnetic field measurements to aid in the initial star identification, while the method in Section 5.3 correlates observed star sightings with entries in a reduced star catalog. The convergence of the on-board filtering algorithm is demonstrated in Section 5.4. Initialization of the fine control mode appears to pose no problems for L-D.

Once a precise inertial attitude reference of the spacecraft has been established, L-D ephemeris data is used to convert the inertial reference to an earth pointing reference. Then ACS commands are issued that cause the spacecraft to maneuver from an inertial hold mode to its normal on-orbit attitude: yaw ($\hat{z}_b$) to nadir, pitch ($\hat{y}_b$) normal to the orbit plane, and roll ($\hat{x}_b$) in direction of orbital motion. The RW's will be used to perform this maneuver. Any further maneuvers performed during the life of the spacecraft, such as stationkeeping, for example, will not require a reinitialization of the ARS. At the end of even the longest of any such maneuvers, the inertial reference unit (gyros) provides an attitude reference that will certainly be accurate enough to identify the stars sighted by the trackers. Attitude and gyro bias updates can then be computed.

The TDRS antenna should be deployed once coarse sun acquisition has been completed. Since MMS/L-D will probably acquire the sun with the negative yaw ($-\hat{z}_b$) axis, the antenna dish could find itself looking directly into the sun, a situation rarely encountered during normal on-orbit operations. To assure thermal loads compatible with normal on-orbit conditions the antenna elevation angle should be commanded to its

maximum dip angle of -26° and the azimuth to +90° so that the antenna looks away from the sun and in the positive pitch direction.

The solar array will be placed into normal operation (see Section 3.5) once the spacecraft has maneuvered to its nominal earth pointing orientation. Correct initial positioning of the array will be accomplished by ground command. Spacecraft ephemeris in ECI coordinates and time of year are sufficient information to compute the correct array angle relative to the solar array/spacecraft scribe-mark. The correct array orientation can be verified from telemetry data of the coarse sun sensor which is mounted on the solar array.

5.1 Normal MMS/L-D Acquisition Sequence

During launch the ACS is in a standby condition and the actuators are disabled. After separation from the launch vehicle (shuttle or Delta 3910 booster) the ACS is enabled and the solar array is deployed and subsequently rotated to a predetermined position relative to its scribe-mark. For L-D the solar cells will look toward $-\hat{z}_b$. The normal MMS acquisition sequence is to be autonomous by utilizing the on-board computer.

Coarse Sun Acquisition

After array deployment the spacecraft acquires the sun with its negative yaw axis ($-\hat{z}_b$ axis) and the spacecraft rates are reduced to an appropriate level. This maneuver is accomplished by the on-board computer using coarse sun sensors located on the solar array, the Inertial Reference Unit (gyros) for rate information, and the reaction control jets, magnetic torquers and/or reaction wheels to provide control torques. Normally coarse sun acquisition seeks an orientation with the solar array normal to the sun line. Because of the array cant angle of 37.5° (9:30 am orbit) the sun line would then not be aligned with one of the principal control axes of the spacecraft. Since it may be required to perform a rotation about the sun line to acquire appropriate stars into the fields of view of the star trackers, it is preferred to align the $-\hat{z}_b$ axis with the sun which keeps the solar array at 52.5°(90°-37.5°) to the sun line. The 20 percent

loss in generated electrical power is not critical since the payload sensors, which consume more than 50 percent of the power, are not yet activated. For one axis, the output signals of the array-mounted coarse sun sensors must then either be biased by 37.5° to account for the array cant angle, or the coarse sun sensors must be mounted to the uncanted portion of the solar array shaft.

Utilizing the mass expulsion system, the ACS is capable of completing a coarse sun acquisition sequence within 15 minutes in a sunlit segment of the orbit for initial rates of up to 2 deg/sec about each control axis. This would apply to acquisition after separation from a Delta 3910 launch vehicle. Utilizing reaction wheels, which would apply to acquisition after a shuttle launch, the ACS can complete coarse sun acquisition within 30 minutes in a sunlit segment of the orbit for initial rates of up to 0.25 deg/sec about each control axis. Coarse sun acquisition is considered complete when the attitude error between the sun line and the coarse sun sensor reference axis (biased) is less than ten (10) degrees (including albedo effects), the maximum rate about each of the control axes is less than 0.05 degree per second and control is maintained by the reaction wheels. Following coarse sun acquisition, the magnetic torquers and/or the mass expulsion system are used to reduce the reaction wheel speeds to less than 25 percent of no load speed.

Fine Sun Acquisition Mode

In the fine sun acquisition mode the coarse sun sensor is replaced by the fine digital sun sensor located in the ACS module with reference axis aligned with the $-\hat{z}_b$ axis. The initial conditions for the fine sun acquisition mode are defined by the final conditions of the coarse sun acquisition mode. Fine sun acquisition shall be considered complete when the attitude error between the sun line and the fine sun sensor reference is less then 0.1 degree, the maximum rate about each of the control axes is less than 0.05 degree per second, and the reaction wheel speeds are less than 25 percent of no load speed. Fine sun acquisition can be completed within ten (10) minutes of entering the mode.

After completion of the fine sun acquisition mode the spacecraft enters the stellar acquisition mode, which, as was mentioned above, is part of the main topic of this section.

Stellar Acquisition Mode

The initial conditions for the stellar acquisition mode are defined by the fine sun acquisition mode. Stellar acquisition shall be considered complete when the attitude of the ACS reference (optical cube) in the ACS module is aligned within 0.1 degree (each of three axes) of a specified inertial attitude (including verification of required guide stars), the maximum rate about each of the control axes is less than 0.01 degree per second, and the reaction wheel speeds are less than 25 percent of no load speed. Stellar acquisition must be completed within four hours after entering the mode. At the end of stellar acquisition for spacecraft is considered to be in an inertial hold mode from which its normal on-orbit orientation is acquired by performing the appropriate maneuver.

5.2 Star Identification/Attitude Determination From Magnetic Field Measurements

Conditions at the completion of fine sun acquisition establish the initial conditions for the start of attitude determination from magnetometer measurements. The conditions are that the negative yaw axis is within 0.1 degree of the sun line and that the maximum rates are 0.05 deg/sec about any of the control axes. The attitude about the sun line is unknown and is to be estimated. The preferred way to do this for low orbit missions is to wait for a point in the sunlit portion of the orbit at which the earth's magnetic field is oriented more or less orthogonal to the sunline (60° or more). For high inclination missions, such as L-D, the portion of the orbit around the poles is generally not satisfactory. One purpose here is to point out angular error sources in the overall magnetic attitude determination scheme.

5.2.1 Magnetic $\vec{B}$ Field Modeling

Autonomous attitude determination is desired and to do this a sufficiently accurate magnetic $\vec{B}$ field model must be available on-board at the

time of attitude determination. Comparisons of a simple tilted dipole field model and the standard spherical harmonic model reveal that the $\vec{B}$ field vectors computed by the models may differ in direction by as much as 10-15° or more. This rules out the possibility of using the tilted dipole model on-board for autonomous attitude determination since the star tracker field-of-view is only 8° x 8° and a 10° - 15° uncertainty would also be unsatisfactory for star identification. Since launch date and therefore approximate vehicle location in the $\vec{B}$ field is known before launch, a local portion of the spherical harmonic model may be stored into the on-board processor. This would still permit autonomous attitude determination. However, storage of a complete harmonic model may be prohibitive, and if it should be required, the model would have to be computed on the ground and sent up for use at the proper time.

Finally, the agreement between the harmonic model and nature has to be determined since it is a direct error source in the attitude determination. Estimates of the divergence between the harmonic model and nature are not well known because of a lack of data, but published results [7] show that solar-magnetic field attitude determination produces accuracies of 1 to 3.5 degrees from field measurements that are in error by up to 9.2 degrees. Repeated measurements at successive points in orbit do, however, help to reduce the field uncertainty effects.

To be of use in the attitude estimation process, the magnetic field must be available in a proper coordinate frame for on-board use. This coordinate frame is referred to as the sun frame and is defined in detail in the next section. Typically, the tenth order harmonic model $\vec{B}$ field is computed in spherical coordinates as

$$\vec{B} = \begin{bmatrix} B_r \\ B_\lambda \\ B_\theta \end{bmatrix}$$

where r is the radius from the geocenter to the field point, λ is the East longitude, and θ is the colatitude. This field vector is then transformed

by suitable routine orthogonal transformations to obtain it finally in sun coordinates. Possible errors in the final field vector as a result of unknown angular errors in the transformations are discussed after the coordinate systems are defined. In any event, the magnetic field is assumed to be transformed error-free into a standard set of Earth-Centered-Inertial coordinates which will be related to the sun coordinates by standard orbit transformations. The error-free assumption is justified because up to that point the transformation does not involve orbital geometry.

5.2.2 Coordinate Transformations and Frames

It is convenient to have a set of Earth-Centered-Inertial coordinates $\hat{x}_I\ \hat{y}_I\ \hat{z}_I$ with $\hat{x}_I$ toward the vernal equinox point, $\hat{z}_I$ normal to the equatorial plane, and $\hat{y}_I$ completing the set. It is in this set that the magnetic field is assumed available by error-free transformation from magnetic coordinates.

To perform the attitude determination, it is convenient to establish a set of sun coordinates $\hat{x}_S$, $\hat{y}_S$, $\hat{z}_S$ centered in the spacecraft with $-\hat{z}_S$ toward the sun, $\hat{x}_S$ in the orbital plane, and $\hat{y}_S$ completing the set. Then the vehicle body coordinate set $\hat{x}_B$, $\hat{y}_B$, $\hat{z}_B$ is defined by the respective rotations α, β, γ where α is about the $\hat{x}_S$ axis, β is about the intermediate $\hat{y}$ axis, and γ is about the final $\hat{z}_B$ axis. Angles α and β are less than or equal to 0.1 degree as noted earlier, and γ is arbitrary about the $\hat{z}_B$ axis which is nominally the anti-sun line. Figure 5-1 shows the frames and angles involved.

The transformation from sun to body coordinates is $[A]_{BS}$ given by

$$[A]_{BS}=\begin{bmatrix} \cos\gamma\cos\beta & \cos\gamma\sin\beta\sin\alpha+\sin\gamma\cos\alpha & -\cos\gamma\sin\beta\cos\alpha+\sin\gamma\sin\alpha \\ -\sin\gamma\cos\beta & -\sin\gamma\sin\beta\sin\alpha+\cos\gamma\cos\alpha & \sin\gamma\sin\beta\cos\alpha+\cos\gamma\sin\alpha \\ \sin\beta & -\cos\beta\sin\alpha & \cos\beta\cos\alpha \end{bmatrix}$$

and is explicitly required for the least-squares attitude determination in Section 5.2.3.

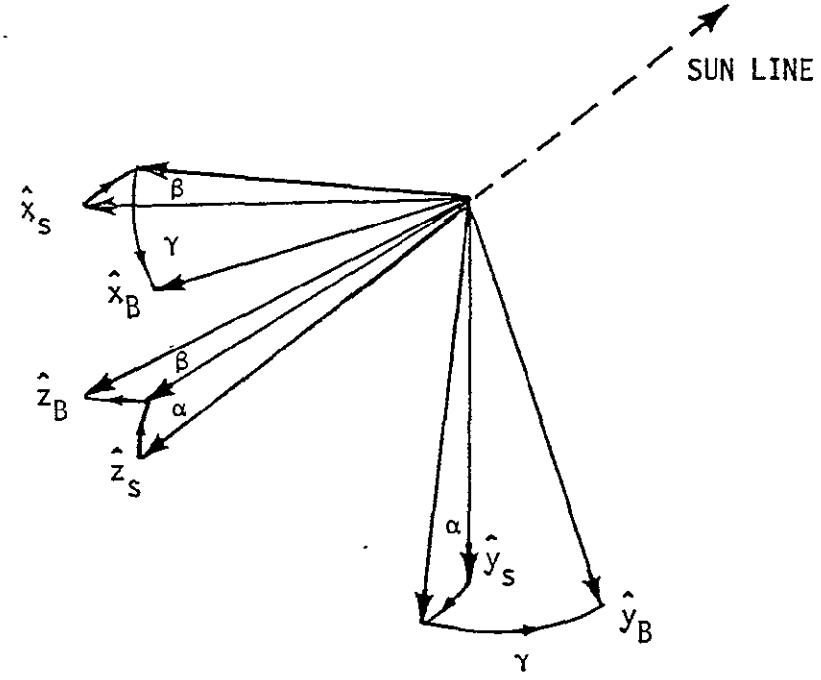

Figure 5-1. Sun-Body Coordinate Conventions

Additional transformations are required also, but those involve angular quantities such as orbit inclination, orbit position angle, and angle of the ascending node which are all known quite accurately. For instance, spacecraft position is assumed known to within 100 meters which, at an altitude of 705 km (388 nautical miles) creates an angular error of approximately 3 arc-sec. Errors such as this in the computation of transformations are entirely negligible compared to the potential disagreement between the magnetic model and nature so they may be ignored. The errors are also negigibly small compared to the 8° x 8° field-of-view for the star tracker. Thus the overall transformation from ECI coordinates to sun coordinates is designated as $[A]_{SI}$ and with it the magnetic field available in ECI coordinates may be transformed to the sun coordinates by

$$\bar{B}_s = [A]_{SI}\, \bar{B}_I$$

for use in the attitude determination.

5.2.3 Attitude Determination

Magnetic field measurements are obtained from the magnetometers in body axes, and since the field model is known in sun coordinates as $\vec{B}_s$, the measurement equation may be written as

$$\bar{z} = [A]_{BS}\, \vec{B}_s + \bar{V}$$

where $\bar{z}$ is the vector of three measurements

$$\bar{z} = \begin{bmatrix} B_{xs} \\ B_{ys} \\ B_{zs} \end{bmatrix}$$

The additive noise is represented by the vector $\bar{V}$, and since the measurements are processed at discrete times in orbit, the covariance matrix of $\bar{V}$ may be written as

$$E[\bar{V}(t_i)\,\bar{V}^T(t_j)] = [R]\,\delta_{ij}$$

where [R] is a constant matrix. Modeling the noise as uncorrelated between the axes and with equal variance in all axes permits writing [R] as

$$[R] = \begin{bmatrix} \sigma_v^2 & 0 & 0 \\ 0 & \sigma_v^2 & 0 \\ 0 & 0 & \sigma_v^2 \end{bmatrix}$$

For the magnetometers considered here, the resolution is 0.004 gauss which yields a $\sigma_v = 0.001$ gauss if a rounding-error model with a uniform distribution is used. The noise is considered zero mean although bias may result since the accuracy of the magnetometers is $\pm 1\%$ of the full scale value of ± 0.5 gauss.

The emphasis here is on a computationally simple algorithm that will produce estimates for the angle about the sun line accurately enough so that unambigous star identifications can be made and the stellar-inertial attitude reference system can be initialized. Thus the extended Kalman filter is not considered for magnetic attitude determination. Also of importance is the fact that rates about the sun line can be appreciable at this time and thus the yaw attitude may change between successive magnetometer attitude determinations. Thus the yaw gyro rate has to be integrated so that the yaw angle change can be propagated between successive attitude determinations. Since the yaw axis is within 0.1 degree of the sunline, α and β are always small and accurate enough for stellar convergence; however they may also readily be estimated by the least squares procedure if desired. The procedure is as follows.

Let $\bar{x}^0$ represent the initial best estimate of the vector $\bar{x} \triangleq (\alpha,\beta,\gamma)^T$. Since the measurement equation is nonlinear and implicitly involves $\bar{x}$, it may be written as

$$\bar{z} = h(\bar{x}) + \bar{V}$$

$$h(\bar{x}) = \begin{bmatrix} c\eta c\beta B_{xs} & + (c\gamma s\beta s\alpha + s\gamma c\alpha)\, B_{ys} & + (-c\gamma s\beta c\alpha + s\gamma s\alpha)\, B_{zs} \\ -s\gamma c\beta B_{xs} & + (-s\gamma s\beta s\alpha + c\gamma c\alpha)\, B_{ys} & + (s\gamma s\beta c\alpha + c\gamma s\alpha)\, B_{zs} \\ s\beta B_{xs} & - c\beta s\alpha\, B_{ys} & + \quad c\beta c\alpha\, B_{zs} \end{bmatrix}$$

and linearized about $\bar{x} = (0\ ,\ 0\ ,\ \gamma^{o})$ to obtain the matrix H defined as

$$H = \left.\frac{\partial h(\bar{x})}{\partial \bar{x}}\right|_{\bar{x} = \bar{x}^{o}}$$

$$H = \begin{bmatrix} \sin\gamma^{o}\, B_{zs} & -\cos\gamma^{o}\, B_{zs} & -\sin\gamma\, B_{xs} + B_{ys} \\ \cos\gamma^{o}\, B_{zs} & \sin\gamma^{o}\, B_{zs} & -\cos\gamma\, B_{xs} - \sin\gamma\, B_{ys} \\ -\, B_{ys} & B_{xs} & 0 \end{bmatrix}$$

The complete linearization may now be written as

$$\Delta\bar{z} = H\, \Delta\bar{x} + \bar{V}$$

where the $\bar{x}$ and $\bar{z}$ are defined as

$$\Delta\bar{x} = \bar{x} - \bar{x}^{o}$$

$$\Delta\bar{z} = \bar{z} - [A(\bar{x}^{o})]_{BS}\, \bar{B}_{s}$$

These equations would be suitable for estimating the attitude $\bar{x}$ based on $\Delta\bar{x}$ computed from the relation

$$\Delta\bar{x} = H^{-1}\, \Delta\bar{z}$$

However, in the present case α and β are known within 0.1° if the fine sun sensor is operative. This accuracy is probably greater than can be obtained from the magnetic field, and thus α and β do not normally have to be estimated. The preceding formulation is still applicable with some notational changes as follows.

Using only the last column of matrix H, define

$$M = \begin{bmatrix} -\sin\gamma^{o} B_{xs} + B_{ys} \\ -\cos\gamma^{o} B_{xs} - \sin\gamma^{o} B_{ys} \end{bmatrix}$$

Then the measurement equation may be condensed to

$$\begin{bmatrix} \Delta z_1 \\ \Delta z_2 \end{bmatrix} = M \Delta\gamma + \begin{bmatrix} V_1 \\ V_2 \end{bmatrix}$$

from which a least squares estimate for $\Delta\gamma$ may be obtained as

$$\Delta\gamma = (M^T M)^{-1} M^T \begin{bmatrix} \Delta z_1 \\ \Delta z_2 \end{bmatrix}$$

The attitude γ is then obtained from

$$\gamma = \gamma^{o} + (M^T M)^{-1} M^T (\Delta\bar{z} - [A'(\bar{x}^{o})_{BS}]\, \bar{B}_s) \qquad (5.2\text{-}1)$$

where $\Delta\bar{z}$ is understood to be

$$\Delta\bar{z} = \begin{bmatrix} \Delta z_1 \\ \Delta z_2 \end{bmatrix}$$

and the primed transformation $A'(\bar{x}^{o})_{BS}$ is obtained from $A(\bar{x}^{o})_{BS}$ by deleting the last row, as

$$[A']_{BS} = \begin{bmatrix} \cos\gamma\cos\beta & \cos\gamma\sin\beta\sin\alpha + \sin\gamma\cos\alpha & -\cos\gamma\sin\beta\cos\alpha + \sin\gamma\sin\alpha \\ -\sin\gamma\cos\beta & -\sin\gamma\sin\beta\sin\alpha + \cos\gamma\cos\alpha & \sin\gamma\sin\beta\cos\alpha + \cos\gamma\sin\alpha \end{bmatrix}$$

The first estimate of γ^o will be determined shortly, and then $\bar{B}_s$, $[A'(\bar{x}^o)]_{BS}$, and the measurement $\bar{z}(t_i)$ are all known so that γ may be computed. Let the first estimate be $\gamma(t_1)$, and determine the incremental attitude change γ_g up to time b_2 by integration of the gyro outputs. Then the new initial estimate for the second least-squares determination is given by

$$\gamma^o(t_2) = \gamma(t_1) + \gamma_g(t_2)$$

Using this $\gamma^o(t_2)$, the computation in (5.2-1) may be repeated to determine the second attitude estimate $\gamma(t_2)$. The process is repeated until $\gamma(t_i)$ has converged, i.e., successive computed updates $\Delta\gamma$ are small and have zero mean.

The first estimate $\bar{x}^o(t_1)$, i.e., $\gamma^o(t_1)$, may be determined as follows. Since α and ρ are within 0.1 degree, they may be set to zero in the measurement equation

$$\bar{z} = [A]_{BS}\,\bar{B}_s$$

Writing the equation out and solving for the remaining unknown γ^o yields the expression

$$\gamma^o = \cos^{-1}\left[\frac{z_1 B_{sx} + z_2 B_{sy}}{B_{sx}^2 + B_{sy}^2}\right]$$

which provides the starting estimate.

The flow diagram which follows contains the main steps for the magnetometer attitude estimation.

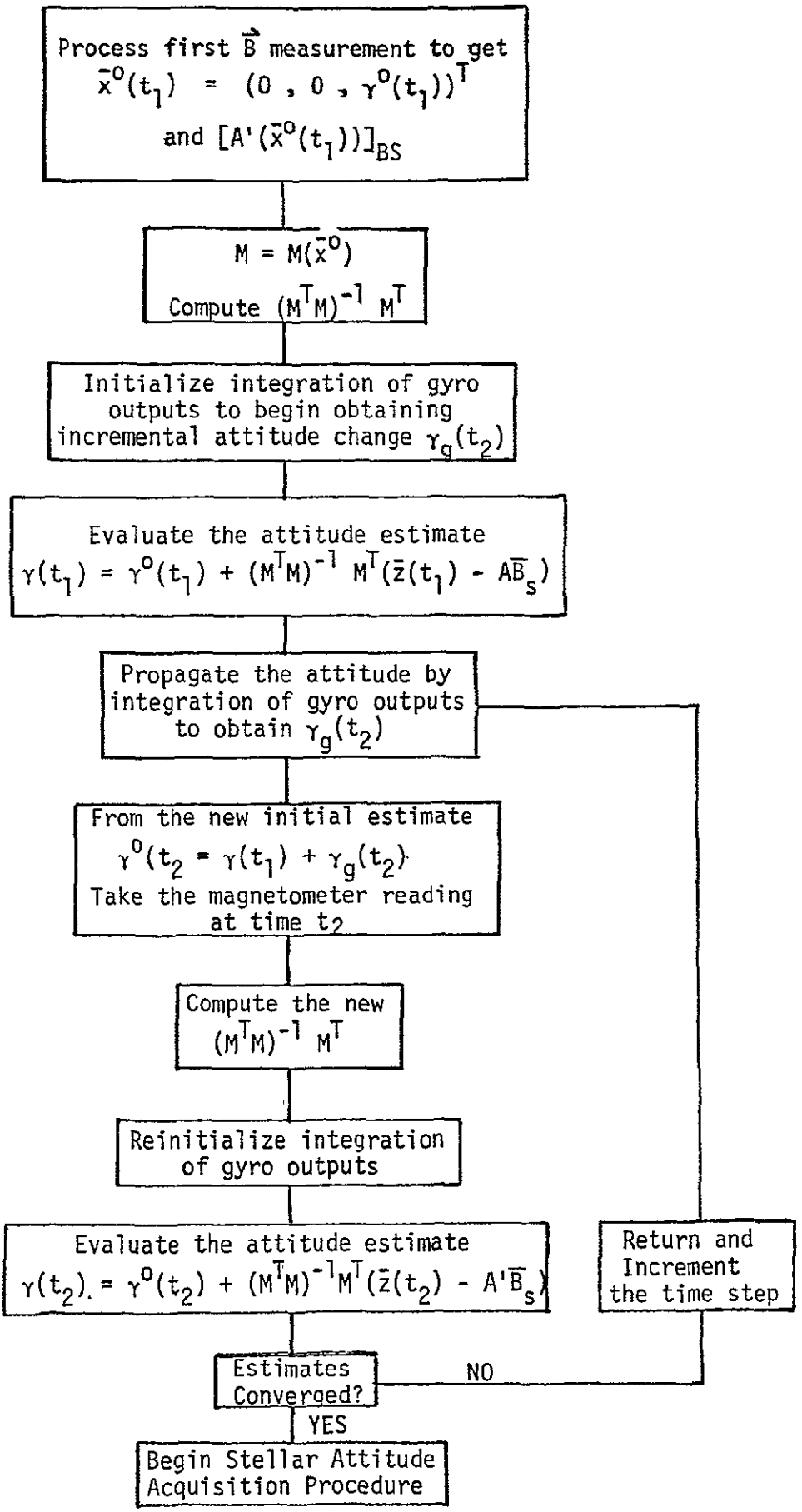

Figure 5-1a. Attitude Processing Flow Chart

The arrangement of the preceding flow chart is arbitrary in several places, and it is implicitly assumed that the computational time per estimate is negligible compared to the time difference $t_i - t_j$ between estimates.

5.2.4 Error Sources and Effects

This section summarizes the potential error sources and indicates the accuracy expected for the magnetic attitude determination. The error sources and their effects are:

(1) Divergence between the magnetic model and nature. A mean angular error is 4.3° extracted from Reference 1, with a maximum error of 9.2°. Effects of this divergence are reduced by repeated measurements at several points along the orbit.

(2) Magnetometer measurement noise of 0.004 gauss. These effects are also reduced by repeated measurements along the orbit.

(3) Errors in coordinate transformations. Since the transformations involve angular quantities that are accurately known, the error in attitude determination that results from an inaccurately transformed $\overline{B}$ field is negligible.

Results in Reference 7 show that attitude errors on the order of 1.56° (average) with a maximum of 3.5° are achievable. Such errors are well within the 8° x 8° field-of-view of the star tracker, and thus the solar-magnetic determination should be accurate enough to permit initiation of stellar acquisition.

5.3 Star Identification By Correlation

Another method of determining the orientation of the spacecraft about the sun line is by correlating star tracker observations with a star catalog. The star catalog contains only those stars above a certain brightness M_v which should be encountered by the spacecraft's star tracker as it sweeps out at a swath about the sun line. The correlation method will now be briefly described.

5.3.1 Description of Method

The spacecraft is commanded to rotate about the sun line at a fixed rate, say 0.1 deg/sec, and the star tracker sensitivity threshold is set such that it will detect only stars above a specified brightness which matches the brightness of the stars included in the catalog. At the beginning of the spacecraft rotation, or scan, the inertial reference system is initialized with a guess of zero rotation angle about the sun line, the rotation angle being referenced to a suitably defined sun pointing reference frame. The stars in the star catalog are sequentially ordered according to this reference point and each star is specified by an azimuth or scan angle ϕ_c measured from the reference (in the direction of spacecraft rotation) and a declination relative to the swath plane, δ_c (the subscript c stands for catalog). Then, as the star tracker sweeps out the swath, the time and the scan angle for each star encountered by the tracker will be recorded. The scan angle is obtained from the inertial reference unit, i.e., integrated gyro rate, and is denoted by ϕ_T (subscript T for tracker). If the spacecraft is controlled so that it remains well aligned with the sunline, one can start to correlate the sequence of star observations to the catalog entries after one revolution. If the spacecraft rotation axis does not remain well aligned with the sunline, some stars may be missed due to the resulting wobble, and 2-3 revolutions of data taking may be required. LANDSAT D will be maintained sun pointing to within 0.1 degree when using the fine digital sun sensor or an attitude reference and one revolution should suffice.

The correlation proceeds then as follows. The first star encountered by the tracker is assumed to be the first star in the catalog and the difference ϕ_0 of the scan angles is computed,

$$\phi_0(1) = \phi_c(1) - \phi_T(1)$$

The angle $\phi_0(1)$ may be considered the first update on the initial zero estimate for the orientation angle of the spacecraft about the sun line and it is added to all the observed scan angles $\phi_T(n)$. All the observed stars are now correlated with the entries in the star catalog, considering

all possible combinations, and the number of successful correlations or matches are recorded. A successful match is considered to occur between two stars when the observed star scan angle $\phi_T(n)$ falls within a specified ε of the catalog scan angle $\phi_c(m)$, i.e.,

$$|\phi_c(m) - \phi_T(n)| < \varepsilon$$

The process is then repeated for the next pair of stars, for example the first star encountered by the tracker is assumed to be star No. 2 in the catalog and the number of successful correlations are determined under this assumption. This process is repeated until all possible star pairs have been exhausted, and the pairing that produced the most matches is declared the winner and the corresponding scan phasing angle ϕ_0 is the final estimate of the orientation angle of the spacecraft about the sun line. ϕ_0 is not selected as the angle computed for the first forced pair in the sequence, but once good correlation for a particular sequence has been established, all star measurements are considered and a least squares fit to ϕ_0 can be obtained. Initial calibration of the scan axis gyro bias can also be obtained. In principle, the elapsed time between two star observations, the $\Delta\phi_T$ scan angle as obtained from the gyros, and the $\Delta\phi_c$ for the two stars as obtained from the catalog, contain all the information to compute gyro bias. Namely

$$b_{g_{scan}} = \frac{\Delta\phi_c - \Delta\phi_T}{\Delta t}$$

In practice one uses all the data and computes a least squares fit estimate for the gyro bias.

Using this method the spacecraft orientation about the sun line can usually be determined within about 0.2 degree and the gyro bias estimate within 0.2 deg/hr. The errors are mainly due to bias and noise imperfections in the tracker and gyros. Residual gyro bias appears to be the main error source in the estimate of the scan phasing angle ϕ_0. The number of stars also influences the accuracy; the more data, the better the

estimate. The latter is, however, of little concern to LANDSAT D since one is not so much interested in the accuracy during initialization, as one is interested in a fast correlation process using only a few good stars.

A potential disadvantage of the correlation method is the length of time that may be required to obtain enough stars since trackers will not read accurately above a certain angular rate which limits the speed of commanded rotation about the sun line. Depending on the number of stars in the swath/catalog, a more serious requirement is the rather large amount of computation required to perform the correlation tests. Since the correlation is nominally only performed at the beginning of the mission the software, which includes the swath catalog, should not be left in the computer. But erasing it and reading a new software from a special memory would require a ground command which does not fit the desired autonamous operation plan. Also, the ground command may have to be delayed until a certain favorable orbit position is reached. Since autonomous operation seems hard to attain with this method, it is recommended to perform the correlation task on the ground. In this case the star tracker data is telemetered to the ground and after convergence of the correlation procedure, the correct scan phasing angle about the sun line and the initial gyro bias calibration results are sent back to the spacecraft.

5.3.2 Simulated Star Identification by Correlation

Star identification by correlation has been simulated for L-D by a digital program using real star locations as obtained from the Yale star catalog. The time of year was assumed to be around July 20th such that the right ascension of the sun was exactly 120 degrees. The negative yaw axis of L-D was pointed to the sun with an accuracy of 0.1 degree and the spacecraft rotated about the sun line at 0.1 deg/sec. The cross-axis rates were assumed in a sinusoidal limit cycle with peak rates of 0.05 deg/sec and position amplitude limited to 0.1 degree. Initial uncalibrated gyro biases were set at values averaging to 1.5 deg/hr and the sensitivity threshold of the 8° x 8° FOV star tracker (BBRC CT-401) was set

to M_v = +4. The latter will result in a small star catalog for the swath and provide for faster and less ambiguous star identification/correlation thereby taking full advantage of the relatively large field-of-view (FOV) of the tracker.

The tracker slant angle ϕ_s relative to the ACS module, see Figure 2-5, has been assumed as $\phi_s = 30°$, and the angle between the lines of sight of the two trackers as 70°, i.e., $\pm$ 35° from the projection of the pitch axis onto the plane defined by the lines of sight of the trackers. Since both trackers make the same angle of 65.8° with the negative yaw axis, only one tracker is used.

Figure 5-2 shows a plot of all stars of 4th order magnitude and brighter and also shows the line traced out by the tracker boresight on the celestial sphere. Figure 5-3 removes all stars which do not fall into the swath traced out by the field-of-view of the tracker and marks those which are eclipsed by the earth. As can be seen, only four stars are left making correlation of tracker observations with the catalog very simple. Figure 5-3 also shows the assumed starting point of the scan according to which the sequence of stars in the star catalog is organized, and also shows the actual starting point. Thus, the first star encountered by the tracker is actually the star with Yale number 3487 but the tracker assumed at first that it was star number 1038. During the correlation process all stars are eventually correctly identified and a scan phasing angle of $\hat{\phi}_0 = 224.9$ degrees is determined. This is within 0.1 degree of the actual scan phasing angle of $\phi_0 = 225$ degrees between the initially assumed scan starting point and the actual starting point. The yaw gyro bias was estimated as 1.2 deg/hr and its actual value was 1.4 deg/hr.

It is seen that the accuracy of the correlation method is much better than determination if the orientation about the sun line using magnetic field measurements. However, as shall be shown in the following section, this improved accuracy is not required to initialize the stellar-inertial attitude reference system and the magnetic method will work just fine.

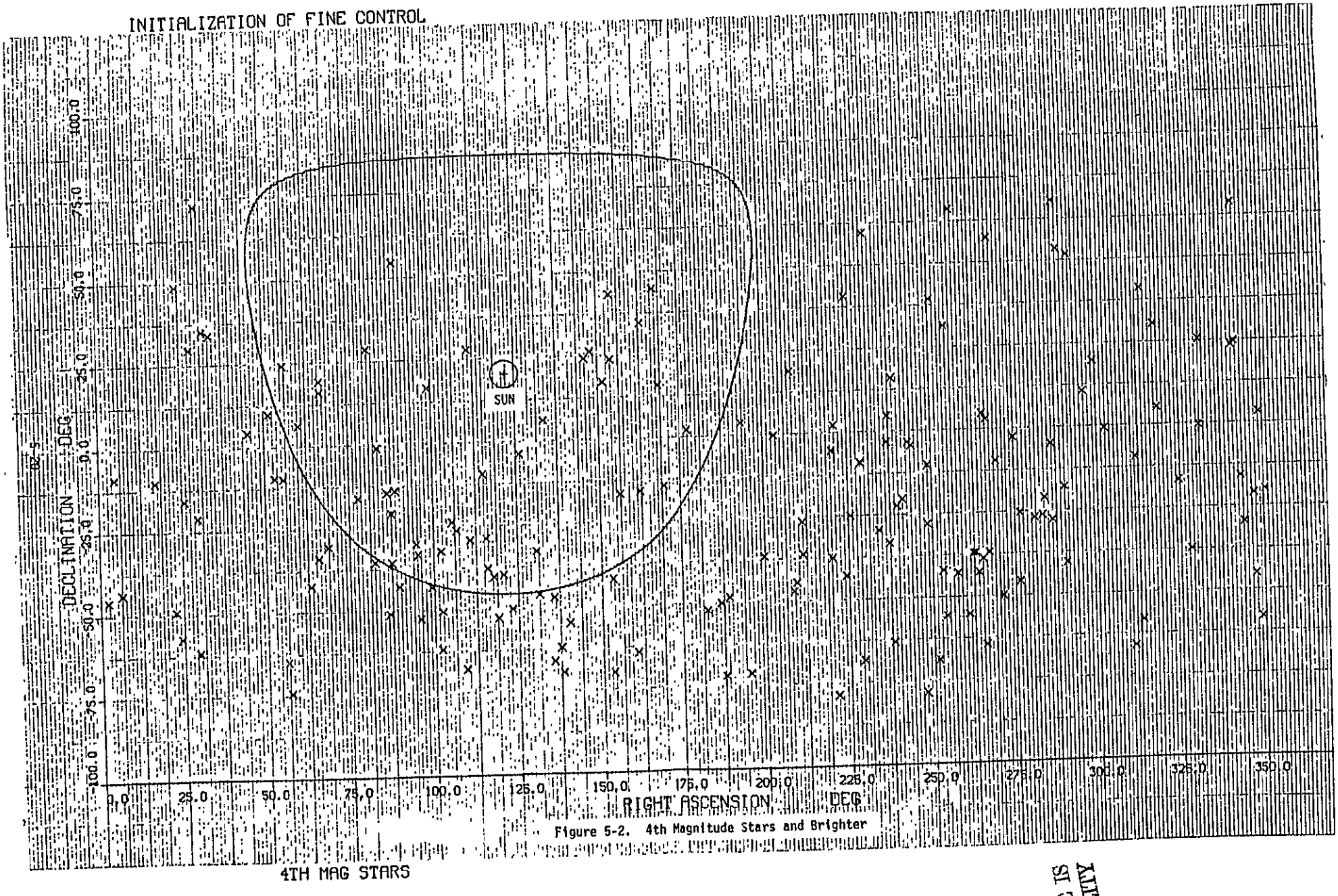

Figure 5-2. 4th Magnitude Stars and Brighter

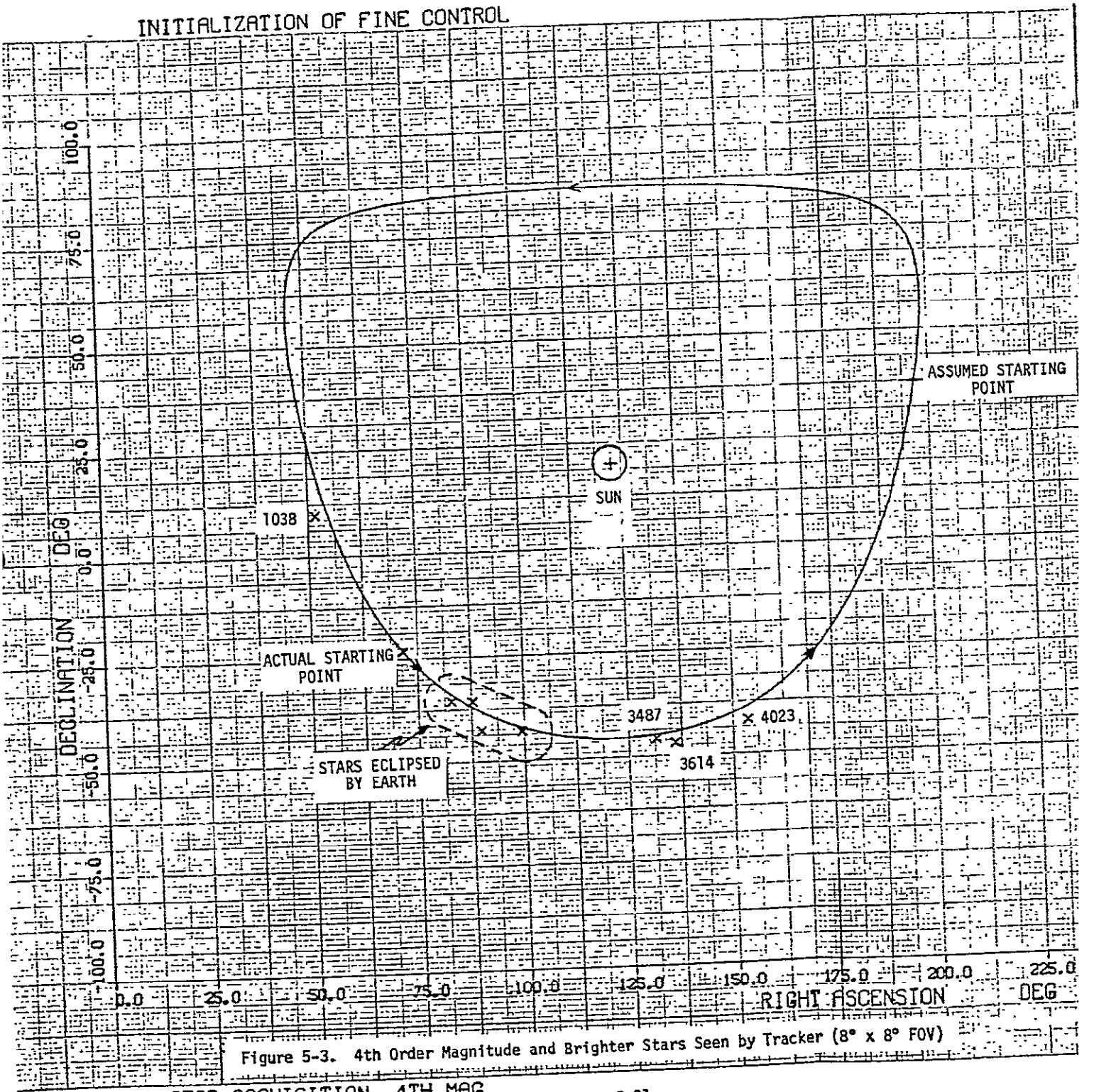

Figure 5-3. 4th Order Magnitude and Brighter Stars Seen by Tracker (8° x 8° FOV)

5.4 Convergence of On-Board Attitude Reference Filter

Attitude of the spacecraft about the sun line was estimated to within about 2° when magnetic field measurements were used, and to within about 0.1° when the star catalog correlation method was used. The magnetic method is simpler and faster and is preferred.

To demonstrate convergence of the on-board attitude reference filter with initial conditions corresponding to the nominal conditions at the end of magnetic-solar acquisition, an attitude estimation simulation was performed using an extended Kalman filter. For the spacecraft this is a part of the stellar acquisition mode. Since the negative yaw axis is sun pointing to within 0.1 degree, roll and pitch attitude uncertainties are a maximum of 0.1 degree at the initiation of fine stellar acquisition. These errors along with a nominal 2.0 degree estimation error about yaw resulting from the magnetic-solar attitude determination are used as initial conditions for the filter.

Actual stars that the star tracker would see are determined by selecting a time of year for the sun position. As in Section 5.3, the time around the 20th of July is again selected with the sun angle at 120° measured in the ecliptic plane. As described earlier, when the spacecraft is sun pointing the star trackers are inclined at an angle of 65.82° to the sun line. The star tracker sensitivity threshold has been set to $M_V = 5$ so that the tracker will sweep out a swath of fifth magnitude or brighter stars as shown in Figure 5.4 when the spacecraft is commanded to rotate about the sun line. The field-of-view is 8° x 8°, and stars eclipsed by the earth are not shown. Also several other stars satisfying the $M_V = 5$ or brighter criterion, are not shown and the stars indicated in Figure 5-4 represent the reference star catalog to be used in stellar convergence. The stars are listed in Table 5-1.

With a 2° attitude uncertainty about yaw at the end of solar-magnetic acquisition, it is doubtful whether the stars that happen to appear in the field-of-view of the trackers at that time are sufficiently separated from neighboring stars to yield an unambiguous star identification. To avoid

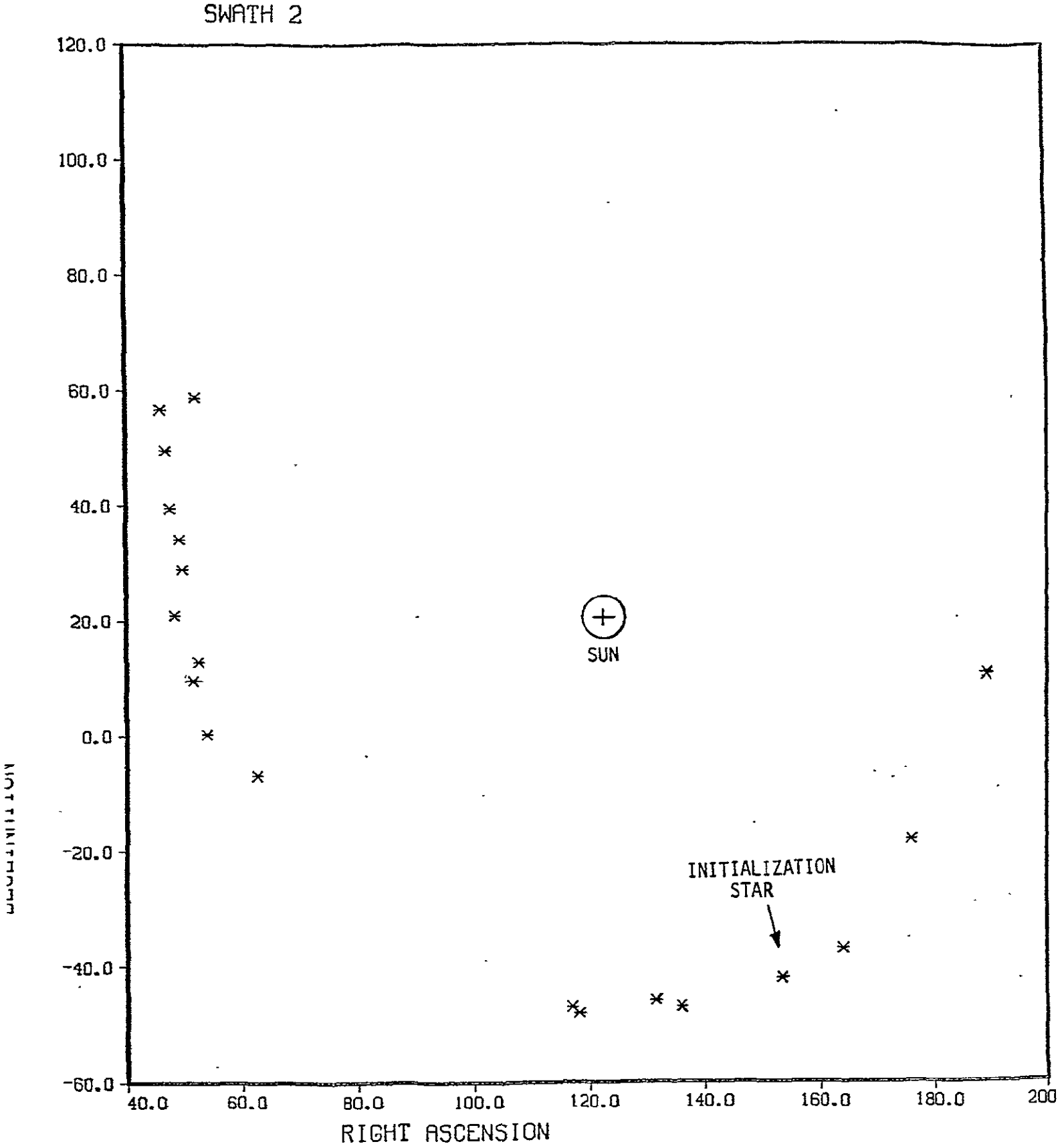

Figure 5-4. Reference Stars, M_v = +5 and Brighter

Table 5-1. Reference Star Catalog, Sun Pointing Mode

	Scan Angle in Swath Plane	Declin. Rel. Swath Plane	Yale Catalog Number	No Multiple No Variable	Right Ascension	Declination	Spectral Class	Galactic Longitude	Galactic Latitude	Visual Brightness, M_V		
1	2.6072	24.049	4826	00	190.2175	10.343	A0	294.8	73.0	4.88		
2	23.0780	21.641	4983	00	197.7333	27.983	G0	43.2	85.4	4.26		ECLIPSED
3	36.2469	23.332	4997	00	198.2025	40.257	K0	104.9	76.2	4.92		
4	69.5707	26.022	4795	00	188.4717	70.127	K2	125.0	47.0	4.94		
5	86.4601	28.145	3751	00	143.5592	81.407	K3	130.7	32.7	4.28		
6	93.3292	27.435	2350	00	100.0692	82.133	A2	131.8	26.6	4.09	R	
7	109.0924	26.971	1148	00	57.0633	71.257	A3	136.3	13.3	4.65		
8	123.2687	27.416	1040	00	52.0758	58.813	A0	142.2	2.1	4.56		
9	125.8670	24.293	918	00	46.0075	56.637	K0	140.6	-1.5	4.75		
10	133.6778	24.658	937	00	46.9058	49.540	G0	144.6	-7.4	4.05		
11	144.6668	24.250	947	00	47.4983	39.540	K0	150.2	-15.7	4.61		
12	150.7687	25.026	991	00	49.3667	34.143	K2	154.6	-19.5	4.82		
13	156.4468	24.537	999	00	49.7808	28.977	K4	158.1	-23.5	4.47		
14	164.6785	21.632	972	00	48.4375	20.960	A0	162.4	-30.6	4.90		
15	174.2046	23.179	1066	00	52.4408	12.880	K0	172.1	-34.3	4.11		
16	177.2319	21.358	1036	00	51.5208	9.663	B8	174.0	-37.3	3.72		
17	187.5103	20.497	1101	00	53.9617	.337	F8	185.1	-41.7	4.26		
18	198.5253	25.597	1298	00	62.7225	-6.887	F2	199.3	-38.4	4.05		
19	235.7477	22.880	1862	00	82.6267	-35.497	K1	239.9	-30.9	3.86		ECLIPSED
20	239.3896	25.150	2040	00	87.5650	-35.773	K2	241.4	-27.1	3.11		
21	241.0633	24.581	2067	00	88.6992	-37.120	G8	243.1	-26.5	4.96		
22	245.1220	20.234	2120	00	89.6342	-42.817	K0	249.5	-27.2	3.95		
23	252.0060	23.242	2451	00	99.2883	-43.167	B8	251.9	-20.5	3.17		
24	259.5687	21.870	2740	00	107.9592	-46.733	F0	257.7	-16.0	4.48		
25	266.1247	22.620	3046	00	116.9383	-47.033	K0	260.7	-10.7	4.70		
26	267.1163	21.662	3090	00	118.1783	-48.063	B1	262.1	-10.4	4.23		
27	276.9083	23.325	3467	00	131.3350	-45.977	A0	265.4	-1.9	3.90		
28	279.9879	21.677	3614	00	135.8650	-47.020	K2	268.2	-.1	3.74		
29	294.4717	21.397	4023	00	153.4733	-42.033	A2	274.3	11.9	3.84	←	INITIALIZATION STAR
30	304.6007	20.565	4273	00	163.9458	-37.027	G5	278.9	20.3	4.59		
31	327.5218	24.782	4514	00	175.9383	-18.240	G8	281.5	41.7	4.72		

false identification, a bright star is selected that is sufficiently separated from neighboring stars, even if dimmer. The spacecraft is commanded to rotate about the sun line, look for this star, and use it to initialize the attitude filter. This assures correct identification of the star used in the first attitude update. This first update significantly improves attitude knowledge and identifications of subsequent stars of 5th order magnitude and brighter will pose no problems.

The required rotation about the sun line is the main reason why it was recommended that L-D should align the yaw axis with the sun line and not the (canted) solar array normal. Rotation about a non-principal axis that is not a spacecraft control axis and to which the star tracker lines of sight are not symmetric, appears undesirable.

The bright and isolated star selected here for initializing the filter is indicated by an arrow in Figure 5-4. It is star number 29 in Table 5-1 and it has the Yale Number 4023. In the filter simulation, the forward looking star tracker encounters this star almost immediately and convergence is rapid as shown in Figure 5-5. An enlarged plot of the same data is shown in Figure 5-6 where it is seen that the errors in all axes have converged to approximately 5 arc-sec (1σ) at the end of half a revolution (0.5 hr) about the sun line. Gyro biases were calibrated to within 0.0013 deg/hr (1σ). Both trackers were read in this simulation every 30 seconds. If both trackers are read only every 300 seconds, the results of Figures 5-7 and 5-8 are obtained where convergence to about 10 arc-sec (1σ) is achieved with gyro bias calibration being about the same, i.e., 0.0013 deg/hr (1σ). Both performances satisfy the requirements for successful stellar acquisition and the spacecraft can be considered in inertial hold mode.

With a precision stellar inertial attitude reference successfully established, spacecraft ephemeris data is used to obtain an earth pointing attitude reference. This may be done as follows. Let A_{br} denote the direction cosine matrix describing the spacecraft's attitude relative to the

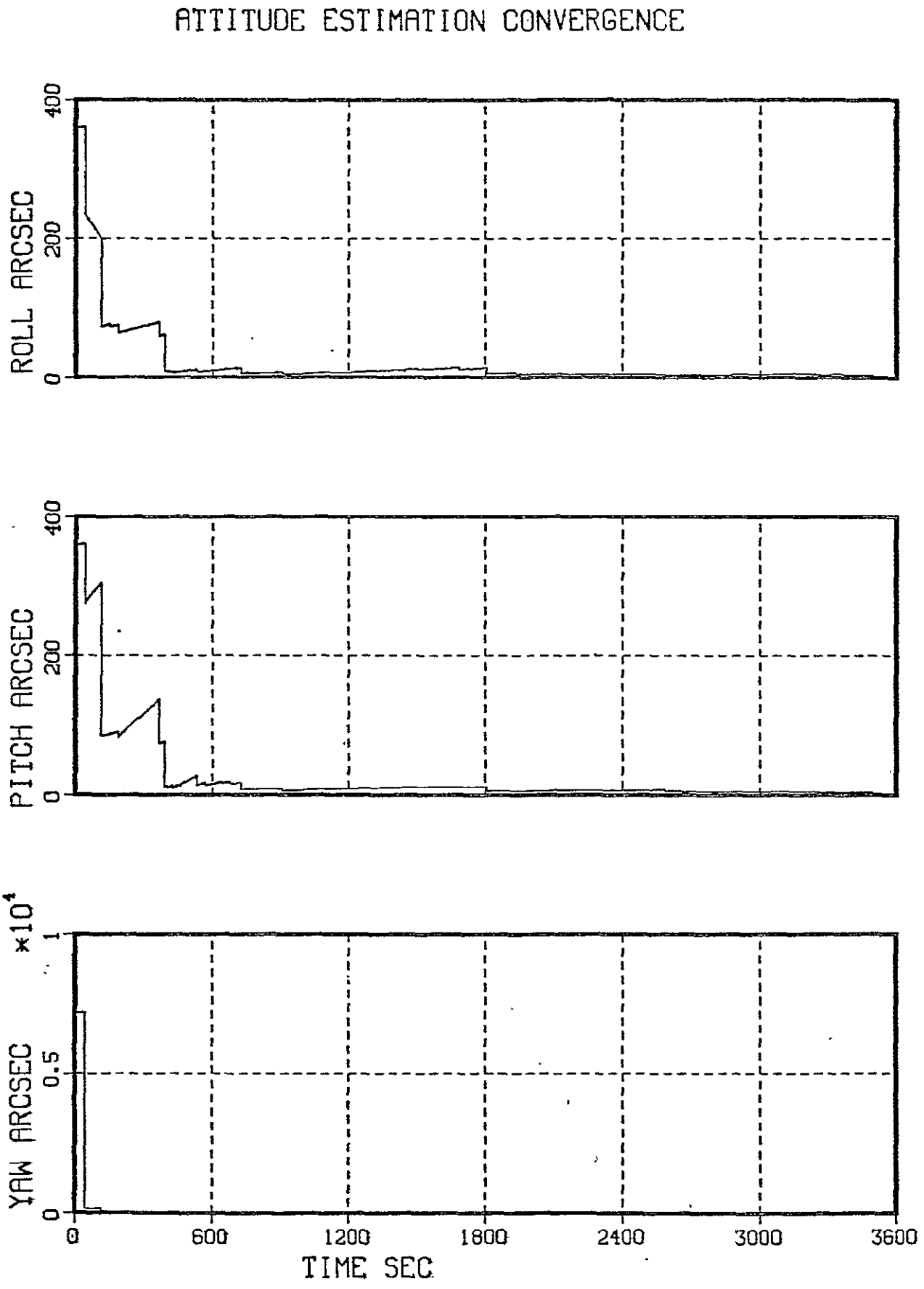

Figure 5-5. Attitude Reference Filter Convergence After Initialization from Large Attitude Uncertainties (30 Second Update Interval)

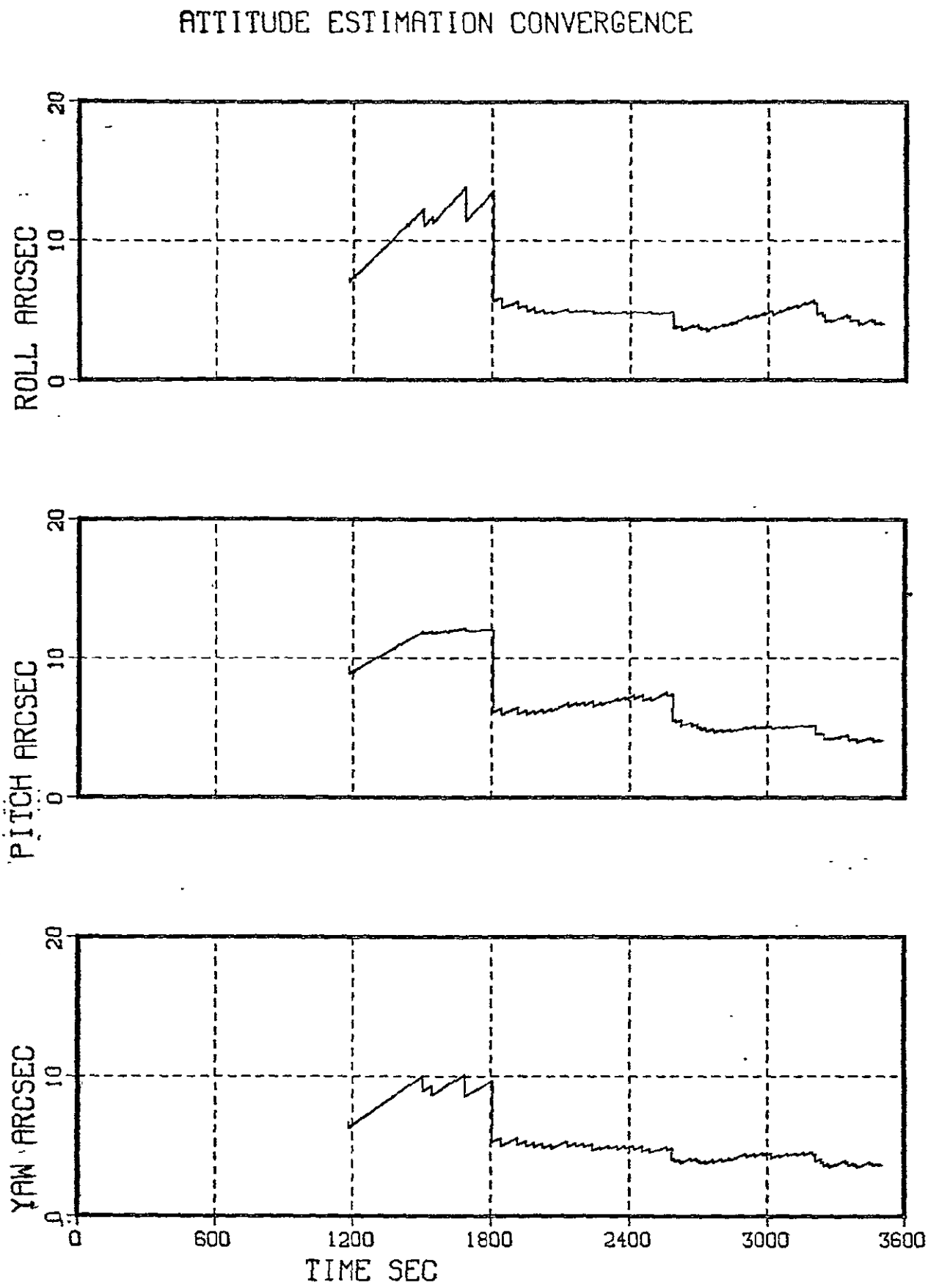

Figure 5-6. Attitude Reference Filter Convergence After Initialization (Expanded Scale Figure 5-5)

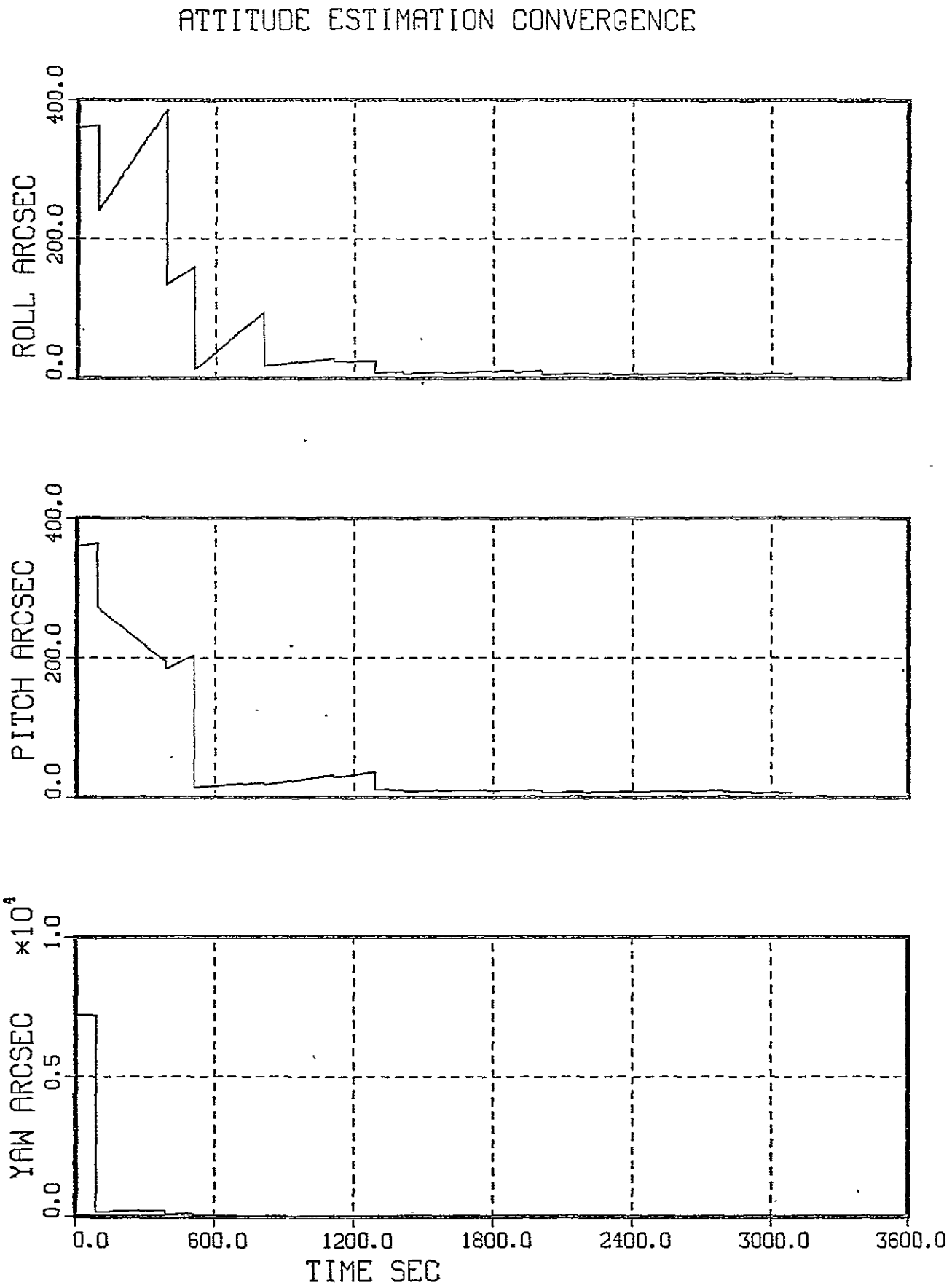

Figure 5-7. Attitude Reference Filter Convergence After Initialization from Large Attitude Uncertainties (300 Second Update Interval)

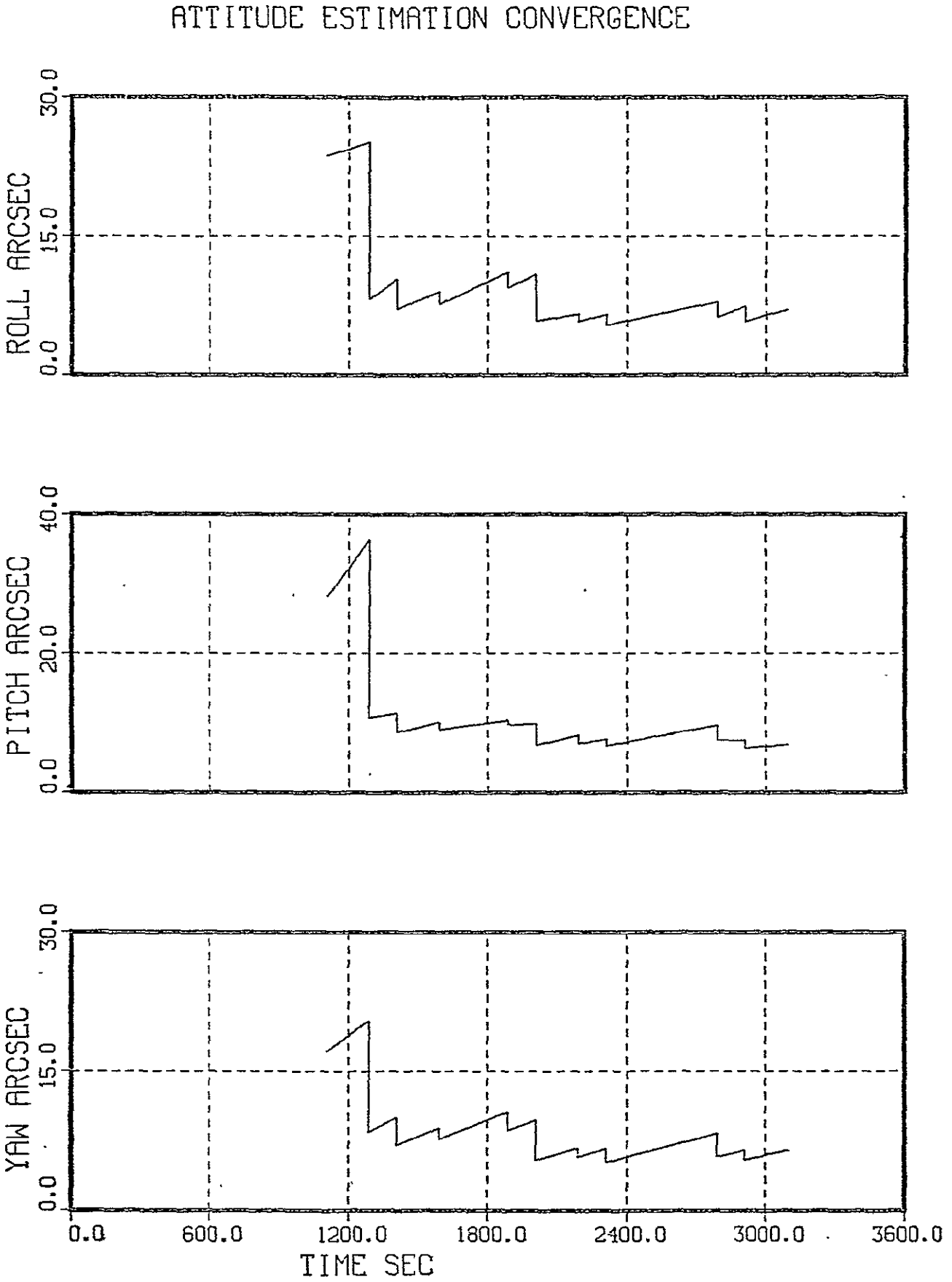

Figure 5-8. Attitude Reference Filter Convergence After Initialization (Expanded Scale Figure 5-7)

the earth pointing orbital reference frame $\{\hat{x}_r, \hat{y}_r, \hat{z}_r\}$. Then A_{br} is the desired earth pointing attitude reference. The stellar inertial attitude reference system provides the spacecraft's attitude relative to ECI given by the direction cosine matrix A_{bI}; the ephemeris provides the attitude of the earth pointing , orbital reference frame relative to ECI by the direction cosine matrix A_{rI}. Hence, the desired earth oriented attitude reference A_{br} is given by

$$A_{br} = A_{bI} A_{rI}^{T}$$

The above could have also been done in terms of quaternions and quaternion algebra, but frequently direction cosine matrices are required in any event and it is advantageous to perform the computations as indicated. Figure 5-9 shows a functional block diagram of the on-board attitude reference system.

With A_{br} established, tne spacecraft is commanded to slew away from the sun and assume its earth pointing orientation. After attitude settling, the spacecraft is in the normal on-orbit fine pointing mode and ready to turn on the payload sensors and take data. A_{br} represents then a very-small-angle rotation matrix, and single axis, i.e., roll, pitch and yaw, control errors can be extracted from the appropriate off-diagonal terms of A_{br}.

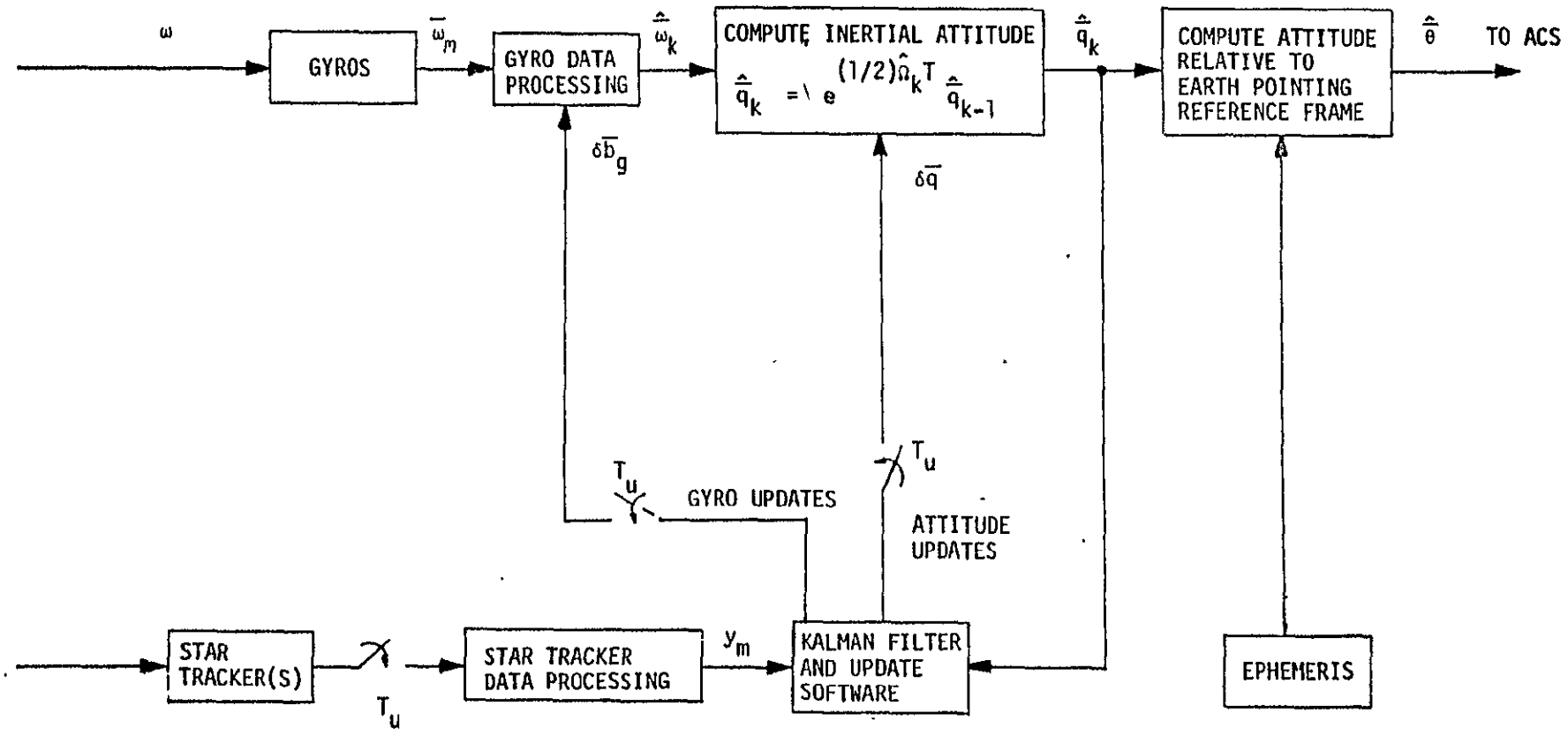

Figure 5-9. Functional Block Diagram Stellar Inertial ARS

REFERENCES

1. "Low Cost Modular Spacecraft Description," NASA/GSFC Report Number X-700-75-140, May 1975.

2. "Specification for Multi-Mission Modular Spacecraft (MMS) Attitude Control Subsystem," F. J. Kull, NASA Document GSFC-S-700-17, April 1976.

3. "Telecommunicator Service Via a Tracking and Data Relay Satellite System. Phase II, Implementation and Operations," Proposal to NASA by TRW DSG, Part 2, Vol. 4, 15 January 1976.

4. "Precision Pointing Control System (PPCS) System Design and Analysis," TRW Technical Report No. 13900-6012-RO-01, 1 July 1972.

5. "Design Study Landsat Follow-On Mission Unique Communications System," prepared by TRW DSG for NASA/GSFC, TRW Report No. 14897-6007-RU-00, August 1976.

6. "ALLMAG, GDALMG, LINTRA: Computer Programs for Geomagnetic Field and Field-Line Calculations," E. G. Stassinopoulos and Gilbert D. Mead, NASA/GSFC Report No. NSSDC 72-12, February 1972.

7. "The Attitude Determination System for the Orbiting Astronomical Observatory," P. B. Davenport, Proceedings of the Symposium on Spacecraft Attitude Determination, pp. 249-256, held at the Aerospace Corporation, El Segundo, Ca., October 1969.

PROGRAM LFO

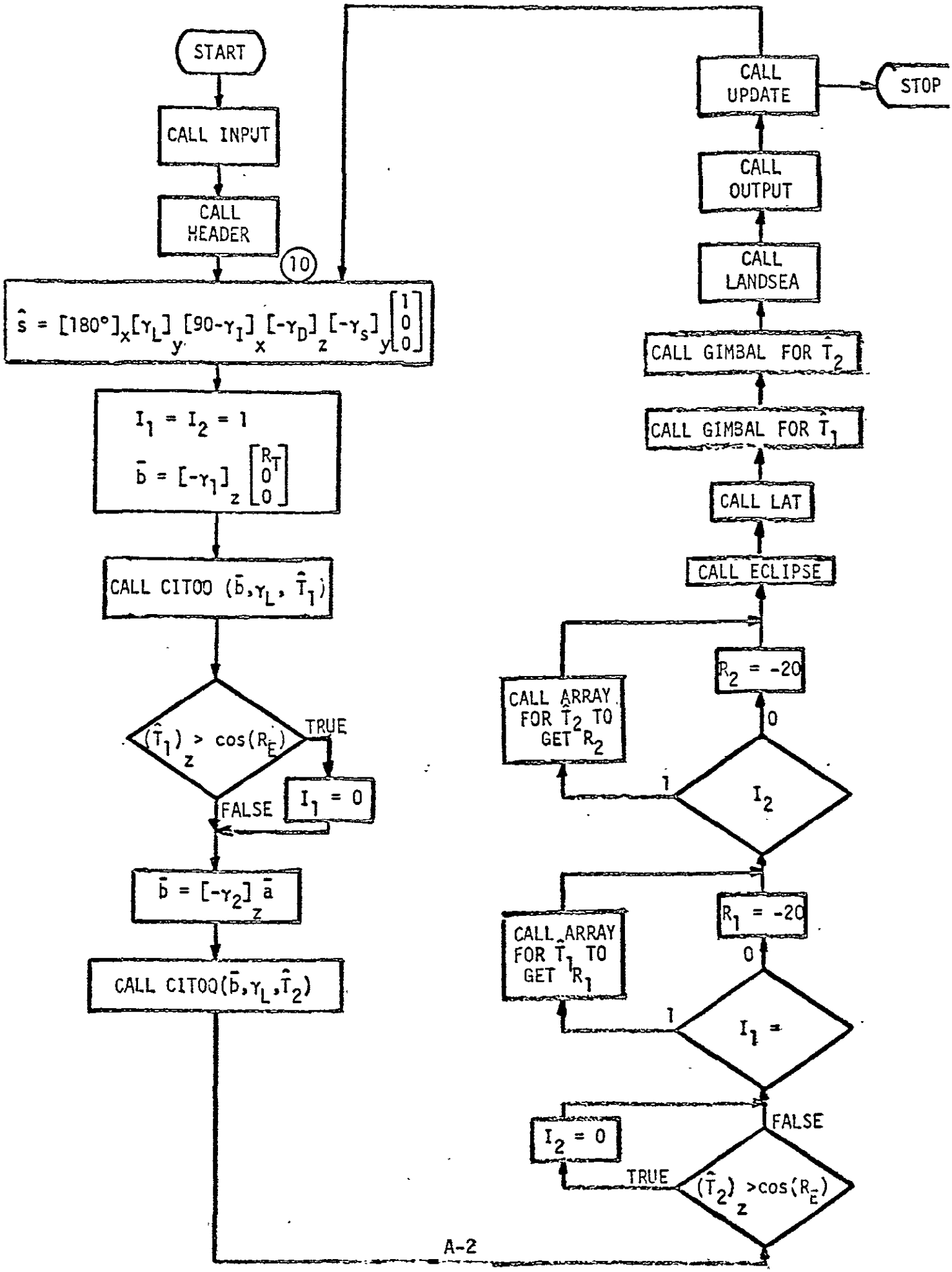
START
CALL INPUT
CALL HEADER
10
$\hat{s} = [180°]_x[\gamma_L]_y [90-\gamma_I]_x [-\gamma_D]_z [-\gamma_s]_y \begin{bmatrix}1\\0\\0\end{bmatrix}$
$I_1 = I_2 = 1$
$\bar{b} = [-\gamma_1]_z \begin{bmatrix}R_T\\0\\0\end{bmatrix}$
CALL CITOO $(\bar{b}, \gamma_L, \hat{T}_1)$
$(\hat{T}_1)_z > \cos(R_E)$
TRUE
$I_1 = 0$
FALSE
$\bar{b} = [-\gamma_2]_z \bar{a}$
CALL CITOO$(\bar{b}, \gamma_L, \hat{T}_2)$
CALL UPDATE
STOP
CALL OUTPUT
CALL LANDSEA
CALL GIMBAL FOR $\hat{T}_2$
CALL GIMBAL FOR $\hat{T}_1$
CALL LAT
CALL ECLIPSE
$R_2 = -20$
0
I_2
1
CALL ARRAY FOR $\hat{T}_2$ TO GET R_2
$R_1 = -20$
0
I_1 =
1
CALL ARRAY FOR $\hat{T}_1$ TO GET R_1
FALSE
$I_2 = 0$
TRUE
$(\hat{T}_2)_z > \cos(R_E)$

SUBROUTINE OUTPUT

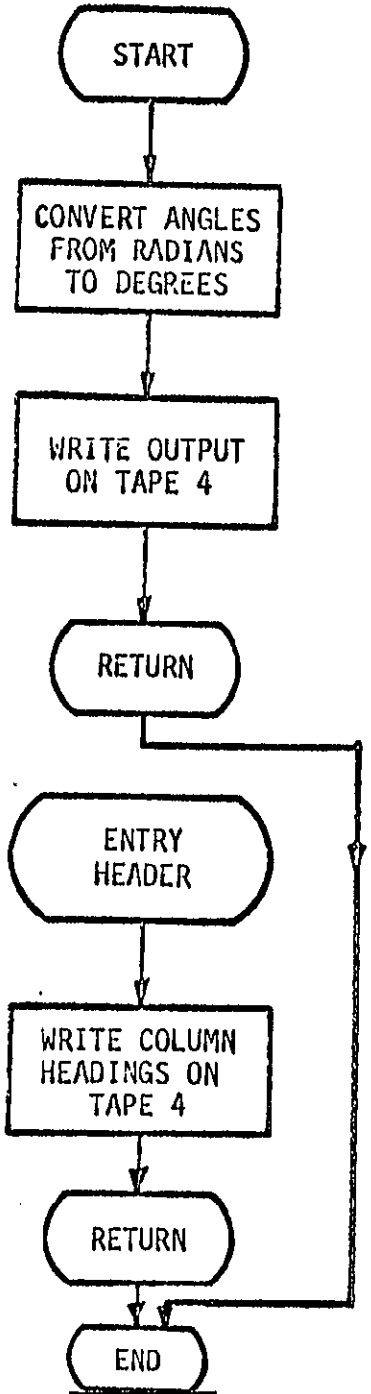

SUBROUTINE UPDATE

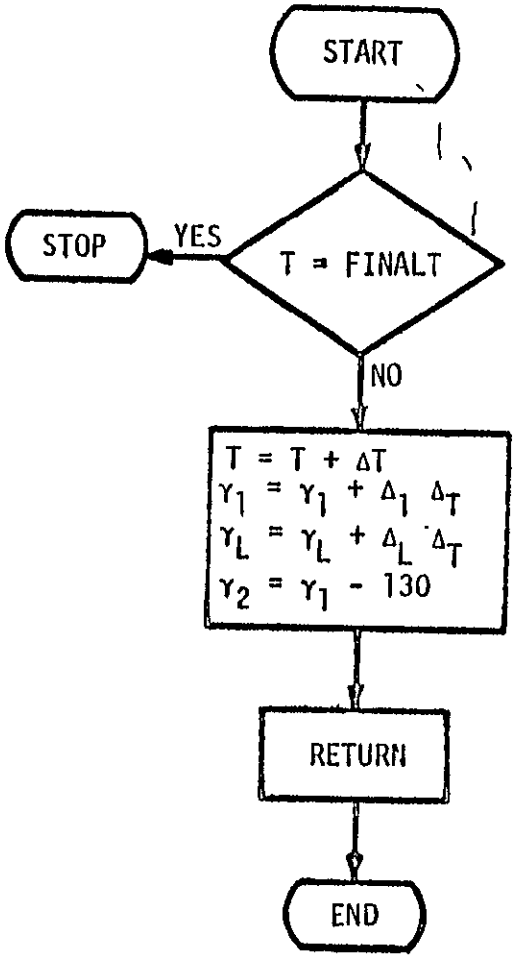

SUNROUTINE INPUT

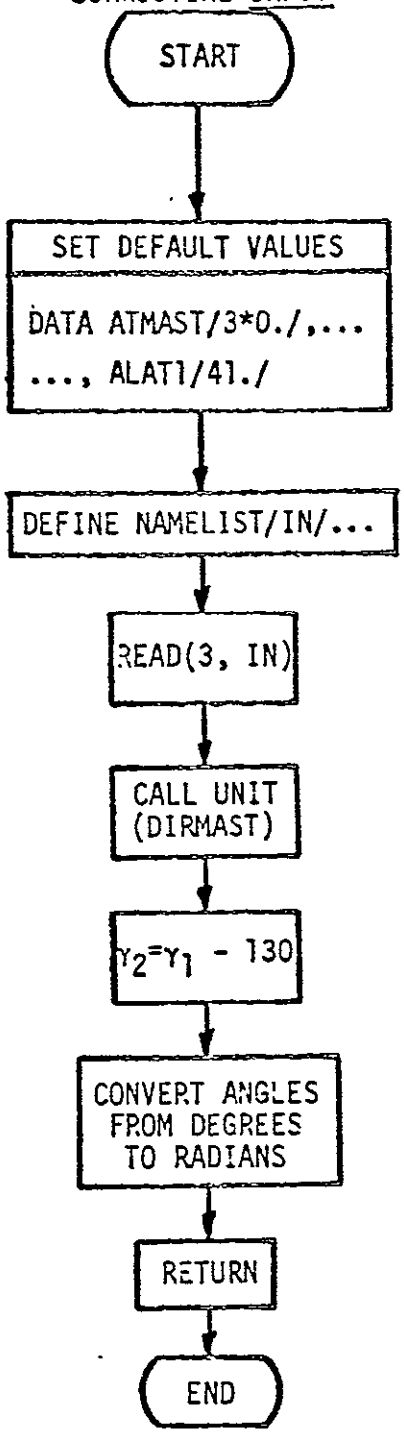

SUBROUTINE BASIS (a, e, d)

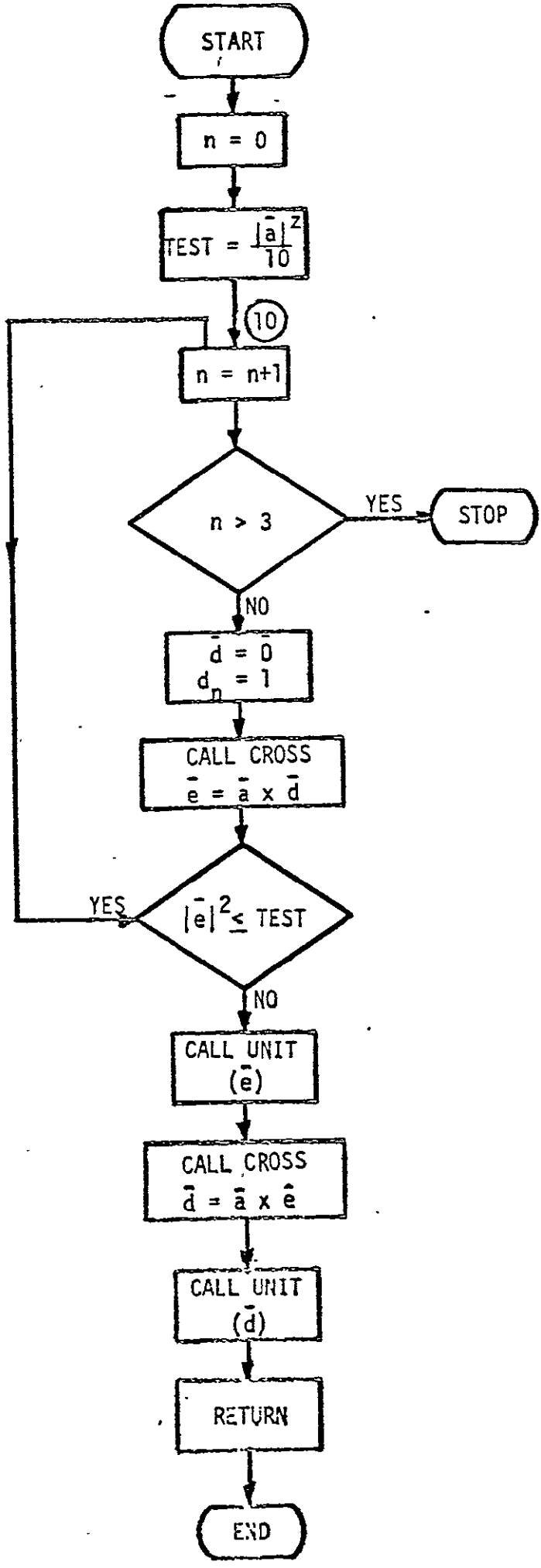

SUBROUTINE ARRAY ($\bar{T}$, $\bar{S}$, R)

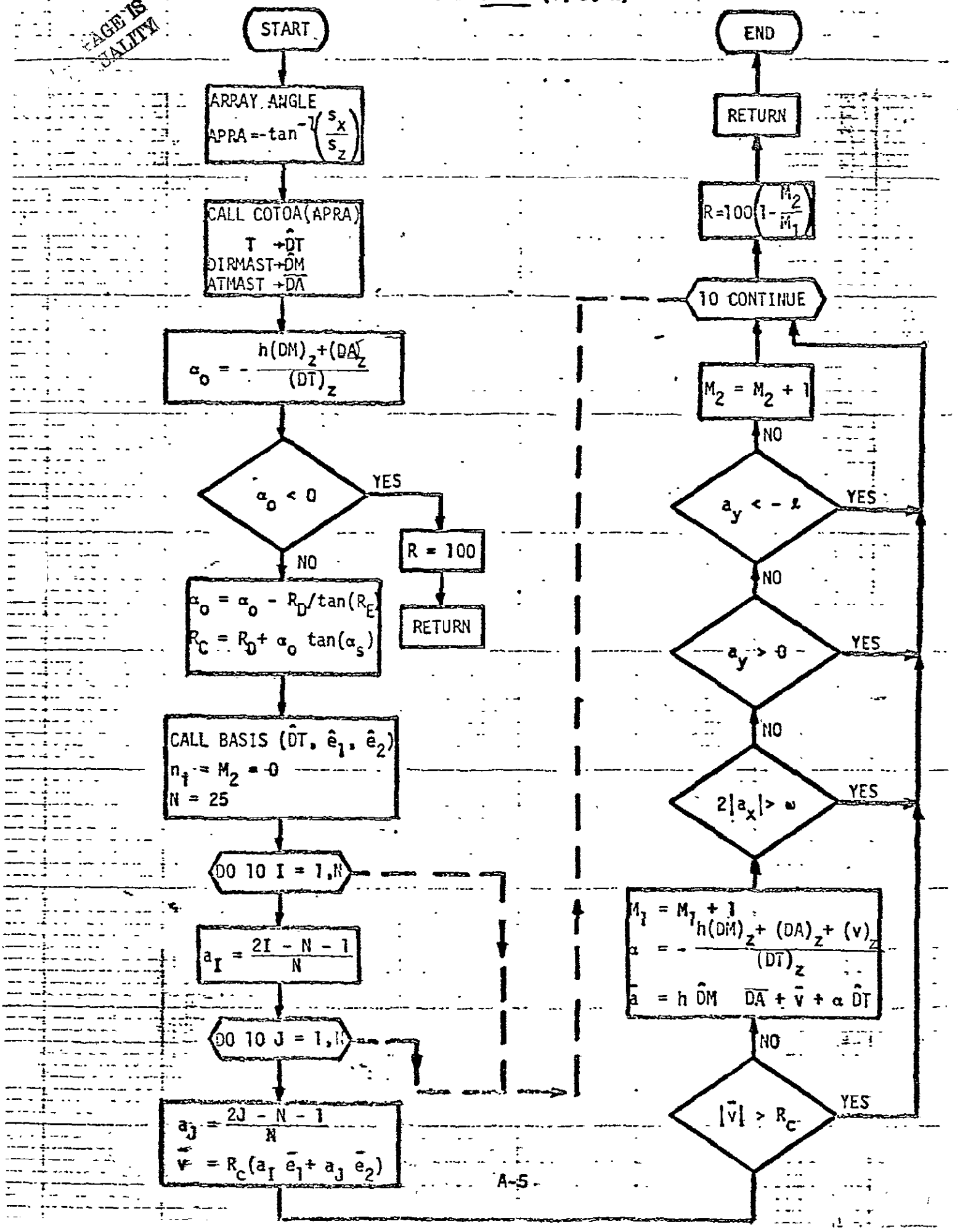

SUBROUTINE LAT

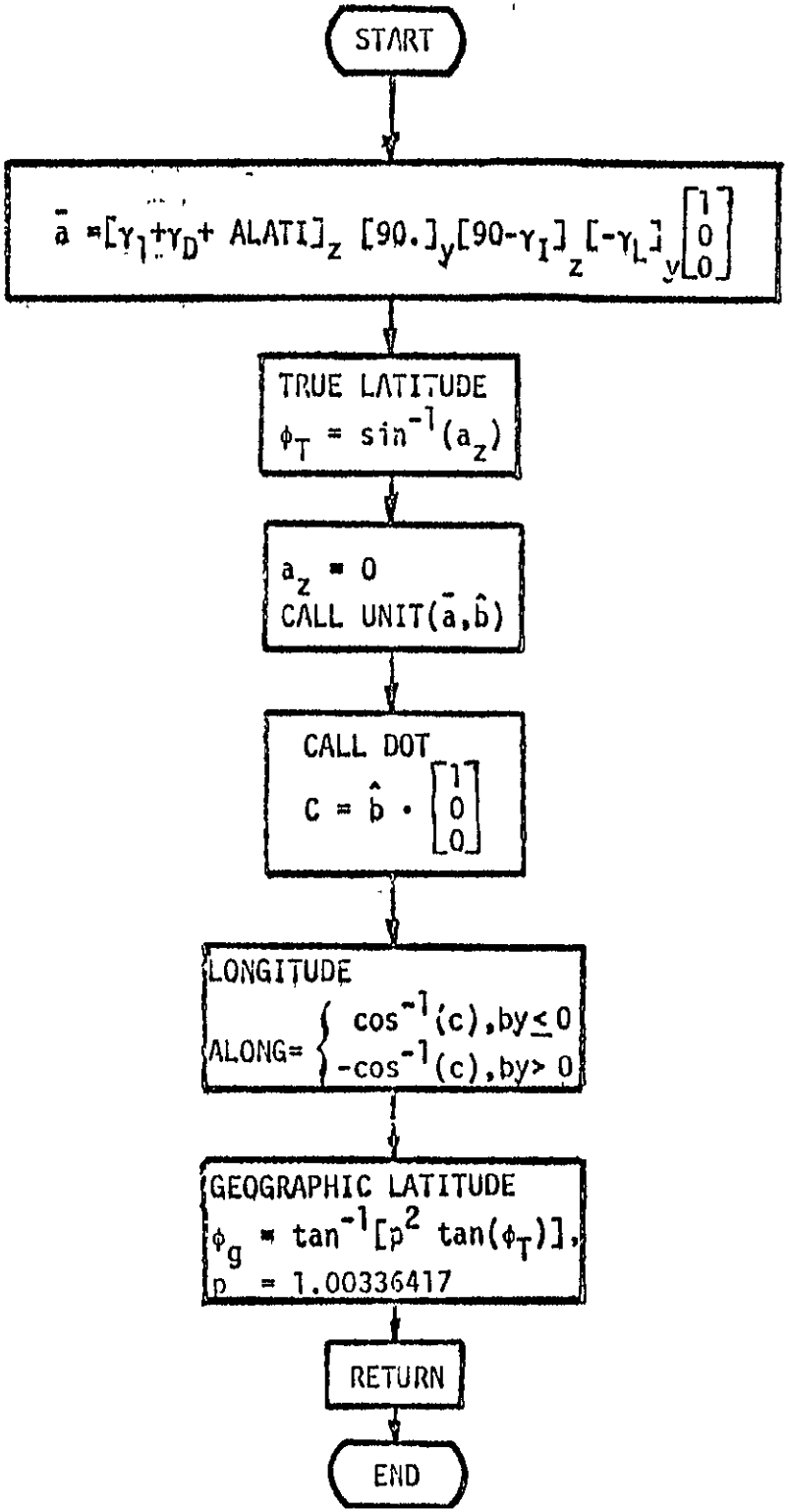

SUBROUTINE LANDSEA

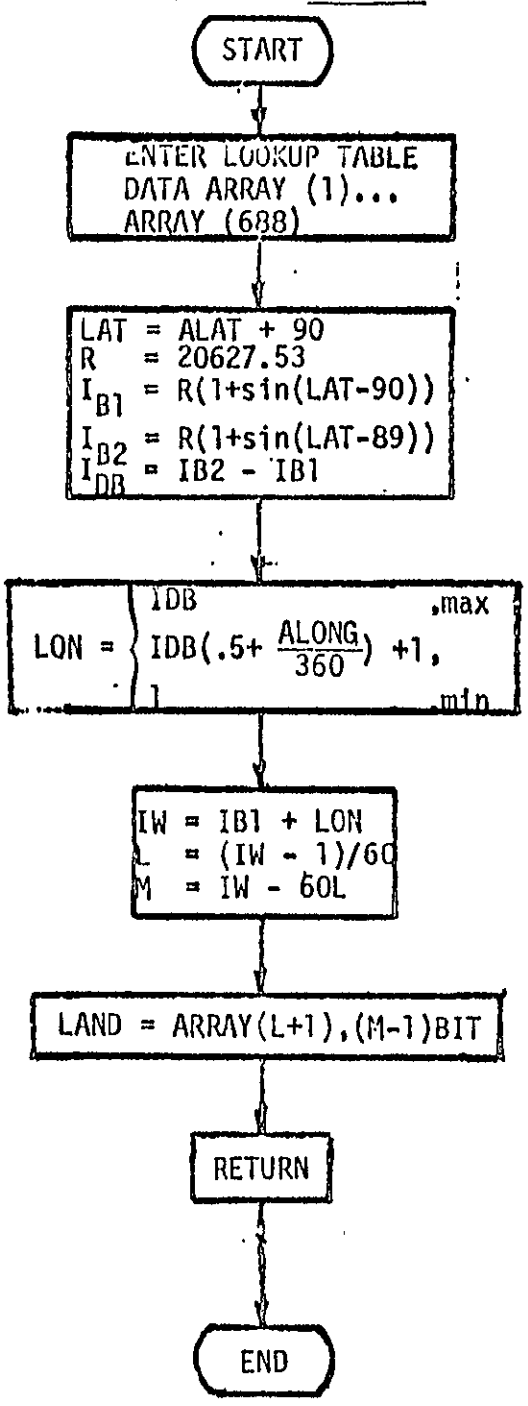

SUBROUTINE GIMBAL ($\bar{T}$, G_1, G_2, G_3)

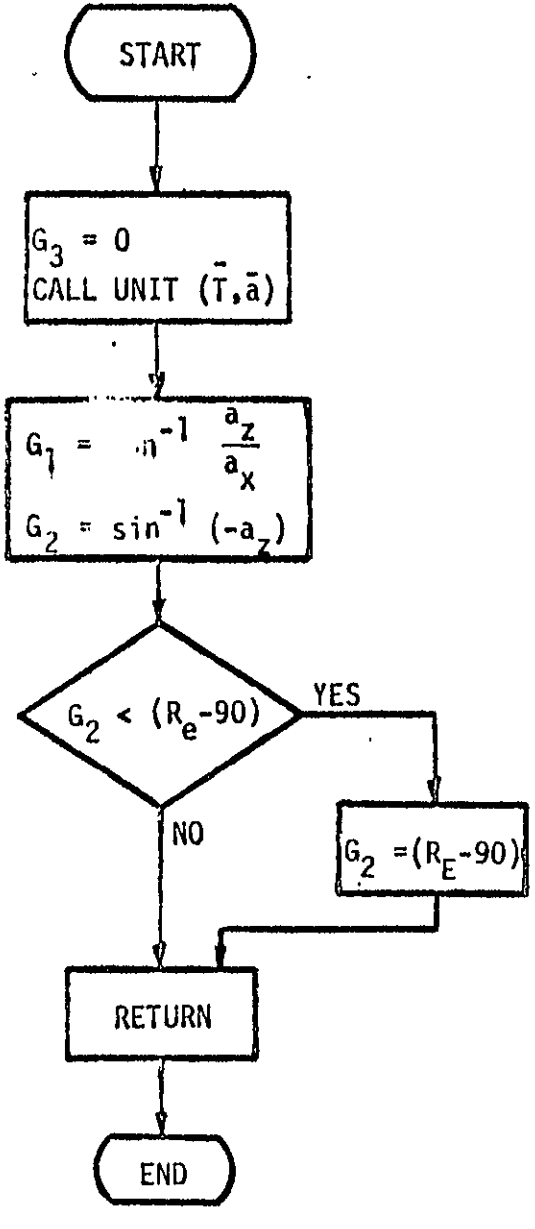

SUBROUTINE ECLIPSE

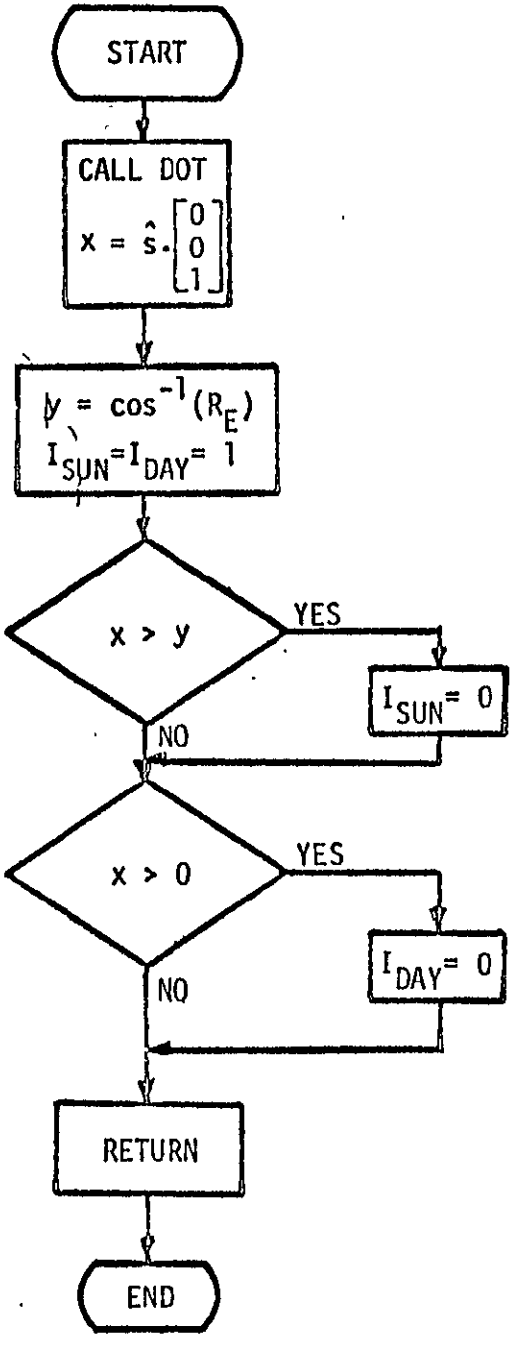

SUBROUTINE CITOO ($\bar{a}, \gamma_L, b$)

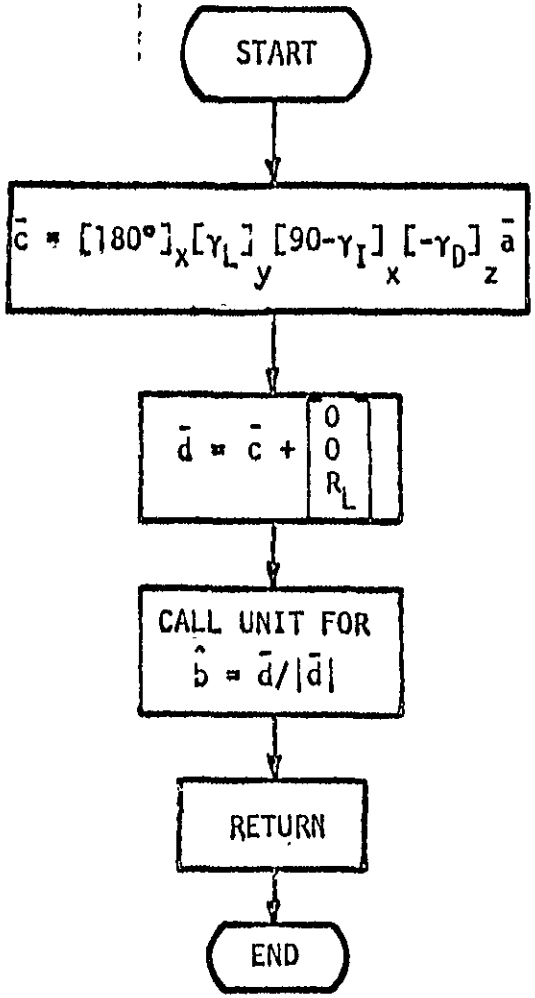

SUBROUTINE COTOA($\bar{a}, \rho, \bar{b}$)

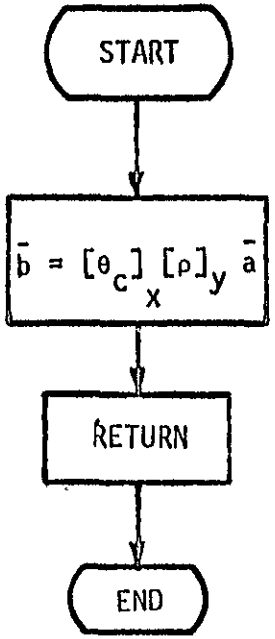

SUBROUTINE ROT($\bar{x}_I$,a,n,$\bar{x}_0$)

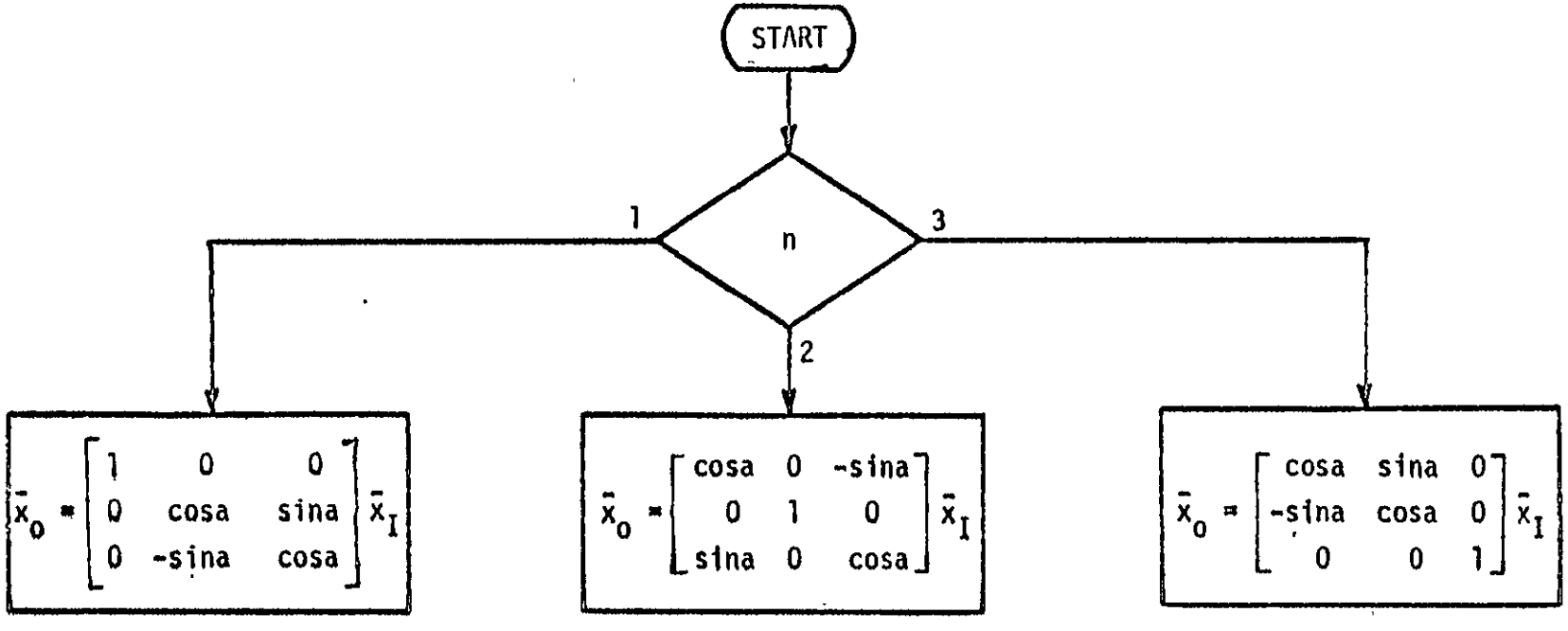

SUBROUTINE UNIT ($\bar{x}$, $\hat{y}$)

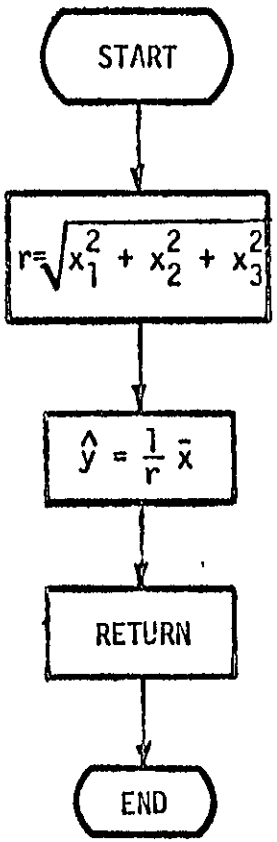

SUBROUTINE DOT ($\bar{x}$,$\bar{y}$,a)

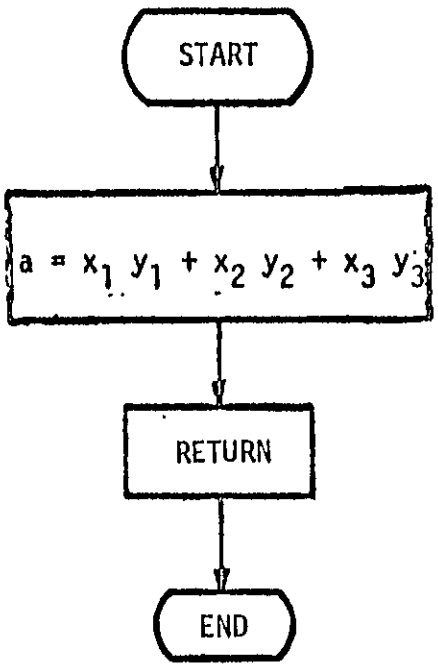

SUBROUTINE CROSS ($\bar{a}$,$\bar{b}$,$\bar{c}$)

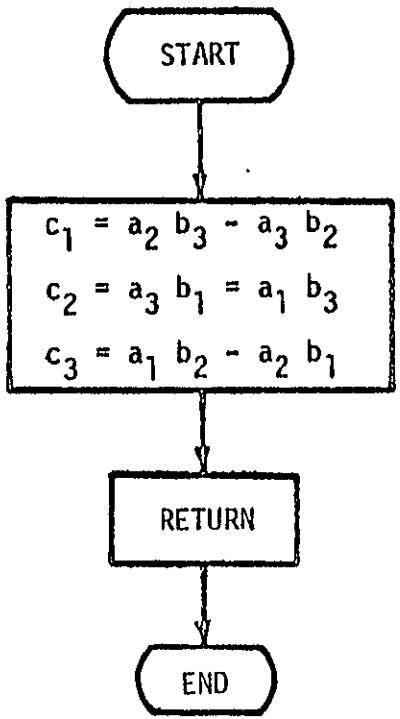

```
00100       PROGRAM LFO(TAPE3,INPUT,OUTPUT,TAPE1=INPUT,TAPE2=OUTPUT,TAPE4)
00110       COMMON/CARR/ATMAST(3),DIRMAST(3),HMAST,RDISH,ALPHAS,
00120      1     ARRW,ARRL,CANT,REARTH
00130       COMMON/CORB/GAMMAI,GAMMAD,RL
00140       COMMON/CML/GAMMAS,GAMMA1,GAMMA2,GAMMAL,RT,ALAT1
00150       COMMON/CUP/DELTA1,DELTAL,DELTAT,FINALT
00160       COMMON/COUT/T1(3),T2(3),S(3)
00170       DIMENSION A(3),B(3),C(3)
00180       F(ARG)=ARG*3.141592654/180.
00190       CALL INPUT
00200       REWIND 4
00210       LAND=2
00220       CALL HEADER(TIME,RL,RT,GAMMA1,GAMMAS,GAMMAL)
00230    10 CONTINUE
00240       A(1)=1.
00250       A(2)=0.
00260       A(3)=0.
00270       CALL ROT(A,-GAMMAS,2,B)
00280       CALL ROT(B,-GAMMAD,3,S)
00290       CALL ROT(S,(F(90.)-GAMMAI),1,B)
00300       CALL ROT(B,GAMMAL,2,C)
00310       CALL ROT(C,F(180.),1,S)
00320       I1=1
00330       I2=1
00340       A(1)=RT
00350       CALL ROT(A,-GAMMA1,3,B)
00360       CALL CITOO(B,GAMMAL,T1)
00370       IF(T1(3).GT.COS(REARTH)) I1=0
00380       CALL ROT(A,-GAMMA2,3,B)
00390       CALL CITOO(B,GAMMAL,T2)
00400       IF(T2(3).GT.COS(REARTH)) I2=0
00410       IF(I1.EQ.1) CALL ARRAY(T1,S,R1)
00420       IF(I2.EQ.1) CALL ARRAY(T2,S,R2)
00430       IF(I1.EQ.0) R1=-20.
00440       IF(I2.EQ.0) R2=-20.
00450       CALL ECLIPSE(S,REARTH,ISUN,IDAY)
00460       CALL LAT(GAMMA1,GAMMAL,GAMMAI,GAMMAD,ALAT1,ALAT,ALONG)
00470       CALL GIMBAL(T1,REARTH,G11,G12,G13)
00480       CALL GIMBAL(T2,REARTH,G21,G22,G23)
00490       CALL LANDSEA(ALAT,-ALONG,LAND)
00500       CALL OUTPUT(TIME,R1,R2,GAMMA1,GAMMA2,GAMMAL,ISUN,IDAY,
00510      1ALAT,ALONG,G11,G12,G21,G22,LAND)
```

```
00520       CALL UPDATE(TIME,GAMMA1,GAMMA2,GAMMAL)
00530       GO TO 10
00540    11 CONTINUE
00550       END
00560       SUBROUTINE INPUT
00570       COMMON/CARR/ATMAST(3),DIRMAST(3),HMAST,RDISH,ALPHAS,
00580      1   ARRW,ARRL,CANT,REARTH
00590       COMMON/CORB/GAMMAI,GAMMAD,RL
00600       COMMON/CML/GAMMAS,GAMMA1,GAMMA2,GAMMAL,RT,ALAT1
00610       COMMON/CUP/DELTA1,DELTAL,DELTAT,FINALT
00620       DIMENSION A(3)
00630       DATA ATMAST/3*0./,DIRMAST/0.,0.,-1./,RDISH/3./,CANT/37.5/,
00640      1ALPHAS/2./,DELTA1/15./,DELTAL/220.31/,RL/7074./,RT/4.224E4/,
00650      2REARTH/64.2/,GAMMA1/0./,GAMMAL/0./,GAMMAS/0./,GAMMAI/98.2/
00660      3,GAMMAD/37.5/,ALAT1/41./
00670       NAMELIST/IN/GAMMA1,GAMMAL,GAMMAS,GAMMAI,REARTH,RL,RT,ATMAST,
00680      1DIRMAST,HMAST,RDISH,ALPHAS,ARRW,ARRL,CANT,DELTAT,FINALT,
00690      2DELTA1,DELTAL,GAMMAD,ALAT1
00700       F(ARG)=ARG*3.141592654/180.
00710       READ(3,IN)
00720       DO 10 I=1,3
00730    10 A(I)=DIRMAST(I)
00740       CALL UNIT(A,DIRMAST)
00750       GAMMA2=GAMMA1-130.
00760       CANT=F(CANT)
00770       REARTH=F(REARTH)
00780       GAMMAS=F(GAMMAS)
00790       GAMMA1=F(GAMMA1)
00800       GAMMA2=F(GAMMA2)
00810       GAMMAL=F(GAMMAL)
00820       GAMMAI=F(GAMMAI)
00830       DELTA1=F(DELTA1)
00840       DELTAL=F(DELTAL)
00850       ALPHAS=F(ALPHAS)
00860       GAMMAD=F(GAMMAD)
00870       ALAT1=F(ALAT1)
00880       RETURN
00890       END
00900       SUBROUTINE UPDATE(TIME,GAMMA1,GAMMA2,GAMMAL)
00910       COMMON/CUP/DELTA1,DELTAL,DELTAT,FINALT
00920       IF(TIME.GE.FINALT) STOP
00930       TIME=TIME+DELTAT
```

```
00940       GAMMA1=GAMMA1 + DELTAT*DELTA1
00950       GAMMAL=GAMMAL + DELTAT*DELTAL
00960       GAMMA2=GAMMA1 - 130.*3.141592654/180.
00970       RETURN
00980       END
00990       SUBROUTINE OUTPUT(TIME,R1,R2,GAMMA1,GAMMA2,GAMMAL,ISUN,
01000      1IDAY,ALAT,ALONG,G11,G12,G21,G22,LAND)
01010       COMMON/COUT/T1(3),T2(3),S(3)
01020    50 FORMAT(1X,1X,F8.3,9(1X,F6.1),4X,I1,3X,I1,2(1X,F6.1),3X,I1)
01030       F(ARG)=ARG*180./3.141592654
01040       AL=F(GAMMAL)
01050       A1=F(GAMMA1)
01060       A2=F(GAMMA2)
01070       ALAT=F(ALAT)
01080       ALONG=F(ALONG)
01090       G11=F(G11)
01100       G12=F(G12)
01110       G21=F(G21)
01120       G22=F(G22)
01130       WRITE(4,50)TIME,AL,A1,R1,G11,G12
01140      1,A2,R2,G21,G22,IDAY,ISUN,ALAT,ALONG,LAND
01150       RETURN
01160       ENTRY HEADER
01170    51 FORMAT(1X,5X,*TIME*,3X,*LF/O*,2X,*TDRS1*,2X,
01180      1*TRANS*,2X,*GIMBAL ANGLES*,1X,*TDRS2*,2X,*TRANS*,
01190      22X,*GIMBAL ANGLES*,2X,*DAY*,1X,*SUN*,2X,*LAT*,3X,*LONG*,3X,*LAND*)
01200       WRITE(4,51)
01210       RETURN
01220       END
01230       SUBROUTINE ARRAY(T,S,RESULT)
01240       COMMON/CARR/ATMAST(3),DIRMAST(3),HMAST,RDISH,ALPHAS,
01250      1    ARRW,ARRL,CANT,REARTH
01260       DIMENSION V(3),E1(3),E2(3),DT(3),DM(3),DA(3),A(3),T(3),S(3)
01270 C     TRANSFORM VECTORS TO ARRAY COORDINATES
01280       ARRA=-ATAN2(S(1),S(3))
01290       CALL COTOA(T,ARRA,DT)
01300       CALL COTOA(DIRMAST,ARRA,DM)
01310       CALL COTOA(ATMAST,ARRA,DA)
01320 C     FIND ANTENNA PATTERN DIAMETER
01330       TEMP=-((HMAST*DM(3) + DA(3))/DT(3))
01340       IF(TEMP.LT.0.) GO TO 300
01350       ALPHAO=TEMP - RDISH/TAN(REARTH)
```

```
01360       RC=RDISH + ALPHAO*TAN(ALPHAS)
01370 C     DETERMINE EXTENT OF INTERFERENCE
01380       CALL BASIS(DT,E1,E2)
01390       M1=0
01400       M2=0
01410       N=25
01420       DO 10 I=1,N
01430       AI=(2.*I-N-1.)/N
01440       DO 10 J=1,N
01450       AJ=(2.*J-N-1.)/N
01460       DO 11 K=1,3
01470    11 V(K)=RC*(AI*E1(K) + AJ*E2(K))
01480       TEMP=0.
01490       DO 12 K=1,3
01500    12 TEMP=TEMP + V(K)*V(K)
01510       CHECK=SQRT(TEMP)
01520       IF(CHECK.GT.RC) GO TO 10
01530       M1=M1 + 1
01540       ALPHA=-(HMAST*DM(3) + DA(3) + V(3))/DT(3)
01550       DO 13 K=1,2
01560    13 A(K)=HMAST*DM(K) + DA(K) + V(K) + ALPHA*DT(K)
01570       TEMP=2.*ABS(A(1))
01580       IF(TEMP.GT.ARRW) GO TO 10
01590       TEMP=A(2)
01600       IF(TEMP.GT.0.) GO TO 10
01610       IF(TEMP.LT.-ARRL) GO TO 10
01620       M2=M2 + 1
01630    10 CONTINUE
01640       RESULT=100.*(1.-M2/M1)
01650       RETURN
01660   300 RESULT=100.
01670       RETURN
01680       END
01690       SUBROUTINE COTOA(A,PHO,B)
01700       COMMON/CARR/ATMAST(3),DIRMAST(3),HMAST,RDISH,ALPHAS,
01710      1     ARRW,ARRL,CANT,FEARTH
01720       DIMENSION A(3),B(3),C(3)
01730       CALL ROT(A,PHO,2,C)
01740       CALL ROT(C,CANT,1,B)
01750       RETURN
01760       END
01770       SUBROUTINE BASIS(A,B,C)
```

```
01780       DIMENSION A(3),B(3),C(3),D(3),E(3)
01790       N=0
01800       TEMP=0.
01810       DO 9 I=1,3
01820     9 TEMP=TEMP + A(I)*A(I)
01830       TEST=TEMP/10.
01840    10 N=N+1
01850       IF(N.GT.3) GO TO 70
01860       DO 11 I=1,3
01870    11 D(I)=0.
01880       D(N)=1.
01890       CALL CROSS(A,D,E)
01900       TEMP=0.
01910       DO 12 I=1,3
01920    12 TEMP=TEMP + E(I)*E(I)
01930       IF(TEMP.LE.TEST) GO TO 10
01940       CALL UNIT(E,B)
01950       CALL CROSS(A,B,D)
01960       CALL UNIT(D,C)
01970       RETURN
01980    70 DISPLAY*NO BASIS FOUND*
01990       STOP
02000       END
02010       SUBROUTINE ECLIPSE(S,REARTH,ISUN,IDAY)
02020       DIMENSION S(3),A(3)
02030       A(1)=0.
02040       A(2)=0.
02050       A(3)=1.
02060       CALL DOT(S,A,X)
02070       Y=COS(REARTH)
02080       ISUN=1
02090       IDAY=1
02100       IF(X.GT.Y)ISUN=0
02110       IF(X.GT.0.)IDAY=0
02120       RETURN
02130       END
02140       SUBROUTINE LAT(GAMMA1,GAMMAL,GAMMAI,GAMMAD,ALAT1,ALAT,ALONG)
02150       DIMENSION A(3),B(3)
02160       F(ARG)=ARG*3.141592654/180.
02170       G(ARG)=ARG*180./3.141592654
02180       A(1)=1.
02190       A(2)=0.
```

```
02200       A(3)=0.
02210       CALL ROT(A,-GAMMAL,2,B)
02220       CALL ROT(B,(F(90.)-GAMMAI),3,A)
02230       CALL ROT(A,F(90.),2,B)
02240       CALL ROT(B,(ALAT1+GAMMAD+GAMMA1),3,A)
02250       TLAT=ASIN(A(3))
02260       A(3)=0.
02270       CALL UNIT(A,B)
02280       A(1)=1.
02290       A(2)=0.
02300       A(3)=0.
02310       CALL DOT(B,A,C)
02320       ALONG=ACOS(C)
02330       IF(B(2).GT.0.) ALONG=-ALONG
02340       PARAM=(1.00336417)**2
02350       ALAT=ATAN(PARAM*TAN(TLAT))
02360       RETURN
02370       END
02380       SUBROUTINE GIMBAL(T,REARTH,G1,G2,G3)
02390       DIMENSION T(3),A(3)
02400       F(ARG)=ARG*3.141592654/180.
02410       G3=0.
02420       CALL UNIT(T,A)
02430       G1=ATAN2(A(2),A(1))
02440       G2=ASIN(-A(3))
02450       TEMP=REARTH - F(90.)
02460       IF(G2.LT.TEMP) G2=TEMP
02470       RETURN
02480       END
02490       SUBROUTINE CITOO(X,GAMMAL,Y)
02500       DIMENSION X(3),Y(3),Z(3)
02510       COMMON/CORB/GAMMAI,GAMMAD,RL
02520       F(ARG)=ARG*3.141592654/180.
02530       CALL ROT(X,-GAMMAD,3,Y)
02540       CALL ROT(Y,(F(90.)-GAMMAI),1,Z)
02550       CALL ROT(Z,GAMMAL,2,Y)
02560       CALL ROT(Y,F(180.),1,Z)
02570       Z(3)=Z(3) + RL
02580       CALL UNIT(Z,Y)
02590       RETURN
02600       END
02610       SUBROUTINE UNIT(X,Y)
```

```
02620       DIMENSION X(3),Y(3)
02630       TEMP=0.
02640       DO 10 I=1,3
02650    10 TEMP=TEMP + X(I)*X(I)
02660       TEMP=SQRT(TEMP)
02670       DO 20 I=1,3
02680    20 Y(I)=X(I)/TEMP
02690       RETURN
02700       END
02710       SUBROUTINE DOT(X,Y,A)
02720       DIMENSION X(3),Y(3)
02730       A=0.
02740       DO 10 I=1,3
02750    10 A=A + X(I)*Y(I)
02760       RETURN
02770       END
02780       SUBROUTINE ROT(XI,A,N,XO)
02790       DIMENSION XI(3),XO(3)
02800       IF(N.EQ.2) GO TO 10
02810       IF(N.EQ.3) GO TO 20
02820       XO(1)=XI(1)
02830       XO(2)=XI(2)*COS(A) + XI(3)*SIN(A)
02840       XO(3)=-XI(2)*SIN(A) + XI(3)*COS(A)
02850       GO TO 30
02860    10 XO(1)=XI(1)*COS(A) - XI(3)*SIN(A)
02870       XO(2)=XI(2)
02880       XO(3)=XI(1)*SIN(A) + XI(3)*COS(A)
02890       GO TO 30
02900    20 XO(1)=XI(1)*COS(A) + XI(2)*SIN(A)
02910       XO(2)=-XI(1)*SIN(A) + XI(2)*COS(A)
02920       XO(3)=XI(3)
02930    30 CONTINUE
02940       RETURN
02950       END
02960       SUBROUTINE CROSS(A,B,C)
02970       DIMENSION A(3),B(3),C(3)
02980       C(1)=A(2)*B(3) - A(3)*B(2)
02990       C(2)=A(3)*B(1) - A(1)*B(3)
03000       C(3)=A(1)*B(2) - A(2)*B(1)
03010       RETURN
03020       END
```